N E T C

NEW ENGLAND TRANSPORTATION CONSORTIUM

EFFECTIVENESS OF HIGH STRENGTH COMPOSITES AS STRUCTURAL & PROTECTIVE COATINGS FOR STRUCTURAL ELEMENTS

P. Balaguru, Principal Investigator
K. Wayne Lee, Principal Investigator

Prepared for
The New England Transportation Consortium

May 2001

NETCR 28 Project No. 96-3

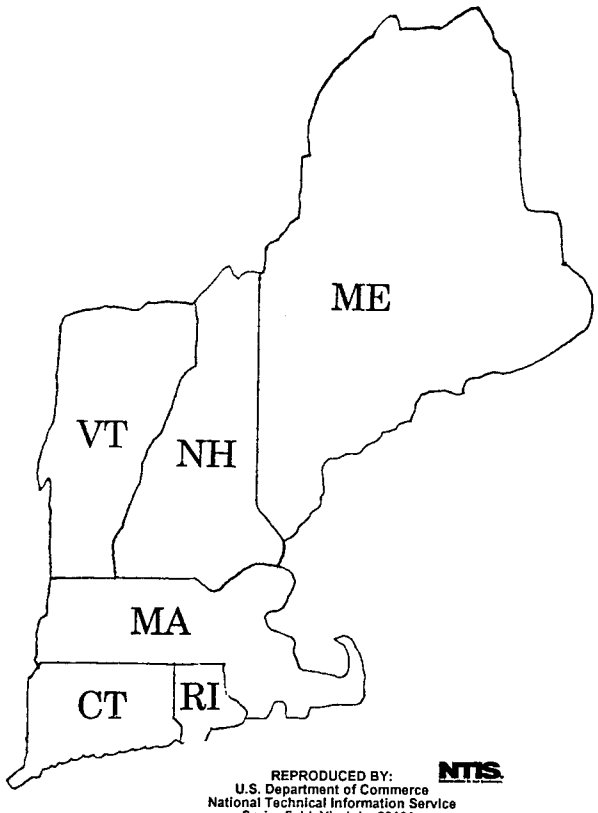

TRANSPORTATION INNOVATIONS AND IMPROVEMENTS FOR THE FUTURE

EFFECTIVENESS OF HIGH STRENGTH COMPOSITES AS STRUCTURAL & PROTECTIVE COATINGS FOR STRUCTURAL ELEMENTS

P. Balaguru, Principal Investigator
K. Wayne Lee, Principal Investigator

Prepared for
The New England Transportation Consortium

May 2001

NETCR 28 Project No. 96-3

1. Report No	2. Government Accession No.	3. Recipient's Catalog No.
NETCR 28	N/A	N/A

4. Title and Subtitle	5. Report Date
Effectiveness of High Strength Composites as Structural & Protective Coatings for Structural Elements	May 3, 2001
	6. Performing Organization Code: N/A

7. Authors(s)	8. Performing Organization Report No.
P. Balaguru & K. Wayne Lee	

9. Performing Organization Name and Address	10. Work Unit No. (TRAIS)
Rutgers-The State of University of New Jersey 623 Bowser Road, Piscataway, NJ 08854 & University of Rhode Island, Bliss Hall, 212 Kingston, RI 02881	N/A
	11. Contract or Grant No.: N/A
	13. Type of Report and Period Covered: Final

12. Sponsoring Agency Name and Address	14. Sponsoring Agency Code
New England Transportation Consortium 179 Middle Turnpike University of Connecticut, U-202 Storrs, CT 06269-5202	NETC 96-3 A study conducted in cooperation with the U.S.DOT

15. Supplementary Notes
N/A

16. Abstract

The primary objective of the research presented in this report is to identify a cost-effective composite system that will provide protection and strengthening of transportation structures under wet-dry, freeze-thaw and deicing salt environments.

The inorganic alumino silicate being developed as a fireproof matrix for high strength composites was used as coating mater. All of the systems performed well in wetting and drying conditions. Under scaling conditions, damage to the surface of the samples could be slowed down or prevented. The coatings were durable under freezing and thawing but they could not protect concrete without entrained air. Therefore, if the structure is susceptible to freezing and thawing, coating alone will not protect the structure.

The inorganic matrix in combination with tows and sheets was used to strengthen plain concrete member. Evaluation of prismatic members in flexure indicates that the carbon does not reach its fracture strain of 0.015 at failure. The fracture strain of carbon is higher when organic matrix was used for strengthening. Wetting and drying and scaling conditions do not reduce the effectiveness of the strengthening system. The analytical procedure provides reasonable accurate results. The factor that is most difficult to estimate is the carbon strain at failure for both the inorganic and organic matrices.

Three structures in Rhode Island were used for field evaluation: New Jersey Barriers, Curbs, and Abutments. All three applications are performing well. The first application is two years old.

17. Key Words	18. Distribution Statement
High Strength Composites, Structural Coatings, Protective Coatings, Inorganic Alumino Silicate, Freeze and Thaw, Fracture Strain	No restrictions. This document is available to the Public through the National Technical Information Service, Springfield, Virginia 22161

19. Security Classif. (of this report)	20. Security Classif. (of this page)	21. No. of Pages	22. Price
Unclassified	Unclassified	237	N/A

Form DOT F 1700.7 (8-72) Reproduction of completed page authorized (art. 5/94)

Executive summary

The primary objective of the research presented in this report is to identify a cost-effective composite system that will provide protection and strengthening of transportation structures under wet-dry, freeze-thaw and deicing salt environments. The major tasks were: (i) identification of promising material combinations through literature search and discussing with product manufacturers and users, (ii) evaluation of the chosen material combinations in the laboratory under accelerated test conditions, (iii) field trials, and (iv) final recommendations. Details of the literature search and selection of promising material combinations are presented in chapter 2 followed by expanded scope and objective of the investigation. The laboratory studies under wetting and drying, freezing and thawing, and sealing conditions are presented in chapters 3, 4 and 5 respectively. Performance of an inorganic coating on steel beams is presented in chapter 6. Strengthening systems using high strength carbon fibers are discussed in chapters 7 and 8. Conclusions and recommendations are presented in chapter 9.

Details of Laboratory and Analytical Investigations

Matrix:

Three formulations of alumino silicate inorganic matrices.

Two polymer modified cementitous systems (Five Star coating and Miracote)

One organic polymer with low molecular weight that will not form a film (low molecule methyl metha crylate, 3H).

The matrices could be used as plain coatings, or discrete fiber reinforced systems. For discrete fiber reinforced systems, 6mm (0.25in) long carbon fibers were used.

Reinforced strengthening systems:

Both organic and inorganic matrices were used to strengthen plain and reinforced concrete members. In addition, inorganic matrix was used to strengthen steel beams.

Test methods:

Coating and strengthening systems were evaluated under wet-dry and scaling conditions. Coated samples were also evaluated under freezing and thawing conditions. The performance was evaluated using non-destructive testing and strength tests under flexure.

Modelling: Analytical procedures were developed for designing the strengthening system. Limited field evaluations were conducted using structures in Rhode Island.

Field applications:

The coatings were applied in three structures located in Rhode Island. In the first application the coating was applied over a New Jersey barrier located over backwater. The second set of coatings was applied on curbs of sidewalks and abutments on a bridge in Route 1 in South County. The third application was done using a sprayer under a bridge carrying Route 295 near Providence.

Conclusions:

Based on the literature search, laboratory investigation and field trials the following major conclusions can be drawn.

Study of existing literature:

- Coating material should be less permeable than concrete and should not form an impermeable membrane. If the water inside the member is not allowed to escape, the impermeable membrane will delaminate.
- Polymer modified cementitous materials can be formulated to develop matrices with low permeability.
- The inorganic alumino silicate being developed as a fireproof matrix for high strength composites can also be used as a coating material.

Laboratory evaluation: Coating

- All of the systems performed well in wetting and drying conditions. The coatings and interfaces were durable.
- Under scaling conditions, damage to the surface of the samples could be slowed down or prevented. Each of the matrices performed well.
- The coatings were durable under freezing and thawing but they could not protect concrete without entrained air. Therefore, if the structure is susceptible to freezing and thawing, coating alone will not protect the structure.

Laboratory evaluation: Strengthening

- The inorganic matrix in combination with tows and sheets can be used to strengthen plain concrete members.
- Evaluation of prismatic members in flexure indicates that the carbon does not reach its fracture strain of 0.015 at failure. Since the inorganic matrix cracks, stress concentrations at these cracks result in early

failure. The fracture strain of the carbon was also found to be dependent upon the amount of carbon reinforcement. As the amount of reinforcement increases, the fracture strain decreases.

- The fracture strain of carbon is higher when organic matrix was used for strengthening. However, the increase was not very significant.
- Wetting and drying and scaling conditions do not reduce the effectiveness of the strengthening system.
- With proper design and construction process, failure by delamination of composite can be eliminated.
- Reinforced or prestressed concrete members can be strengthened with carbon fibers and inorganic matrix.
- The performance of the inorganic matrix is better than organic polymer in terms of adhesion. In addition, it is fire resistant, durable under UV light and does not involve any toxic substances. The alumino silicate matrix is water based and no special protective equipment other than gloves is needed. Excess material can be discarded as ordinary waste. This aspect is very important during the construction phase.

Analytical methods:

- The analytical procedure provides reasonably accurate results. The factor that is most difficult to estimate is the carbon strain at failure for both the inorganic and organic matrices.

- The parametric study indicates that carbon strain and carbon modulus do not significantly affect the moment capacity. Therefore, small errors in the assumption of carbon fracture may not significantly affect the strength calculations.
- A flow chart and design examples are provided for the analysis at working load levels and strength design.

Field evaluation:

Three structures in Rhode Island were chosen for field evaluation. The components consisted of New Jersey Barriers, Curbs, and Abutments. For the first two structures the coating was applied using brush or squeeze. For the third structure the coating was applied using sprayer.

Based on the first application, the matrix was modified to increase the pot life. The second application was successful. For the third application the air pressure was not sufficient. However, the coating was placed successfully.

All the three applications are performing well. The first application is two years old.

Recommendations:

All the inorganic matrices are suitable for protective coating.

More field trials should be carried out using local contractors and their equipment. These applications should be monitored for atleast 3 years.

For strengthening applications the existing systems can be used with organic or inorganic matrices. However the authors recommend the following field demonstration project. One of the reasons for this recommendation is that

most studies have been conducted for beams. But a large number of piers need rehabilitation. The column rapping method used in California is expensive and not needed for most cases.

The bridge carrying Route 1 traffic near south county hospital in Rhode Island is a best candidate for the field evaluation. The prestressed concrete beams carrying the deck are in excellent shape but the supporting piers are in distressed condition. Rehabilitating these piers with composites will be much more economical than replacing them. It is proposed to repair the columns using inorganic matrix and inexpensive carbon tows. The carbon tows can be used as a replacement for axial (along the height) reinforcement and confining the piers (columns). The recommend repair and evaluation procedure is as follows:

- Remove the spalled concrete.
- Remove the rusted reinforcement.
- Using the inorganic matrix and carbon tows place longitudinal and spiral reinforcement.
- Coat the outside to match the color of the existing structure.
- Instrument the column to measure the axial and hoop strains over a period of 3 years.
- Take small cores to confirm the integrity of repairs over a period of 3 years.
- Prepare specifications for the application of the system.

Acknowledgements

The authors would like to thank NETC for providing the financial support. The input of the technical committee and their encouragement and greatly appreciated. The technical committee consisted of:

Mr. Andy Tahmassian, Eric C. Lohrey, Deborah S. Loiselle, Warren Tripp, Clem Fung and Joel C. Kittredge.

The authors also thank Mr. Gerald M. McCarthy and his staff and CONDOT research contract office for their help. The authors also acknowledge the contribution of graduate students : Ronald Garon, Dharm Bhatt and technical assistance of Mr. Edward Wass.

Finally the authors acknowledge the contribution of Rutgers University and URI and thank Mr. Colin Franco for initiating the project and constant encouragement throughout the investigation.

Table of Contents

Chapter 8 – Analytical Investigation

List of Tables

List of figures

Chapter 1

Introduction

1.1 Scope and Objective of This Study

In the United States, maintenance and rehabilitation of the infrastructure is becoming a technical challenge. Deterioration occurs more rapidly in northern regions because of the cold weather during the winter season. In these regions, deterioration is accelerated because the concrete is subjected to freezing and thawing cycles. The salts used to prevent freezing during the winter months result in chloride induced corrosion. This deterioration occurs in bridge decks and various other superstructures. In coastal regions, exposure to chlorides is a year round problem. Piers and bridge decks are constantly subject to chloride corrosion. Although various methods have been proposed, an urgent need still exists to find an effective an economical solution to the problem of deterioration.

Recently, high strength fiber composites have been evaluated for rehabilitation of the transportation infrastructure and been found to shown excellent potential. Fiberglass boats have been known to provide excellent service for 50 years with little or no maintenance. Some of these boats are constantly exposed to sea water, the same type of aggressive environment exposed to bridge decks and other structural elements. Therefore, a number of projects have been sponsored to evaluate these composites as protective layers.

The first step in the development of these composites is the selection of a matrix. The matrix can be broadly defined as either organic or inorganic. The organic matrices are generally comprised of acrylics, epoxies, latexes, or polymers. They are usually

either single or multi-component systems, the latter of which exhibits better mechanical properties. The first part is usually a resin while the second part is an activator. Once the two parts are mixed, setting time varies between 15 minutes to 2 hours at which point they can be formulated to adhere to most materials. These organic matrices have been used to improve the performance of concrete for several decades. The strengths of the organic matrices are their almost total impermeability, dimensional stability, and high elongation before rupture. Although impermeability is a strength in many applications using composites, it is the biggest weakness when using the matrices for concrete protection. Because they are totally impermeable, the matrices are unable to release vapor pressure buildup within the structure of the concrete. Vapor pressure build-up is known to cause delamination of the matrix and can be quite damaging to the concrete.

In an attempt to improve upon the performance of the organic matrices, a number of inorganic matrices that contain polymer additives have been developed. The matrices have permeabilities lower than concrete but are not totally impermeable. It is believed that when used as a protective layer, the matrix can slow the ingress of water but at the same time allow the vapor pressure to be released. The most widely used inorganic matrix thus far has been a portland cement based system. Because of the large grain sizes of the cement, it has been difficult to develop thin and workable matrices. In addition to the portland cement based systems, alumino silicates and phosphate based compounds are used in inorganic matrices. The major advantages of their use are stability under UV light, hardness, and compatibility with concrete. A potassium aluminosilicate, one of a family of Geopolymer materials, is currently available. It has shown a pot life of over three hours and is compatible with organic, mineral, and steel fibers.

Reinforcement for the composites is available in a wide variety of materials and sizes. The common fiber types used in the construction industry are carbon, glass, nylon, polyester, and steel. In many applications, steel fibers would be preferred because of their strength and durability. In the current study, it is not feasible to use steel fibers because the coatings are expected to be quite thin. Therefore, only fine steel fibers would be acceptable. Micro steel fibers are available, but are quite expensive and would impair the development of a cost effective system. Carbon fibers are more expensive than glass and nylon fibers but are the most durable. They are inert and can be used with a number of other matrices while withstanding temperatures up to 400° C. The glass fibers deteriorate in alkali environments and the nylon is quite dense and difficult to impregnate with the matrix. Each of the fibers is available in microfibers, discrete fibers 3 to 6 mm in length, tows and fabrics.

For the current investigation one organic matrix, two polymer modified cements, and three formulations of inorganic matrix were chosen. They were evaluated as a coating material and matrix for strengthening applications.

The main focus of the study was the durability of the composite as a protective and strengthening system for concrete. Several test chambers were developed to simulate field exposure conditions in the laboratory. These include a salt-water wet-dry machine to simulate marine environments, a freeze-thaw machine mimicking the effects of a harsh winter climate, and scaling tests to study the effect of ponded water as it freezes on the surface. Both destructive and non-destructive tests were used for the evaluation. The cumulative effects of a series of wet-dry or freeze-thaw cycles were evaluated with a non-destructive test. This was accomplished by computing the dynamic modulus of elasticity

of the specimens from their natural frequencies. Trends or variations in these values were used to gage the composite's performance. Effectiveness of strengthening was measured using flexure testing.

Steel is another material that has widespread use in the construction industry. It is frequently subject to the same destructive environments as concrete. Although the damage to the steel may not be as severe, repairs may still be necessary to preserve the integrity of the structural element. For this reason, the ability to strengthen steel I-beams with the inorganic based composite system was also studied. Because the steel and carbon have comparable strengths, only minimal strength gains were expected. The ability of the matrix to bond with the steel surface and how this may prevent deterioration of the element was studied.

The current state of the knowledge on coatings and strengthening systems is presented in Chapter 2. Chapter 3 deals with the performance of the coatings under wet-dry conditions. In Chapter 4, the durability of the coatings after exposure to freeze-thaw conditions is determined. Environmental exposure is also modeled in Chapter 5, where the performance of the coatings under scaling conditions is evaluated.

In Chapter 6, the ability of the coatings to protect and strengthen steel elements is determined. A comparison between strengthening systems comprised of organic and inorganic matrices is made in Chapter 7. In Chapter 8, both organic and inorganic matrix based strengthening systems are modeled analytically. Both design and analysis techniques are covered.

Chapter 2

State of the Art

2.1 Introduction

One of the objectives of the research presented in this dissertation was to "identify a cost effective composite system that will provide long-term performance under wet-dry, freeze-thaw, and deicing salt environments." The first task was to select promising materials based on the current knowledge. This chapter presents information on the current state-of-the-art.

The focus areas are: matrix, reinforcement, and construction techniques. The matrix could be either organic or inorganic. The reinforcement could be whiskers(short micro fibers), discrete fibers(three to six mm long), tows, or fabrics made of carbon, glass, polymer, or metals. The construction techniques vary based on the type of reinforcement.

2.2 Matrix

The matrix can be broadly classified as organic or inorganic. Organic matrices have been used to improve the properties of concrete for more than two decades. The major drawback of these systems when used as a coating is total impermeability or the inability to release vapor pressure buildup. Even though total impermeability is good to prevent the ingress of liquids, vapor pressure buildup on the interface of the concrete and the coating lead to delamination. Therefore, a number of inorganic matrices that contain polymer additives have been developed. These matrices have very low permeability and

at the same time allow for vapor pressure release. In addition, two recently developed inorganic systems are discussed.

2.2.1 Organic Matrix

The organic matrices are generally grouped into acrylics, epoxies, latexes, and polymers. They are either single component or multi-component systems. Typically, multi-component systems have better properties in terms of adhesion and mechanical properties. Part A consists of resin and Part B consists of hardener or activator. Once the two components are mixed, they start to set with a pot life varying from fifteen minutes to two hours at 70°F.

Organic matrices can be formulated to adhere to most materials. The primary drawback is the surface preparation. For most compositions, the surface should be dust free, dry, and contain no loose particles. In addition, the temperature should be at least 40°F. The strong points are: impermeability, dimensional stability, and high elongation before rupture. The following sections present the pertinent details for the major groups of inorganic matrices.

Epoxies

Typical epoxy consists of a two-part system that does not have to be formulated for a specific use. The compressive and tensile strengths range from 500 to 12,000psi and 500 to 7000psi, respectively (ACI Committee 503). The elongation ranges from 0.2 to 150 percent. They are resistant to wet-dry cycling, chloride deicing salts, muriatic

acids, gasoline, oil, alkalis and sulfates. Note that most of the transportation structures are exposed to these chemicals.

Epoxies have been used as both protective and decorative coatings. The coatings vary in thickness, ranging from thin films to high-build coatings. The system has to be properly designed so as to avoid or relieve excessive shrinkage and thermal stresses between the coatings and the concrete surface in order to prevent delamination of the coating through loss of bond or failure of the concrete. Epoxies work well in tile-like coatings, but in some instances, the surface was found to "chalk" in outdoor exposure. They have been successfully used in swimming pools and a number of industrial applications (ACI Committee 503).

Even though epoxies can be sprayed, the preferred method to obtain good contact with concrete is application by brush and roller. For very porous surfaces more than one coat may be necessary.

Glass reinforced epoxy resins have been tried as protective barriers with thickness ranging from 0.5 to 6mm. These systems were applied in four steps (ACI Committee 515).

Step 1. Apply a low viscosity epoxy resin that is about 0.125mm thick on a properly prepared surface.

Step 2. Apply an activated and filled epoxy resin. This one millimeter thick layer that contains fine inert filler is applied using a trowel.

Step 3. Place woven glass fabric and embed in the wet epoxy applied in Step 2. Apply another activated epoxy coating with a brush.

Step 4. Apply another heavy coat as in Step 2 after the epoxy in Step 3 becomes tack free.

These applications are similar to the fabric reinforced systems discussed in later sections. The performance of these systems, which is a major parameter for the current study, is also discussed in those sections.

Polyester Resins

Even though a large number of commercial formulations are available, the one based on maleic anhydride and bisphenol A was found to be the most chemically resistant. Vinylester that contains acrylic acid and epoxy is another successful combination. These resins are typically mixed with fifty percent styrene monomer to lower the viscosity.

The curing or solidification is initiated by adding hardeners such as benzoyl peroxide. The reaction rate can be accelerated using accelerators such as dimethylaniline. When using polymer resins, contact with water should be avoided because water will inhibit curing. It is good practice to apply a primer that is not water sensitive. In some formulations, air was found to inhibit the curing process. This problem was solved by covering the polyester coat with a one to two percent paraffin coating.

Woven and non-woven glass fabrics and glass flakes (1.5mm diameter and 0.125mm thick) have also been used in combination with polyesters for protective barriers.

Polyurethane Resins

Urethane barrier systems consist of a resin component called polyol and a curing agent called isocynate. Because a large number of commercially available formulations are available, a careful screening is necessary for the selection of the right product for a given application.

Urethanes provide protection from deicing salts, other chemicals, and fungal growth. They can also be mixed with pigments to obtain decorative colors. Even though most urethanes are supplied as a two-part system, single component air curable systems are also available. They should be applied on a dry surface.

Latexes

Latexes represent a large variety of organic matrices. Some authors include epoxies and bituminous materials in this category. However, this section covers only elatomeric and thermoplastic latexes.

The elastomeric latex can be divided into natural rubber latex and synthetic latex. The popular synthetic latexes include: styrene-butediene, polychloroprene (Neoprene), and acrylonitrile butadiene.

The common formulations in thermoplastic areas consist of : polyacrylic ester, styrene-acrylic, vinyl acetate copolymers, polyvinyl acetate, vinylidene chloride copolymers, polyvinyl proponate, and polypropylene. Epoxies are grouped under the thermosetting latexes. In addition, there are also mixed latexes.

Typical formulations of latexes used in conjunction with concrete are shown in Table 2.1(ACI Committee 548). Acrylic polymers are a family of polymers that contain

acrylic and methacrylic acids such as butyl acrylate and methyl methacrylate. Studies have shown that cementitious coatings modified with acrylic latex maintain adhesion over many years of exposure to sunlight, rain, and snow (Lavell, 1988).

Redispersable Polymer Powders

Redispersable powders are manufactured by drying the wet spray of latex polymer (Lavell, 1988, Walters, 1992). These powders are normally white and free-flowing. They are puffy with a bulk density of about twenty-five percent lower than portland cement and the particle sizes are about 80 microns. Properly dispensed powders will have a particle size of about one or one and a half microns.

2.2.1.1 Evaluation of Organic Matrices as a Coating Material

Over the years, a large number of studies have been conducted on the performance of organic polymers used as protective coatings. Three recent studies conducted under the sponsorship of NCHRP, Army Corp of Engineers, and Canada provide a comprehensive evaluation (Marusin, 1989, Husbande and Causey, 1989, Carter, 1989, Bean, 1988). The following is a brief study of their findings.

The study sponsored by the NCHRP was conducted by Wiss, Janney, Elstner Associates and the results were published in the report NCHRP Report No. 244, "Concrete Sealers for Protection of Bridge Structures." The study focused on the following sealers.

Boiled linseed oil with mineral spirits
Chlorinated Rubber
Three methacrylate based latexes

Two butadiene based latexes

Five epoxies with different concentrations of solids

Two epoxies containing polysulfide

Two polyurethenes

Silane

Siloxane

Silicate

Siliconate

Mixture of polyisobutylene and aluminum stearate

The tests were conducted using 10 cm(4in) cubes coated with the various matrices. These cubes were immersed in chloride solutions for a twenty-one day test period. The weight gain and net chloride gain were used for evaluation. The chloride ion content was determined using ground half cubes or six millimeter cores and digestion potentiometric titration procedure. The results are shown in Table 2.2.

Both the salt-water absorption and chloride ion penetration vary widely. Even within the same generic type, such as epoxy, the variations are large. Six materials showed weight changes that are greater than plain concrete. A good correlation was found to exist between weight gain and chloride ion content. Linseed oil, a silane, and siloxane was found to penetrate concrete well and hence were classified as penetrating sealers. The results are further discussed in the following sections.

Boiled Linseed Oil

Linseed oil is one of the most widely used sealers. It was found that two coats did not improve the properties significantly. However, four coats reduced the weight gain by fifty-two percent. The chloride ion content was reduced by sixty percent for four coats.

The depth of penetration varied from zero to two millimeters and the vapor transmission was not affected by multiple coats.

The chloride content at various depths is shown in Table 2.3. It can be seen that even four coats did not bring down the chlorides to threshold levels of 0.03 percent.

Epoxies

The epoxies used consisted of two component systems with solid contents varying from seventeen to one hundred percent. In most cases, two coats were applied. The performance improved with increase in solid contents. Two epoxies with solid contents of fifty and one hundred percent provided the best results with seventy-nine and ninety percent reduction in weight gain. The corresponding reduction in chloride ion contents were eighty-one and ninety-one percent respectively. Epoxies with lower solid contents performed better when the samples were pretreated with linseed oil. The two polysulfide epoxies did not perform well.

Silane primer in combination with water based epoxies seem to perform well in reducing chloride ingress.

Urethanes

Urethane containing twenty to forty percent solids was applied in two and three coats. Two component urethanes reduced weight gain and chloride penetration by about eighty percent. The one component system was much less effective. Some urethanes are very sensitive to UV exposure, and pigments play an important role in their behavior. The coverage rate also influences the behavior as shown in Table 2.4.

Latexes

Acrylic type containing methacrylate was found to be more effective than a styrene butadiene type. Both styrene-butadiene sealers studied had very little influence in the reduction of weight gain and chloride ion penetration.

Silanes

Typically silanes do not form a continuous film and hence are not as effective as continuous film forming systems. They do penetrate concrete to form a hydrophobic zone repelling liquid water. Since the film is not continuous, silane treated concrete is permeable to water vapor.

The silanes investigated reduced chloride content up to seventy-nine percent. Their performance is highly influenced by the amount of silane in the system and the amount used per area. The choride content range was 0.08, 0.02, 0.01, and 0.007 percent at depths of 12, 25, 37, and 50mm respectively. The threshold levels of 0.03 percent was reached at depths larger than 12mm.

The penetration depth of silane varied from 1 to 8mm. Deeper penetration did not improve the chloride ion ingress but could protect the concrete for a longer duration. Since silanes are penetrating sealers, they are not recommended for previously treated surfaces.

Siloxanes

Siloxanes by themselves were found to be poor performers. But when they were combined with silanes, their performance becomes synergistic. The chloride levels for

three samples are shown in Table 2.5. The threshold levels of 0.03 percent chloride can be achieved at 12mm or deeper. Siloxanes are also very sensitive to their formulation. The depth of penetration varied from 1 to 9mm.

Chlorinated Rubbers

Chlorinated rubbers were found to have no influence on concrete permeability. This confirms the results reported in earlier studies.

Silicates and Siliconates

Both silicates and siliconates were also found to be ineffective. The formulations were found to have significant influence on performance.

The following overall conclusion reported in Husbande and Causey, 1989, summarizes the performances of various organic matrices.

> "Certain specific chemical materials used as sealers over the concrete exposed surfaces can enhance concrete durability and limit corrosion of embedded steel by reducing the intrusion of chloride laden water into the concrete. Among the most successful materials are epoxies, urethanes, latexes, silanes, and silane-siloxanes. However, performances of all these materials varied from excellent through unsatisfactory. Effectiveness of all these sealers is greatly influenced by their chemical formulations, concrete quality, surface preparation, and application conditions. Generally, epoxies exhibited glossy surfaces, urethanes and latexes varied

in color, and penetrating silanes or silane-siloxanes did not change concrete appearance."

The authors feel that epoxies and methaerylates are the most promising organic matrices. The selection should be based on their compatibility and ease of application with glass and carbon fibers and fabrics. These aspects are further discussed in the later sections.

The study conducted by the U.S. Army Corps of Engineers dealt with the concrete sealers and concrete coatings. Their focus was to evaluate the commercially available materials for resistance to chemical attack, erosion, and freeze-thaw.

The generic types of sealers that were evaluated are acrylics, epoxies, polyurethanes, silicates, silanes, silicones, siloxanes, stearates, and hydrocarbons. Their study complements the NCHRP study discussed earlier. Overall, sixty-eight commercial products were evaluated. The generic coating types evaluated were epoxy resins, polyester resins, acrylics, vinyls, polyurethanes, silicons, neoprenes, butyle rubbers, and cementitious coatings. Typically, coatings were thicker than sealers and in most cases they bridge the micro cracks that are present on the parent concrete surface.

Tests were conducted to determine water absorption, water vapor transmission, resistance to scaling, bond strength of coating to concrete, and weathering. A water absorption test was conducted by immersing coated 100 mm cubes. The concrete mixture had a water-cement ratio of 0.62 and a 28 day compressive strength of 26 Mpa (3800psi). Cubes were weighed after immersing them for 1, 2, 3, 4, and 7 days.

For the water-vapor transmission test, 13mm holes were drilled to a depth of 50mm through coated 100 mm cubes and immersed in water for five days to saturate

them. The holes were then sealed and the samples were dried at 38°C and thirty percent relative humidity. Weight of the cubes after drying periods of 2, 4, and 7 days were used to determine the water-vapor transmission rate.

Resistance to sealing, bond strength of coating, and accelerated weathering tests were conducted using ASTM C 672-84, D 4541-45, and G 53-84 respectively. For the sealing test, four percent calcium solution was used as the deicer and the samples were evaluated for fifty cycles. The concrete had a 28 day compressive strength of 36Mpa (5200psi). For the accelerated weathering tests, UV-B fluorescent ultraviolet lamps with peak emission occurring at 313 nanometers were used. The samples were tested at 50° C with 5 and 3 hours for UV and condensation respectively. The test samples were 150 X 75 X 13 mm (6 X 3 X 0.5 in.) mortar prisms.

The results are presented in Tables 2.6 and 2.7. The control samples had water absorption of 4.7 percent after 2 days and water vapor transmission of 3.2 percent after four days. As in the case of an earlier study, a wide range of variation was observed. The primary variables that affected the absorption were : solid content, application rate, and porosity and texture of the concrete. Silanes, silicates, and silicones were found to be poor performers. Acrylics with less than ten percent solids also performed badly.

In the area of water vapor transmission, siloxanes performed better than silanes. Acrylics had more than fifty percent water vapor transmission. They concluded that if the water absorption is limited to twenty percent and water vapor transmission should exceed thirty percent, only 13 of the 68 sealers tested would satisfy the requirements.

Silanes, siloxanes, and silicones performed better in the accelerated weathering test. The acrylic sealers that performed better in water absorption tests did not perform well under UV exposure. Linseed oil was found to perform better.

As expected, epoxy resins performed well in scaling tests. Silanes and siloxanes did not perform well. Overall, about fifty percent of the sealers tested provided satisfactory performance.

When the sealers were applied as thicker coatings difficulty was encountered specifically at the edges and corners. Most of the coatings adhered well to the concrete and their performance under UV and weathering were better than the counterpart sealers. Polyurethanes, specifically two component systems, were found to perform well under accelerated weathering conditions. Acrylics had mixed results.

The general conclusion was that siloxanes and linseed oil showed promise as sealers. The only drawback was their resistance to freezing and thawing. Acrylic formulations also showed promise for coatings.

The research conducted in Canada generally confirms the results of the American study. The Canadian study focussed more on sealers than coatings. Again, epoxies and siloxanes were found to perform better than other composites.

2.2.2 Inorganic Matrix

The most widely used inorganic matrix is the portland cement based system. However, the grain sizes of cement are not conducive to formulating thin matrices. Hence, they are quite often used in conjunction with organic matrices as discussed in the next section.

Other than portland cement, the other common room-temperature matrices are alumino silicates and phosphate based compounds. The major advantages in using inorganic systems are their resistance to high temperature, stability under UV light, hardness, and compatibility with concrete and non-toxic characteristics. Special precautions are not needed during the construction and disposal of excess or old material is easier. One of the inorganic resins which is currently available is a potassium aluminosilicate, or poly(sialate-siloxo), with the general chemical structure.

$$K_n\{-(SiO_2)_z - AlO_2\} \bullet wH_2O \qquad (2.1)$$

where z>>n. This resin hardens to an amorphous or glassy material, and is one of a family of inorganic Geopolymers materials (Davidovits, 1991A, Davidovits, 1991B). It has a pot life of more than three hours and is compatible with organic, mineral, and steel fibers.

Geopolymers have been evaluated for use with carbon, glass, nylon, steel fibers, and fabrics. The results are quite encouraging (Balaguru et al., 1996, Lyon et al., 1997, Foden et al., 1997, Foden et al., 1996, Foden et al., 1996b, Foden et al., 1996c). It has also been successfully used for strengthening a reinforced concrete beam (Balaguru et al., 1996).

The matrix is stable in alkali and acids but not evaluated for wet-dry or freeze-thaw durability. If this composite is selected for further evaluation, durability tests will be conducted as part of the current investigation.

The phosphate matrix has been used in mortar form for about 20 years but has not been used as a coating material. Preliminary tests conducted at Rutgers show that this

material has excellent prospects. The primary strength of the matrix is its fast setting characteristics. It is possible to obtain a stable system in about two hours.

2.3 Fibers

The common fiber types used in the construction industry consist are aramid, carbon, glass, nylon, polypropylene, polyester, polyvynal alcohol, and steel. For the current project it may not be feasible to use steel fibers because the coatings are expected to be thin and hence only very fine steel fibers can be used. Even though micro steel fibers are available, they are very expensive (about $30/lb). Aramid fibers are also expensive as compared to other fibers. Therefore, the discussion is focused on carbon, glass and polymeric fibers. It should be noted that the word fibers encompasses discrete fibers, continuous fibers and fabrics.

Carbon is inert and has been used with a number of matrices. By itself carbon can withstand up to 400^{o}C, and is available in discrete fibers (whiskers to 12mm long), tows, and fabrics. The only concern is cost. They are more expensive than glass or polymeric fibers.

Glass is also available in a variety of forms and is inexpensive as compared to carbon. It is not as durable as carbon and it deteriorates in alkali environments. A large number of studies are available on the behavior of various types of glass in alkaline environments (Balaguru and Shah, 1992). The commonly used E glass degrades rapidly in an alkali environment. If glass fibers are used near concrete, they should be well protected with impermeable matrices. Alkali resistant fibers are also available, but their

durability is still questionable for long durations. This aspect is further discussed in the composites section.

All the polymeric fibers are available in discrete fiber form. Only polypropyle fibers are readily available in loose fabric form. The fabrics made of nylon and other fibers seem to be too dense and hence cannot be readily impregnated with the matrix. The only disadvantage with polymeric fibers is their suseptibility to fire and a low modulus. However, they are very flexible and hence easy to work with an inexpensive.

Polyester fibers degrade under alkaline environment and most of the polypropylene fibers degrade under UV exposure (Balaguru and Shah, 1992, Balaguru and Slattum, 1995).

2.3.1 Polymer Modified Cement Coatings

A number of proprietary polymer modified cement coatings are available in the market. Their performance is closely related to the performance of polymers used in the system. The major difference is the vapor transmission. Most cement systems allow for the release of vapor pressure. Most of the data available on the performance is provided by the manufacturers and not based on a systematic study. In general, modified cement mortars are more water resistant and they adhere to the parent concrete better.

2.4 Fiber Composites

Most popular fiber composites are made using either carbon or glass. These composites have been used in aerospace industries for more than three decades. Their

use in civil infrastructure is relatively recent. In most cases, these composites have been used for repair and rehabilitation of structures.

The structural elements studied include the following:

- Beams bonded with FRP composites at the tension face.
- Beams bonded with FRP composites at the tension face and sides.
- Columns confined using various types of wrapping.
- Masonry structures bonded with FRP fabrics and wires.

Bonding of steel plates using epoxy resins to the tension zone of concrete beams had been used extensively in the rehabilitation of bridges and buildings. However, corrosion of steel plates has been found to cause deterioration of the bond at a glued steel-concrete interface, rendering the structure vulnerable under overload and possible failure. Hence, FRP's are now being considered as a potential replacement for steel plates to avoid corrosion. In addition, FRP's have a low volume to weight ratio, and eliminate the need for joints since the composite sheets can be obtained in long lengths. FRP sheets made of carbon, glass, or aramid fibers bonded with a polymer matrix are being used as a substitute for steel (ACI Committee 440, Nanni, Sadatmanesh and Ehasani, 1996, MPA, Meier, 1987). Epoxy, polyester, or vinylester are the common adhesives used to bond the FRP sheets to the concrete. A number of researchers have conducted experimental and analytical investigations on the strength and stiffness of beams with bonded FRP composites (Meier, 1987, Plevris and Triantafillou, 1993). These investigations have shown that beams strengthened with FRP fabrics exhibit much higher ultimate strength and stiffness than reference beams.

As in the case of beams, columns retrofitted with FRP fabrics or wires have been investigated primarily for strength behavior. The elements investigated include building columns (Plevris and Triantafillou, 1993, Plevris and Triantafillou, 1993b), bridge columns(Ritchic et al., 1991, Saadatmanash and Ehsani, 1991), and chimneys(Harmon and Slattery, 1992, Priestley et al., 1992). Chimneys were repaired without having to take them out of service. It has been shown that wrapping FRP fabric around the perimeter of both circular and rectangular concrete columns to create a confinement effect resulted in improving the ductility and the strength. In addition, it has been shown that confinement with FRP's may improve the behavior of columns subjected to seismic loading (Priestley et al., 1992). Other FRP confinement techniques have also been shown to improve the behavior of normal and high strength concrete (Harmon and Slattery, 1992). Retrofitting of concrete columns by lateral confinement with FRP wires has also demonstrated an increase in strength and ductility. Results showed significant increases in compressive strength and psuedo-ductility under uniaxial compression. Analytical studies have also been conducted to evaluate the strength and durability behavior (Li et al., 1992, Berset, 1992).

Bonding masonry structures with FRP's enhances their strength and deformation characteristics. Test results have shown that bonding unreinforced masonry structures with composite fabrics is a very effective technique for increasing flexural strength and ductility of these elements. One study has shown that the specimen carried loads more than twenty times its own weight (in flexure) and exhibited large deflections, in excess of 1/50 times the span (Ehsani et al., 1993). Other work has revealed an increase in strength of masonry walls under compression, in-plane bending, and out-of-plane bending by 3-

fold, 12-fold, and 14-fold, respectively, when retrofitted with FRP fabrics (Hamid et al., 1993). There are a number of studies in progress in the U.S.A. and Canada including the active programs at the University of Arizona, Penn State, Iowa State, Wyoming, Rutgers, University of Toronto, Manitoba, and Sherbrooke.

Even though a large number of applications have been carried out, available information on durability is limited (Toutanji and Balaguru, 1998, Soudki and Green, 1996, Saadatmanash and Tannous, 1998, Gomez and Casto, 1996). Durability studies can be grouped to cover specific areas.

- durability of fiberglass bars or composites
- durability of carbon bars or composites
- durability of concrete repaired with glass or carbon composites.

A number of studies are still in progress, the most comprehensive one is being conducted by CALTrans. The authors have listened to a number of presentations at Transportation Research Board Meetings, American Concrete Institute and American Society of Civil Engineers conventions, and International workshops of Fiber Reinforced Polymers. The following are the broad conclusions.

Carbon either in fabric or fiber form or composite plate can be used with no durability problems provided that the matrix is durable. The interface between the coating (or composite repair) and concrete is governed by the quality of the concrete and the liquids that get through uncovered areas.

Glass composites have some problems. Glass by itself is very susceptible to alkali and when alkali reaches the fiber from concrete or other source it will deteriorate.

Extensive research has been conducted to alleviate these problems. If the fabrics are well protected by the matrix the durability problem is minimized.

The following are some of the conclusions of different authors who evaluated the composites.

The durability of pultruded fiberglass composite systems, isophthalic polyester and vinylester, were studied by Gomez and Casto by placing coupons in a 2% NaCl-water solution and subjecting to freeze-thaw (Gomez and Casto, 1996). Periodically the coupons were removed and tested to failure in flexure. Results showed significant loss in flexural strength, rigidity, and toughness due to freeze-thaw cycles.

The durability of identical steel and S-2 glass-epoxy pre-tensioned beams subjected to wet-dry conditions simulating tidal effects was investigated by Sen et al., 1993. Half of the tested beams were pre-cracked at the mid-span section. Test results showed a complete loss in the effectiveness of the fiberglass strands exposed to wet-dry cycles after an average of six months for the pre-cracked and fifteen months for the uncracked beams. There was no comparable loss of capacity in the identical steel pre-tensioned specimens.

The durability of beams externally bonded with different composite systems was investigated by Chajes et al., 1994. A number of beams were exposed to cycles of wetting and drying and another set was subjected to freeze and thaw cycles. Results showed that the beams experienced a reduction in flexural strength due to the degradation in the bond between the concrete and the fiber composite. The results also show degradation in the fiber composites themselves.

The effect of acidic and alkaline conditioning under varying and constant temperature on strength and stiffness of concrete beams wrapped with carbon fiber sheets was also studied by Javed et al., 1996. Results showed that the bond shear strength of the samples exposed to environmental conditioning decreased with respect to unconditioned samples. The percentage decrease was 17% for samples in acidic condition, 24% for samples in alkaline condition, and 29% for samples exposed to hygrothermal condition.

Specimens made of carbon FRP grid and glass-carbon FRP grid with junctions at 100 mm spacing were exposed for up to a year to solutions of salt and alkali, UV radiation with wet-dry cycling, and freeze-thaw action by Rahman et al., 1996. The tensile strength of these specimens was found to remain unaffected by the environmental conditions wheras the junction strength was found to be sensitive to salt, alkali, and freeze-thaw action.

The results reported in Toutanji and Balaguru, 1998, deal with an experimental study on the performance of concrete columns wrapped with carbon and glass FRP composite sheets subjected to wet-dry and freeze-thaw conditions. Concrete columns were wrapped with three different types of FRP tow sheets, two carbon and one glass. Test variables included the type of fiber (C1, C5, and GE) and the environmental exposure conditions. The specimens were conditioned in three different environments as follows: a) room temperature (20°C), b) 300 cycles of wet-dry using salt water, c) 300 freeze-thaw cycles. At the end of each exposure period, stress-strain behavior in compression was obtained in order to evaluate their strength stiffness, and ductility, which were compared to the performance of unconditioned samples. The following are the conclusions of this recent paper.

- The results of this study are in agreement with others that have shown that carbon fiber reinforced polymer is superior to glass when exposed to harsh environments.
- Exposure to wet-dry environments has little effect on the compressive strength of CFRP wrapped specimens; however, exposure improves the stiffness of the specimens. The CFRP wrapped specimens exhibited a reduction in strength of 10% but exhibited no effect on stiffness due to wet-dry conditions.
- Exposure to freeze-thaw environments showed a significant degradation in strength in both CFRP and GFRP wrapped specimens. Specimens wrapped with each of the carbon fiber sheets C1 and C5 experienced similar reduction in strength. The glass fiber wrapped specimens exhibited a higher degree of degradation as compared to the carbon fiber wrapped specimens. The freeze-thaw exposure seems to exhibit no effect on the stiffness of CFRP or GFRP wrapped specimens.
- Exposure to wet-dry environments caused no loss in ductility in specimens wrapped with CFRP; however, specimens wrapped with GFRP sheets exhibited a reduction in ductility. Exposing wrapped specimens with either CFRP or GFRP sheets to freeze-thaw environments exhibited a significant reduction in ductility.
- The wrapped specimens subjected to freeze-thaw cycling exhibited more catastrophic failure behavior as compared to the unconditioned and wet-dry conditioned specimens.

2.5 Application Techniques

The common application techniques are brush, roller, squeegee, spraying, and troweling. For the organic matrices, the preferred methods are by brush or roller because they provide better wetting. If sprayers are used, airless sprayers are recommended. In addition, a larger thickness is needed to ensure complete coverage.

A large number of commercial sprayers are available. Most of them deal with single components and are not suitable for multi component matrices. In general, two component systems have better properties than single component systems. For adding fibers, chopper guns are attached at the top. There are at least three companies that sell sprayers that can handle two components and fibers. The boat building industry also uses two component systems with a fiber chopping gun.

The following are the major factors that should be considered in the area of application techniques.

2.5.1 Surface Preparation

Surface preparation is extremely important especially for organic matrices. They should not have loose aggregates or conglomerates, dust, or water. Surface preparation could add a considerable amount of expenditure. Inorganic matrices are more forgiving because they can be applied on a wet surface and the surface need not be totally dust free.

Special equipment has been developed for sandblasting, cleaning, automatic metering, and application on horizontal surfaces, but this heavy equipment is not suitable for application on vertical surfaces.

2.5.2 Working Time and Temperature Requirements

In most cases the working time, or pot life, is limited to about two hours. Both ambient and concrete surface temperatures must be higher than 40°F, preferably higher than 50°F for proper application and cure. These requirements are the same for both organic and inorganic matrices.

2.5.3 Precautions During Application

Most of the organic matrices have some requirements in terms of protection equipment for the construction crew. In addition, special enclosures may be needed when work is done in urban area where the structures are located close to residential or commercial buildings.

Use of the chopped glass fibers provides another challenge because the fibers are thrown on the stream of the matrix and some of the fibers become air-born creating a health hazard. It is proposed to develop a special system to minimize the air-born fibers. In this respect, hand placed fabrics are a better option in terms of efficiency and placement technique. The disadvantages are their cost and application in hard to reach places.

2.5.4 Curing Requirements

Most systems need to be protected for at least 24 hours from rain, freezing, or other contamination such as excessive dust. In some cases, a heating blanket is recommended for accelerating the cure.

2.5.5 Case Studies

Spraying of organic matrices is being carried out on a regular basis for factory and industrial buildings. In some occasions, chopped glass fibers, glass fiber mats, and polypropylene fiber mats are being utilized. Chopped glass and organic matrix are commonly used by the boat building industry but the operation is not clean. Extensive protective equipment is needed to prevent dust and chemical inhalation.

In the area of the infrastructure, a large number of projects have been carried out in California using carbon and glass tows and fabrics. In the New England area, we have installations in Connecticut and Vermont. To the best of the authors' knowledge, these systems are expensive and may not be economically feasible for applications as protective coatings. The cost could be reduced if the market volume increases. In addition, light glass, polypropylene or nylon fabrics could be used instead of expensive unidirectional glass and carbon. Note that the current installations are used for strength and ductility enhancement for which the fibers should be embedded with the least amount of disturbance. In the protective coatings, fiber could have slight weaves that will not adversely effect the performance. Additionally, the stiffness (Young's Modulus) of fibers is not critical.

2.6 Recommendations

Review of the various organic, inorganic, modified cementitious matrices, fiber, tow, fabric reinforcement, and application techniques lead to the following selection of materials and construction techniques.

2.6.1 Matrix

It was decided to study one organic matrix, two polymer modified cement systems, and a few formulations of inorganic matrix.

The organic matrix provides total impermeability but no avenue for vapor pressure release. This seems to result in delamination of the concrete at the interface. However, the chosen system has a low molecular weight and allows for vapor pressure release.

The inorganic matrix works similar to concrete but is much more impermeable than concrete. The major advantages are their compatibility with the concrete resulting in a chemical bond that eliminates the well defined interface. It also allows for vapor pressure release. The recommended matrix is an alumino silicate that has been evaluated with carbon and glass fibers and fabrics.

The polymer modified systems are expected to behave similar to the inorganic matrices but they can not be used for strengthening.

2.6.2 Reinforcement

In the area of fibers; whiskers, discrete fibers, and continuous fiber reinforcements made of carbon were selected. All of the fiber types are commercially available.

The primary contribution of the fibers is to provide a continuous thin film of fiber reinforced mat. Fabrics will provide strength increase. Whiskers and short fibers are expected to provide strain enhancement resulting in more ductility and less spot cracking.

2.6.3 Application Techniques

All application techniques should be tried both in the laboratory and small field trials. It is expected that spraying with short fibers and hand laying technique for fabrics will prevail as the economical and viable techniques.

Sprayers are available for glass fiber reinforced panels, boat builders, and commercial organic matrices. However, for the research presented in this study, the applications were made using a spatula.

Table 2.1
Typical formulation for latexes used with portland cement(ACI Committee 548)

Vinyl acetate, homo- and copolymer latexes	
Item	Parts by Weight
Vinyl acetate	70-100
Comonomer	0-30
Partially hydrolyzed polyvinyl alcohol	6
Sodium bicarbonate	0.3
Hydrogen peroxide(35%)	0.7
Sodium formaldehyde sulfoxylate	0.5
Water	80
Acrylic copolymer latex	
Ethyl acrylate	98
A vinyl carboxylic acid	2
Nonionic surfactant	6
Anionic surfacatant	0.3
Sodium formaldehyde sulfoxylate	0.1
Caustic soda	0.2
Peroxide	0.1
Water	100
Styrene-butadiene copolymer latex	
Styrene	64
Butadiene	35
A vinyl caroxylic acid	1
Nonionic surfactant	7
Anionic surfactant	0.1
Ammonium persulfate	0.2
Water	105

Table 2.2

Summary of average weight gain and loss, chloride ion content and reduction of weight gain and chloride ion content when compared to uncoated cubes, Marusin, 1989

No.	Material	Weight gain after 21 days 15%NaCl	Reduction of Weight Gain(%)	Weight loss 21 days air dry(%)	Chloride ion Content (%)	Reduction of Chloride ion in Concrete(%)
1	Siloxane	2.87	None	1.01	0.287	None
2	Linseed Oil(2 Coats)	2.19	21	0.89	0.209	11
	(4 Coats)	1.34	52	0.79	0.094	60
3	Siliconate	2.84	None	0.97	0.258	None
4	Urethane	0.63	77	-0.05	0.048	80
5	Chlorinated Rubber	2.54	8	0.94	0.223	6
6	Silane	0.82	70	0	0.05	79
7	Styrene butadiene	2.8	None	1.11	0.271	None
8	Methyl methacrylate	0.61	78	-0.12	0.047	80
9	Sodium Silicate	2.41	13	0.78	0.247	None
10	Polyisobutyl	1.34	52	0.3	0.126	47
11	Vinyl toluene	2.42	13	0.91	0.209	12
12	Al stearate	2.5	10	0.87	0.246	None
13	Methyl meta	2.47	11	0.96	0.233	1
14	Vinyl toluene	2.32	16	0.83	0.22	7
15	Al stearate	0.57	79	0.23	0.044	81
16	Epoxy	0.29	90	0	0.008	97
17	Epoxy-polysulfide	1.78	36	0.78	0.158	33
18	Epoxy	1.7	39	0.56	0.161	32
19	Epoxy	2.53	9	0.95	0.233	1
20	Epoxy-polysulfide	1.99	28	0.87	0.172	27
21	Epoxy	2.23	20	1.01	0.201	15
22	Plain Concrete	2.77	-	0.93	0.236	-

Table 2.3

Chloride content, percent at depths in mm (Linseed Oil)

Depth	0-12	12-25	25-37	37-50
Two coats	0.45	0.2	0.08	0.05
Four Coats	0.4	0.1	0.05	0.04

Table 2.4
Performance of urethane sealants

Urethane Sealant Number	Coverage (ft2/gal*)	Weight Gain (% weight gain)	Chloride ion content (% by weight)
1	300/300	0.29	0.004
	400/400	0.44	0.022
	500/500	0.63	0.069
2	300/300	0.43	0.016
3	100/100	0.14	0.007
3**	100/100	1.2	0.095

* Two coats, coverage per inch coat

** Urethane with pigment

Table 2.5

Chloride content, percent at various depth interval, mm (Siloxanes)

Depth	0-12	12-25	25-37	37-50
A	0.136	0.03	0.028	0.024
B	0.1	0.021	0.013	0.007
C	0.076	0.018	0.012	0.007

Table 2.6

Accelerated Weathering Test Results, (Husbande and Causey, 1989)

	Water Absorption % Before Testing (Material No.)				Water Absorption % 1600 hr Testing (Material No.)			
Generic Type	1	2	3	4	1	2	3	4
Acrylic	0.55	0.61	0.72	0.87	2.56	3.12	4	3.94
Hydrocarbon	0.47	0.65	0.4		0.94	3.57	4.61	
Linseed Oil*	4.5	1.57			0.54	0.88		
Polyurethane	0.34	0.53	0.22		0.87	1.44	0.87	
Silane	0.52	0.56	0.6	0.44	0.66	0.7	0.8	0.57
Silicone	0.44				0.47			
Siloxane	0.56	0.54	0.59		0.71	0.68	0.73	
Stearate	0.93	0.67			1.96	1		

* Material 1 is an emulsion and 2 is linseed oil in mineral spirits.

Table 2.7

Resistance to Scaling, Concrete Sealers, (Husbande and Causey, 1989)

Generic Type	Number Tested	Visual Rating of Surface (No. Materials for each Rating) 0	1	2	3	4	5
Control	2					1	1
Acrylic	9	2	3	3		1	
Epoxy	4	4		1			
Hydrocarbon	3			1		1	1
Linseed Oil	1						
Methyl Methacrylate	1	1					
Polyurethane	5	3					2
Silane	5	1		1	1	1	2
Siloxanes	6				3	1	1
Stearate	2				1		1

Rating 0-no scaling, 1-slight scaling, 2-slight to moderate scaling
3-moderate scaling, 4-moderate to severe, 5-severe

Chapter 3

Durability Under Wet-Dry Conditions

3.1 Introduction

Continuous exposure to wet-dry conditions is detrimental to concrete used in construction. The degradation is more rapid for structures located in marine environments because of the presence of salt. Elements exposed to such environments are gradually weakened and will eventually have to replaced or repaired. Typically concrete on the exposed surface is weakened more rapidly than concrete within the structure. During placement, the presence of water near the formwork makes the surface concrete weaker because of an increase in the water-cement ratio resulting in faster degradation. Epoxy coatings have been used to increase the durability of exposed surfaces. High strength fibers made of aramid, glass, or carbon have been used in conjunction with epoxies when strengthening is required. The external bonding of Fiber Reinforced Plastics, (FRP), to the tension face of an element is one such method of repair. Acceptance of high strength composites in the construction industry in this capacity has grown at a rapid pace during the last decade (ACI Committee 440). They are very popular for repair and rehabilitation because of their light weight, high strength, and corrosion resistance.

Epoxies and other organic matrices have been utilized as a protective coating for several decades because they seal the surface of the concrete. Their main drawback is their inability to release vapor pressure buildup that causes damage in the concrete and delamination of the dried epoxy (ACI Committee 503). The effect is minimized for air

entrained concrete. The results presented in this chapter focus on the inorganic matrices that comprise the next generation of barrier and strengthening systems. They are less permeable than concrete thus slowing the flow of water through the weakened exterior surfaces. Vapor pressure is released because the matrices are not totally impermeable. In strengthening applications, the matrices form a strong bond between the surface of the concrete and the fiber reinforcement. Based on the literature search one cementitious, three inorganic, and one organic matrix were chosen for this study. The organic matrix was made of very low molecule sizes that allowed penetration of the matrix and vapor pressure release.

The objective of this part of the investigation was to evaluate the effect of wet-dry cycles found in marine environments. In barrier applications, the objective was to evaluate the coatings and the durability of coated concrete. In strengthening applications, the effectiveness of the matrices used in conjunction with carbon reinforcement was studied.

3.2 Experimental Evaluation

As mentioned earlier, one cementitious, one organic, and three inorganic matrices were evaluated as protective coatings. For a strengthening system, an inorganic matrix was used in combination with short discrete and continuous carbon fibers. For parent concrete, a high and low strength mortar with low and high water-cement ratios were chosen. The specimens with protective coating were subjected to wet-dry cycles using salt water. Dynamic modulus was measured after exposure to wet-dry cycles using a non-destructive test method. The non-destructive testing allows the same samples to be

tested after various levels of exposure. In strengthening applications, the effectiveness of the matrix was studied using flexure tests after exposure to wet/dry conditions.

3.2.1 Independant Variables

The independant variables for the wet-dry durability testing consisted of the unprotected parent samples along with six sets of coated samples. One set of samples was coated on all sides and the second set was coated on only three sides. The sequences were chosen to simulate different field elements such as piers and abutments. Piers can be protected on all sides minimizing water penetration where as in abutments, water can penetrate from back fills. The following sections provide more details.

Polymer modified cement.

This system commercially known as Five Star consisted of a cementitious powder and water. The liquid to solid ratio was 0.30. Six millimeter long carbon fibers were added at a dosage of 2%. The fibers were added to improve the tension strain capacity.

Inorganic matrices.

Three inorganic matrices consist of a potassium silicate solution and silicafumes from three different sources. The first one contained 0.5% carbon and the second had about 0.2% carbon. The third silicafume was a refined naturally occurring fume. All of the fumes had a minimum silica content of 80%. They were mixed in a solid to liquid ratio of 1:1. Microfibers and ground sand were added as fillers. The ratio of fillers to matrix was 0.55. Carbon fibers at a rate of 2% were added to all three matrices. Samples coated with the third silicafume were tested at the end of the test cycle after previous tests had

shown that samples totally coated and coated on only three sides performed equally well. Therefore, the third silicafume was applied to all sides of the specimens.

Organic system.

This commercially available epoxy system is known as 3M Concrete Protector and Restorer. It is made of low molecular weight methal methacrylate. This matrix penetrates the pores rather than forming a film, thus allowing for vapor pressure release. Coating three sides was successful in protecting the concrete so totally coated samples were not tested, because total sealing will provide better protection.

Strengthening systems.

An inorganic matrix was used to bond continuous carbon fibers in the form of tows or fabrics. The reinforcement consisted of one, two, or three tows or one and two layers of unidirectional fabric. The area of one carbon tow was 0.00286 in^2 and the carbon fabric had an area of 0.0115 in^2. In addition, samples were strengthened with a discrete fiber reinforced mix. This matrix was comprised of potassium silicate solution and silicafume with no carbon. The pure silicafume was needed to obtain a matrix that could be used to wet the carbon fibers. The standard formulation was as follows.

Liquid : 100 g

Silicafume : 125 g

Wetting Agent : 1g

3.2.2 Preparation of Concrete Prisms

Two mix proportions were used to prepare the concrete prisms. The dimensions of the prisms were 2 X 2 X 13 in. For the first mix the cement : fine aggregate : course

aggregate ratio was 1 : 2.14 : 1.79. The maximum size of the course aggregate was 0.375 in. The water/cement ratio was 0.5. This concrete was designated as high strength concrete. For the second concrete mix, the cement : fine aggregate : course aggregate ratio was 1 : 2.95 : 2.04. Again, the maximum size of the course aggregate was 0.375 in. The water/cement ratio was 0.6. This mix was designated as the low strength mix. The prisms were cast using 2 X 2 X 13 in. steel molds, covered with polyethylene sheet and kept for 24 hours at room temperature and humidity. At the end of 24 hours, the samples were removed from the molds and cured for 28 days in a room maintained at 100% relative humidity.

3.2.3 Application of Coating or Strengthening Systems

Once the parent samples had been properly cured their surfaces were prepared for the application of the matrices. In specimens protected with coating, the surface was cleaned with a wire brush and etched with a solution comprised of two parts water and one part phosphoric acid. Any excess solution was rinsed off and the prisms were allowed to dry. This preparation was needed to create a rough surface. Note that specimens prepared in the laboratory have a very smooth surface. The concrete surfaces in the field are much rougher because of their large surfaces, form surfaces, and carbonation. This is true even if steel forms are used.

The components of the chosen matrix were then mixed in a high shear mixer for three minutes. An initial thin layer of the matrix was applied to the surface of the prism using a trowel. This was done to fill any voids in the surface of the concrete and to ensure adequate bonding between the specimen and the matrix. A second layer of the

matrix was then applied to the specimen to achieve an approximate thickness of 1 mm. The coated specimens were cured at room conditions for 28 days.

Samples that were used in strengthening applications were prepared using a more stringent procedure. This procedure is similar to the procedure used in the field (ACI Committee 515). This involves sand blasting and cleaning with a wire brush. Sand blasting was performed using silica quartz sand at a pressure of 80 psi. Once the surface was cleaned, a thin layer of the inorganic matrix was applied to fill the small air voids and to create a smooth surface. Pre-cut carbon tows and sheets were impregnated with the matrix and placed on the prepared concrete surface and bonded using grooved rollers. A second layer of the matrix was applied as a protective coating. The samples were cured for at 24 hours at room temperature followed by 24 hours at 80°C. The elevated temperature was used to ensure adequate curing in a two day period. Base on the heat energy required, one day curing at 80°C is equivalent to about one week curing at room temperature (Foden etal. 1996A). The accelerated curing was used to save time.

3.2.4 Test Procedure

The two major steps involved in testing were : exposure to wetting and drying and evaluation of the exposed samples. A special set-up was built for exposing the samples to wetting and drying. A computer data acquisition system was used to measure the natural frequency. The samples with strengthening systems were tested under flexure using a third point loading. The following sections provide the pertinent details.

Wet-Dry Chamber

A special set-up was built for exposing the samples to wetting and drying. A 53 X 27 X 6in. stainless steel basin containing the specimens was elevated to a height of four feet. A reservoir containing twenty-five gallons of a 3% saline solution was installed beneath the basin, Fig. 3.1. In an attempt to more closely duplicate marine environments, a commercial product named Instant Ocean was used to prepare the 3% saline solution. A heater and a temperature gage were attached to the salt water reservoir to ensure that the water remained at a constant temperature of 100^{o} F. Elevated temperature was used to further accelerate the deterioration process. The salt water was transported from the reservoir to the basin containing the samples by a pump installed outside the reservoir. A timing valve attached to the drain of the basin controlled the flow of water back into the reservoir. An 18 inch fan was installed two feet above the basin to help circulate air during dry cycles.

After the test specimens were placed in the stainless steel basin, the timers were set to allow for a three hour wet and three hour dry cycle. At the beginning of each wet cycle, the pump filled the basin to a level that totally submerged the samples with salt water from the reservoir. After three hours, the basin's drain valve opened allowing water from the basin to drain back into the reservoir and the fan began to circulate air above the basin. At the conclusion of the three hour dry cycle, the wet portion of the next cycle began. Visual inspection confirmed the complete drying of the samples.

Determination of Natural Frequency and Dynamic Modulus

ASTM C666 Procedure A (American Society for Testing and Materials, 1993) was used as a guideline for estimating the dynamic modulus of the concrete specimens

exposed to wet-dry cycles. The dynamic modulus of elasticity for a concrete prism, E, is computed using the equation:

$$E=Dw(n')^2 \qquad (3.1)$$

where E is the dynamic modulus of elasticity of the sample in psi, w is the weight of the specimen in pounds, n is the natural longitudinal frequency of the prism in hertz, and D is the shape factor of the tested specimen.

$$D=0.01035(L/bt) \qquad (3.2)$$

where L is the length, b is the width and t is the thickness of the specimen in inches as shown in Figure 3.2.

The natural frequency was obtained using an accelerometer in conjunction with the National Instruments data acquisition software Labview. A schematic of the test set-up is shown in Figure 3.3.

The specimen was supported using a single support at mid-span and the accelerometer was mounted at the center of one end of the specimen. An impact load was then applied at the midpoint of the free end of the prism using an impulse hammer. Voltage output of the accelerometer corresponding to the wave propagation in the prism was recorded by the Labview software. The power spectrum of the signal was then obtained by performing a Fast Fourier Transform on the recorded signal. The number of sampling points was set at 2048. The spectrum was then smoothed and the fundamental frequency was recognized as the highest peak in the spectrum. An average of ten frequency readings was taken as the specimen's fundamental frequency in an attempt to minimize any error in the calculation of dynamic modulus.

Flexure Test

Samples strengthened with carbon reinforcement were tested in flexure using a three point bending test, Fig. 3.4. The load was applied using an MTS testing machine with a 10,000 lb. capacity. The mid-span deflection was measured using an LVDT. Both load and deflection were recorded by a computer.

3.2.5 Frequency of Testing

The samples with protective coating were tested after about 10 cycles of exposure. The testing continued until 200 cycles had been completed. The samples treated with the strengthening systems were exposed to a full series of either 50 or 100 wet-dry cycles before they were removed from the wet-dry machine. These samples were tested in flexure. The non-destructive test method could not be used for these samples because the degradation of the composite or the interface could not be identified by this method.

3.3 Test Results and Discussion: Coatings

The data obtained from the durability testing of barrier coating samples under wet-dry conditions are presented in Figures 3.5-3.36. The dynamic modulus values presented were calculated using the evaluation method described in section 3.2.4 of this report. The Relative Dynamic Modulus, (RDM), was calculated using the equation

$$RDM = (n_n/n_0)^2 \text{ X } 100 \qquad (3.3)$$

where n_n is the specimen's fundamental frequency after n cycles of wet-dry and n_0 is the samples initial fundamental frequency.

Figures 3.5-3.8 present the results for the control specimens exposed to wet-dry conditions. Both high strength samples were able to survive the entire 200 cycle testing sequence and maintain over 99% of their initial dynamic modulus. In the low strength samples, the testing of one sample was concluded midway through the test cycle after a significant drop in strength was observed.

The results obtained from the dynamic modulus testing of samples coated with the polymer modified cement system are shown in Figures 3.9-3.16. High and low strength samples totally coated and having only three sides coated are included in these figures. Positive results were observed for both concrete mixes and coating application types. Strength of the specimens was maintained and the bond between the coating and the parent concrete remained strong.

The performance of the samples coated with the silicafume formulations is shown in Figures 3.17-3.34. All specimens maintained a high percentage of their initial strength for the entire 200 cycles of wet-dry exposure. Each of the silicafume formulations was observed to maintain it's bond with the concrete interface despite the wet-dry exposure.

The organic coating protected the parent concrete samples as well as the polymer modified cement system or the inorganic coating. As seen in Figures 3.35 and 3.36, although only three sides of the samples were protected with the coating, over 99% of the initial dynamic modulus was maintained after 200 cycles of wet-dry exposure. The coating penetrated the surface of the samples so wet-dry exposure did not weaken the bond to the parent concrete specimen.

The samples coated on all sides were exposed to 200 cycles of wetting and drying. Samples with coating on three sides were exposed to only 100 cycles. The

testing was stopped after 100 cycles because there was no sign of deterioration. None of the samples with coating showed any signs of deterioration leading to the following major conclusion.

All of the coating materials, namely; polymer modified cement, three formulations of inorganic matrix, and low molecule methyl methacrylate are durable under wet-dry conditions. The interface between the parent concrete and the coating is also durable. Visual examination of the exposed samples confirmed that the coatings were in excellent condition.

One of the control specimens showed some signs of deterioration after about 100 cycles of wet-dry exposure, Fig 3.7. The low strength concrete is significantly weaker than the high strength mix and is more susceptible to the damaging effects of the wet-dry exposure.

The results were consistent except for one case with the polymer modified cementitious system. The author believes that a change in natural frequency occurred due to accidental cracking of the specimen, Fig.3.11.

3.4 Test Results and Discussion: Strength Tests

As mentioned earlier, the test samples consisted of the following.

- Two control samples
- Two samples strengthened with both 2 and 4 percent discrete carbon fibers
- Two samples strengthened with one, two, and three carbon tows
- Two samples strengthened with one and two layers of carbon

For each variable, two specimens were tested at 0, 50, and 100 cycles of exposure. The objective was to determine whether discrete fibers would add strength and toughness to plain concrete and whether it is possible to add continuous reinforcement to plain concrete. In both cases, the wet-dry cycling provided the information on durability. Note that carbon fibers do not corrode and therefore the failure can occur because of the deterioration of the matrix or the interface.

The response variables were maximum strength, flexural stiffness, and toughness. All of these parameters were obtained from the load deflection response presented in Figures 3.37, 3.41, and 3.45. The strengths of the strengthened samples were compared to the control sample, Figures 3.38, 3.42, and 3.46.

Equivalent flexural stiffness, EI, was computed using the equation:

$$EI = Pl^3 / 48\delta \qquad (3.7)$$

Equation 3.7 was derived from the classical equation for the deflection of a simply supported beam under a center-point load.

$$\delta = Pl^3 / 48EI \qquad (3.8)$$

where EI is the flexural stiffness in lb-in^2, P is the peak load of the specimen in pounds, l is the length of the specimen in inches, and δ is the deflection at peak load in inches. The toughness was calculated as the area under the load-displacement curve. All of the data collected from the flexural testing of the samples is included in Table 3.1.

The load-displacement diagrams for the parent samples and the samples strengthened with two and four percent discrete carbon fibers are shown in Figures 3.37. As expected, each of the sample's behavior was linearly elastic up to peak load, followed by brittle failure. The post-peak curve could be obtained if special loading methods such

as crack mouth opening displacement controls were used. Since the focus of the current research is on strength increase, special test methods were not used to capture the post-peak response. The addition of discrete fibers did not improve the post-peak behavior. This confirms the results obtained using natural frequency presented in section 3.3. Additionally, exposure to wet-dry conditions did not change the behavior.

The results obtained from the control samples and those reinforced with two and four percent discrete carbon fibers are tabulated in Table 3.1. A comparison in the failure loads is made in Figure 3.38. The failure loads are presented as a factor of the failure load of the unexposed control sample. Flexural strength of the control samples was improved by exposure to wet/dry conditions. After 100 cycles of wet/dry, the failure load of the control samples had increased by approximately 50 percent. Exposure to wet/dry conditions had little if any effect on the samples reinforced with two and four percent discrete carbon fibers. In each case, the failure load after 50 cycles of exposure was identical to that of the unexposed sample and a slight decrease was observed after 100 cycles of wet/dry.

Figure 3.39 shows the effect of wet/dry exposure on the toughness factor of the samples. After 50 cycles of exposure, the toughness of the control samples had decreased by about 25% but had risen above their initial value after 100 cycles of exposure. The values for samples strengthened with discrete carbon fibers experienced insignificant changes in toughness after exposure to wet-dry conditions. The author believes that the ductility of the samples was not affected by the wet/dry exposure because they did not exhibit any post crack strength. Variations in toughness factor are typical when testing a

nonhomogeneous material like concrete and do not indicate that exposure affected the performance of the composite system.

The effect of exposure to wet-dry conditions on the flexural stiffness of the control and samples strengthened with discrete fibers is shown in Figure 3.40. In the control samples, a significant improvement in stiffness was observed after exposure. The peak value occurred after 50 cycles. After 100 cycles of wet-dry the flexural stiffness was about 50% greater than in the unexposed control. When discrete fibers were used, only insignificant changes in flexural stiffness were observed. Minimum values were noted after exposure to 50 cycles of wet-dry.

The second type of external carbon reinforcement that was studied in this experiment was the use of carbon tows. Figure 3.41 shows the load-displacement plots obtained from the flexural testing of concrete beams reinforced with carbon tows. The silicate matrix bonds with the concrete chemically by transfer of CaOH and KOH between parent concrete and the adhesive, resulting in the absence of a well defined interlaminar layer. Therefore, when the concrete cracks, the cracks will go through the repair layer, transferring the forces to the carbon fibers. As observed in the control and chopped fiber samples, a linear pre-crack load-displacement plot was generated. The post-crack behavior was significantly improved, however, utilizing the carbon tows for reinforcement. The samples were able to sustain load after the crack had formed. The propagation of the crack through the specimen is slowed and a greater center point displacement is obtained before ultimate failure occurs.

The flexural properties obtained from the specimens reinforced with carbon tows are included in Table 3.1. One of the main advantages of the new inorganic matrices is

the ability to form a strong bond with the parent concrete sample. This is of particular importance when hazardous environments such as wet/dry conditions are present. If the bond between the carbon and the concrete specimen is significantly weakened, the ability of the specimen to sustain load after cracking of the concrete will diminish. In an attempt to verify the effectiveness of the matrix in this capacity Figures 3.42-3.44 are shown. They document the failure loads, the toughness factors, and the flexural stiffness of specimens reinforced with one, two, and three carbon tows after exposure to wet/dry conditions. Each variable is shown as a factor of the unexposed control sample.

In general, the failure loads of specimens reinforced with carbon tows increased slightly after exposure to wet/dry conditions. An increase of about 10 percent can be expected after 100 cycles of wet/dry. This indicates that the bond between the carbon and the concrete is not weakened by this exposure. The slight increase in failure loads may be attributed to strengthening of the concrete after exposure to a wet/dry environment. This was observed during testing of the control samples. The strength of the bond between the concrete and the carbon is further verified by the data shown in Figure 3.43. Variations in the toughness factor caused by the wet/dry conditions are documented here. These values indicate that the ability of the specimens to sustain the applied load after cracking of the concrete was not hindered by the exposure to wet/dry conditions. Slight decreases were observed in samples reinforced with only one tow but the change was not significant enough to conclude that wet/dry exposure negatively affects the strengthening system. Additionally, the flexural stiffness of the samples reinforced with carbon tows after wet-dry exposure is shown in Figure 3.44. In each case, the strength of the bond between the carbon and the concrete is verified by the fact

that the values after 100 cycles of exposure are higher than the initial values. The author believes that this is a result of strengthening of the concrete by the wet-dry exposure.

Carbon is commercially available in unidirectional fabric in addition to the tows that were previously discussed. The load displacement plots generated from the flexure testing of samples reinforced with one and two layers of carbon are shown in Figures 3.45. Loads were sustained after cracking of the concrete specimen just as in the case of the carbon tows. Because the area of the carbon layers was greater than that of the tows, in some cases the peak load was achieved after cracking of the sample. The load was also sustained through a greater displacement. Figures 3.46-3.48 show the effects of the wet/dry exposure on samples reinforced with unidirectional carbon fabric.

Failure loads are compared with that of the unexposed control sample in Figure 3.46. The failure loads increased or remained the same except for the sample reinforced with two carbon layers after 50 cycles of wet/dry. The author believes that this is an experimental error resulting from improper preparation of the surface of the concrete specimen. Additionally, the toughness of each of the samples increased except for the inadequately prepared sample, Figure 3.47. Softening of the samples is indicated by the insignificant decrease in flexural stiffness of the samples after 100 wet-dry cycles, Figure 3.48. It can be concluded that the strengthening system utilizing layered carbon was not significantly weakened by exposure to wet/dry conditions.

Improved strength and durability are the desired results of the application of a strengthening system to a concrete element. They are most accurately measured by the failure loads, toughness factors, and flexural stiffness obtained from the flexure testing of the samples. The failure load represents the strength of the sample because it allows for

an estimation of how much load can be safely supported. Toughness factor indicates ductility of the specimens because it gives an indication of the displacement through which load can be supported. The ability to resist deformation while supporting the externally applied load is represented by the flexural stiffness.

Figure 3.49 shows the failure load of each of the strengthened samples as compared to the control. Each of the reinforcement types increased the flexural strength of the samples. The failure load of the specimen increased with an increase in carbon area in all but one case. Strength improvement from one carbon tow was greater than when two carbon tows were used. Strength increases range from 55 percent when a coating consisting of 2% chopped carbon fiber was used up to almost 100 percent when two layers of carbon were used. The durability of the samples was affected in a similar manner as seen in Figure 3.50. The toughness factor of the sample strengthened with 2 layers of carbon is nearly 500 percent greater than the control. The flexural stiffness of samples reinforced with the carbon composite systems was greater than the control samples, Figure 3.51. Samples reinforced with one and two layers of carbon had stiffness values 70 and 80 percent greater than control, respectively.

3.5 Summary

In this chapter, protective coatings and a strengthening system comprised of an inorganic matrix and carbon reinforcement were exposed to wet-dry conditions. The protective coatings were intended to help concrete elements maintain their strength by preventing the ingress of water. Dynamic modulii were measured throughout the series of wet-dry cycles. In both control and coated samples, the variation in strength was

negligible. Additionally, the coatings themselves were observed to be quite durable. At the conclusion of the wet-dry exposure, no cracking or spalling of the coatings was evident.

The strength and ductility of the concrete samples could be increased by the application of the carbon composite system. Peak load and toughness factor values increased as the area of the carbon reinforcement was increased. Effectiveness of the strengthening system was not diminished by exposure to wet-dry conditions. In many cases, flexural properties of the strengthened samples were enhanced by wet-dry exposure. An analytical method to predict the strengths is presented in Chapter 8.

Table 3.1

Summary of flexural test results obtained using specimens exposed to wet-dry cycles.

Designation	No. of Wet/Dry Cycles	Peak Load, lb.	Modulus of rupture, PSI	Deflection at peak load in.	Flexural stiffness, lb-in^2	Toughness in-lb.
C,00	None	506.47	1139.56	.0162	1.22 X 10^6	6.38
C,50	50	719.7	1619.32	.0124	2.13 X 10^6	5.29
C,100	100	805.11	1811.49	.0158	1.86 X 10^6	6.65
F2,00	None	785.62	1767.65	.0198	1.43 X 10^6	8.35
F2,50	50	784.19	1764.43	.0216	1.34 X 10^6	9.22
F2,100	100	755.7	1700.33	.021	1.2 X 10^6	8.86
F4,00	None	876.71	1972.59	.018	1.76 X 10^6	8.79
F4,50	50	894.74	2013.17	.0205	1.57 X 10^6	9.64
F4,100	100	889.23	2000.77	.0183	1.79 X 10^6	9.27
T1,00	None	897.21	2018.72	.0283	1.23 X 10^6	18.63
T1,50	50	852.39	1917.87	.0148	2.12 X 10^6	13.91
T1,100	100	903.05	2031.85	.0195	1.79 X 10^6	14.16
T2,00	None	732.73	1648.65	.0175	1.61 X 10^6	24.7
T2,50	50	943.23	2122.27	.0207	1.75 X 10^6	27.39
T2,100	100	850.08	1912.68	.0202	1.59 X 10^6	24.31
T3,00	None	934.05	2101.61	.0282	1.55 X 10^6	36.99
T3,50	50	1024.55	2305.24	.0269	2 X 10^6	34.54
T3,100	100	1025.65	2307.7	.0295	1.41 X 10^6	37.89
L1,00	None	962.68	2166.71	.0197	2.08 X 10^6	30.65
L1,50	50	1086.75	2445.19	.0228	1.83 X 10^6	39.91
L1,100	100	923.86	2078.69	.0227	1.86 X 10^6	40.94
L2,00	None	1058.01	2380.52	.0212	2.31 X 10^6	37.37
L2,50	50	845.09	1901.45	.0334	1.26 X 10^6	25.64
L2,100	100	1271.5	2860.87	.0346	2.05 X 10^6	41.77

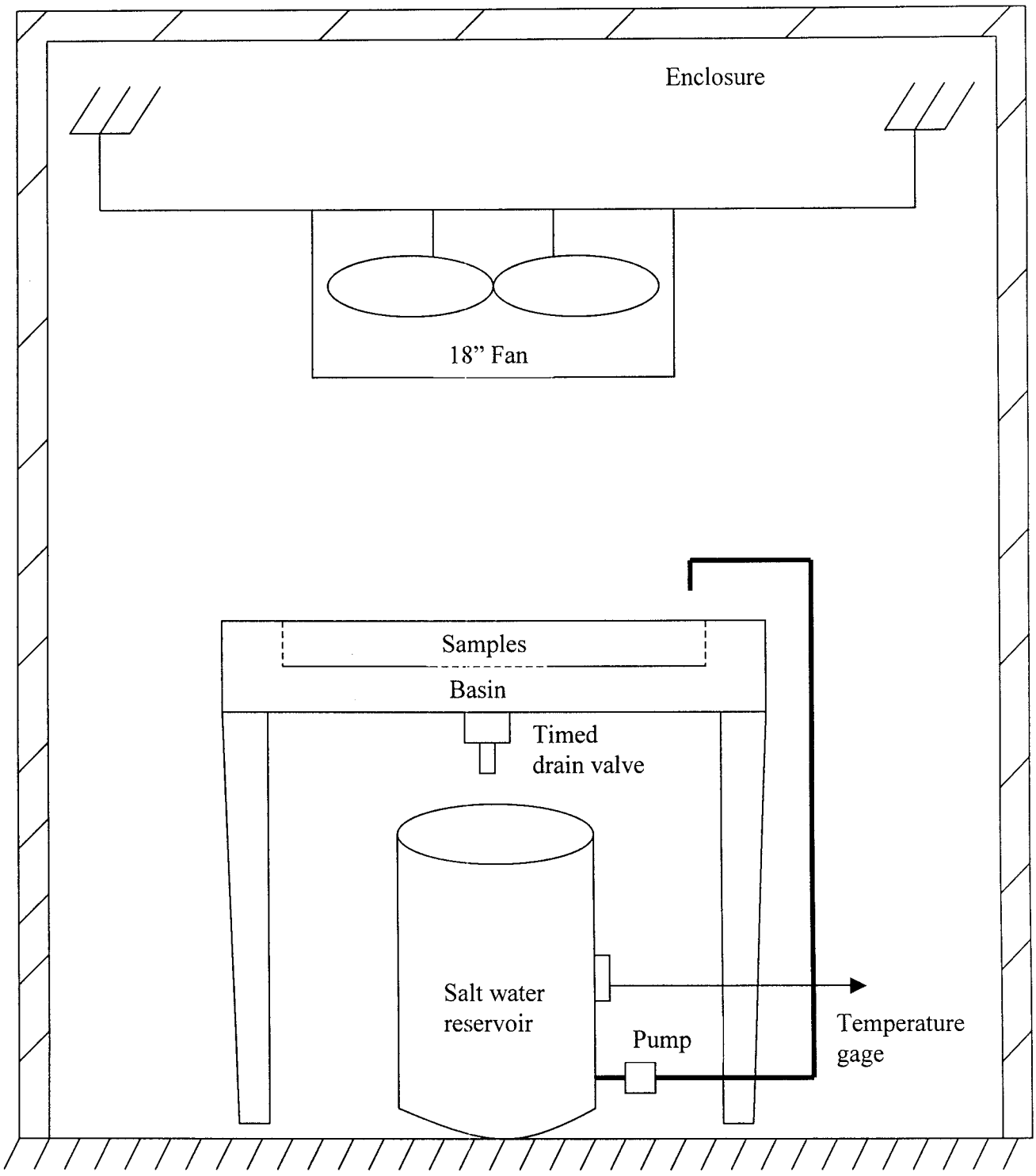

Fig. 3.1. Schematic of wet-dry machine

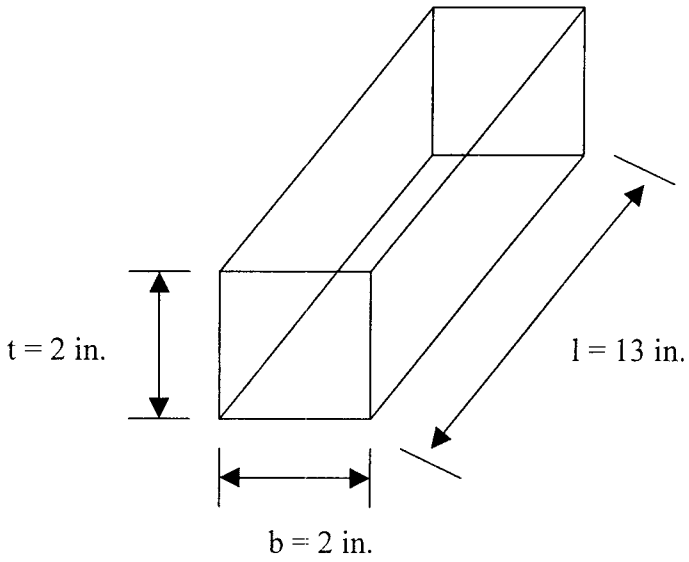

Fig. 3.2. Specimen dimensions for the computation of dynamic modulus

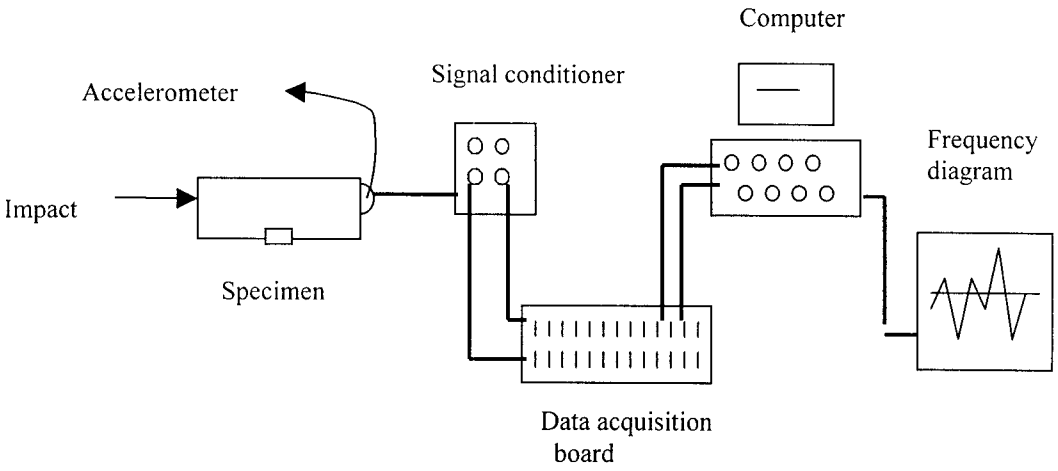

Fig. 3.3. Schematic of dynamic modulus test set-up

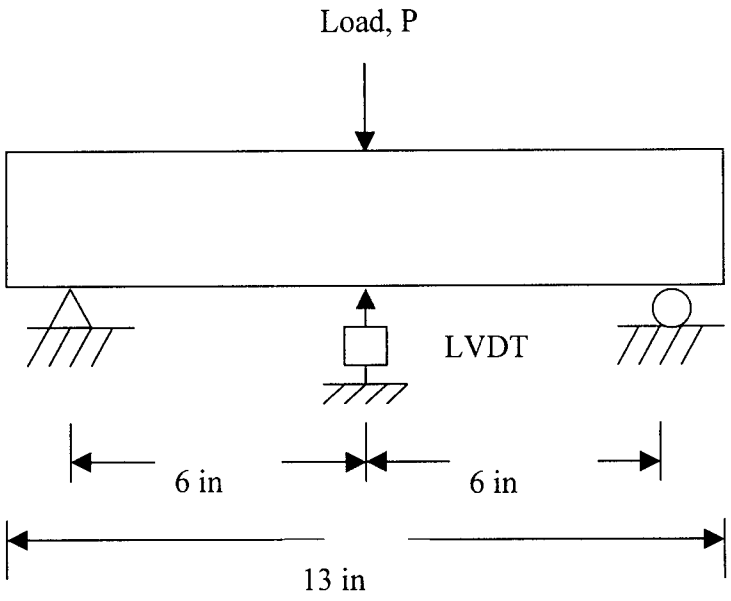

Fig. 3.4. Schematic of flexure test set-up

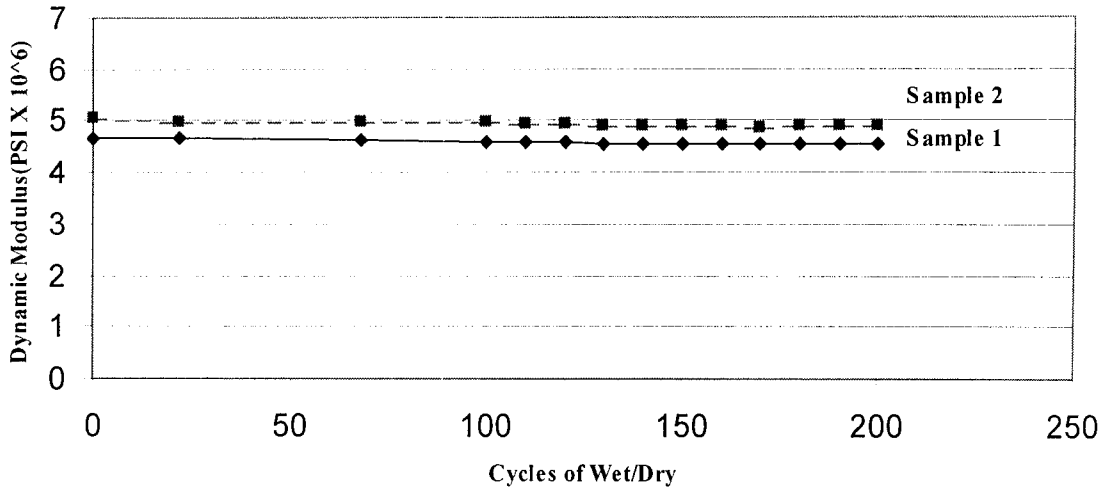

Fig. 3.5. Dynamic modulus vs. number of wet-dry cycles, control, high strength concrete

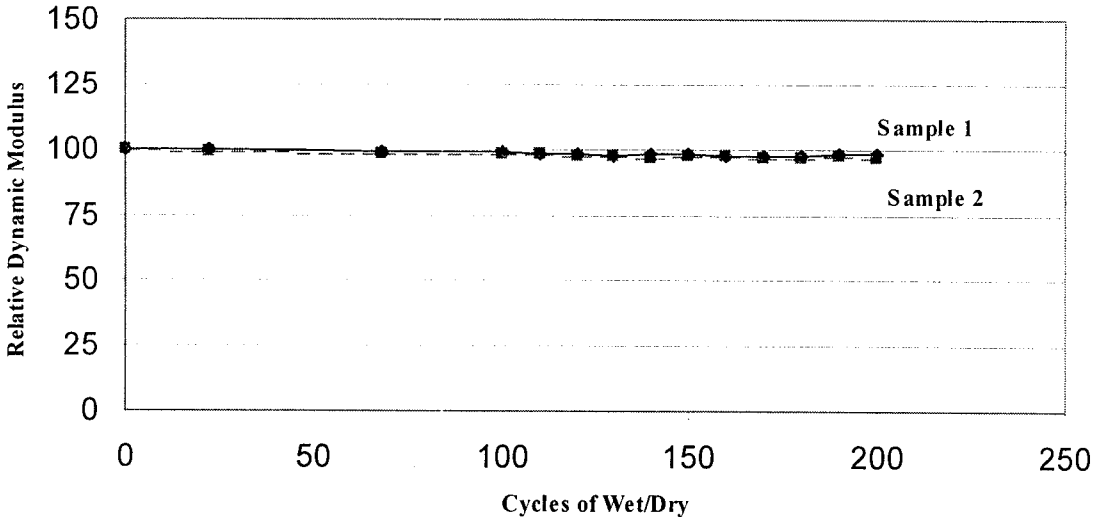

Fig. 3.6. Relative dynamic modulus vs. number of wet-dry cycles, control, high strength concrete

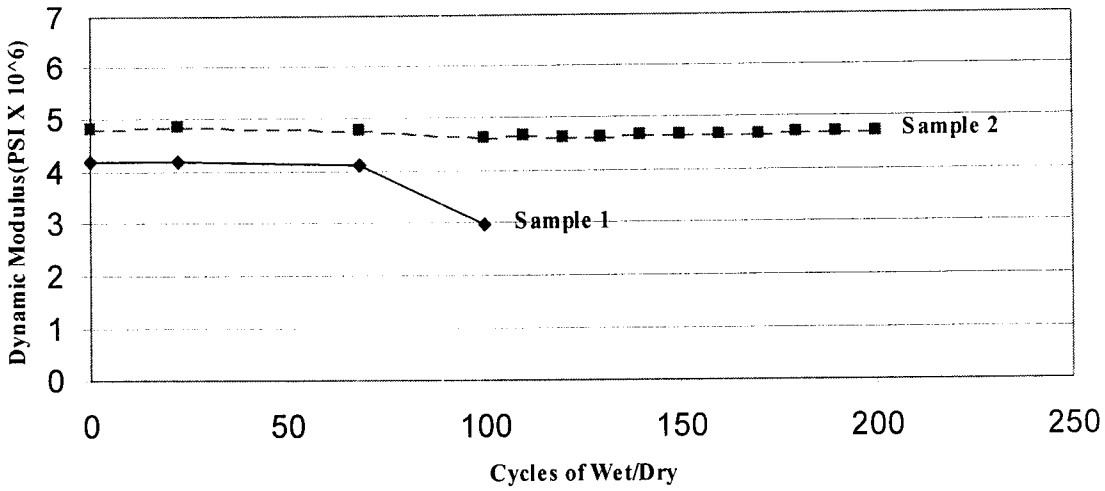

Fig. 3.7 Dynamic modulus vs. number of wet-dry cycles, control, low strength concrete

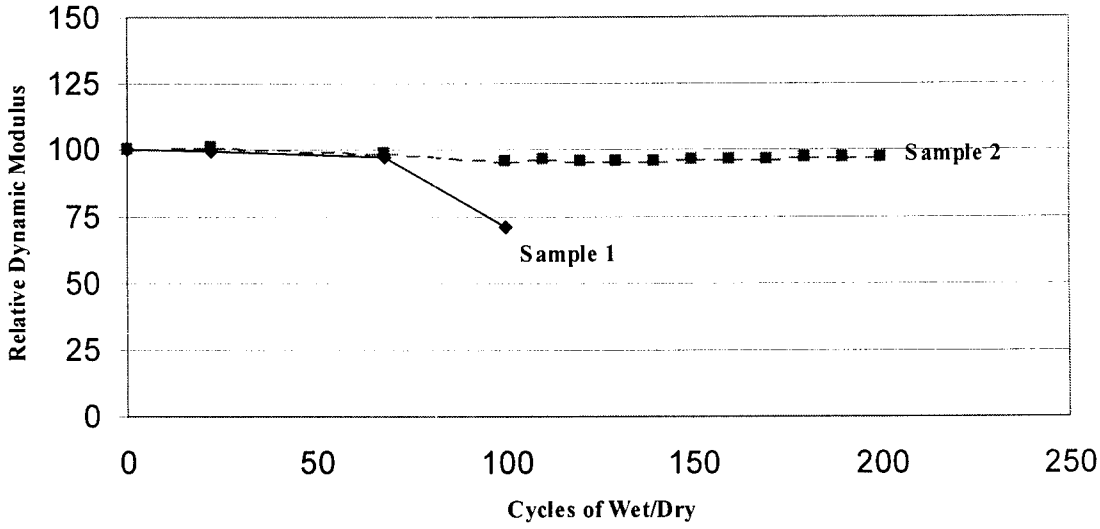

Fig. 3.8. Relative dynamic modulus vs. number of wet-dry cycles, control, low strength concrete

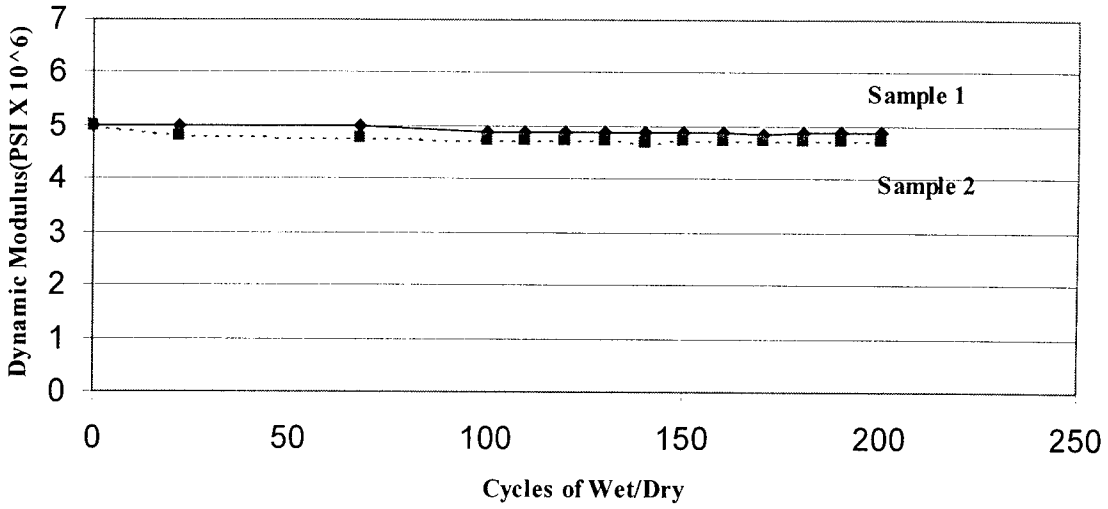

Fig. 3.9. Dynamic modulus vs. number of wet-dry cycles, Five Star, high strength concrete, all sides coated

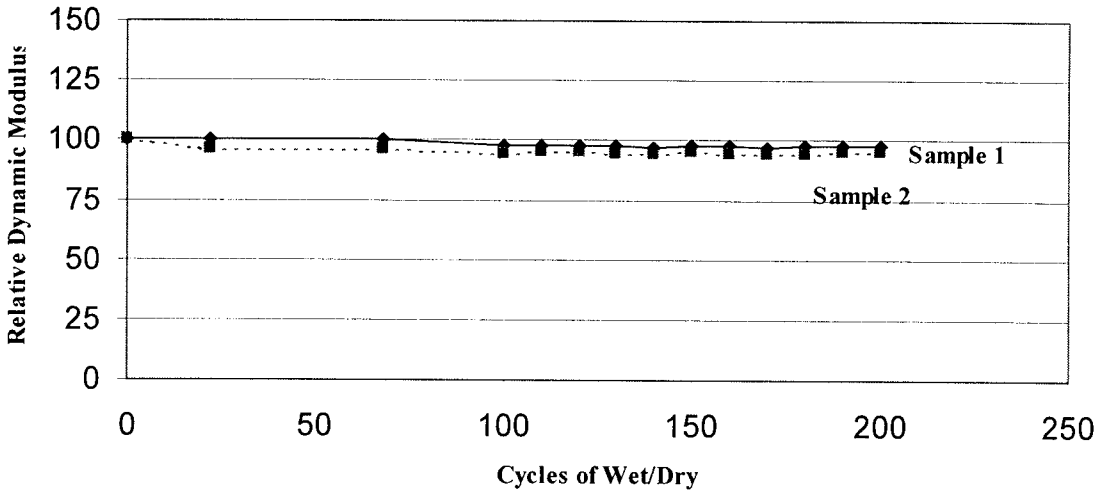

Fig. 3.10. Relative dynamic modulus vs. number of wet-dry cycles, Five Star, high strength concrete, all sides coated

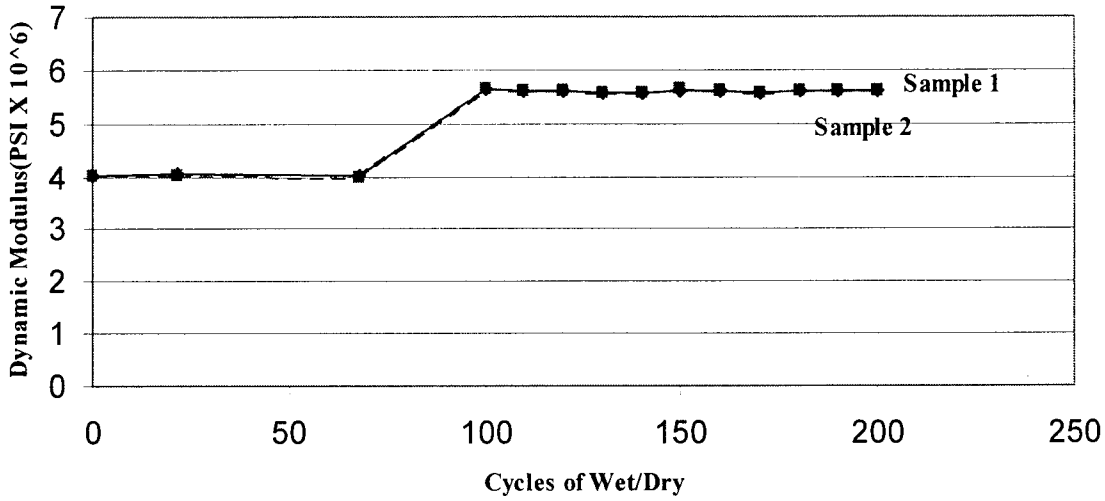

Fig. 3.11. Dynamic modulus vs. number of wet-dry cycles, Five Star, low strength concrete, all sides coated

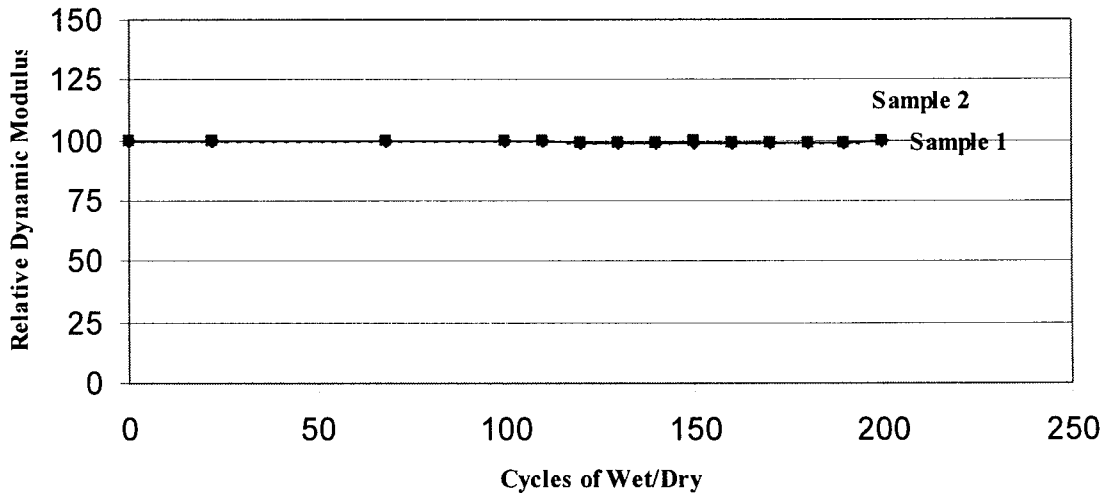

Fig. 3.12. Relative dynamic modulus vs. number of wet-dry cycles, Five Star, low strength concrete, all sides coated

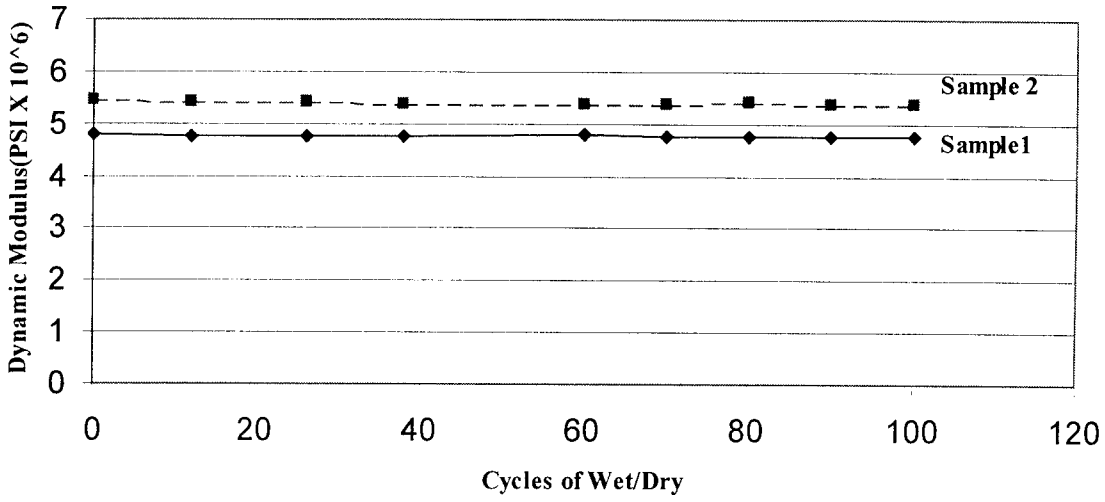

Fig. 3.13. Dynamic modulus vs. number of wet-dry cycles, Five Star, high strength concrete, three sides coated

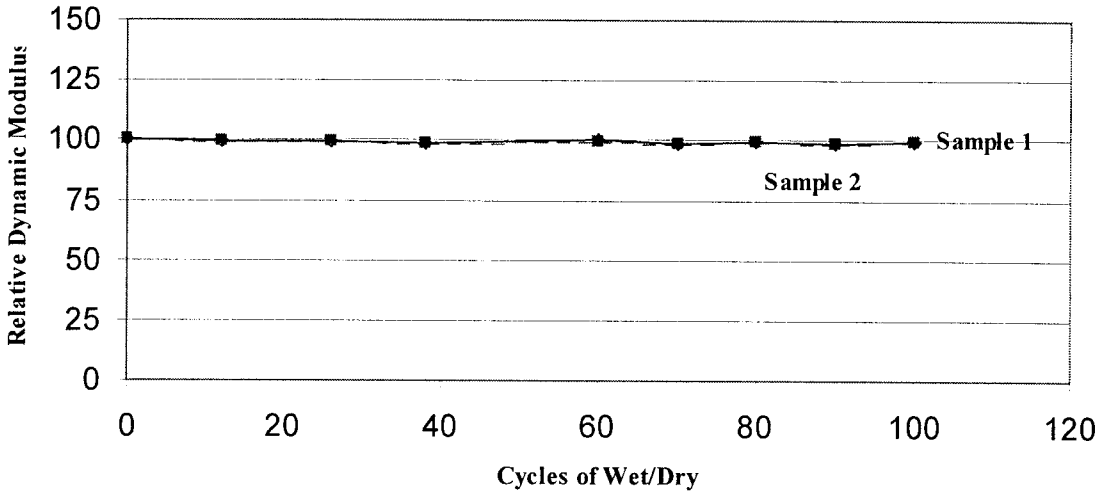

Fig. 3.14. Relative dynamic modulus vs. number of wet-dry cycles, Five Star, high strength concrete, three sides coated

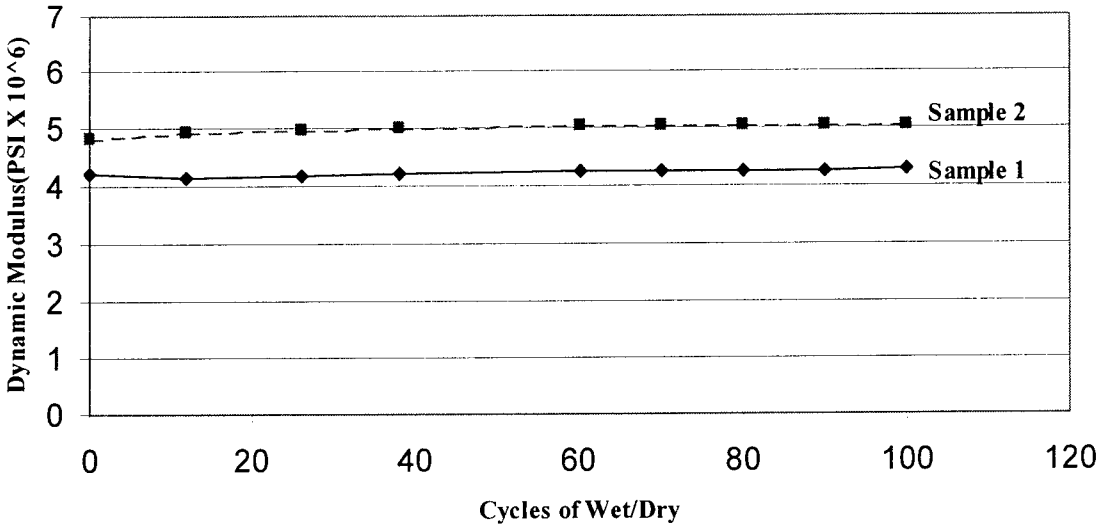

Fig. 3.15. Dynamic modulus vs. number of wet-dry cycles, Five Star, low strength concrete, three sides coated

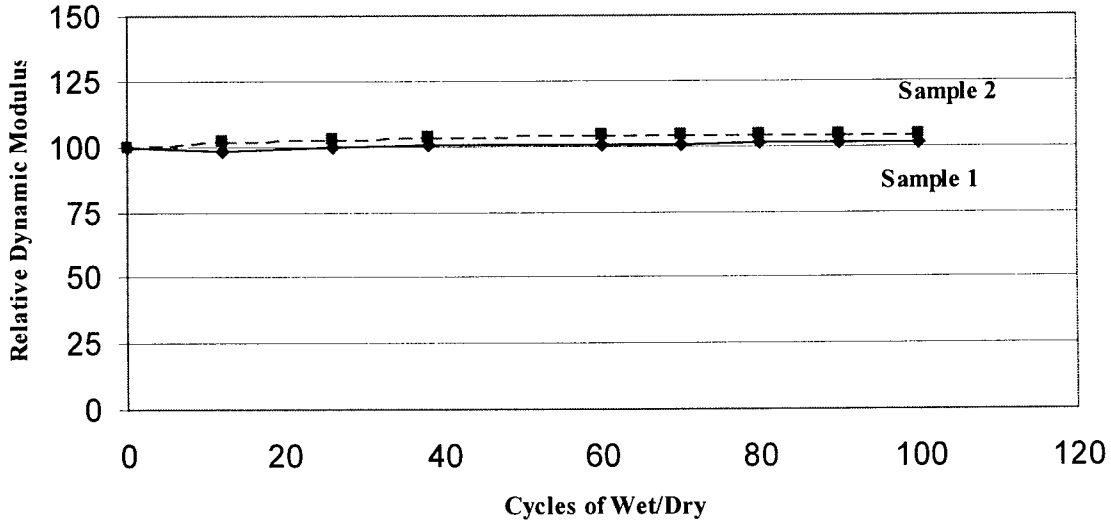

Fig. 3.16. Relative dynamic modulus vs. number of wet-dry cycles, Five Star, low strength concrete, three sides coated

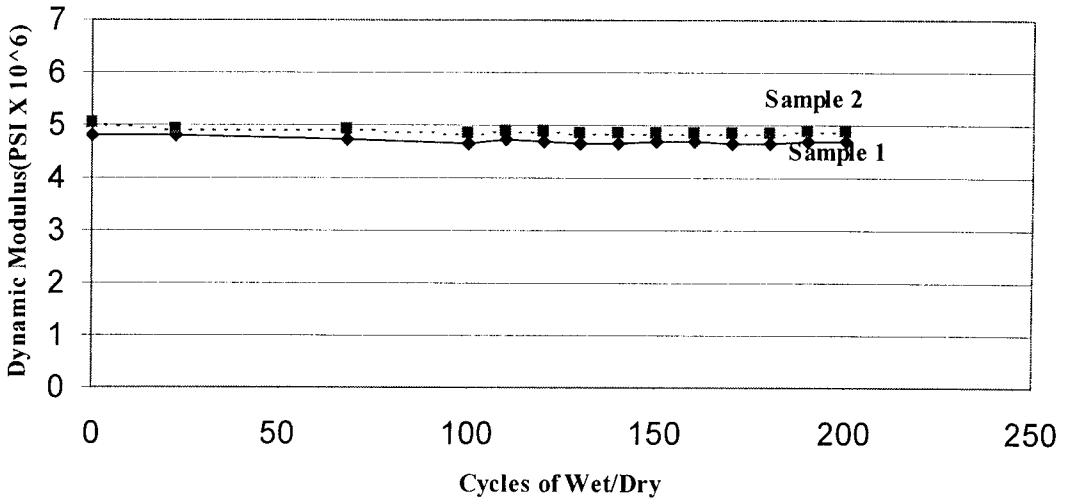

Fig. 3.17. Dynamic modulus vs. number of wet-dry cycles, silicafume1, high strength concrete, all sides coated

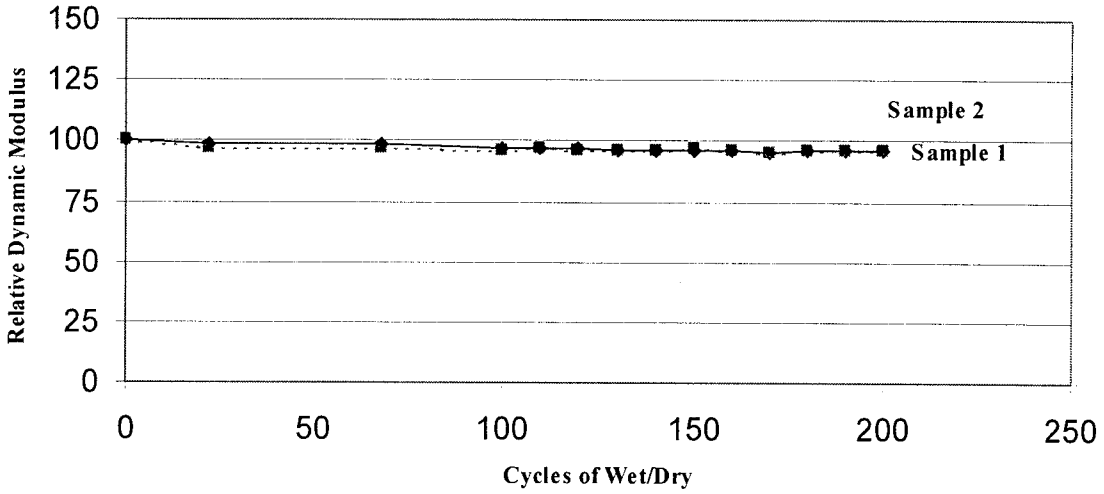

Fig. 3.18. Relative dynamic modulus vs. number of wet-dry cycles, silicafume1, high strength concrete, all sides coated

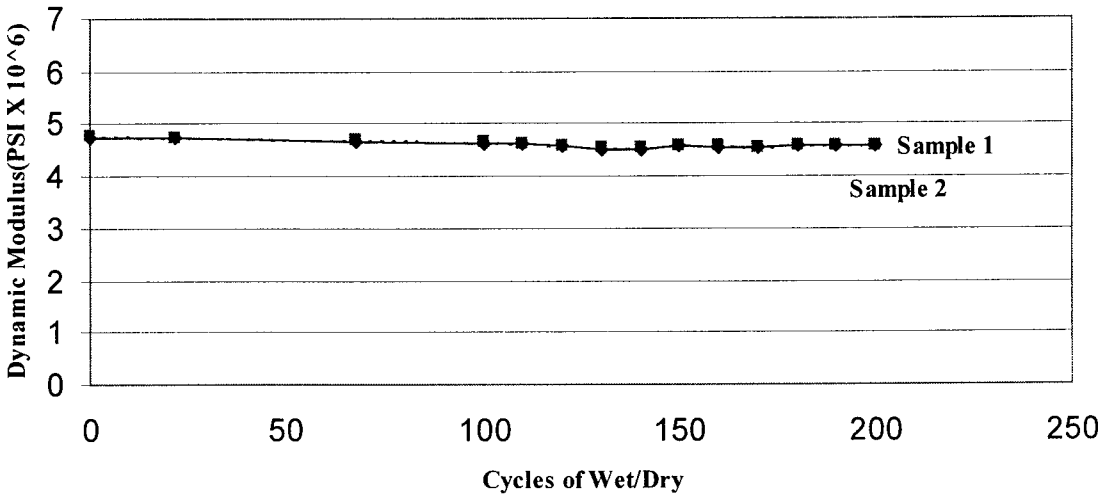

Fig. 3.19. Dynamic modulus vs. number of wet-dry cycles, silicafume1, low strength concrete, all sides coated

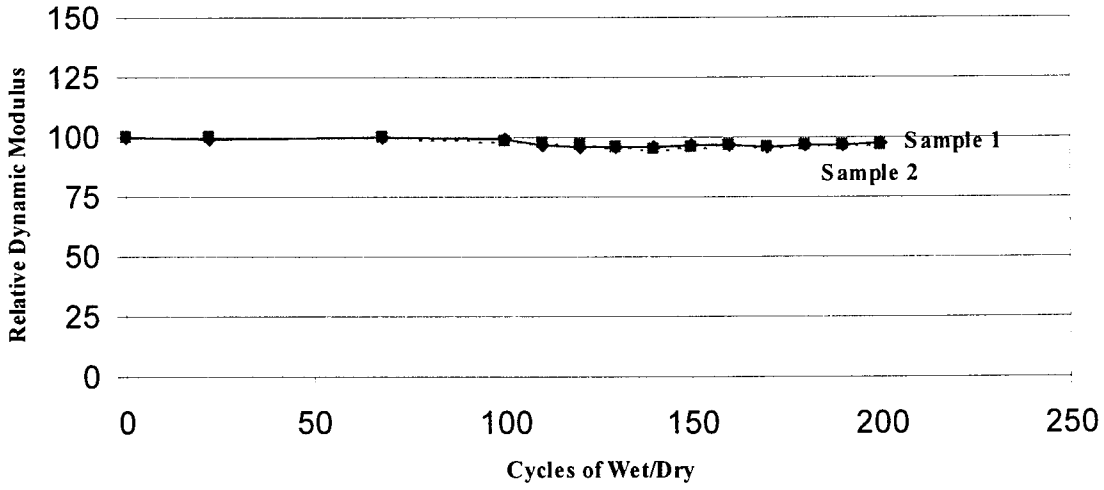

Fig. 3.20. Relative dynamic modulus vs. number of wet-dry cycles, silicafume1, low strength concrete, all sides coated

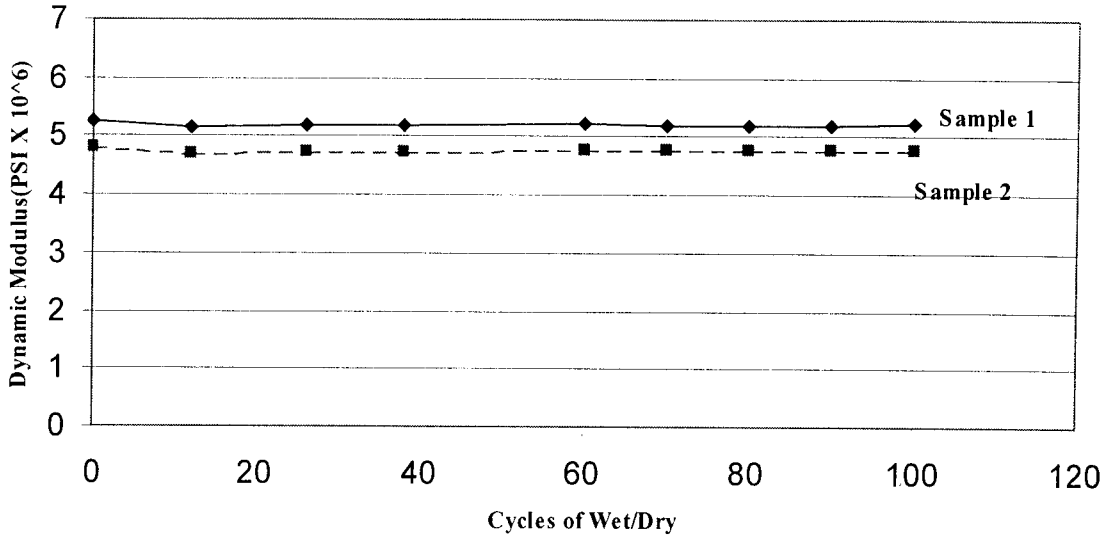

Fig. 3.21. Dynamic modulus vs. number of wet-dry cycles, silicafume1, high strength concrete, three sides coated

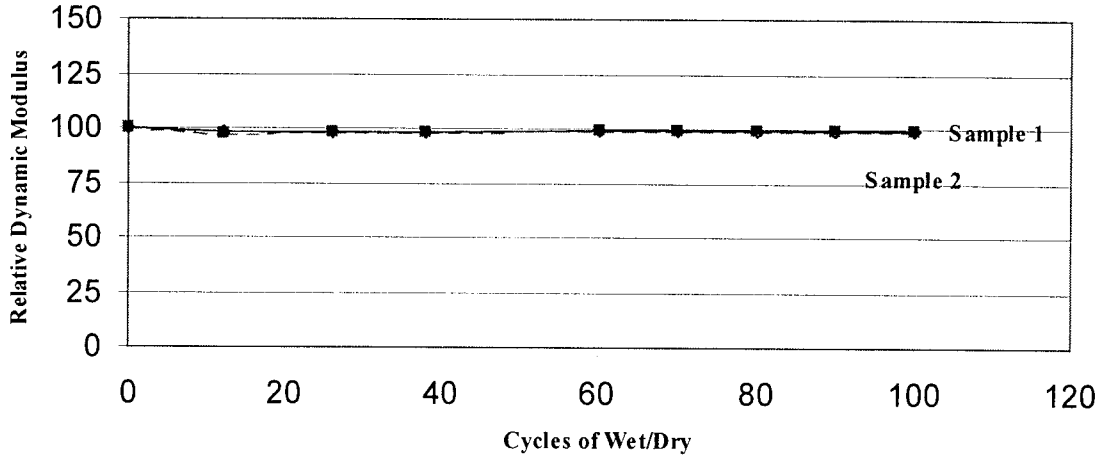

Fig. 3.22. Relative dynamic modulus vs. number of wet-dry cycles, silicafume1, high strength concrete, three sides coated

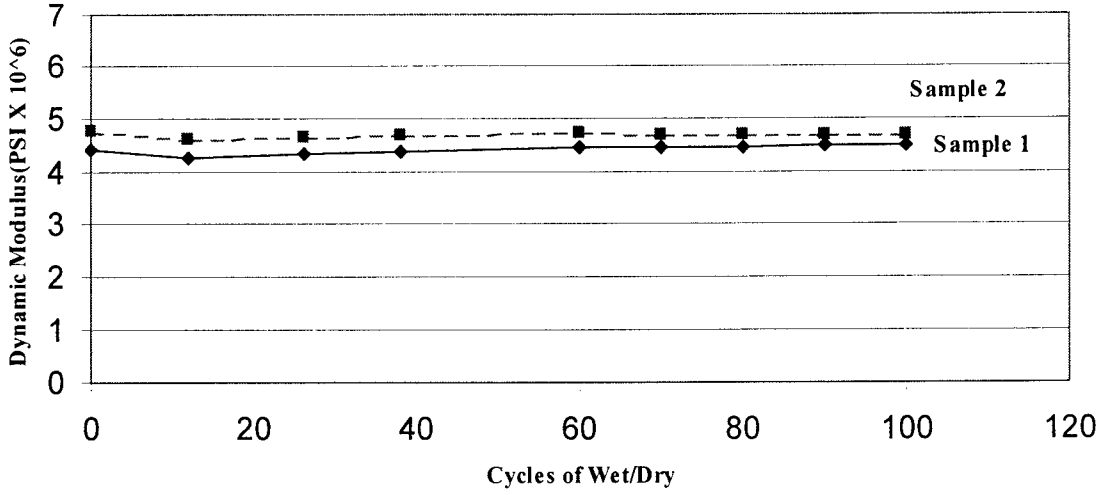

Fig. 3.23. Dynamic modulus vs. number of wet-dry cycles, silicafume1, low strength concrete, three sides coated

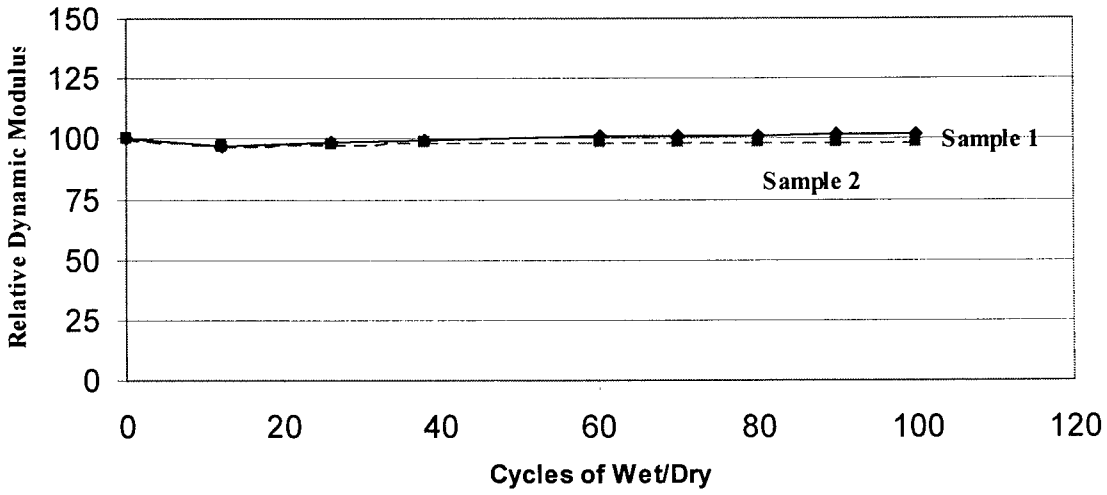

Fig. 3.24. Relative dynamic modulus vs. cycles of wet-dry, silicafume1, low strength concrete, three sides coated

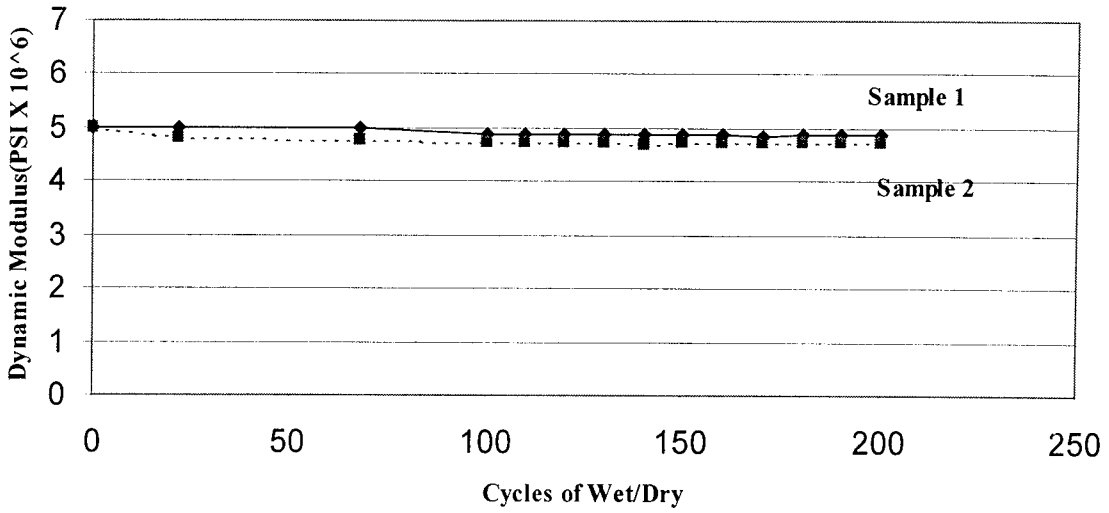

Fig. 3.25. Dynamic modulus vs. number of wet-dry cycles, silicafume2, high strength concrete, all sides coated

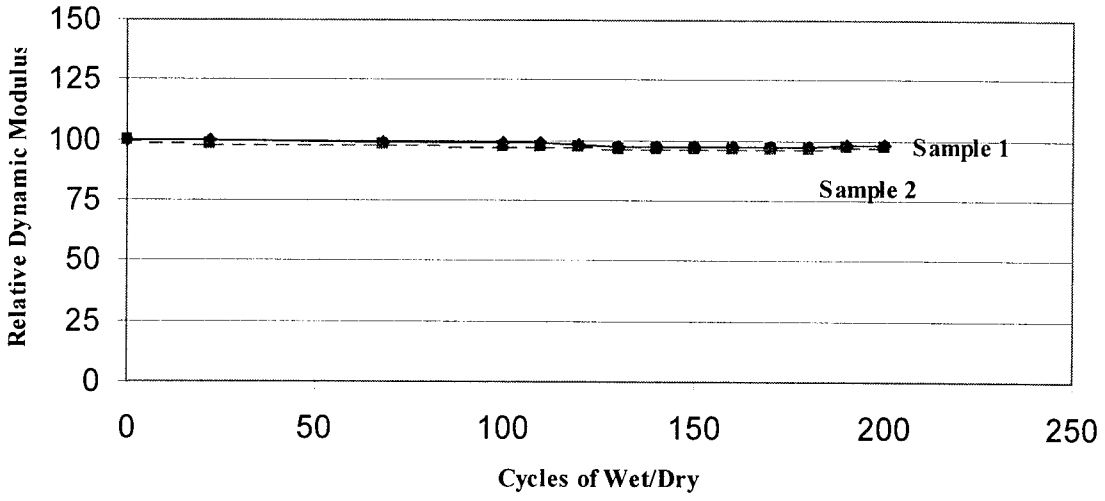

Fig. 3.26. Relative dynamic modulus vs. number of wet-dry cycles, silicafume2, high strength concrete, all sides coated

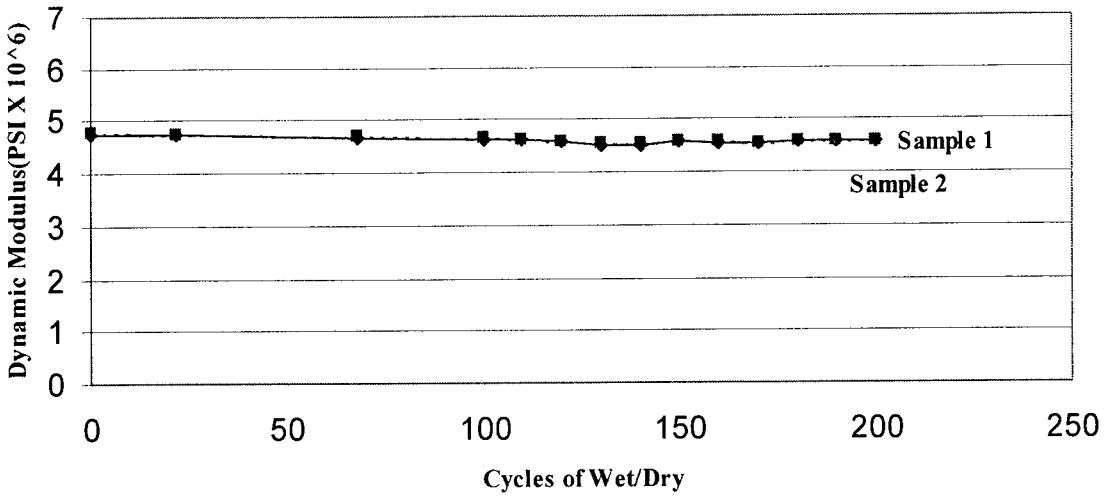

Fig. 3.27. Dynamic modulus vs. number of wet-dry cycles, silicafume2, low strength concrete, all sides coated

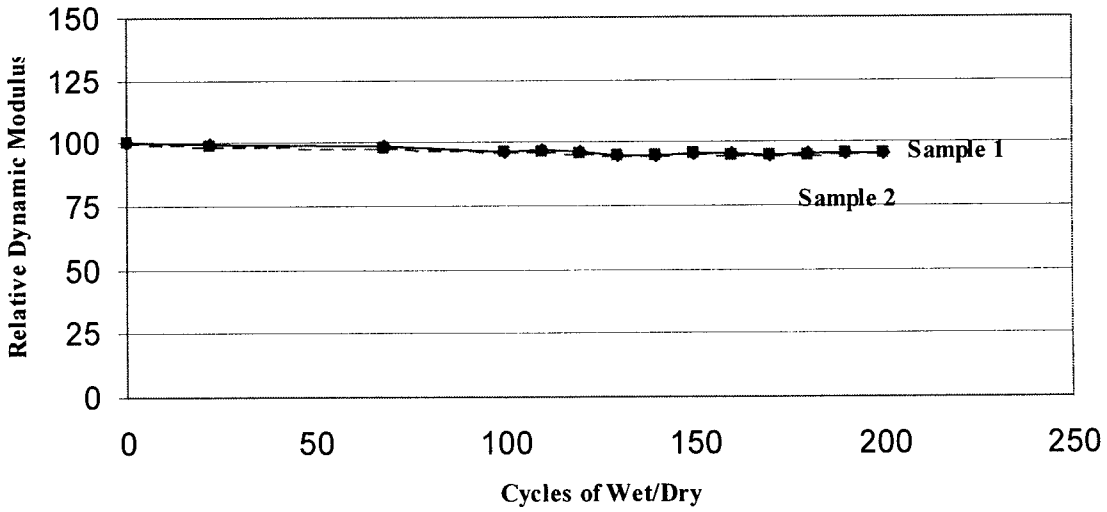

Fig. 3.28. Relative dynamic modulus vs. number of wet-dry cycles, silicafume2, low strength concrete, all sides coated

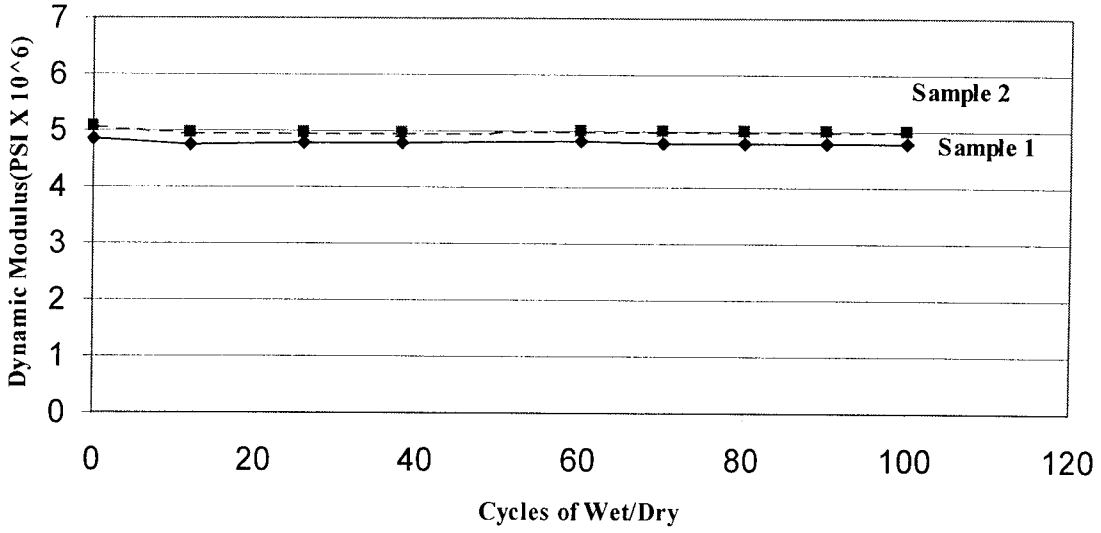

Fig. 3.29. Dynamic modulus vs. number of wet-dry cycles, silicafume2, high strength concrete, three sides coated

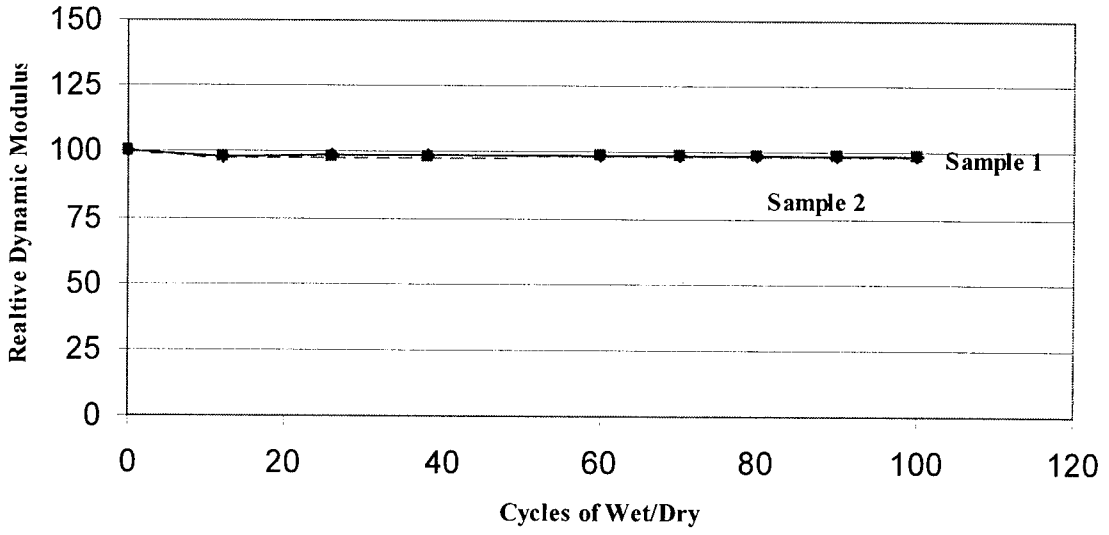

Fig. 3.30. Relative dynamic modulus vs. number of wet-dry cycles, silicafume2, high strength concrete, three sides coated

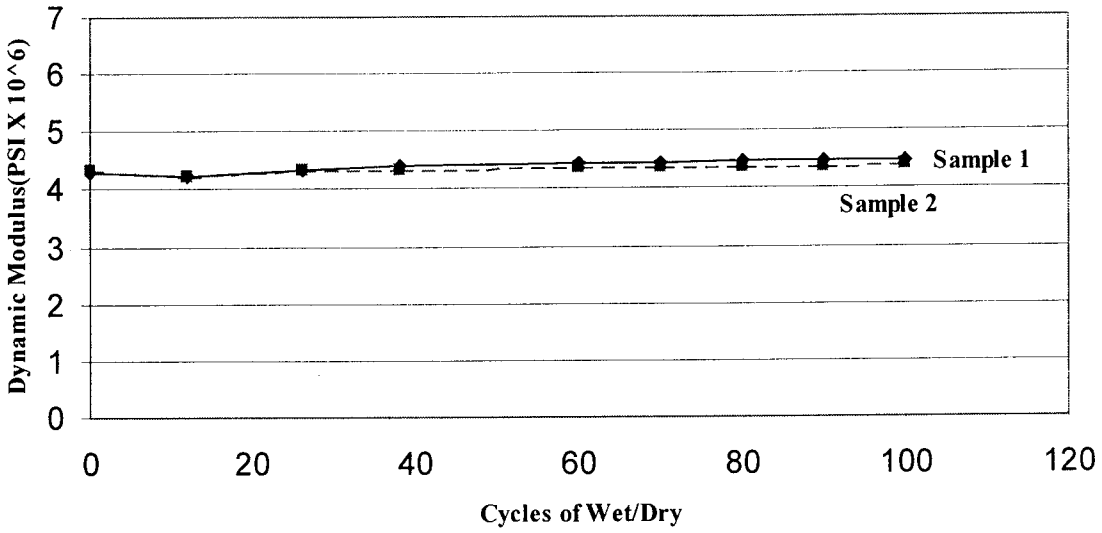

Fig. 3.31. Dynamic modulus vs. number of wet-dry cycles, silicafume2, low strength concrete, three sides coated

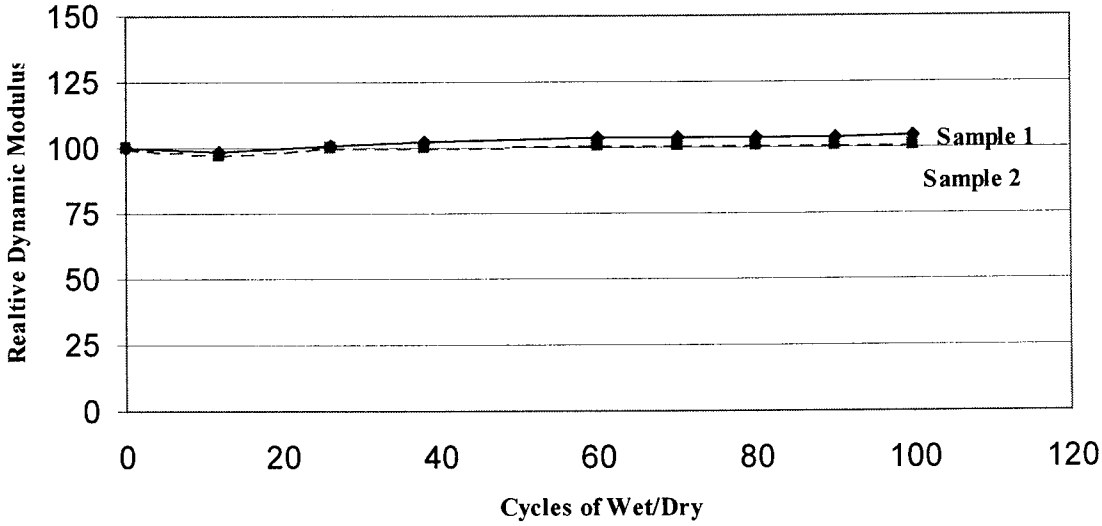

Fig. 3.32. Realtive dynamic modulus vs. number of wet-dry cycles, silicafume2, low strength concrete, three sides coated

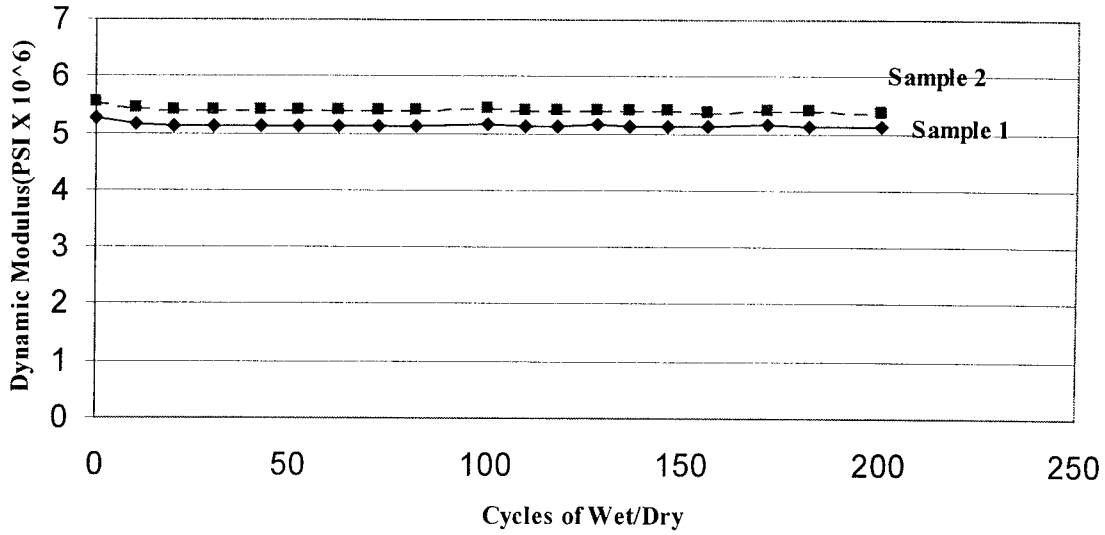

Fig. 3.33. Dynamic modulus vs. number of wet-dry cycles, silicafume3, high strength concrete, all sides coated

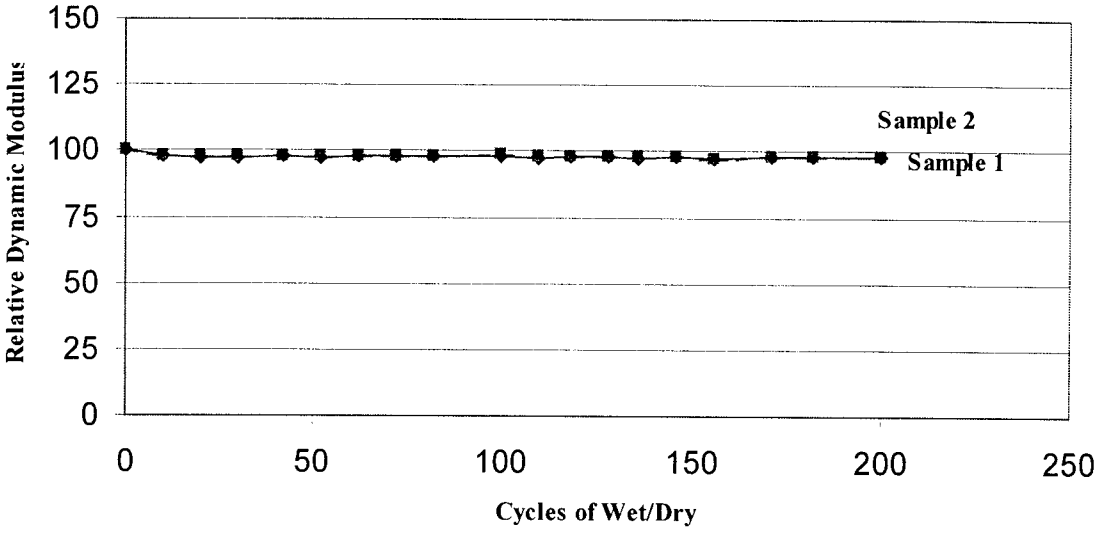

Fig. 3.34. Relative dynamic modulus vs. number of wet-dry cycles, silicafume3, high strength concrete, all sides coated

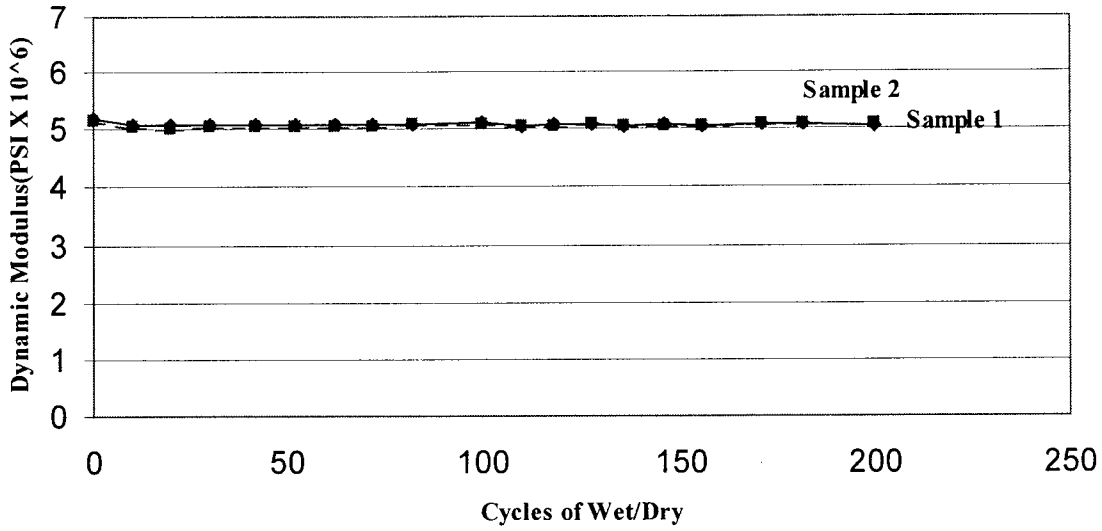

Fig. 3.35. Dynamic modulus vs. number of wet-dry cycles, organic matrix, high strength concrete, three sides coated

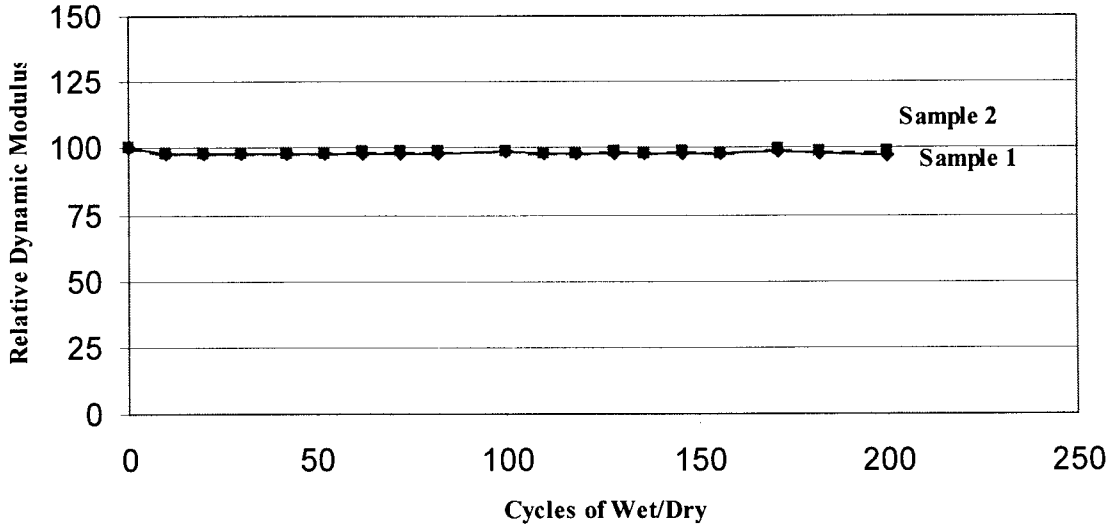

Fig. 3.36. Relative dynamic modulus vs. number of wet-dry cycles, organic matrix, high strength concrete, three sides coated

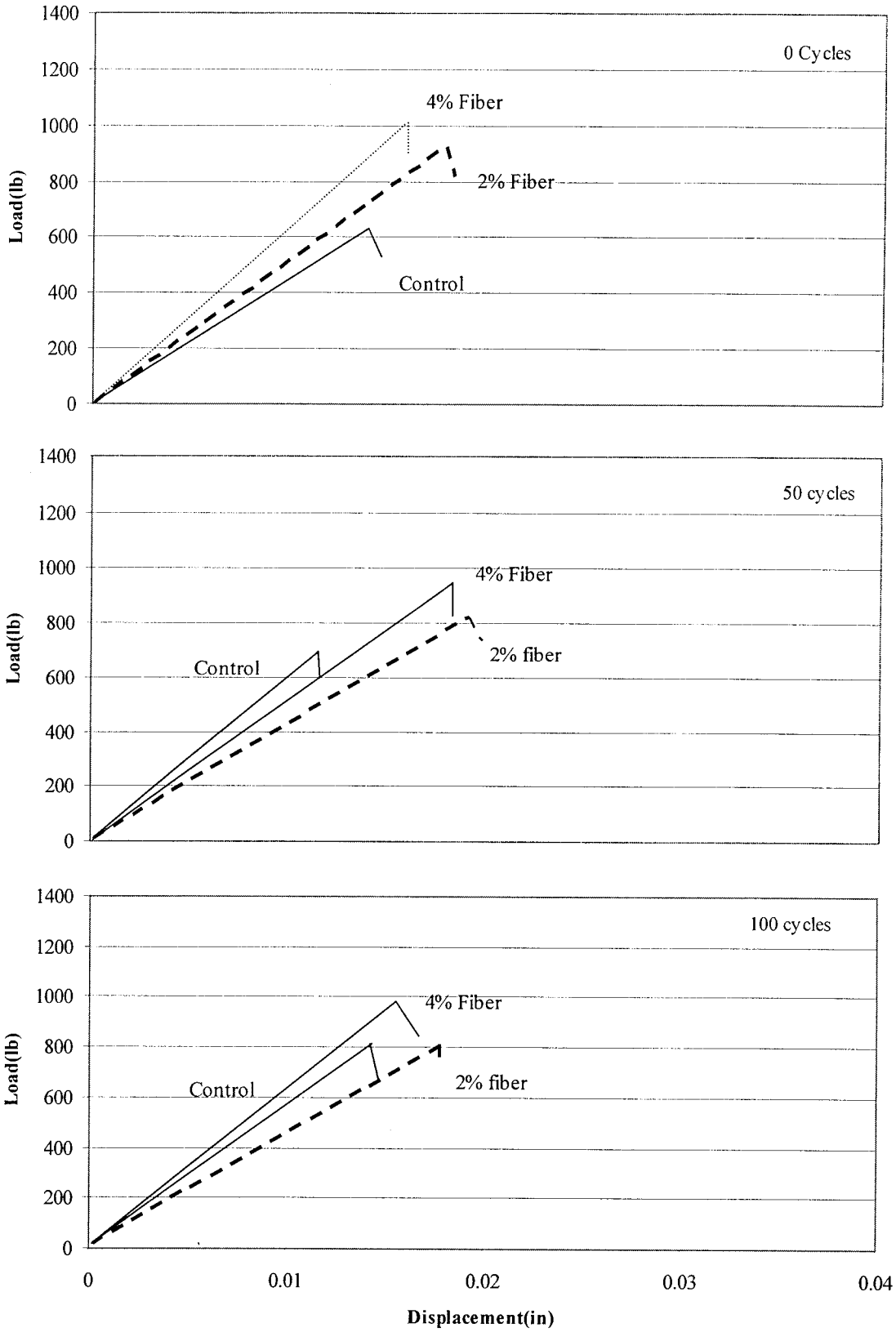

Fig. 3.37. Comparison of load-deflection response; control, 2 and 4 percent discrete carbon fibers

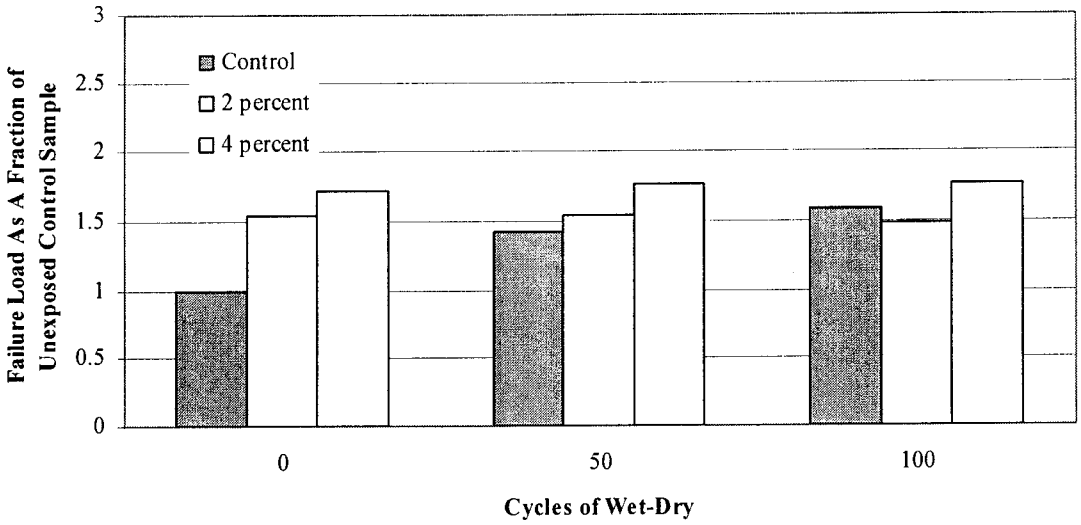

Fig. 3.38. Comparison of failure loads; control, 2 and 4 percent discrete carbon fiber

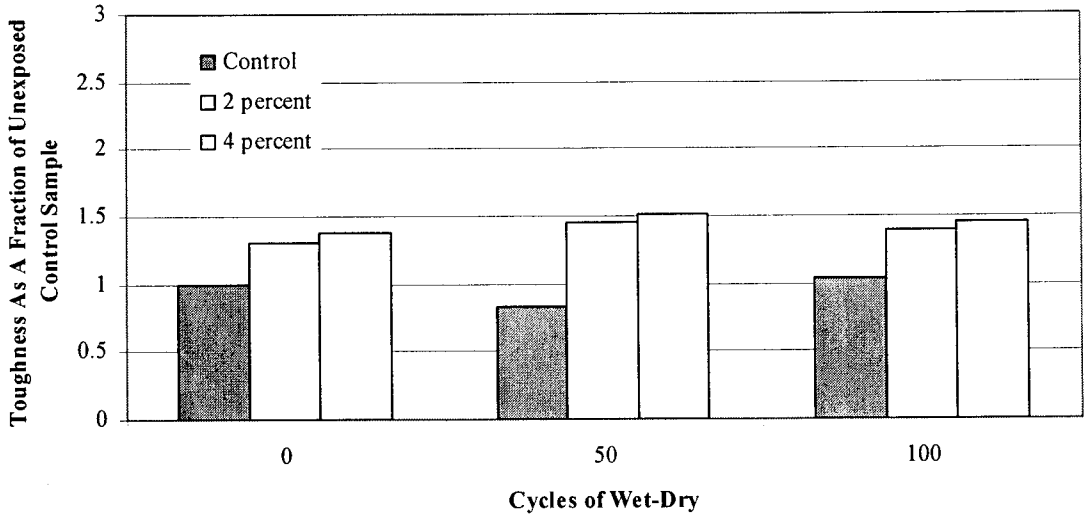

Fig. 3.39 Comparison of toughness; control, 2 and 4 percent discrete carbon fiber

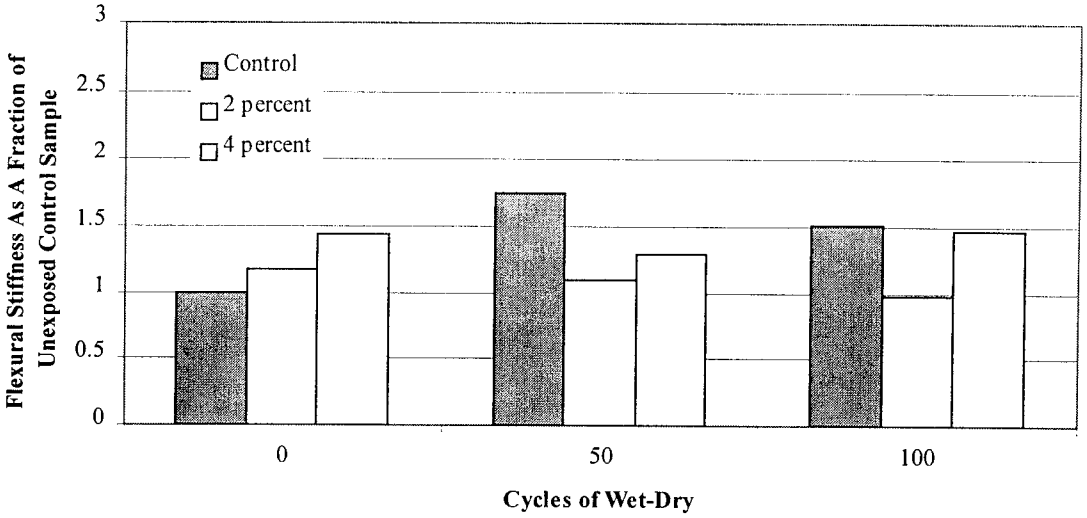

Fig. 3.40 Comparison of flexural stiffness; control, 2 and 4 percent discrete carbon fiber

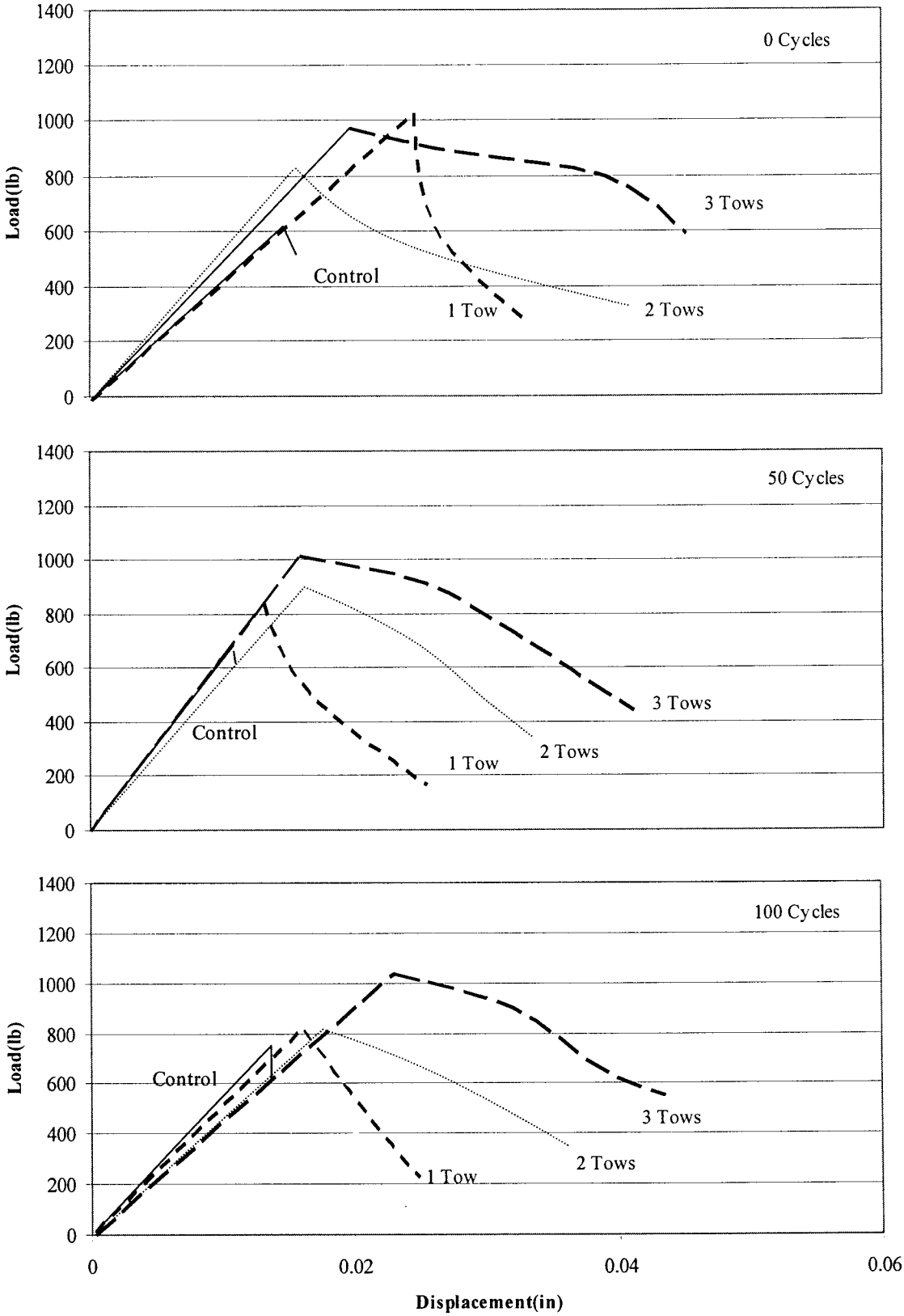

Fig. 3.41. Comparison of load-deflection response; Control, 1, 2, and 3 carbon tows

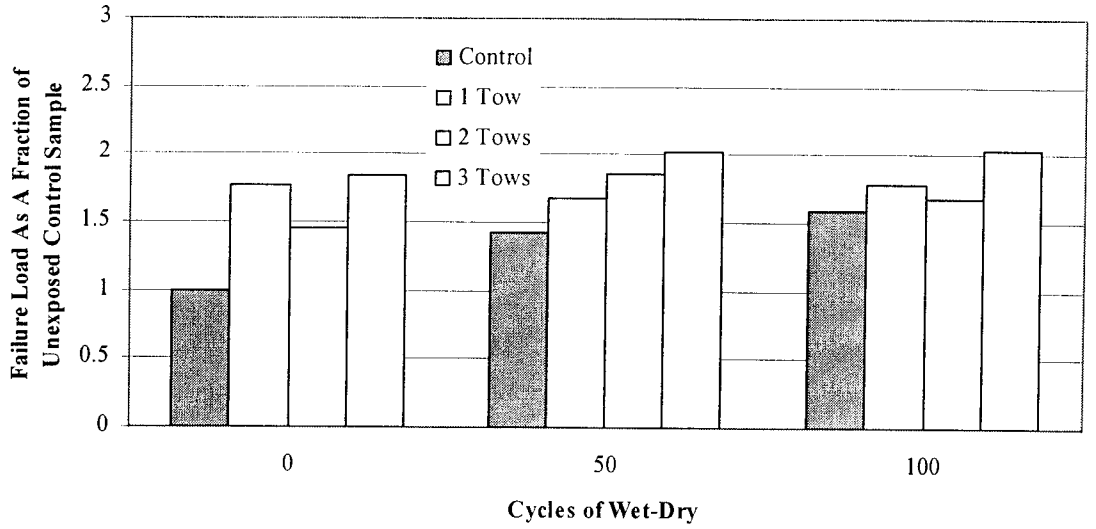

Fig. 3.42. Comparison of failure loads; control, 1, 2, and 3 carbon tows

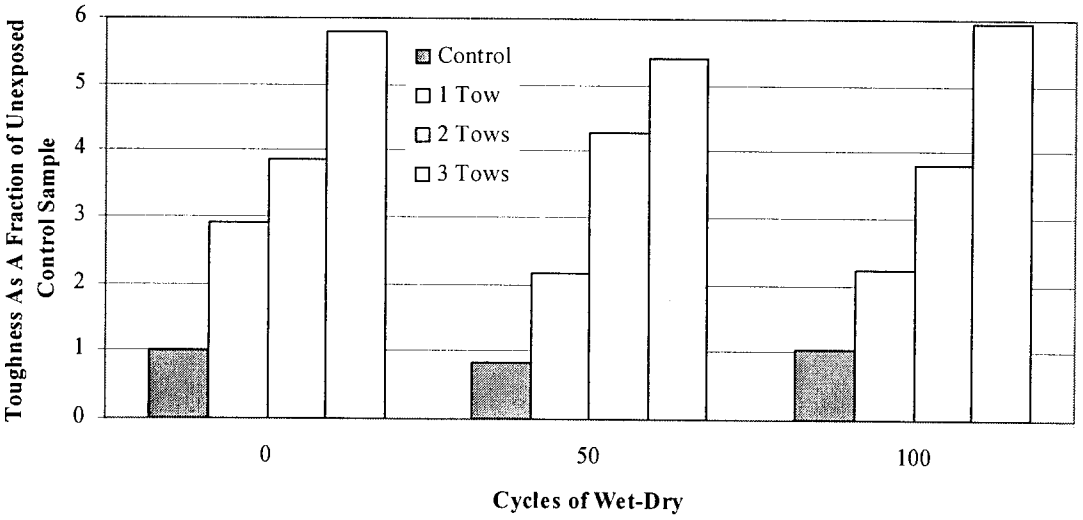

Fig. 3.43. Comparison of toughness; control, 1, 2, and 3 carbon tows

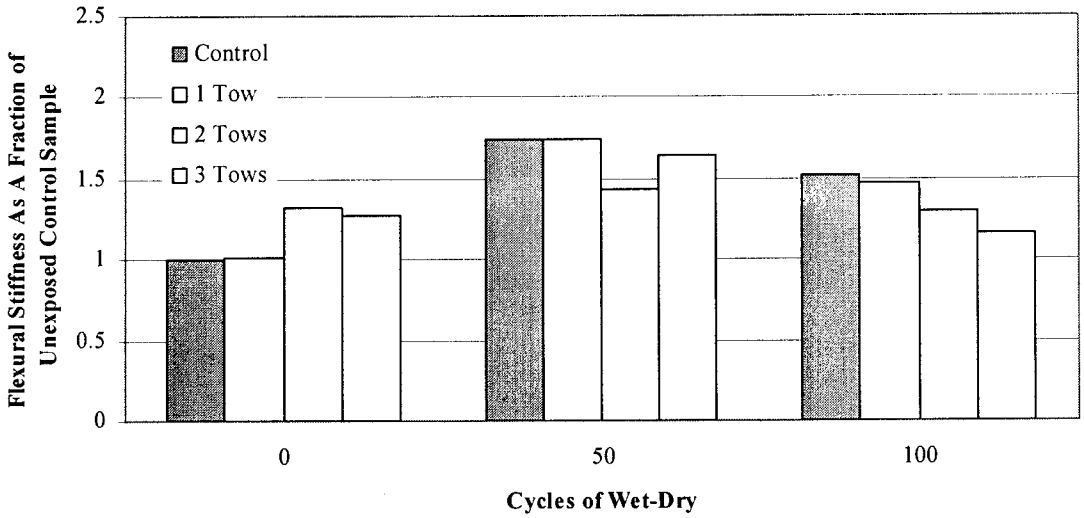

Fig. 3.44. Comparison of flexural stiffness; control, 1, 2, and 3 carbon tows

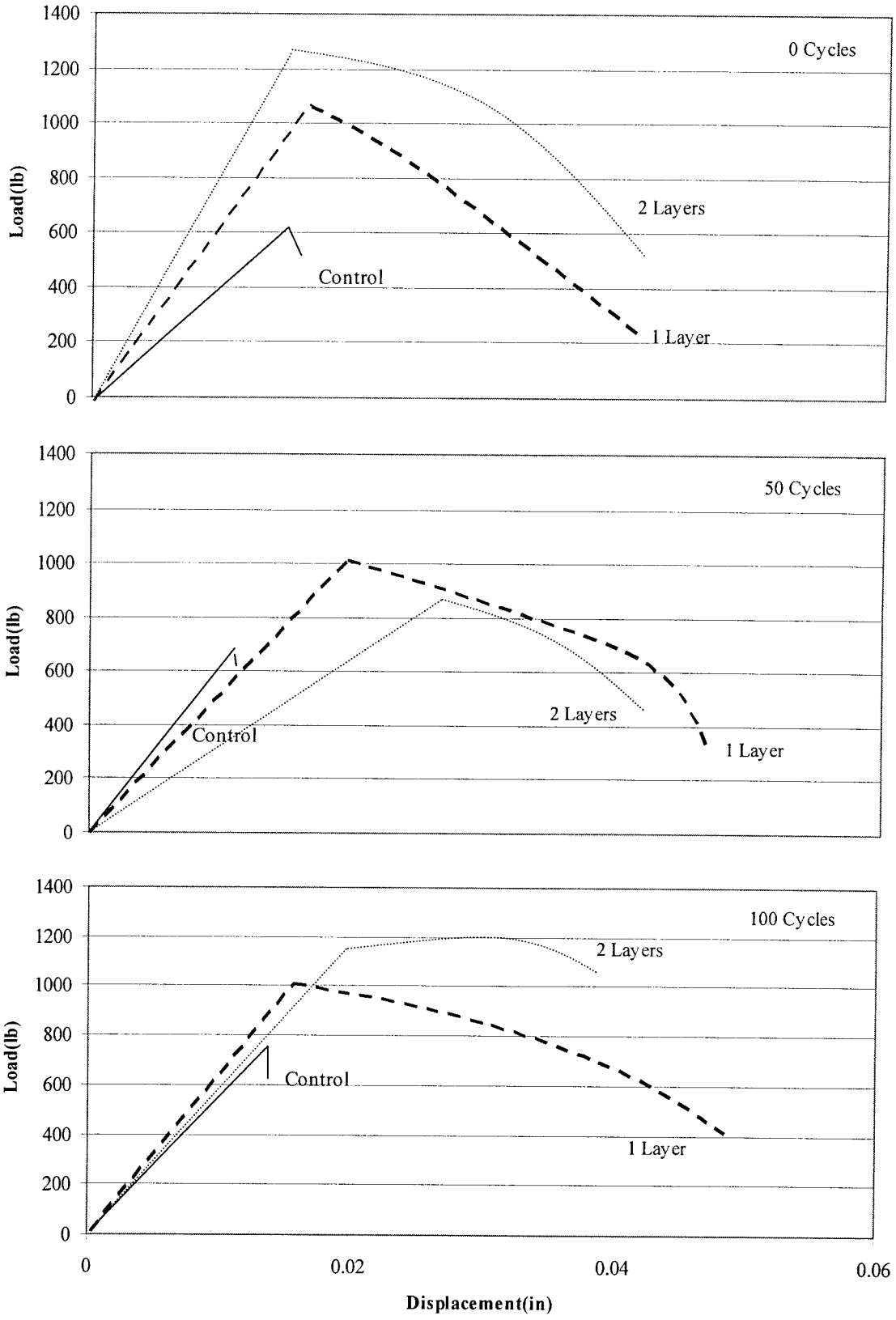

Fig. 3.45. Comparison of load-deflection response; Control, 1 and 2 carbon layers

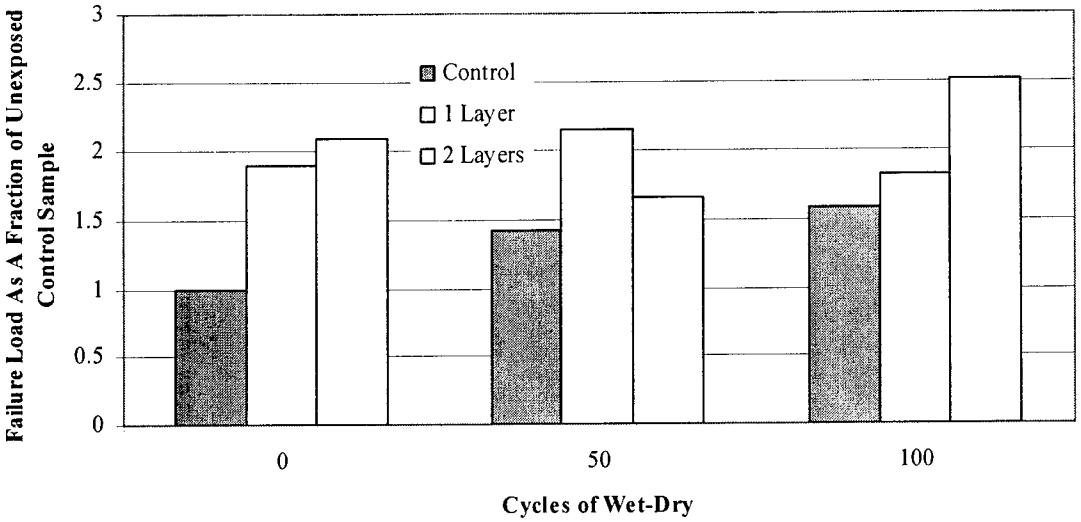

Fig. 3.46. Comparison of failure loads; control, 1 and 2 carbon layers

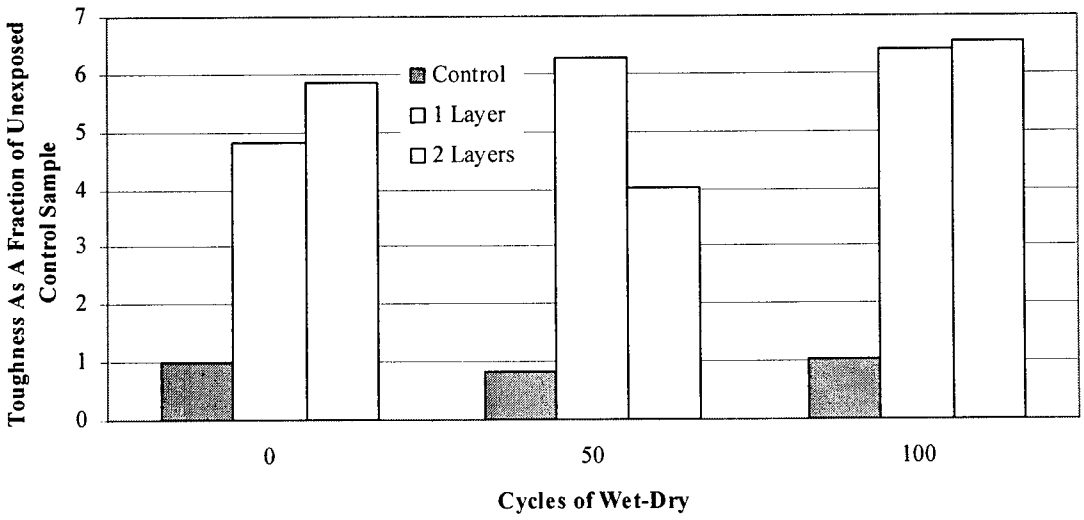

Fig. 3.47 Comparison of toughness; control, 1 and 2 carbon layers

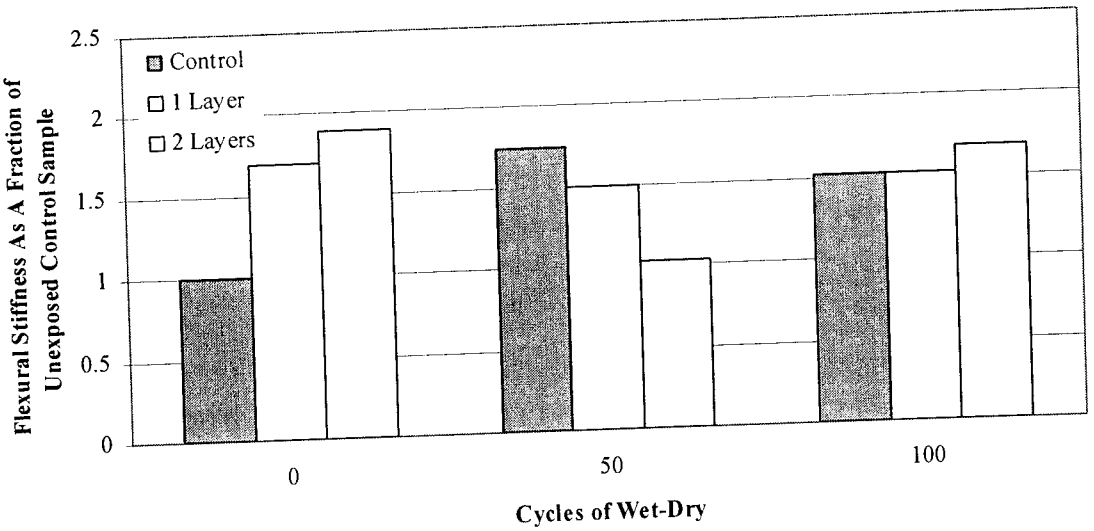

Fig. 3.48 Comparison of flexural stiffness; control, 1 and 2 carbon layers

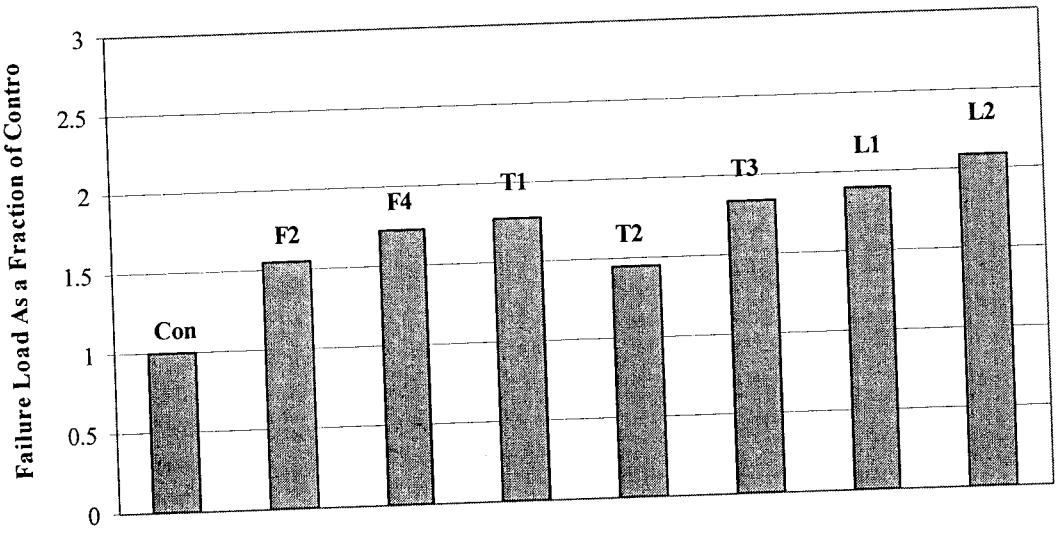

Fig. 3.49. Comparsion of failure loads, zero cycles

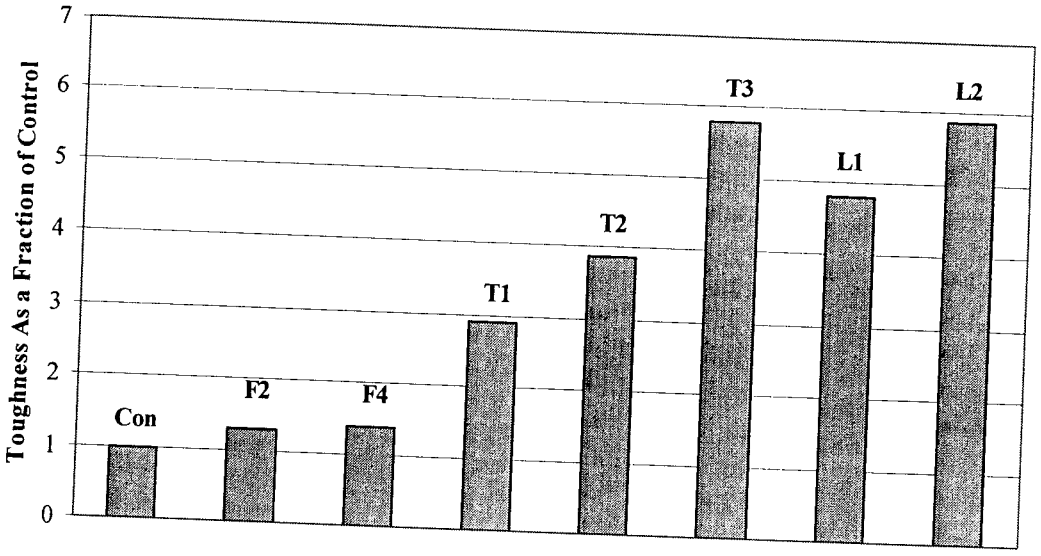

Fig. 3.50. Comparison of toughness, zero cycles

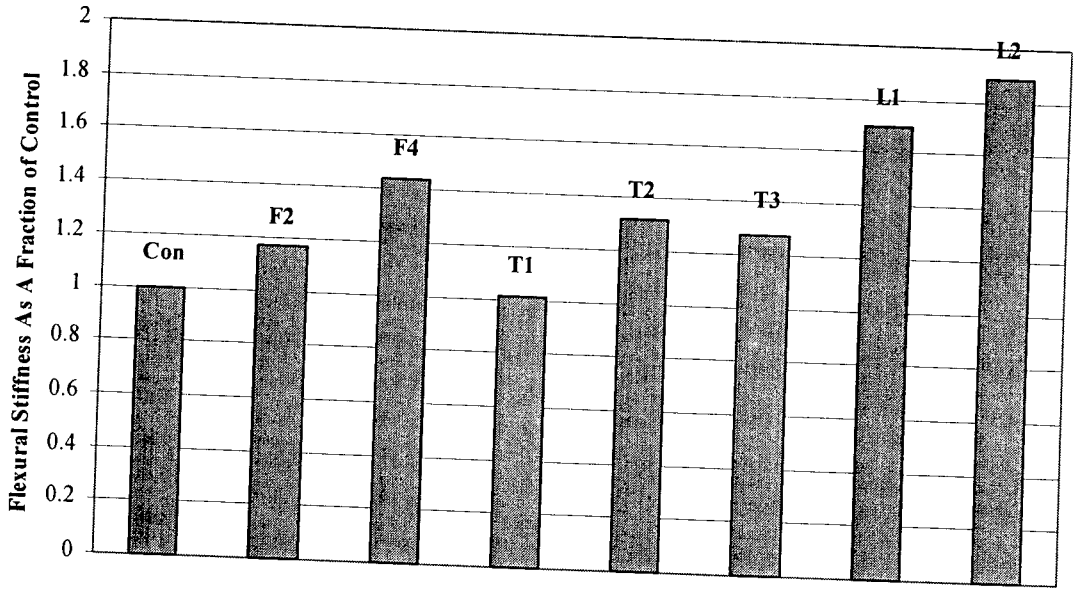

Fig. 3.51. Comparison of flexural stiffness, zero cycles

Chapter 4

Durability Under Freeze-Thaw Conditions

4.1 Introduction

When concrete is subjected to freezing and thawing under water saturated conditions, deterioration occurs due to freezing of the free water. In marine environments, exposure to salt water accelerates the disintegration process.

If the surface of the concrete is porous, water is absorbed through the concrete's surface in wet environments. If the surrounding air temperature drops below freezing, the absorbed water can freeze inside the concrete. This causes a potentially damaging build up of forces within the structure of the concrete. The deterioration process can be substantially controlled by applying a protective coating that will reduce water ingress. The coating will also seal the existing cracks. Epoxies and other organic matrices have been used in this capacity for several decades because they are totally impermeable and effectively seal the surface of the concrete. They have proven to be effective in preventing the ingress of fluids into the concrete's structure. Their main drawback is that while preventing the inflow of any fluid into the concrete's structure, most of them do not allow vapor pressure that builds up inside the concrete to be released. This may cause delamination of the coating and extensive damage to the concrete at the interface. Coating material that is less permeable than hardened concrete can slow the flow of

liquid into the structure of the concrete. Since the matrices are not totally impermeable, damaging vapor pressure can be released.

Such coatings described in Chapter 3 were evaluated under freezing and thawing conditions. The objective was to study the durability of the coating material, the interface, and the level of protection that can be obtained through the use of these coatings.

4.2 Experimental Design

The effectiveness of two cementitious and three inorganic matrices as barrier coatings for concrete was evaluated. Two types of parent concrete with low and relatively high water-cement ratios were chosen for the study. Performance was evaluated using a non-destructive test method. The soundness of the coated samples was determined by comparing initial dynamic modulus values with those after exposure to freezing and thawing.

4.2.1 Independent Variables

The coatings consisted of two polymer modified cementitious materials manufactured by Five Star and Miracote and three inorganic matrices. The Miracote system contained a polymeric liquid : cementitious solid ratio of 19:31. Six millimeter long carbon fibers were added at a rate of 2%. The details of the other coating materials are presented in Section 3.2.1. An outline of the specimen preparation is included in Sections 3.2.2 and 3.2.3.

4.2.2 Freeze-Thaw Machine

The apparatus for the freeze-thaw durability testing consisted of an 84 X 32 X 16 in. insulated stainless steel chamber. A thermocouple on the inside of the chamber was connected to a temperature gage on the outside of the chamber. This permitted the temperature of the samples to be monitored without opening the test chamber. A computer program monitoring this temperature gage controlled the start and stop of both the freezing and thawing cycles. Inside this chamber were seventeen stainless steel water reservoirs. These reservoirs, each measuring 17 X 3.5 X 4.5in., were filled to a level of one half of their depth with a 3% saline solution. Rather than using household sodium chloride, a commercial product named Instant Ocean was used to more closely duplicate the salt water found in marine environments. Cold air was supplied in several locations throughout the chamber to ensure a uniform temperature. Individual heaters were installed in between each of the reservoirs to supply heat during the chamber's thaw cycle. A schematic of the freeze/thaw machine is shown in Figure 4.1

One test specimen was then placed into each of the reservoirs within the freeze-thaw chamber. The thermocouple was attached to the top surface of one of the test specimens as described in ASTM C666 Procedure A (American Society for Testing and Materials, 1993). A freeze cycle began when the power to both the controlling computer and test chamber were turned on. The freeze cycle continued until the temperature inside the chamber was 0^{o} F. At this point, the heaters within the chamber began operating and a thaw cycle began. The thaw cycle was ended when the temperature inside the chamber had reached 40^{o} F. The concrete temperatures could be slightly different.

4.2.3 Evaluation

The deterioration of a concrete specimen occurs gradually throughout the series of freeze-thaw cycles. The effectiveness of a barrier coating designed to slow the ingress of fluids into the concrete had to be determined using the same sample. This was accomplished by using the dynamic modulus test procedure described in section 3.2.4 of this report. Natural frequency was measured after every forty-eight hours. The number of elapsed freeze-thaw cycles in this period was determined by examining the temperature log of the computer. To save time test was stopped at 200 cycles or the complete deterioration of the sample.

4.3 Test Results and Discussion

The low strength control and coated samples were unable withstand even the first fifteen freeze-thaw cycles. All of the low strength samples had either broken into several pieces or had lost a significant percentage of their mass. At this point, the low strength samples were removed from the testing chamber and the focus of the investigation was shifted to the high strength specimens. The results provided a clear indication that coatings can not be used to protect poor concrete. Note that the conditions used in this experiment; namely; freezing and thawing in water under saturated conditions do not normally occur in the field. In addition air entrainment was not used to induce deterioration.

The data obtained from the durability testing of high strength mortar samples under freeze-thaw conditions is summarized in Figures 4.2-4.13. Included in these figures are the dynamic modulus values calculated from the evaluation method described

in section 3.2.4 of this report. In addition the relative dynamic modulus, RDM computed using the equation

$$RDM = (n_n/n_o)^2 \text{ X } 100 \qquad (4.1)$$

is presented. In equation 4.1, n_n is the fundamental frequency after n cycles of freeze-thaw and n_o is the specimen's initial fundamental frequency.

Behavior of the control samples is presented in Figure 4.2 and Figure 4.3. Both samples performed relatively well throughout the first 150 cycles of freeze-thaw, experiencing a minimal loss in dynamic modulus. The strength of sample 1 remained relatively unchanged for the entire 200 cycles. A significant decrease in the strength of sample 2 occurred within the final 50 freeze/thaw cycles. The dynamic modulus of the sample dropped by about 30% in this period. This is verified by Figure 4.3 where the relative dynamic modulus of both samples is shown. At the end of 200 freeze-thaw cycles, the relative dynamic modulus of sample 1 was still above 99% while sample 2 had dropped to about 70% of it's initial strength.

Figures 4.4 and 4.5 present the results of the dynamic modulus testing of specimens protected with the Miracote protective coating system. Failure of both specimens occurred before 150 cycles of freeze/thaw were completed despite the fact that their dynamic moduli remained relatively unchanged. The relative dynamic modulus of each sample did decrease slightly during this period. It is unusual for these two strength indicators to yield conflicting results. This may be attributed to the fact that the Miracote coating was quite porous and was able to absorb a large amount of water. This additional water increased the mass of the test specimens. Mass is one of the variables used to calculate dynamic modulus so the presence of this water exaggerated these values. The

relative dynamic modulus is not mass dependent so it is more reliable for these specimens. Because the Miracote coating was unable to release the absorbed water dynamic modulus values were inaccurate. As the water froze, it caused a buildup of forces that delaminated the coating and ultimately cause failure of the concrete specimens.

The results of the samples protected with the Rapid Star cement coating are summarized in Figures 4.6-4.7. The dynamic modulus and relative dynamic modulus of sample 1 decreased slightly during the first 100 freeze/thaw cycles. The relative dynamic modulus dropped to about 85% during this period. The next strength evaluation yielded a dynamic modulus value that had increased by about 20%. All subsequent attempts at evaluating the natural frequency of the specimen yielded an error message from the computer. This type of error is consistent with the formation of a microcrack within the structure of the concrete. Although not large enough to cause failure of the specimen as in the Miracote Samples, any further evaluation was impossible. Sample 2 performed well during throughout the entire series of freeze/thaw cycles and was able to maintain about 95% of it's strength. The coating was observed to be durable during exposure to the freeze/thaw environment. Small cracks formed but only small chips became dislodged from the samples.

The behavior of samples protected with the Silicafume1 and Silicafume2 coatings is shown in Figures 4.8-11. Failure of each of the samples occurred before 150 freeze/thaw cycles had been completed. In each of the specimens, the dynamic modulus and relative dynamic modulus remained relatively constant during the first 100 freeze/thaw cycles. At this point, sample 1 of both silicafume formulations experienced a

dramatic increase in dynamic modulus similar to the one observed in the first Rapid Star sample. Any further attempts at strength evaluations led to error messages that suggested failure of the specimen. In the remaining samples, the frequency readings remained consistent but cracking caused the samples to break into two pieces. At this point, the samples were removed from the freeze-thaw chamber and the evaluations were concluded. Despite the failure of the specimens, each of the coatings performed well during the freeze/thaw cycles. They remained bonded to the samples and very little cracking and spalling was observed.

The results of the durability testing under freeze-thaw conditions of samples coated with Silicafume3 are shown in Figures 4.12-13. Both of the tested samples were able to survive the entire series of 200 freeze-thaw cycles. The dynamic modulus and relative dynamic modulus values remained constant for a large percentage of the testing cycle. After 150 cycles of freeze-thaw the coating began to delaminate from both specimens. At the conclusion of the evaluation period, coating remained on only about 25% of each sample. Once delamination of the coating began strength evaluations began to yield unreliable results. The dynamic modulus of sample 1 increased by about 25% in a period of 10 freeze-thaw cycles. During the same period, the strength of sample 2 dropped by about 50%. It may be possible to improve the durability of the coating by adding small amounts of organic polymers.

4.4 Summary

The effectiveness of protective coatings applied to concrete samples after freeze-thaw exposure reported in this chapter cover the durability of the coatings, interface, and

the protection provided by the coatings. The results indicate that coating can not be used to protect concrete structures that have very low durability. This observation is based on the poor performance of high water-cement ratio samples coated with various protective coatings.

The coatings are durable and adhere to the parent concrete well except for the third silicafume formulation. However, they do not improve the durability of concrete placed in water saturated conditions. It should be noted that the condition of evaluation is very severe and very rarely occurs in actual field conditions.

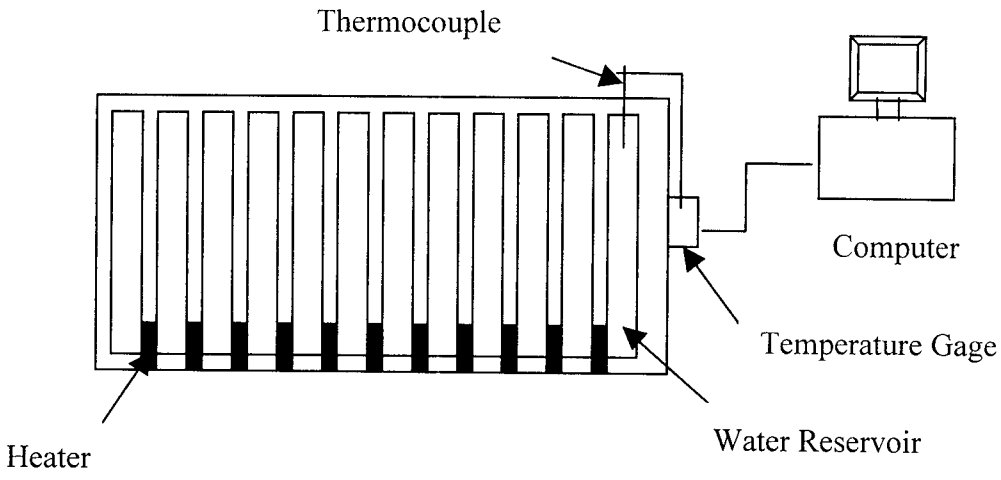

Fig. 4.1 Schematic of freeze/thaw machine

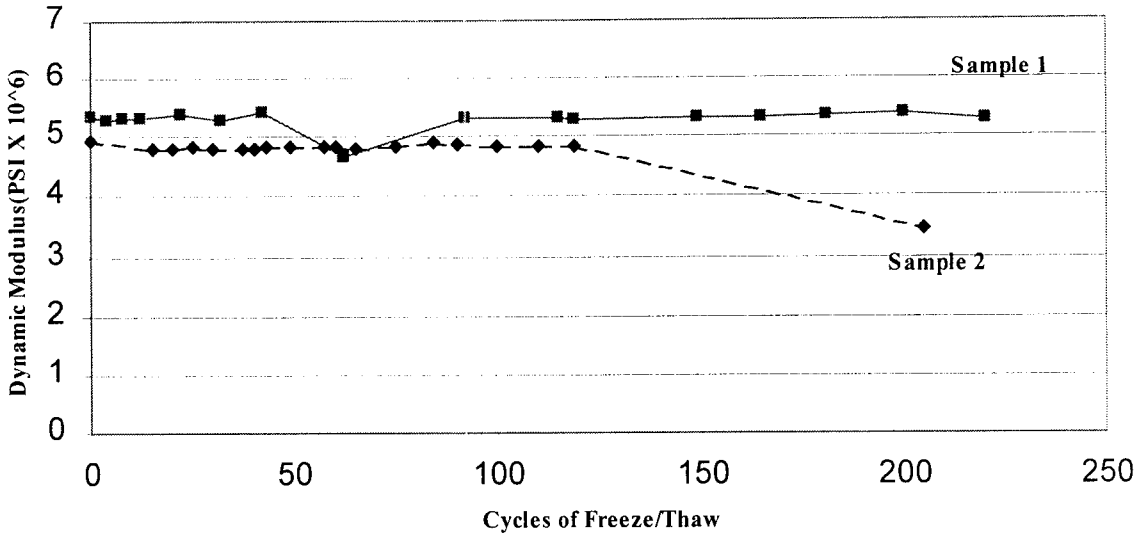

Fig. 4.2. Dynamic modulus vs. number of freeze-thaw cycles, control, high strength mortar

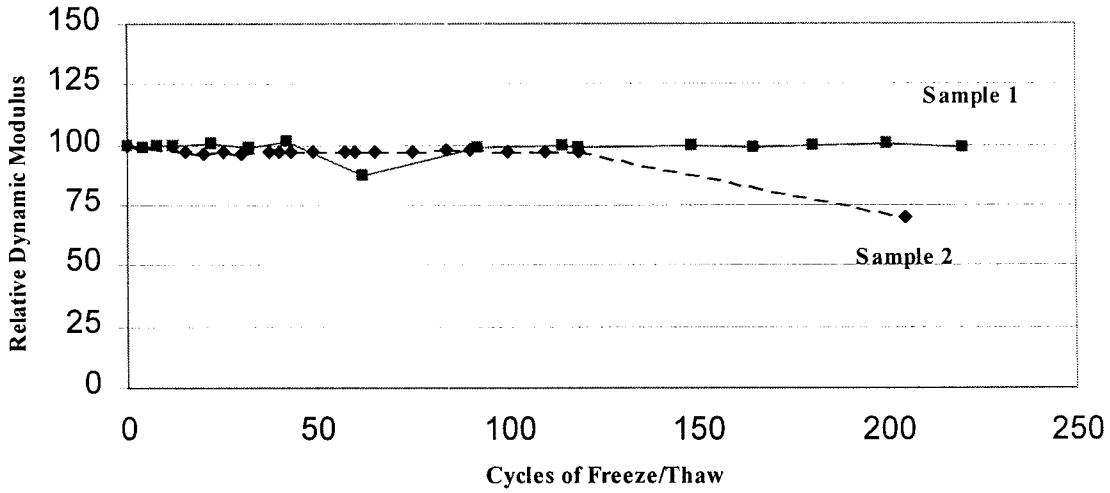

Fig. 4.3. Relative dynamic modulus vs. number of freeze-thaw cycles, control, high strength mortar

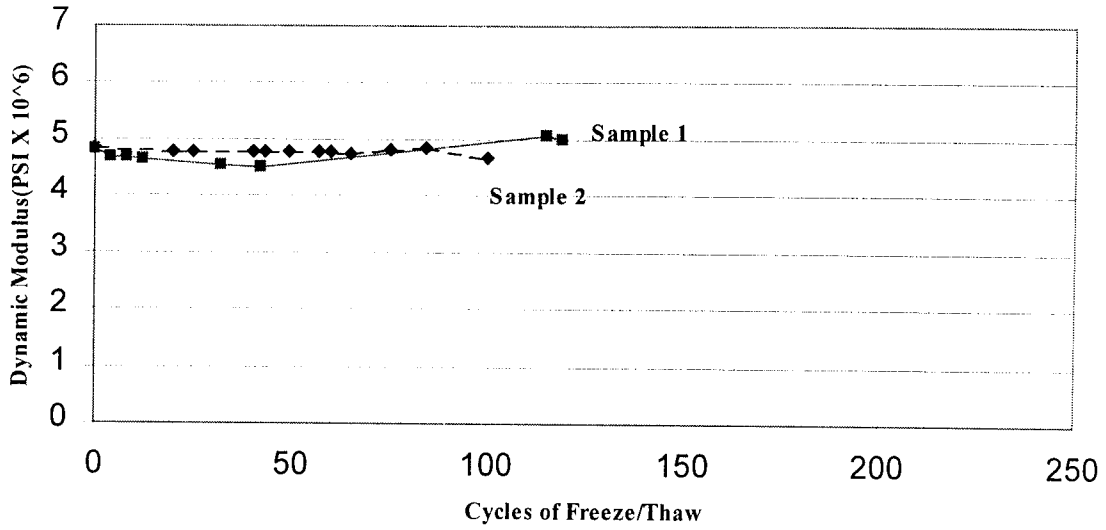

Fig. 4.4. Dynamic modulus vs. number of freeze-thaw cycles, Miracote, high strength mortar

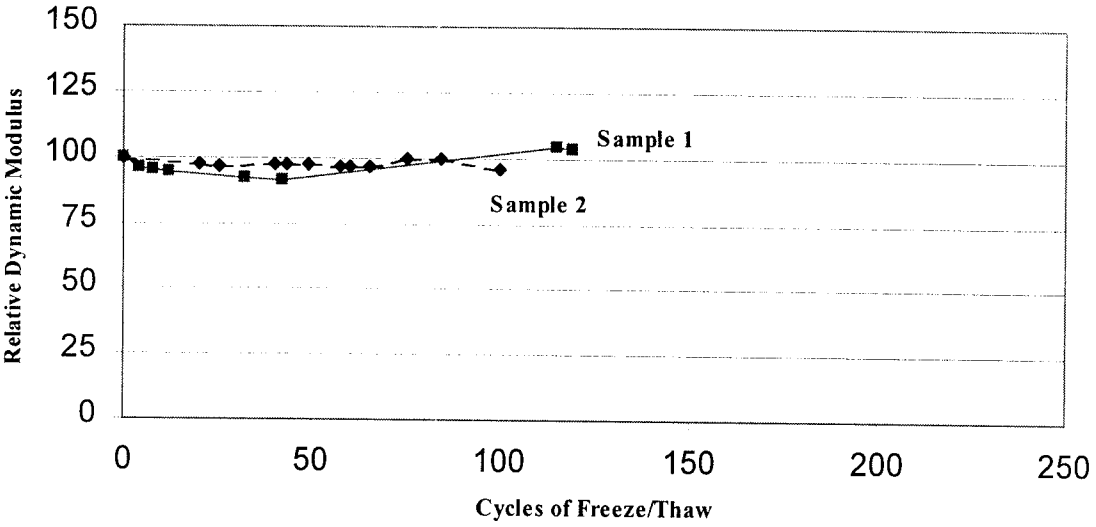

Fig. 4.5. Relative Dynamic Modulus vs. Number of Freeze-Thaw Cycles, Miracote, High Strength Mortar

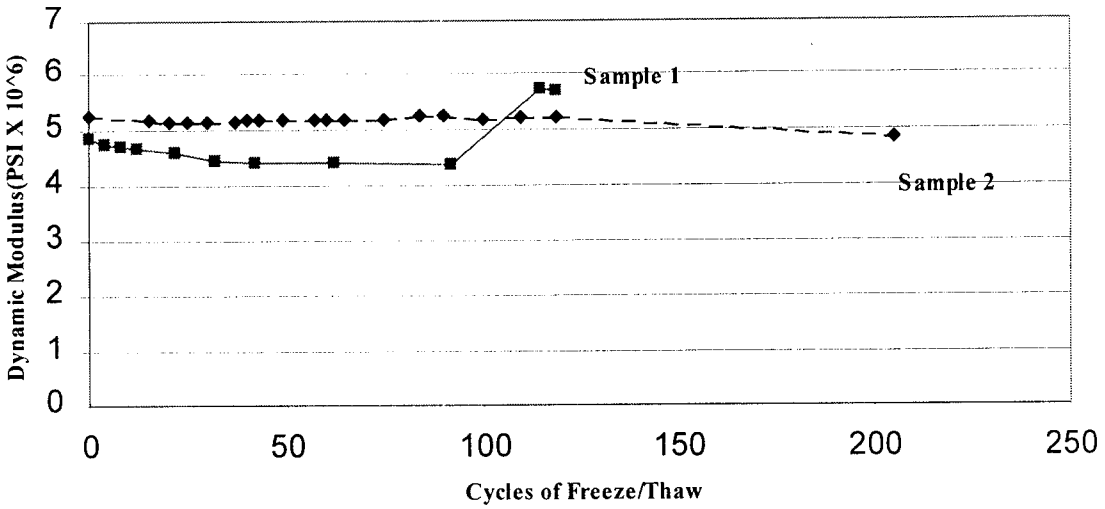

Fig. 4.6. Dynamic modulus vs. number of freeze-thaw cycles, Rapid Star, high strength mortar

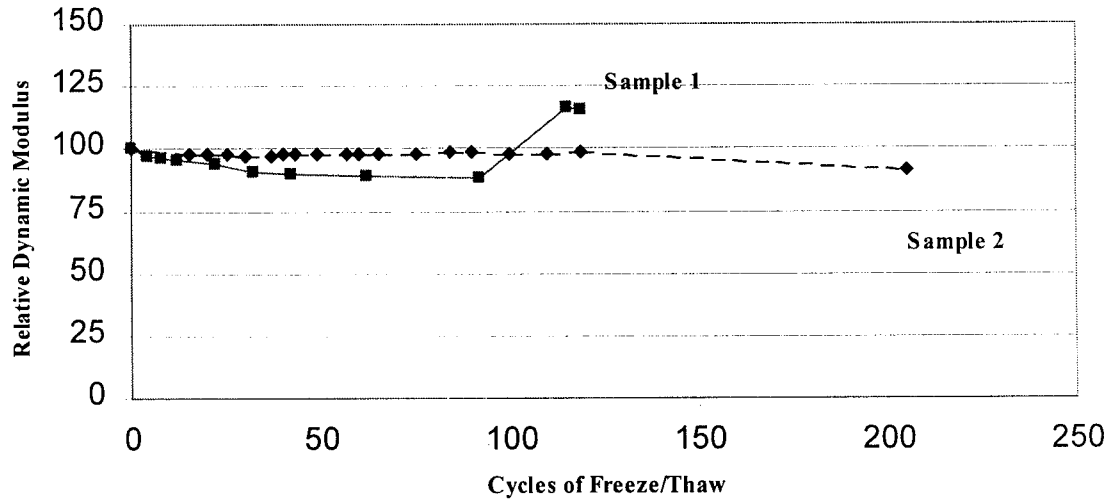

Fig. 4.7. Relative dynamic modulus vs. number of freeze-thaw cycles, Rapid Star, high strength mortar

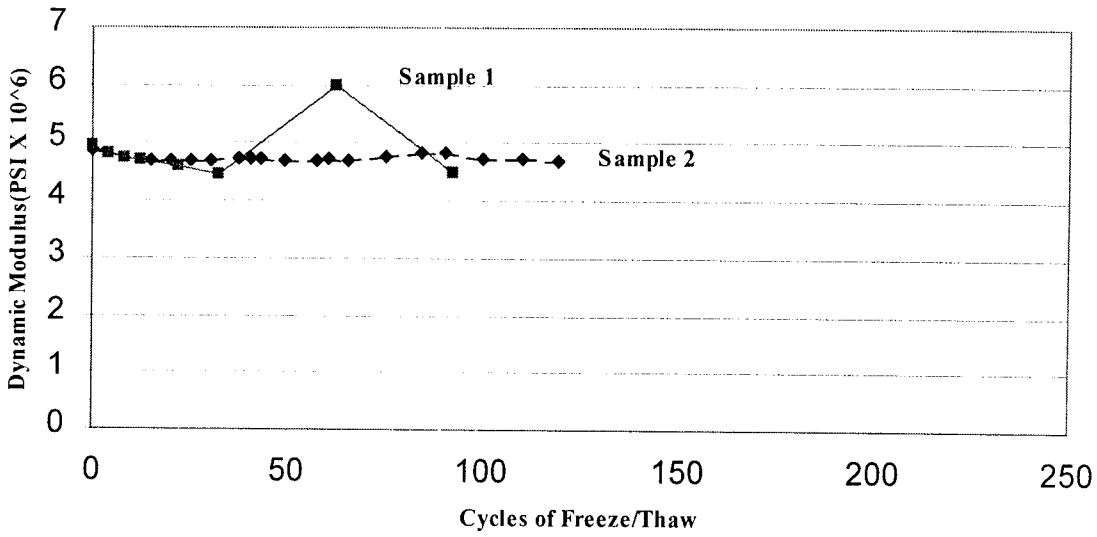

Fig. 4.8. Dynamic modulus vs. number of freeze-thaw cycles, silicafume1, high strength mortar

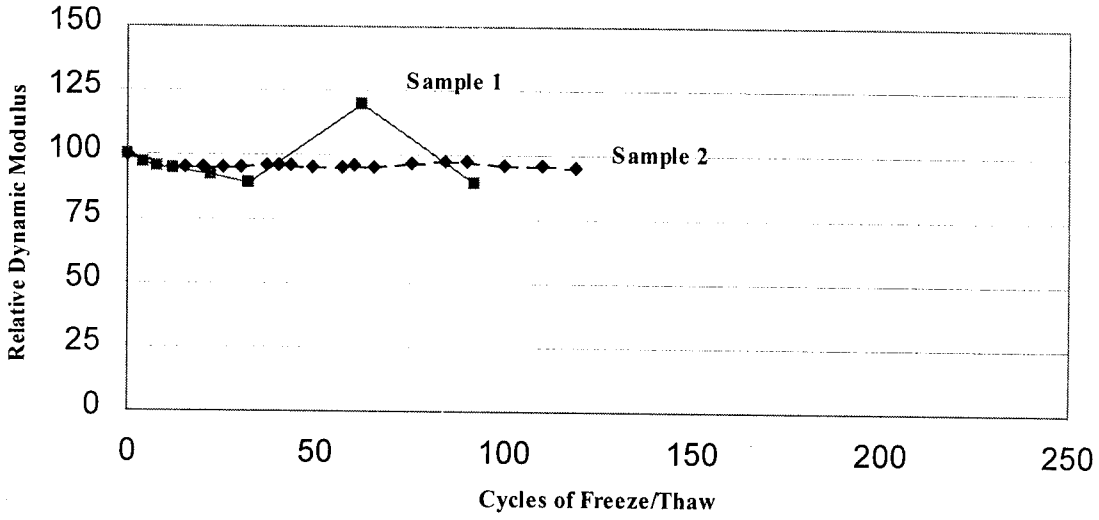

Fig. 4.9. Relative dynamic modulus vs. number of freeze-thaw cycles, silicafume1, high strength mortar

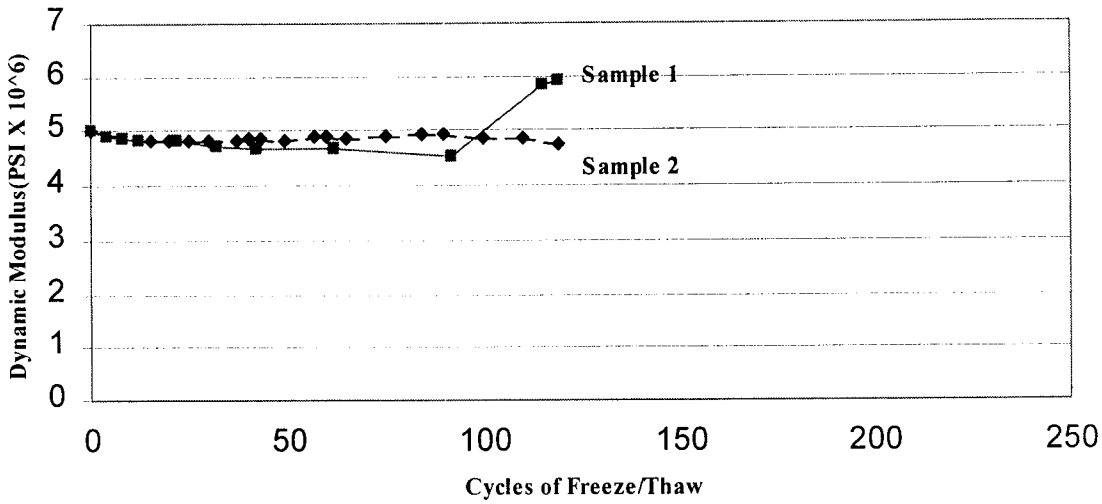

Fig. 4.10. Dynamic modulus vs. number of freeze-thaw cycles, silicafume2, high strength mortar

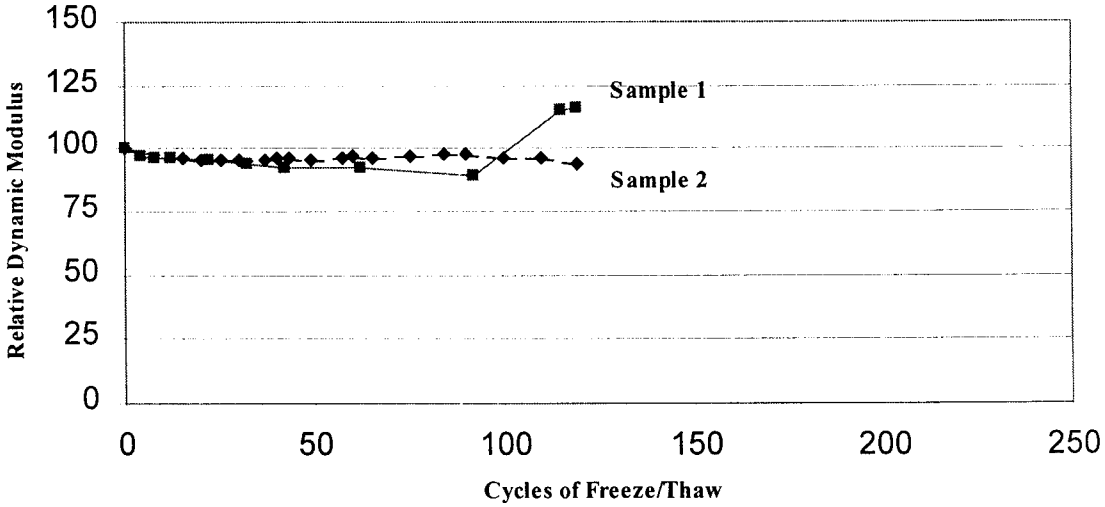

Fig. 4.11. Relative dynamic modulus vs. number of freeze-thaw cycles, silicafume2, high strength mortar

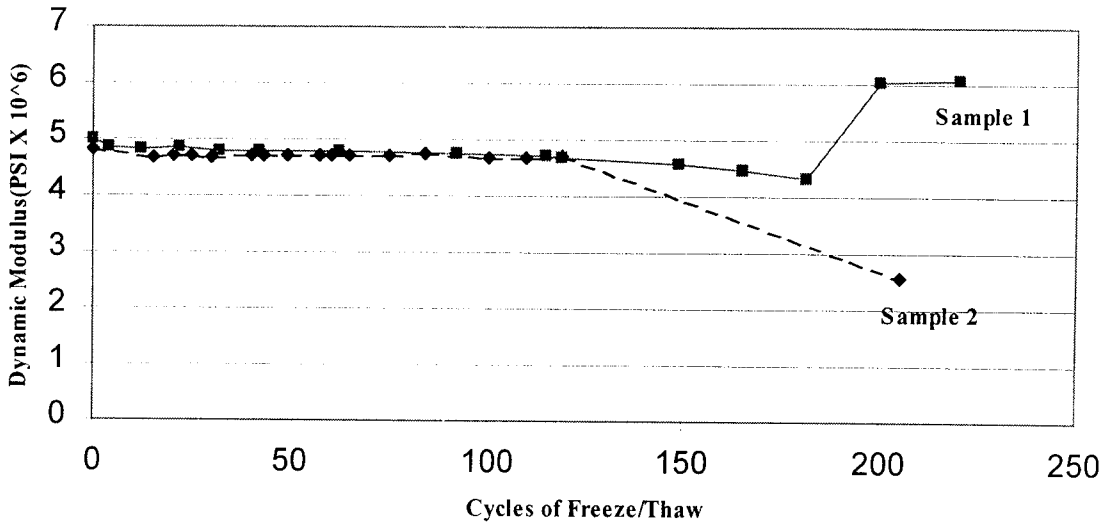

Fig. 4.12. Dynamic modulus vs. number of freeze-thaw cycles, silicafume3, high strength mortar

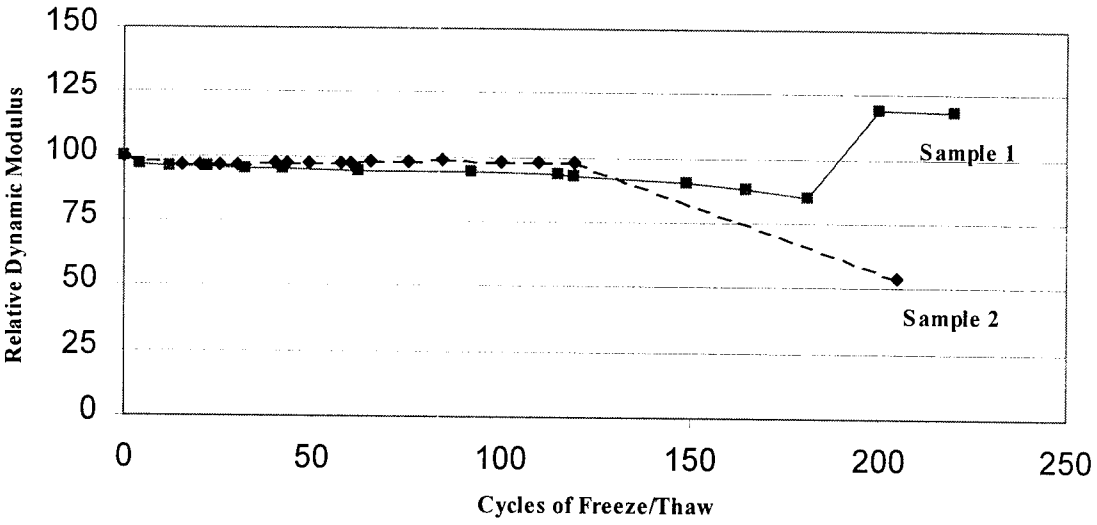

Fig. 4.13. Relative dynamic modulus vs. number of freeze-thaw cycles, silicafume3, high strength mortar

Chapter 5

Durability Under Scaling Conditions

5.1 Introduction

The presence of stagnant, or ponded, water in cold weather environments will lead to the eventual decay of the surface of the concrete. Scaling is one of the results of repeated cycles of freezing and thawing in hardened concrete. When the concrete is permeable, moisture flows through the surface of the concrete into any existing voids. When the temperature drops below 0°C, the absorbed water freezes and expands. This expansion causes stress build up that leads to cracking and spalling of the concrete surface. Scaling occurs when the expansion pressure of the ice exceeds the tensile strength of the concrete causing localized fracture at the element's surface.

One possible solution to the problem of scaling in concrete is to apply a protective coating that will cover existing micro-cracks. The coating should have a lower permeability than the concrete. If the flow rate of the water into the structure of the element is decreased, the damage caused by the freezing cycle can be slowed or prevented. The inorganic matrices evaluated in Chapter 3 have excellent potential in this application. These matrices can also be used to bond glass or carbon reinforcement to structural elements that need strengthening. Scaling of the surface of the concrete reduces the effectiveness of the repair effort. Deterioration weakens the bond between

the surface of the concrete and the carbon and may result in delamination and subsequent failure of the repair.

This chapter presents the results of the scaling resistance study conducted using inorganic matrices and carbon fibers. The system can be used for both coating and strengthening.

5.2 Experimental Investigation

The effectiveness of two cementitious and three inorganic matrices as a surface protector for concrete was evaluated. Additionally, the effectiveness of a strengthening system consisting of an inorganic matrix used in conjunction with several commercially available forms of carbon was studied. The matrices were applied to both a high and low strength mortar and subjected to scaling conditions. The matrices used as a surface protector were evaluated using an ASTM rating system throughout the series of scaling cycles (American Society for Testing and Materials, 1996). In strengthening applications, the effectiveness of the matrix was studied using flexure tests after exposure to scaling conditions.

5.2.1 Details of Specimens

The specimens consisted of:

- Low strength plain concrete
- High strength plain concrete
- Low and high strength prisms coated with three inorganic matrices described in Section 3.2.1

- Low and high strength prisms coated with the Five Star polymer modified cement system described in Section 3.2.1
- Low and high strength prisms coated with the polymer modified cement system commercially known as Miracote described in Section 4.2.1
- Prisms reinforced with discrete carbon fibers, carbon tows and fabrics.

5.2.2 Preparation of Sample

Preparation of the samples was done using the procedure described in Section 3.2.2. First, 2 X 2 X 13 in. prisms were cast and cured. These prisms were coated with the various matrices or strengthened with carbon reinforcement.

5.2.3 Scaling Test Set-Up

A special set-up was built for exposing the test samples to scaling conditions. Rectangular plastic dams were built to fit atop the coated surface of the specimens. The height of the dams was one inch. The dams were attached to the coated surface of the samples with a bead of water proof caulk. Saline solution was contained in the dams atop the samples to a depth of one-fourth of an inch. Commercially available salt, known as Instant Ocean, was used in the saline solution to duplicate marine environments. A schematic of the scaling test set-up is shown in Figure 5.1

The scaling test described in ASTM C672 was designed to allow the completion of one scaling cycle in a 24 hour period (American Society for Testing and Materials, 1993). The samples with the dams containing the saline solution were placed in a freezing chamber. They were kept at 20°F for sixteen hours. At the end of this freezing

cycle, the samples were removed from the freezing chamber and kept at room conditions. After eight hours in this environment, the thaw cycle was completed and a new scaling cycle began as the samples were returned to the freezing chamber. At the completion of five scaling cycles, the surfaces of the samples were rinsed and the saline solution was replaced.

5.2.4 Evaluation Procedure

The barrier coatings were applied to protect the surface of the samples from the damaging effects of repeated scaling cycles. Deterioration is confined to the surface of the specimens, unlike in the freeze-thaw and wet-dry cycles where the concrete was weakened internally. A visual evaluation of the samples was sufficient to determine the effectiveness of the barrier coatings. The rating system described in ASTM C672 was used to evaluate the specimens in this chapter. Scaling of the samples was quantified using the system shown below.

(0) : Little or no scaling

(1) : very slight scaling(1/8 in. depth, max)

(2) : slight to moderate scaling

(3) : moderate scaling

(4) : moderate to severe scaling

(5) : severe scaling

The samples were evaluated and photographed before exposure to scaling conditions. Additional evaluations were made at the completion of every fifth scaling cycle. The samples were exposed to a total of fifty scaling cycles. In certain instances, the testing

was discontinued prematurely because the deterioration of the sample prevented containment of the saline solution.

Flexure testing was used to evaluate the strengthened samples exposed to scaling conditions. The test procedure and set-up are described in Section 3.2.4 of this report. Evaluation was made at the completion of fifty scaling cycles.

5.3 Test Results and Discussion: Coatings

The data obtained from the durability testing of barrier coating samples under scaling conditions is summarized in Figures 5.2-5.13. Included in these figures are the results for both high and low strength concrete samples exposed to scaling cycles and evaluated with the rating system introduced in ASTM procedure C672 and section 5.2.4 of this report. Additionally, photographs are included that illustrate the degradation of the surface of various samples.

Performance of the low strength concrete control samples is presented in Figure 5.2. The first sample degraded to level five in 15 cycles. The second sample degraded to this level within the next 10 scaling cycles.

When polymer modified cementitious coating 1 (Five Star) was applied the deterioration was slowed. Both samples, however, reached the level five in 50 cycles indicating that severe scaling had occurred, Figure 5.3.

The second polymer modified cementitious coating (Miracote) did not experience any deterioration up to 50 scaling cycles.

Silicafume coating 1 showed better performance than matrices 2 and 3 but all three of them showed some signs of deterioration, Figures 5.4-5.6. One specimen with the first matrix (0.5 percent carbon content silicafume) did not develop any damage.

High strength control samples did not develop any damage after 50 cycles of scaling. Both samples with the Five Star coating developed some damage, but performance was superior to low strength samples with the same matrix Figure 5.7. All three inorganic matrices and the Miracote samples did not show any signs of deterioration.

Photographs of various deteriorated surfaces are shown in Figures 5.8-5.13.

5.4 Test Results and Discussion: Strength Tests

The data obtained from the flexure testing of samples strengthened with carbon fibers is shown in Figures 5.14-5.25. Included in these figures are the results obtained from the control samples and samples reinforced with chopped carbon fibers, carbon tows, and layers of carbon. Two samples with each reinforcement type and area were tested. Unexposed samples and samples exposed to fifty cycles of scaling were evaluated. The load-displacement diagrams from each of the tests are presented here. Table 5.1 is a summary of all pertinent information obtained from each of the load-displacement plots. The peak load values and the displacement at these loads for each of the samples are included in this table. The stress in the outer fibers of the specimen at the cracking load, the modulus of rupture, is tabulated for each sample in Table 5.1. The flexural stiffness of each sample was found using the following equations

$$\delta = Pl^3 / 48EI \qquad (5.1)$$

$$EI = Pl^3 / 48\delta \qquad (5.2)$$

where EI is the flexural stiffness in lb-in^2, P is the peak load of the specimen in pounds, l is the length of the specimen in inches, and δ is the deflection at peak load in inches. The ability to measure ductility is also critical when determining the effectiveness of the strengthened samples. The toughness factor of the samples was used as a measure of ductility in this study. It was determined by calculating the area under each of the load-displacement graphs. The values listed in Table 5.1 are the averaged values obtained from the two samples for each reinforcement type with any outlying values omitted. Expected performance of the unexposed samples was previously discussed in Section 3.4 of this report. From the load-displacement graphs presented in Figures 5.14, 5.18, 5.22 and the summarized data in Table 5.1, the following observations can be made regarding the durability of each strengthening type under scaling conditions.

The load-displacement diagrams for the control samples and samples reinforced with discrete carbon fibers are shown in Figure 5.14. Similar behavior was observed in the exposed and the unexposed samples. The load-displacement relationship was linearly elastic until the peak load was achieved. Brittle failure occurred in each of the samples. The post peak response of the specimens was not studied because it was not necessary for this investigation of strength increase and ductility. The addition of the discrete carbon fiber strengthening system did not affect the load-displacement response.

The results obtained from the control samples and samples reinforced with two and four percent carbon are tabulated in Table 5.1. Exposure to scaling conditions caused an increase in the peak load and modulus of rupture values for the control samples. After fifty cycles of scaling, the failure load of the control samples had increased by

approximately fifty percent. Negligible increases in flexural strength were observed in samples reinforced with discrete carbon fibers and subjected to scaling cycles, Figure 5.15. The increases were less than ten percent when two or four percent carbon was used.

Several evaluations of the ductility of the specimens exposed to scaling conditions can also be obtained from the load-displacement graphs. The toughness of the control samples and samples strengthened with two and four percent carbon is shown in Figure 5.16. An insignificant drop was observed for each of the samples after exposure to scaling conditions. Because the samples exhibited no post crack strength, the author believes that this is a result of a lower deflection at peak load. The flexural stiffness of each of the samples increased by at least 50% after fifty scaling cycles, Figure 5.17.

The second reinforcement type that was studied in this chapter utilized carbon tows. The tows were externally bonded to the tension face of the samples with the inorganic matrix. The area of the carbon reinforcement was increased by bunching the tows in groups of one, two, or three. The load-displacement diagrams generated by the testing of samples strengthened with carbon tows are shown in Figures 5.29-5.34. As in the previously discussed samples, linearly elastic behavior was observed prior to cracking of the concrete. The ability of the samples to sustain load after cracking, however, was greatly improved by the carbon tows. As the area of the carbon was increased, a larger percentage of the cracking load was sustained by the sample.

The results of the flexure testing of samples strengthened with carbon tows are included in Table 5.1. Exposure to scaling conditions had minimal effect on the strength capacity of these samples, Figure 5.19. When a single tow was used, weakening occurred

but samples with two or three tows were strengthened by the exposure. In each case, the variation was less than ten percent. When working with concrete, variations of this magnitude are insignificant and the author believes that they should be disregarded.

The effect of the scaling cycles on the ductility of specimens reinforced with tows is shown in Figures 5.20 and 5.21. An inverse relationship was noted between the toughness and flexural stiffness of the samples. When an increase in toughness was observed, the flexural stiffness of the sample decreased. Likewise, decreases in toughness were caused by an increase in flexural stiffness. Softening of the sample, indicated by a drop in flexural stiffness, will allow a greater midpoint displacement to be achieved before failure of the specimen. The toughness will be increased as the load is supported through a greater displacement. The author believes that variations in the ductility observed in this study are consistent with the uncertainty encountered when working with concrete, not indicative of weakening of the carbon composite system.

Along with the carbon tows previously discussed, layered carbon is currently available for strengthening applications and was studied in this chapter. Either a single or a double layer of the carbon was bonded to the specimens before they were tested in flexure. The resulting load-displacement diagrams are shown in Figures 5.22. The behavior was identical to that of the samples strengthened with carbon tows. Linearly elastic pre-crack behavior was observed while the loads were sustained after cracking of the sample.

Insignificant changes in the flexural strength of the samples were noted after exposure to the scaling conditions, Figure 5.23. Exposed samples maintained at least 97 percent of their flexural strength. Ductility of the samples is indicated by Figures 5.24

and 5.25. Any changes in the toughness or flexural stiffness of the samples are consistent with the slight decrease in failure load and do not indicate significant weakening of the samples.

The strengthening system comprised of layered carbon and the inorganic matrix was proven to be durable in scaling environments. The carbon maintained a strong bond with the concrete and delamination did not occur. The flexural properties obtained from the exposed samples were comparable to those that resulted from the unexposed samples.

5.5 Summary

Exposure to scaling environments is detrimental to the surface of concrete elements used in construction. In this chapter, the ability to prevent such degradation by the application of a protective coating was studied. Because structural concrete of various strengths are used, a high and low strength concrete mix were used in the investigation. The protective coatings studied included two polymer modified cement coatings and three inorganic matrices. The high strength concrete used in this investigation was able to resist scaling without the application of a barrier coating. Slight to moderate scaling was observed in heavy duty samples coated with the Five Star cement coating and the Silicafume3 formulation. The low strength samples were susceptible to surface damage when exposed to the scaling conditions. Each of the barrier coatings improved the performance of the low strength samples. The Miracote coating prevented scaling on the surface of the low strength samples for fifty test cycles. The destruction of the surface of

the low strength samples was significantly slowed or prevented by the application of the Silicafume formulations.

The effectiveness of strengthening applications comprised of FRP can be hampered by exposure to scaling environments. The system studied in this chapter was comprised of an inorganic matrix and various forms of carbon. The results obtained from the flexure testing of these samples indicate that the system is resistant to scaling conditions. The flexural strength and ductility of the specimens were determined before and after exposure to the scaling conditions. Comparable results were observed regardless of the type of carbon reinforcement used.

Table 5.1

Summary of flexural test results obtained using specimens exposed to scaling.

Designation	No. of Scaling Cycles	Peak Load, lb.	Modulus of rupture, PSI	Deflection at peak load in.	Flexural stiffness, lb-in^2	Toughness in-lb.
C,00	None	506.47	1139.56	.0162	1.22 X 10^6	6.38
C,50	50	773.32	1739.97	.0132	2.11 X 10^6	5.54
F2,00	None	785.62	1767.65	.0198	1.43 X 10^6	8.35
F2,50	50	843.67	1898.26	.0134	2.27 X 10^6	6.83
F4,00	None	876.71	1972.59	.018	1.75 X 10^6	8.79
F4,50	50	924.25	2079.56	.0143	2.33 X 10^6	7.56
T1,00	None	897.21	2018.72	.0283	1.14 X 10^6	18.63
T1,50	50	847.19	1906.18	.0169	1.80 X 10^6	13.36
T2,00	None	780	1648.65	.0175	1.60 X 10^6	24.7
T2,50	50	847.65	1907.21	.0415	0.74 X 10^6	38.06
T3,00	None	934.05	2101.61	.0282	1.19 X 10^6	36.99
T3,50	50	1007.79	2267.53	.0156	2.33 X 10^6	32
L1,00	None	962.68	2166.71	.0197	1.76 X 10^6	30.65
L1,50	50	942.85	2121.41	.019	1.79 X 10^6	26.9
L2,00	None	1058.01	2380.52	.0212	1.80 X 10^6	37.37
L2,50	50	1031.1	2319.98	.0281	1.32 X 10^6	32.37

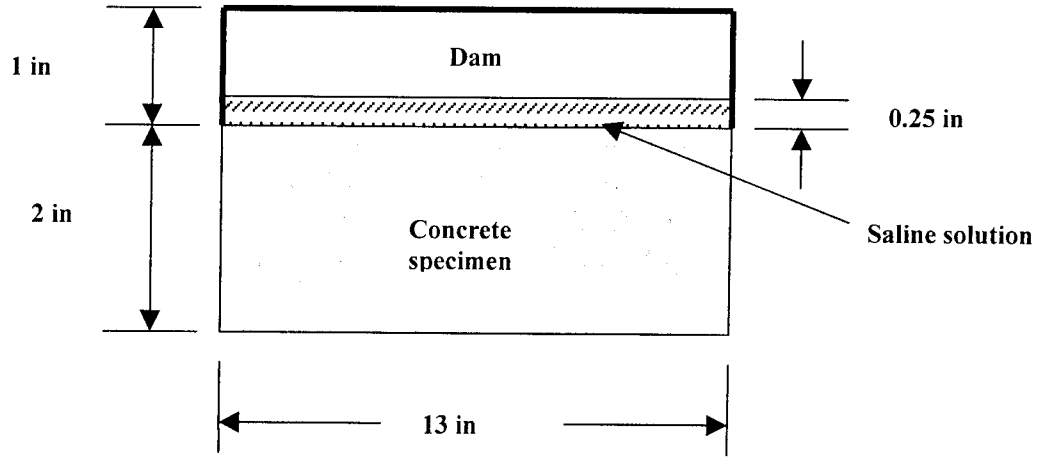

Fig. 5.1. Schematic of scaling test specimen

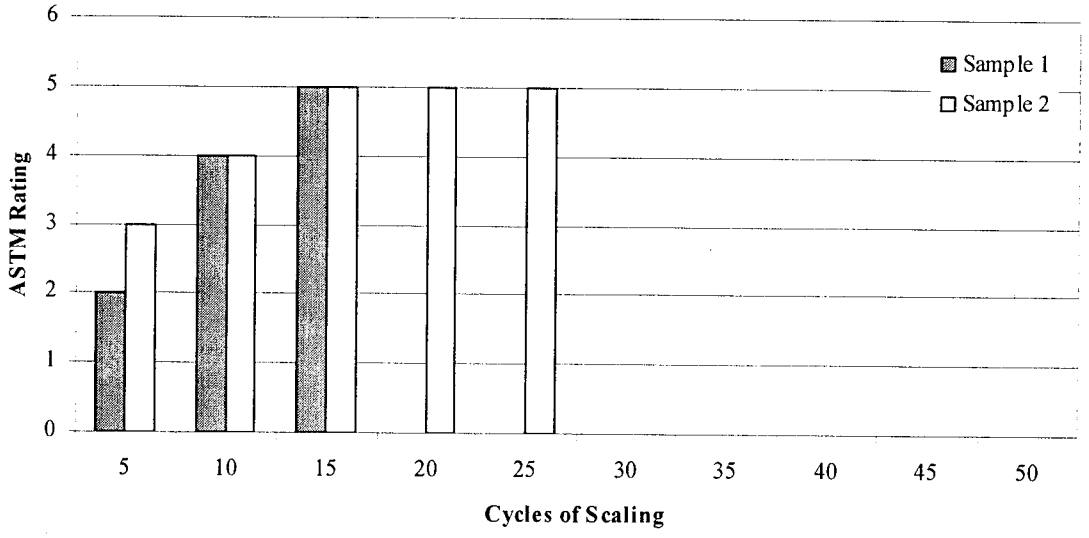

Fig. 5.2. Surface condition of samples subjected to scaling conditions, low strength concrete, control

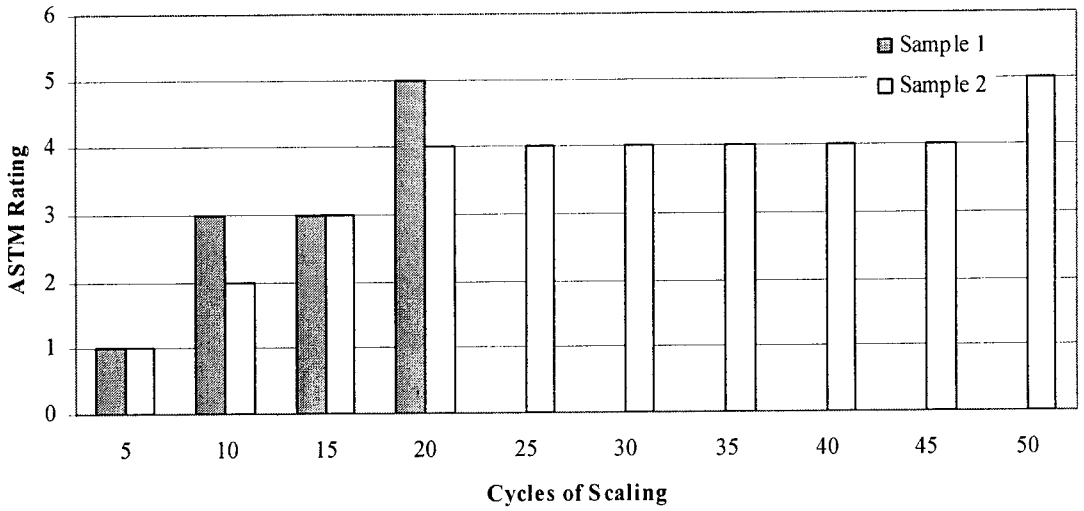

Fig. 5.3. Surface condition of samples subjected to scaling cycles, low strength concrete, Five Star

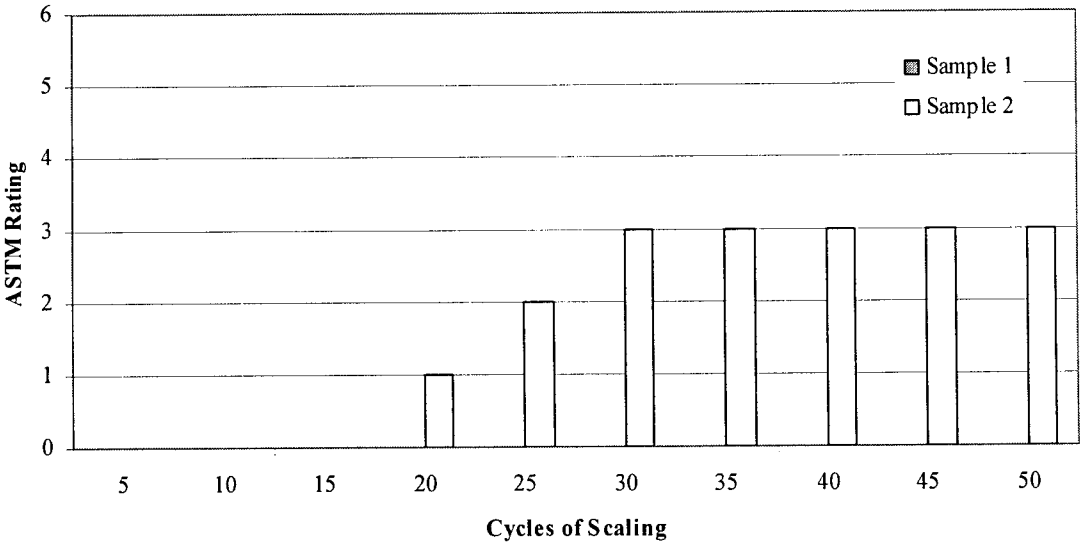

Fig. 5.4. Surface condition of samples subjected to scaling cycles, low strength concrete, Silicafume1

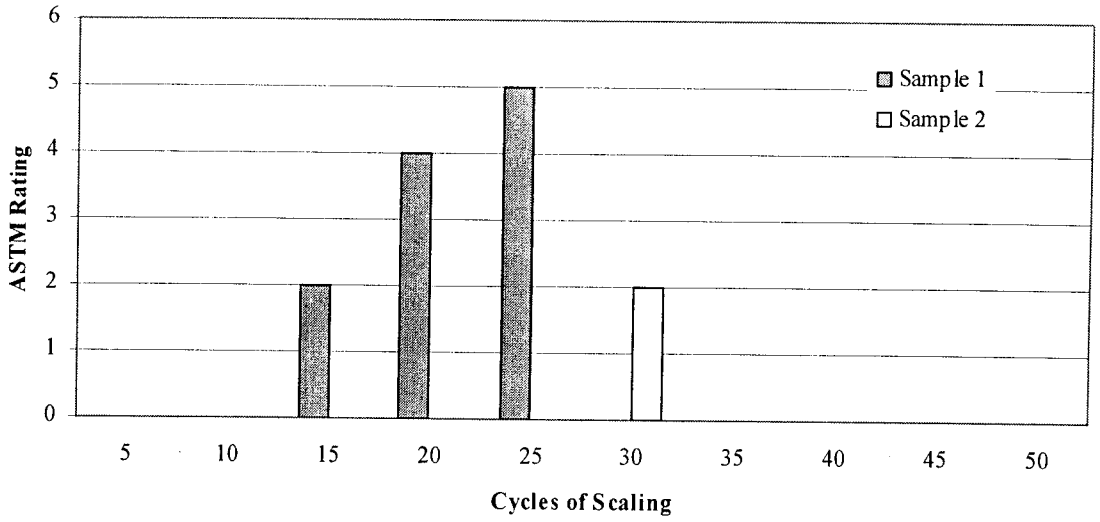

Fig. 5.5. Surface conditions of samples subjected to scaling conditions, low strength concrete, Silicafume2

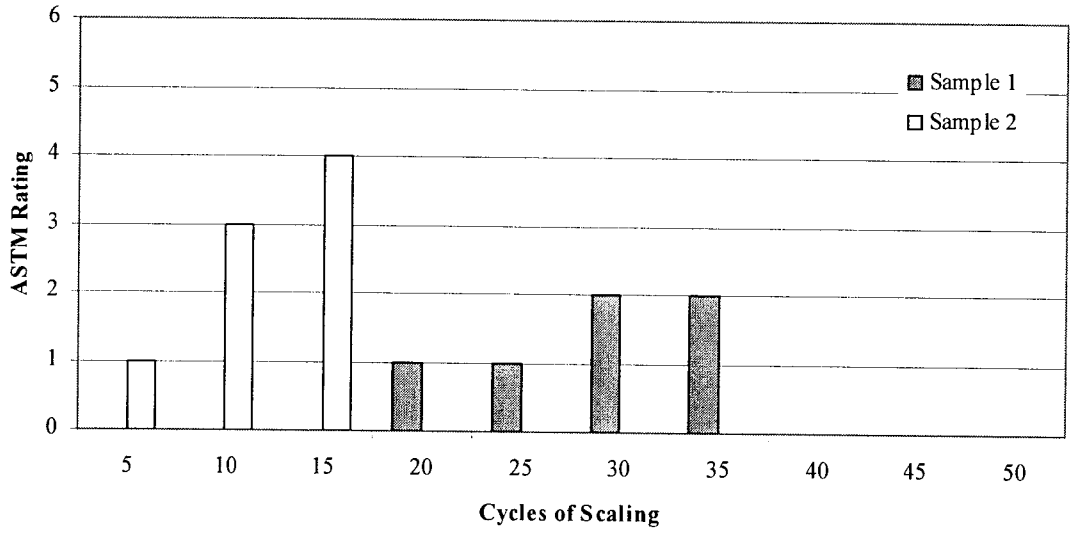

Fig. 5.6. Surface condition of samples subjected to scaling cycles, low strength concrete, Silicafume3

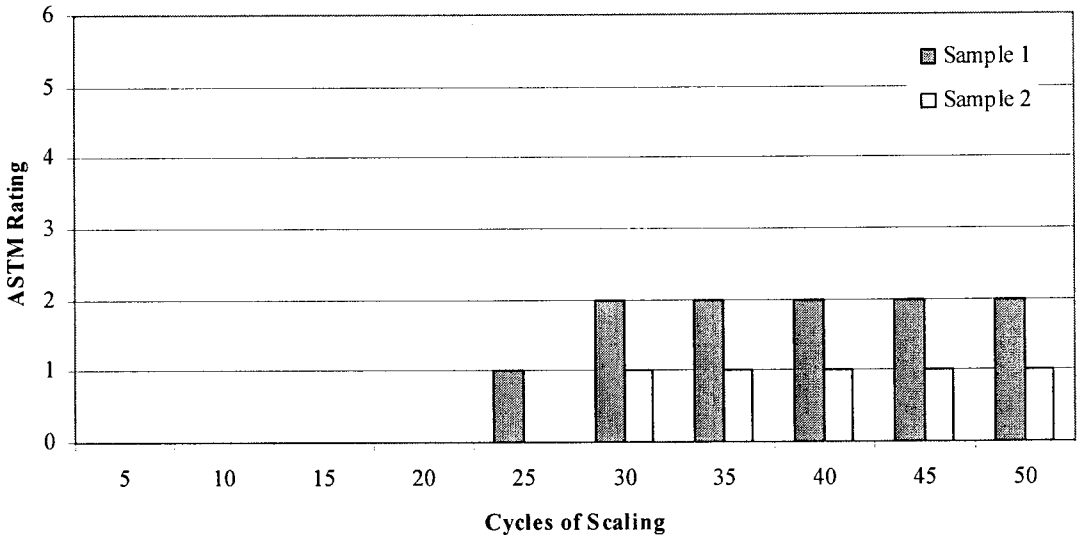

Fig. 5.7. Surface condition of samples subjected to scaling cycles, high strength concrete, Five Star

Fig. 5.8. Control, low strength mortar, 5 cycles of scaling

Fig. 5.9 Five Star, high strength mortar, 35 cycles of scaling

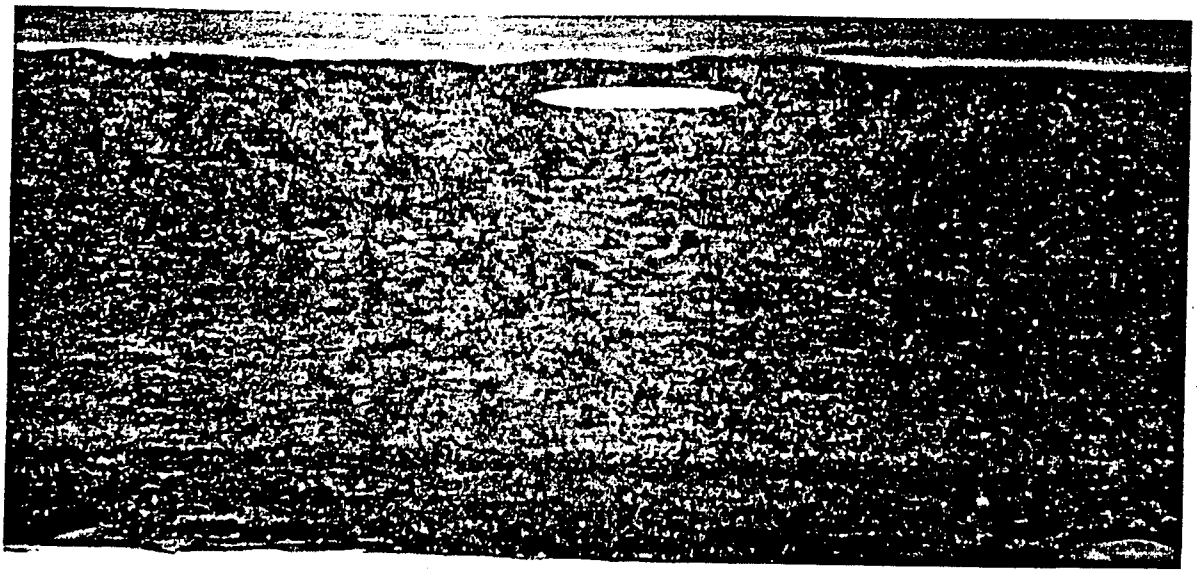

Fig. 5.10. Miracote, low strength mortar, 30 cycles of scaling

Fig. 5.11. Silicafume1, low strength mortar, 20 cycles of scaling

Fig. 5.12. Silicafume2, low strength mortar, 10 cycles of scaling

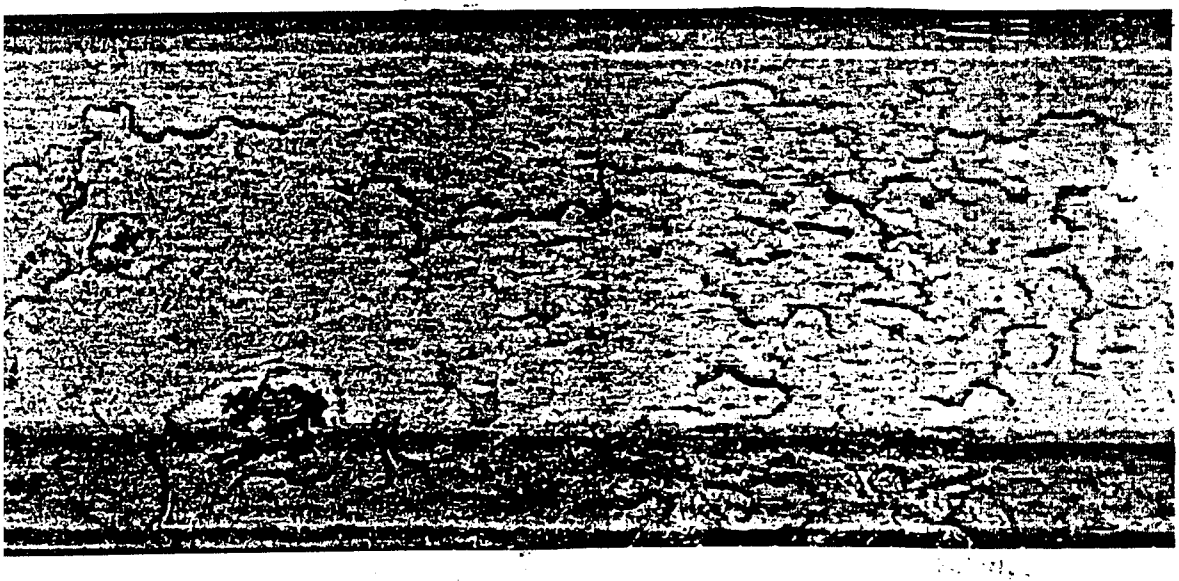

Fig. 5.13. Silicafume3, low strength mortar, 45 cycles of scaling

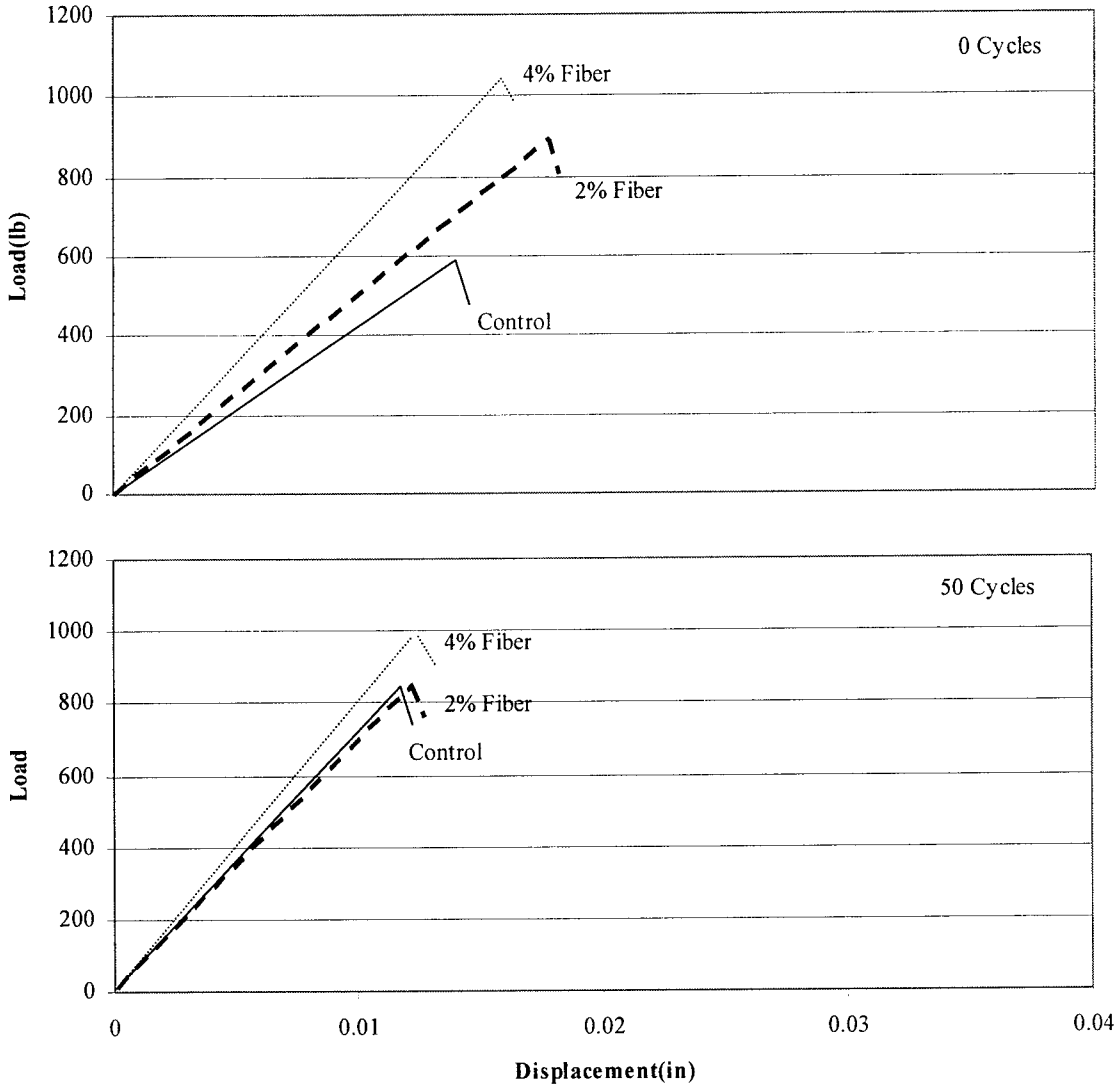

Fig. 5.14. Comparison of load-deflection response; Control, 2 and 4 percent discrete carbon fibers

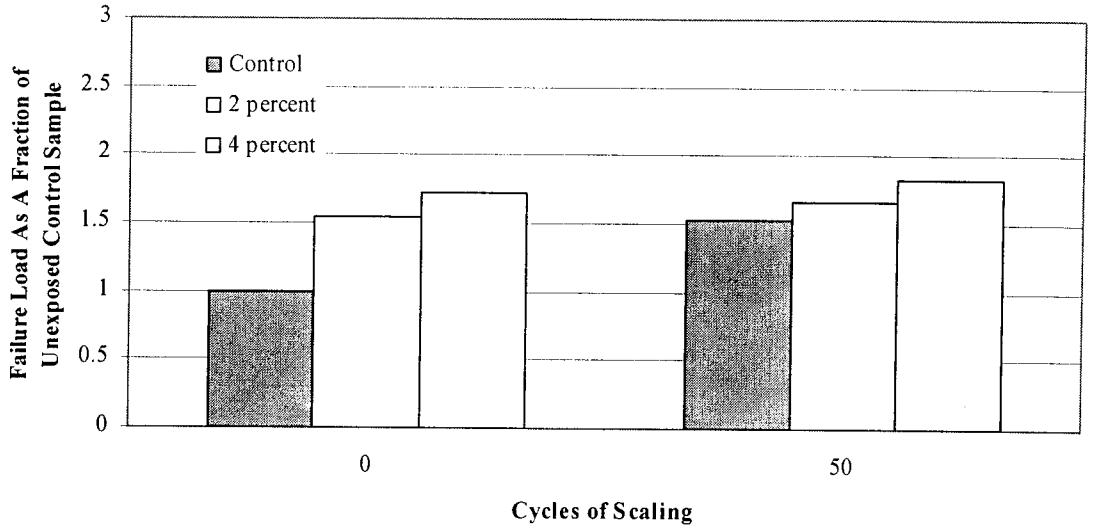

Fig. 5.15. Comparison of failure loads; control, 2 and 4 percent discrete carbon fiber

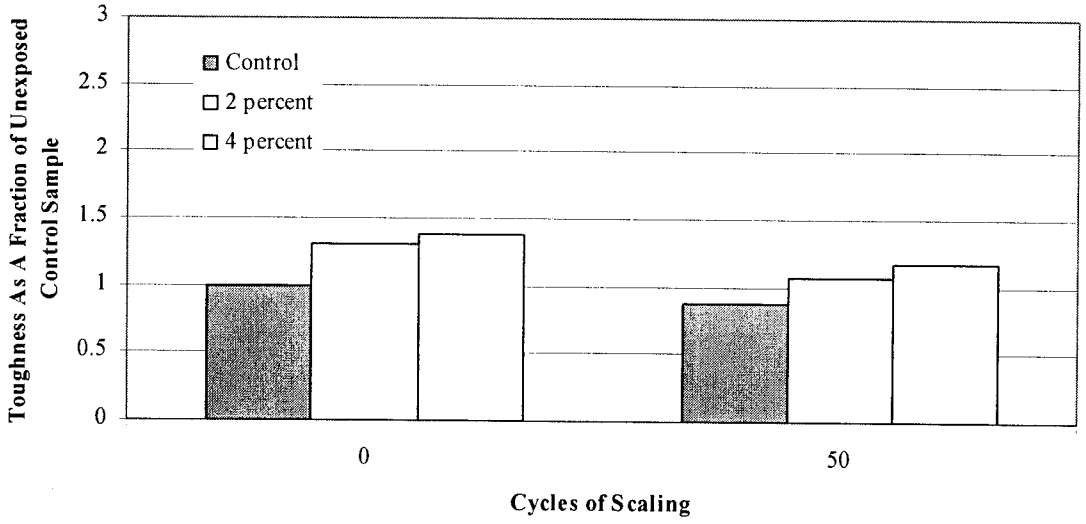

Fig. 5.16. Comparison of toughness; control, 2 and 4 percent discrete carbon fiber

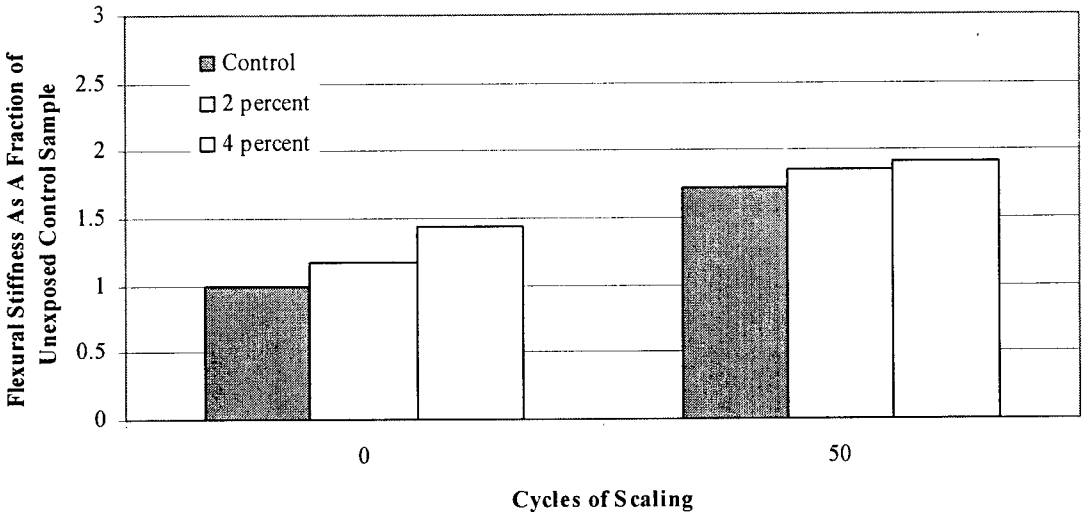

Fig. 5.17. Comparison of flexural stiffness; control, 2 and 4 percent discrete carbon fiber

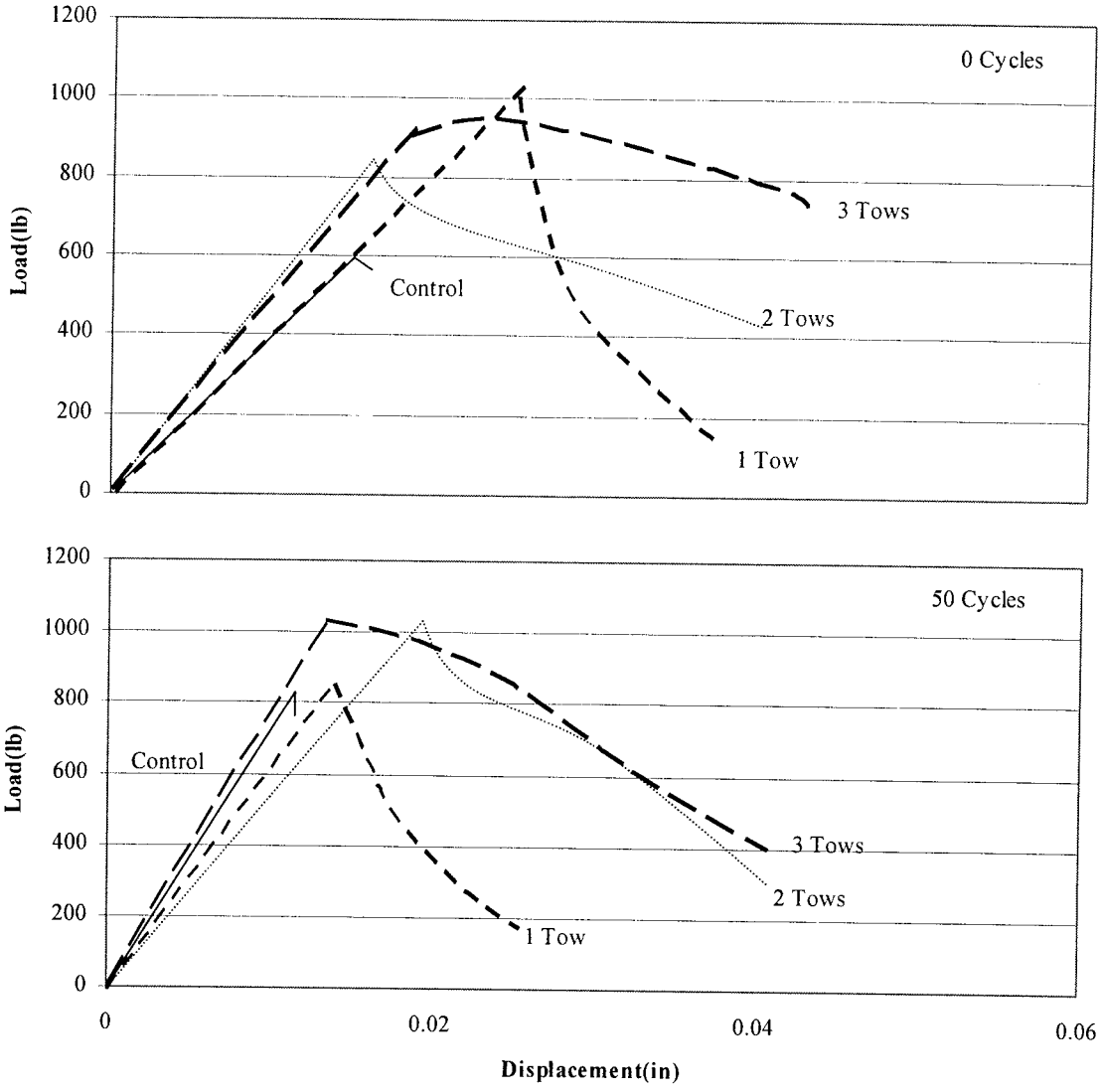

Fig. 5.18. Comparison of load-deflection response; Control, 1, 2, and 3 carbon tows

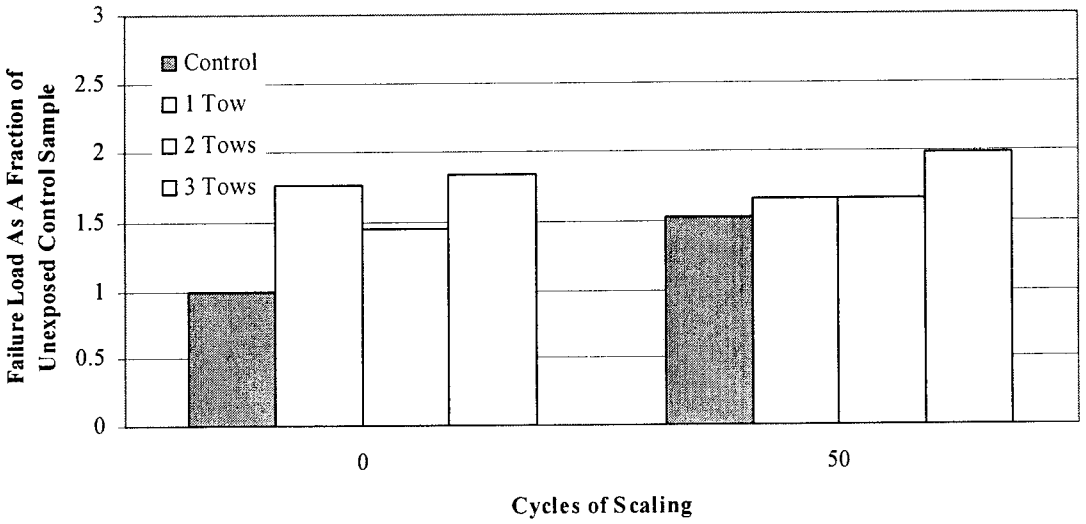

Fig. 5.19. Comparison of failure loads; control, 1, 2, and 3 carbon tows

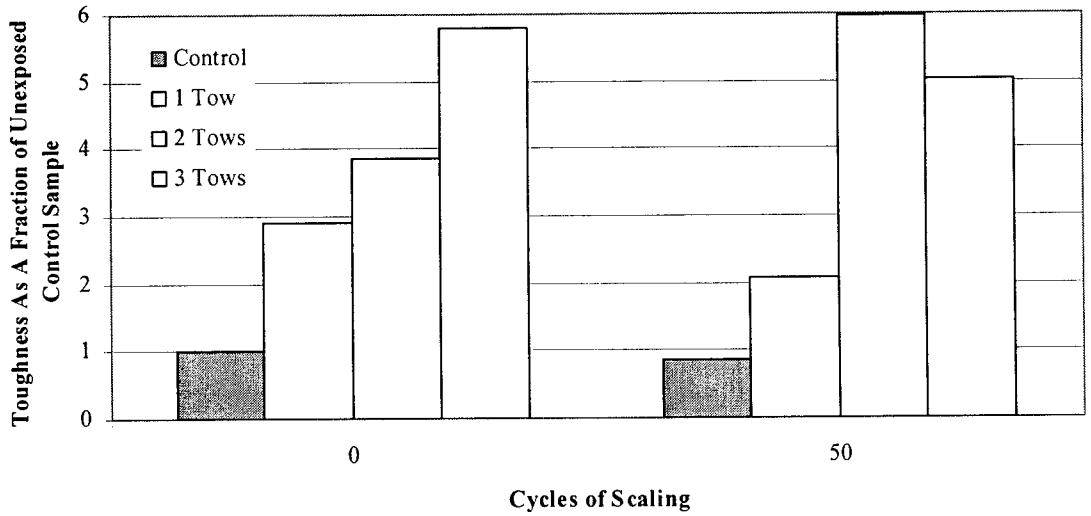

Fig. 5.20. Comparison of toughness; control, 1, 2, and 3 carbon tows

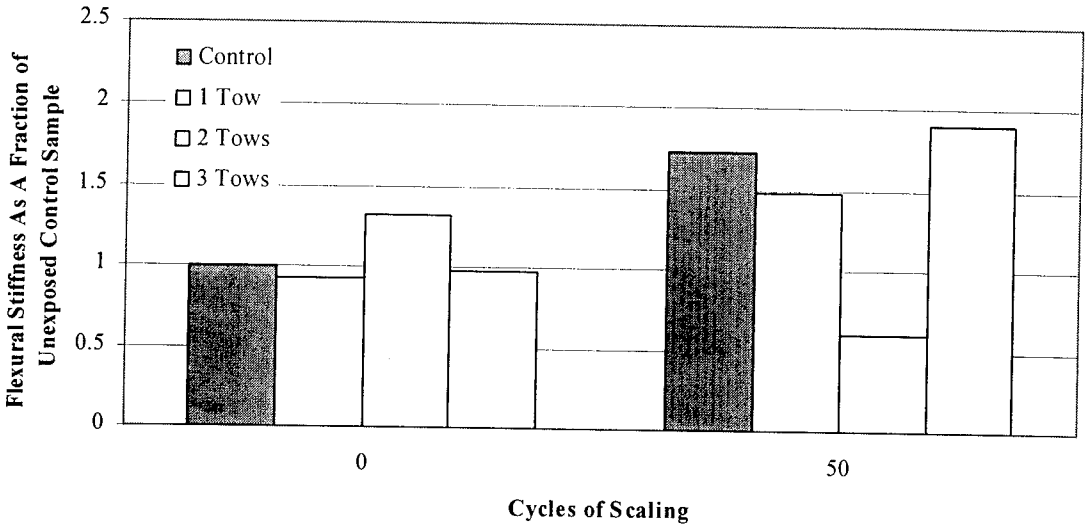

Fig. 5.21. Comparison of flexural stiffness; control, 1, 2, and 3 carbon tows

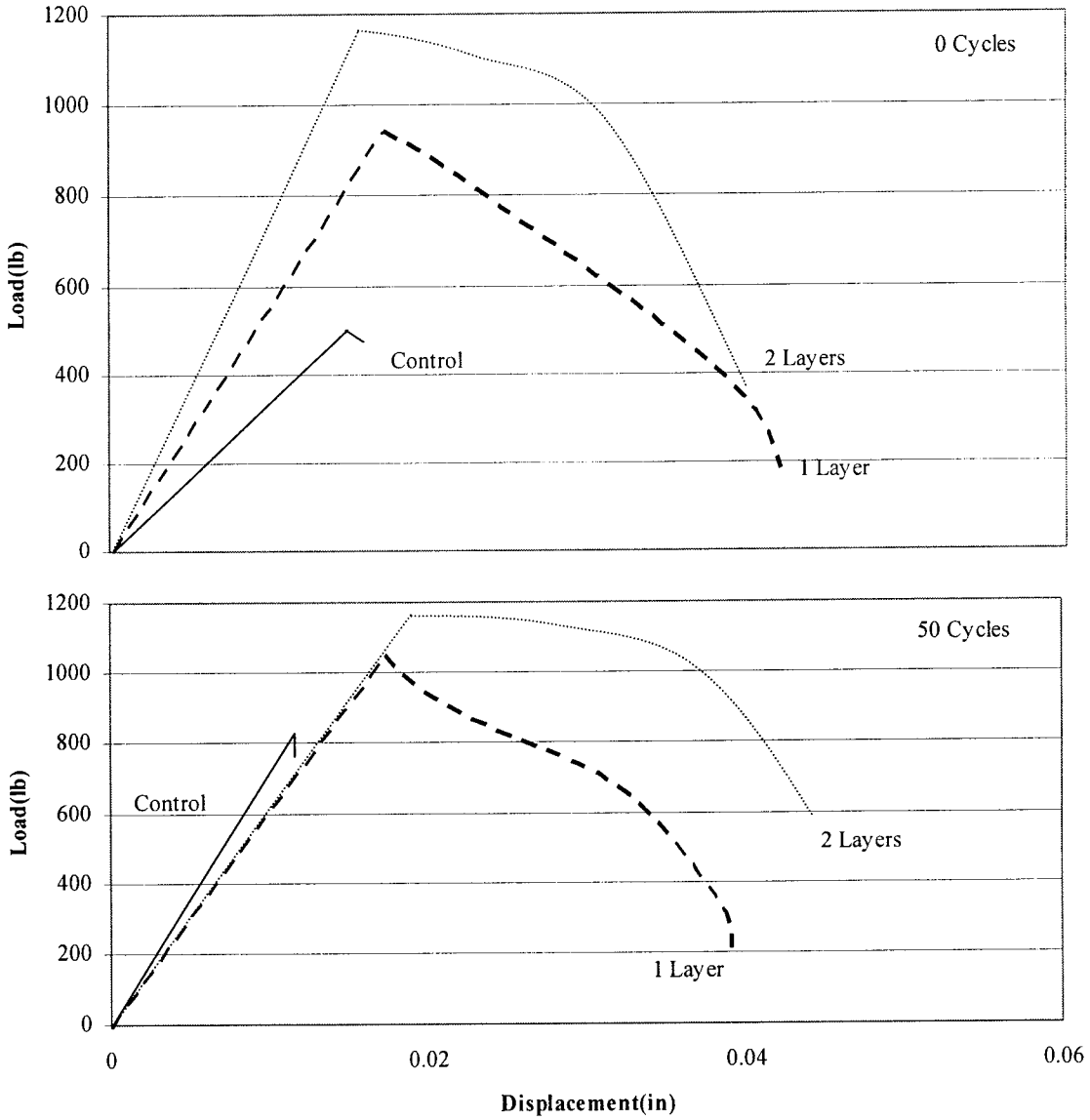

Fig. 5.22. Comparison of load-deflection response; Control, 1 and 2 carbon layers

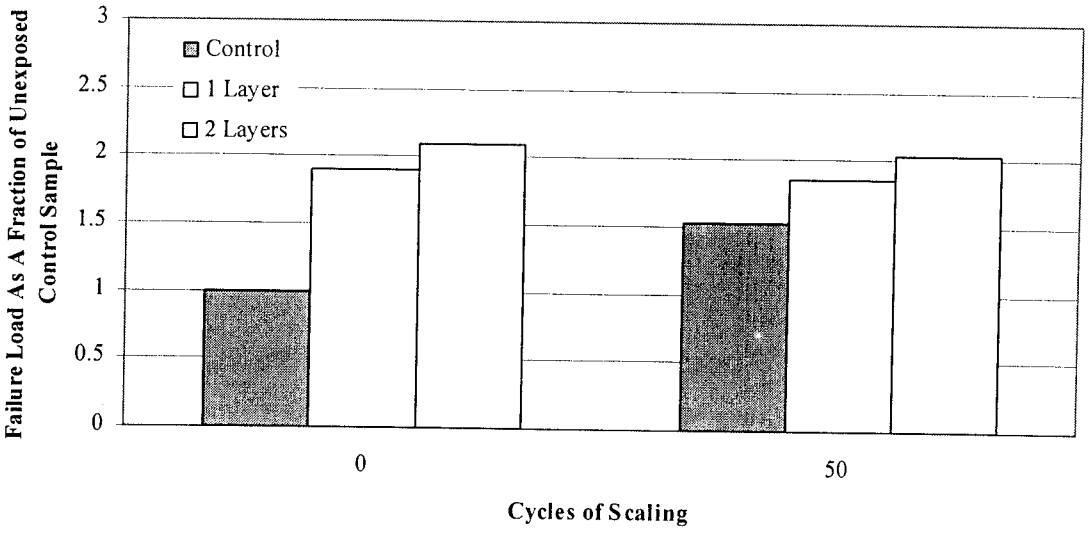

Fig. 5.23. Comparison of failure loads; control, 1 and 2 carbon layers

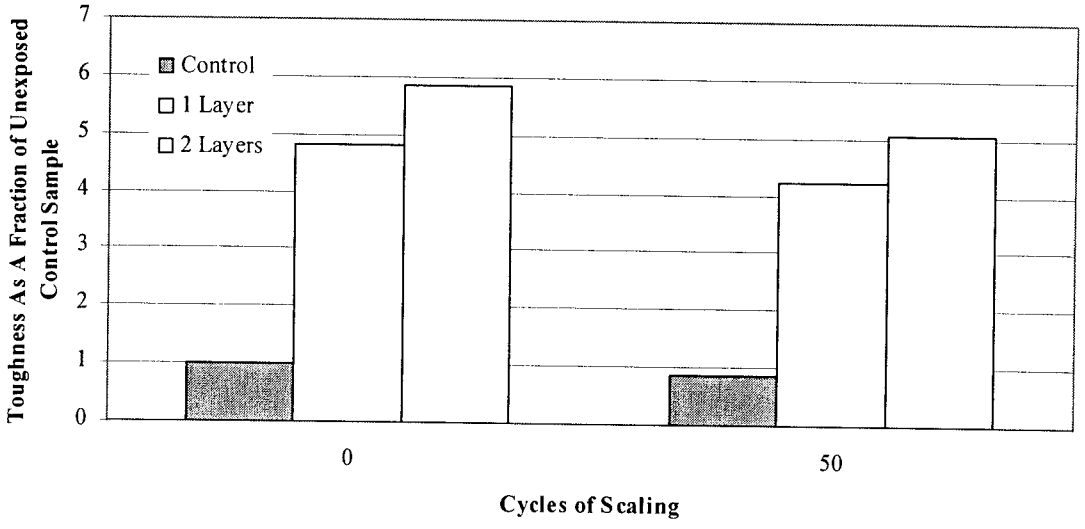

Fig. 5.24. Comparison of toughness; control, 1 and 2 carbon layers

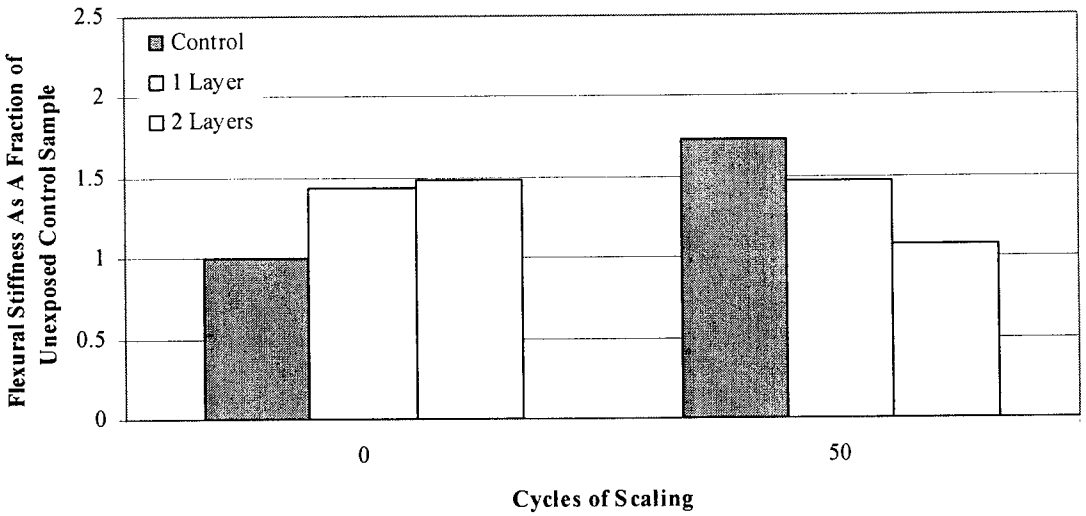

Fig. 5.25. Comparison of flexural stiffness; control, 1 and 2 carbon layers

Chapter 6

Strengthening of Steel Beams

6.1 Introduction

Fiber reinforced composites are currently being evaluated for repairing and rehabilitating concrete and steel elements (Dolan, Rizkalla, and Nanni, 1999). The composites are bonded to the tension face of the elements using a wide variety of currently available matrices. Epoxies and other organic matrices have been used in this capacity for more than five years. Similar results do not exist for the recently developed inorganic matrices. Results presented in this chapter deal with the use of an inorganic matrix for bonding carbon fibers to steel. The study was conducted using steel I-beams which were tested in flexure. Although only minor strength gain was expected, the study was conducted to evaluate the ability of the matrix to form a bond with steel.

6.2 Experimental Design

The effectiveness of a strengthening system consisting of an inorganic matrix used in conjunction with various forms of carbon was evaluated. The matrices were applied to the tension flange of steel I-beams. The strengthening capacity of the system was determined from the flexural properties of the specimens upon completion of flexure testing. The compatibility between the matrix and the steel was also investigated by observing the failure mechanism of each strengthening system.

The study was conducted using commercially available rolled steel sections. Small sections were chosen because the focus was on the feasibility of using an inorganic matrix.

The test samples consisted of I beams strengthened with discrete carbon fibers at two and fours percent, one, two, and three tows of continuous carbon fibers, and one and two layers of carbon fabric. Discrete carbon fiber coating was used as a protective coating.

6.2.1 Preparation of Sample

A standard S3X7.5 steel I-beam was chosen for this study. The dimensions of the section are shown in Figure 6.1. The beams were nineteen inches long.

After the beams had been cut to the appropriate length their surfaces were prepared for the application of the strengthening system. Initially, any excess dirt or rust was removed from the beams with a steel brush. One flange of each sample was then sand blasted with silica quartz sand at a pressure of 100psi. Once again any excess debris or sand was removed from the surface with a wire brush.

The application of the strengthening system occurred in several steps. The components of the inorganic matrix were mixed in a high shear mixer for three minutes to ensure an even distribution of the components. The mix composition is presented in section 3.2.1. An initial thin layer of the matrix was spread across the flange of the beam using a trowel. This was done to fill any voids in the surface of the specimen caused by the high pressure sand blasting. Additionally, this thin layer of matrix helped to ensure proper bonding between the matrix and the specimen. In samples utilizing chopped

carbon fibers in the matrix, a second, slightly thicker layer of the matrix was then applied to the specimens. The total matrix depth was 1mm. When carbon tows or fabrics were used, the carbon was impregnated with the matrix before it was placed on the flange of the specimen. This was accomplished utilizing a hand roller and a spatula. After the carbon was attached to the flanges, an additional protective layer of the matrix was applied. The strengthened specimens were cured for 24 hours at room conditions followed by 24 hours at 80°C. This was done to ensure proper curing at an accelerated rate.

6.2.2 Test Set-Up

A stainless steel testing frame was constructed to support the steel specimens during flexure testing. A schematic of the simple support system is shown in Figure 6.2. The dial gage was attached to the steel support under the testing frame with a magnetic dial gage support. An Ames 282 dial gage with 0.001" precision was used to measure deflection at the center of the beam. A single point load was applied at the mid-span of each specimen.

6.3 Test Procedure

The effectiveness of the strengthening system was determined from the flexural properties of the test specimens. The load was applied to each of the test specimens at a rate of 500 lb/min. At each 500 lb interval, the displacement at the midpoint of the specimen was obtained from the dial gage. This process was continued until the displacement at the center of the test sample was at least two times the displacement when yielding of the specimen began. From these tests, load displacement diagrams for

each of the test specimens were generated. The maximum load and stress were determined from these diagrams along with the modulus of elasticity of the samples. The effectiveness of strengthening was determined by comparing the flexural properties of the control and strengthened samples.

6.4 Analytical Procedure

The strength and stiffness of the strengthened beams were estimated using the standard strength of materials approach. The behavior of the steel was assumed to be elasto-plastic and the behavior of the carbon was assumed to be linearly elastic up to failure. The modulus of elasticity of the carbon and the steel were assumed to be equal. Analysis was completed by calculating the location of the centroid and the moment of inertia of the composite beam. These beam properties used in conjunction with beam bending theory allowed for the prediction of the yield load of each specimen.

The depth of the neutral axis was computed using the first moment of inertia, Figure 6.3.

$$Ay = \sum A_n y_n \qquad (6.1)$$

$$\text{or} \qquad y = (\sum A_n y_n)/A \qquad (6.2)$$

where A_n and y_n are the area and centroidal heights of the individual areas and A and y signify properties of the entire composite beam.

After the centroid of the composite beam was located, the moment of inertia could be determined. Because of the I-shape of the beam, the parallel axis theorem was needed to complete the calculation. The moment of inertia of the individual sub-areas were computed and then shifted to the centroid of the entire composite beam.

$$I = \sum(I_n + A_n d_n^2) \qquad (6.2)$$

where I_n is the moment of inertia in in^4, A_n is the area in in^2, and d_n is the distance to the centroid in inches of the individual sub-areas. I is equal to the moment of inertia of the entire composite beam in in^4. The location of the centroids and the moment of inertia of the control and strengthened samples are presented in Table 6.1.

The load necessary to cause yielding in each of the specimens was determined using the equations associated with simple beam bending. The steel was assumed to yield at a stress of 50,000 psi. Stress in the outermost fiber of each specimen was determined using equation (6.3),

$$\sigma = Mc/I \qquad (6.3)$$

where M is the bending moment at a mid-span of the beam in in-lb., c is the distance from the centroid of the section to the outermost fiber in inches, and I is the moment of inertia of the section in in^4. The yielding stress of the steel was substituted into equation (6.3) and the terms were rearranged to develop an equation for yield moment, M_y

$$M_y = f_y I/c \qquad (6.4)$$

where f_y is the yield stress.

For the simply supported span, yield load, P_y, was computed using:

$$P_y = 4M_y / l \qquad (6.5)$$

where l is the length of the specimen. The upper and lower bounds for the predicted yield load were taken as 5% above and below the result of equation (6.5), respectively.

6.5 Test Results and Discussion

The matrix and the fibers bond well to the steel surface. Matrix reinforced with short discrete fibers can be effectively used as a protective layer for steel. The carbon fiber did not have large delaminations even after yielding of steel.

As expected, the maximum loads did not increase because the carbon area was small compared to the tension flange area. The variations are presented in Figure 6.12.

The load displacement diagrams for samples tested are shown in Figures 6.4-6.11. Two samples were tested for each case. In all samples, behavior was linearly elastic until yielding of the specimen. Then the samples began to exhibit plastic behavior. The slope of the load-displacement curves began to decrease slowly until they were virtually horizontal. The load applied to the mid-point of the specimens began to stabilize as the deflections continued to increase.

The modulus of elasticity of each of the samples was determined experimentally from the elastic part of the load-displacement diagrams. These values are compared in Figure 6.13. The stiffness of strengthened samples increased in all cases except when three tows were used. The authors consider this to be an experimental error.

Moment and load at yielding of the steel, computed using equations (6.4) and (6.5), are presented in Table 6.2 and Figure 6.12. The experimental values were taken from the load-deflection response.

6.6 Summary

The results presented in this chapter indicate that the inorganic matrix can be used as a coating material for steel. Delamination did not occur until the steel had yielded. If

strength improvements are needed, large areas of carbon fiber are necessary. Small amounts of carbon reinforcement can improve the stiffness of steel samples.

Table 6.1

Geometric properties of the specimens

Sample	Carbon Area, in^2	y, in	I, in^4
control	0	1.55	3.5564
2% fiber	0.0019	1.5495	3.5613
4% fiber	0.0039	1.549	3.5662
1 Tow	0.0029	1.549	3.5635
2 Tows	0.0057	1.5486	3.5704
3 Tows	0.0086	1.5477	3.5772
1 Layer	0.0115	1.5471	3.5842
2 Layers	0.023	1.5444	3.6116

Table 6.2

Summary of flexural test results obtained using steel specimens.

Sample	Maximum Load, lb.	Predicted Upper bound, lb.	Predicted Lower bound, lb.	Maximum Stress, PSI	Modulus Of Elasticity PSI
Control	23361	25359	22944	48313	30.9×10^6
2% Fiber	23544	25374	22950	48692	31.4×10^6
4% Fiber	22632	25389	22972	46806	32.3×10^6
1 Tow	22617	25381	22964	46775	32.9×10^6
2 Tows	22051	25399	22980	45604	32.8×10^6
3 Tows	22631	25415	22994	46804	28.8×10^6
1 Layer	22473	25435	23013	46477	34×10^6
2 Layers	23648	25510	23080	48907	34.3×10^6

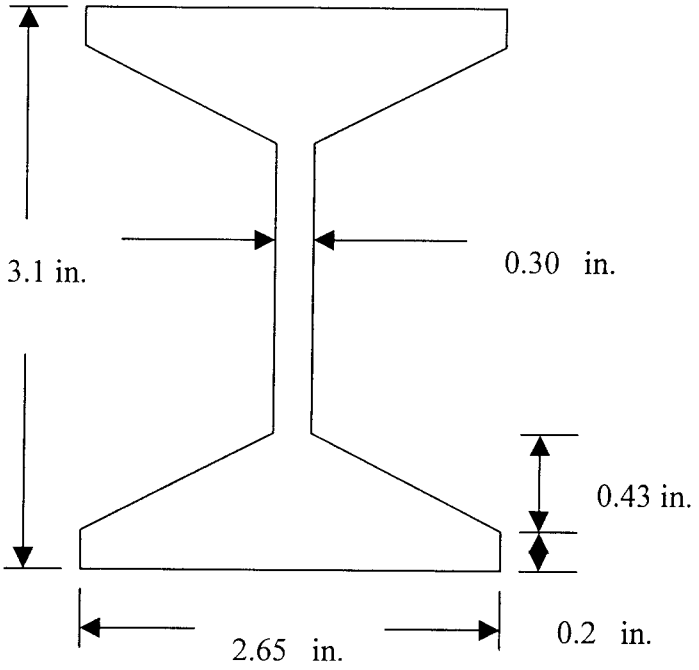

Fig. 6.1 Cross section details of S3X7.5 test specimens

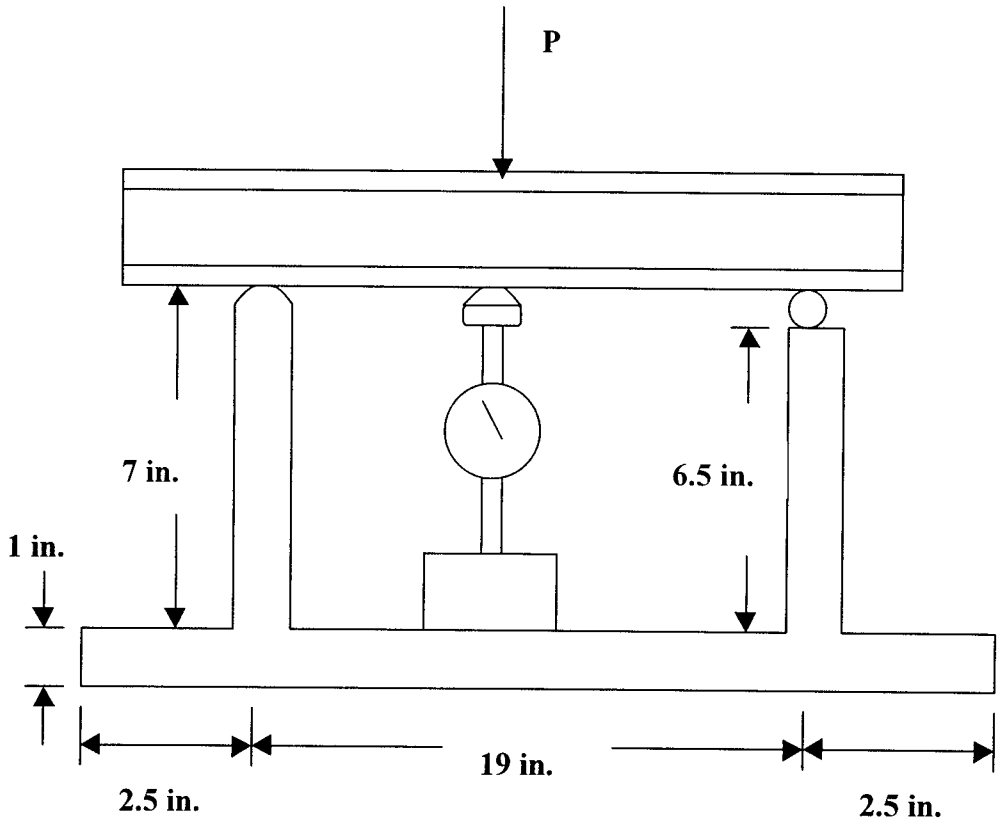

Fig. 6.2. Schematic of test frame for strengthened I-beams

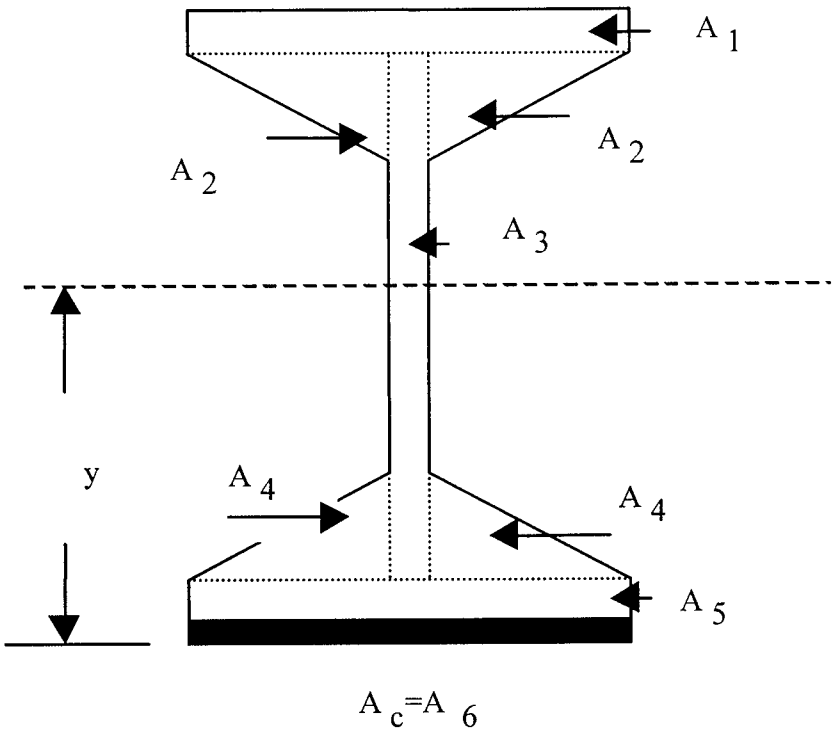

Fig. 6.3. Location of centroidal x-axis in strengthened steel samples.

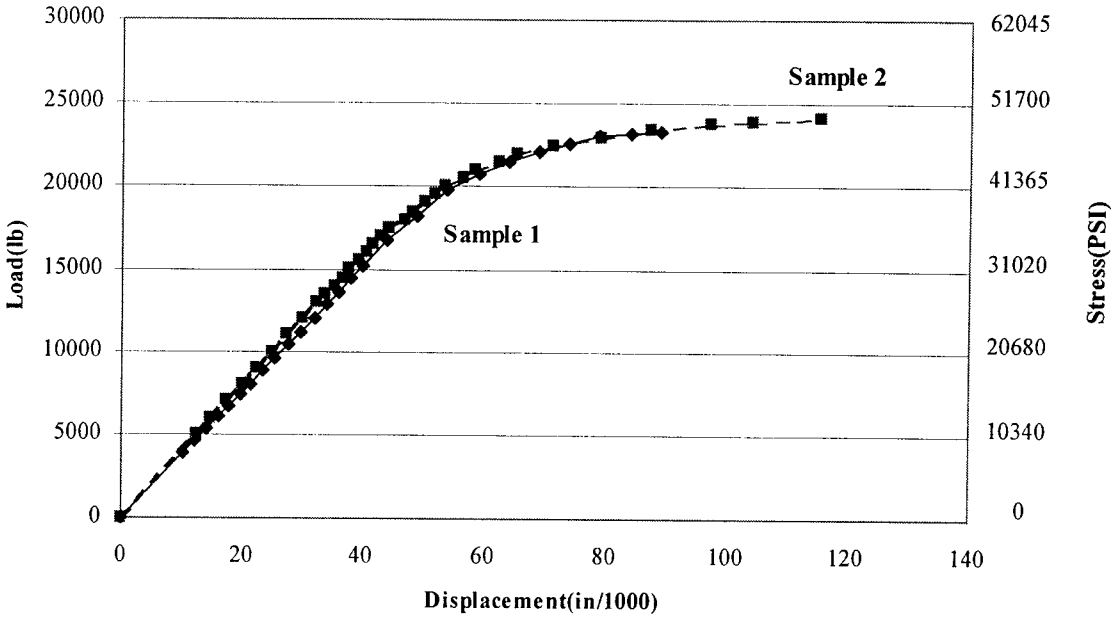

Fig. 6.4. Load vs. displacement, control

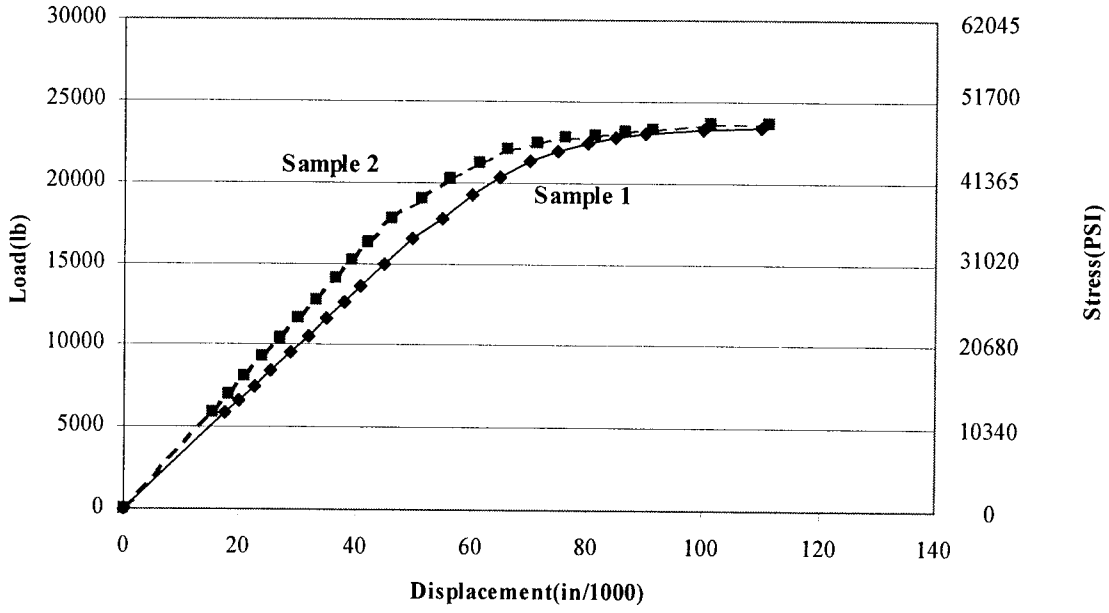

Fig. 6.5. Load vs. displacement, 2% chopped carbon fiber

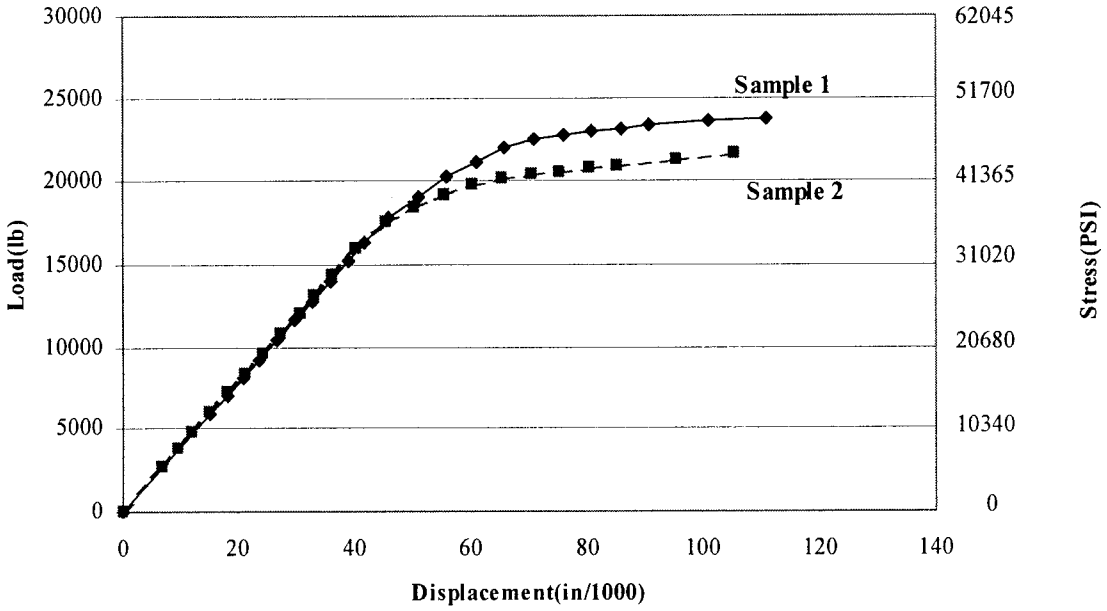

Fig. 6.6. Load vs. displacement, 4% chopped carbon fiber

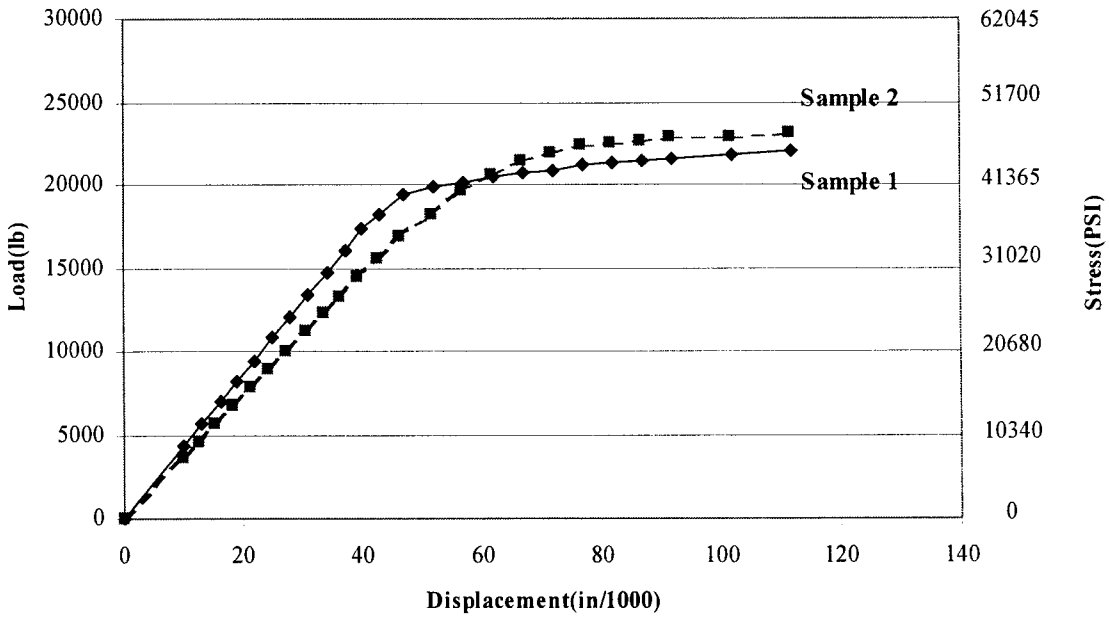

Fig. 6.7. Load vs. displacement, 1 carbon tow

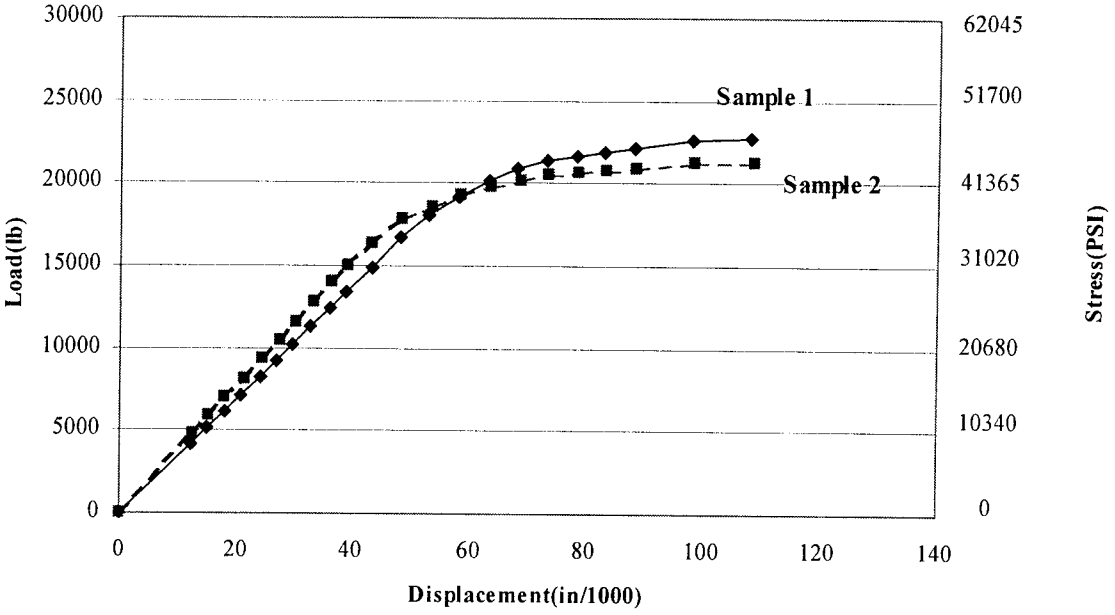

Fig. 6.8. Load vs. displacement, 2 carbon tows

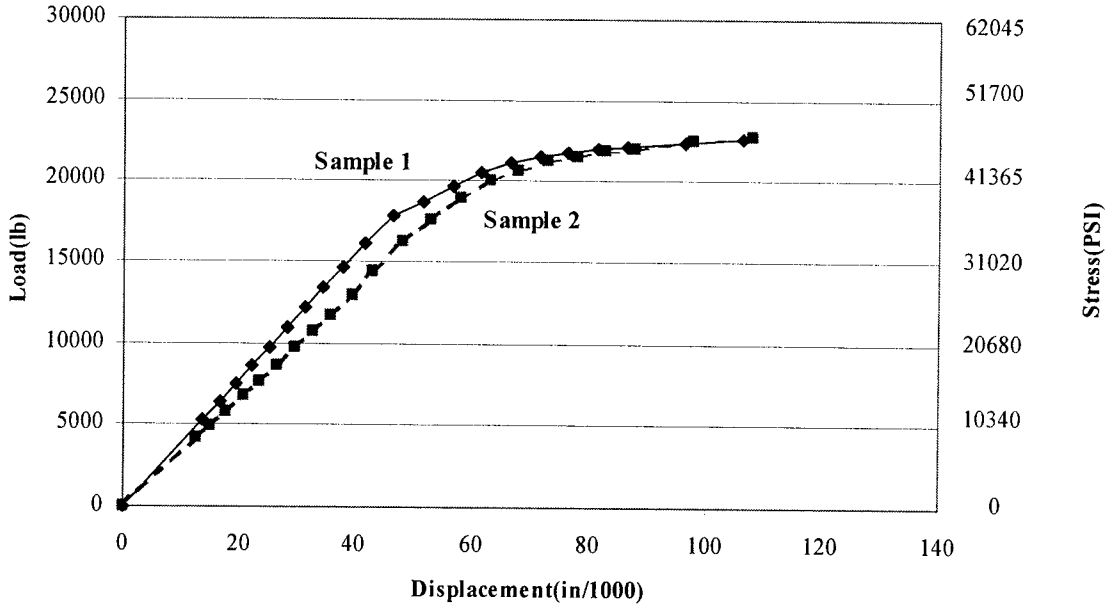

Fig. 6.9. Load vs. displacement, 3 carbon tows

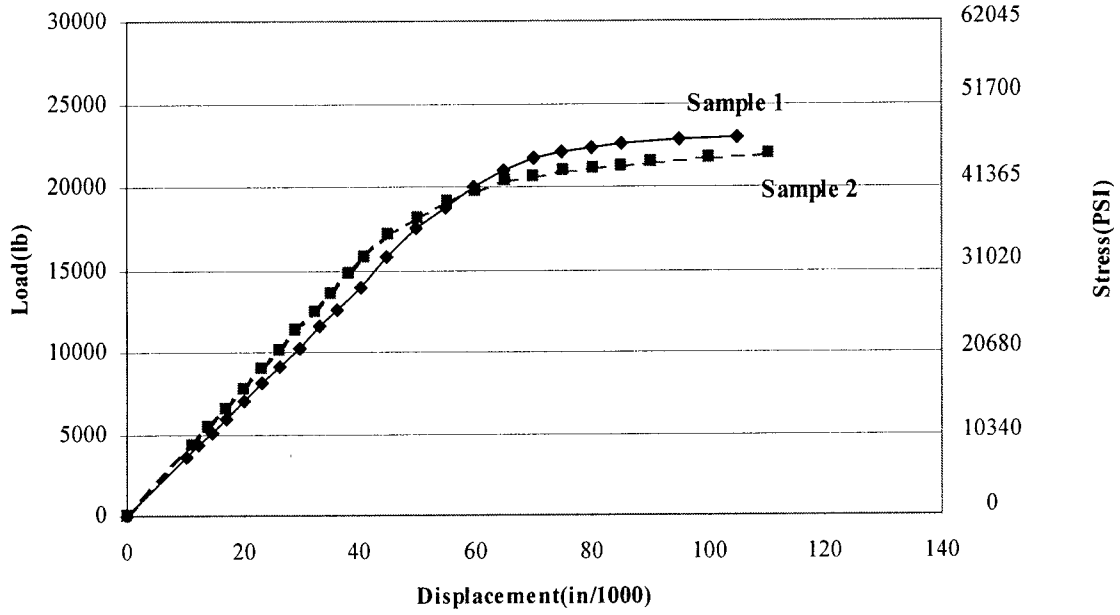

Fig. 6.10. Load vs. displacement, 1 carbon layer

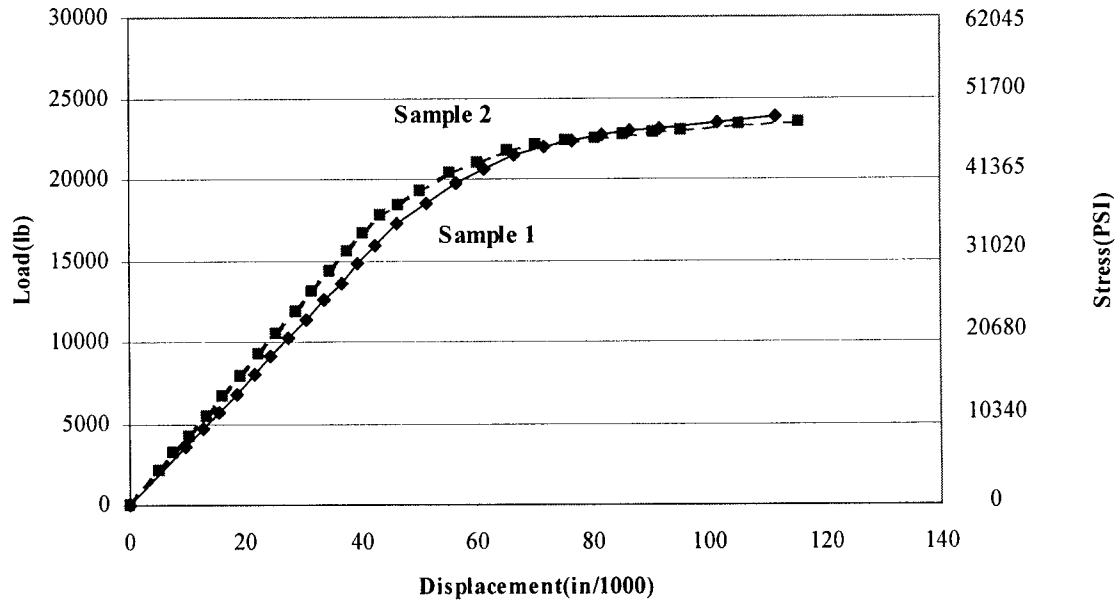

Fig. 6.11. Load vs. displacement, 2 layers of carbon

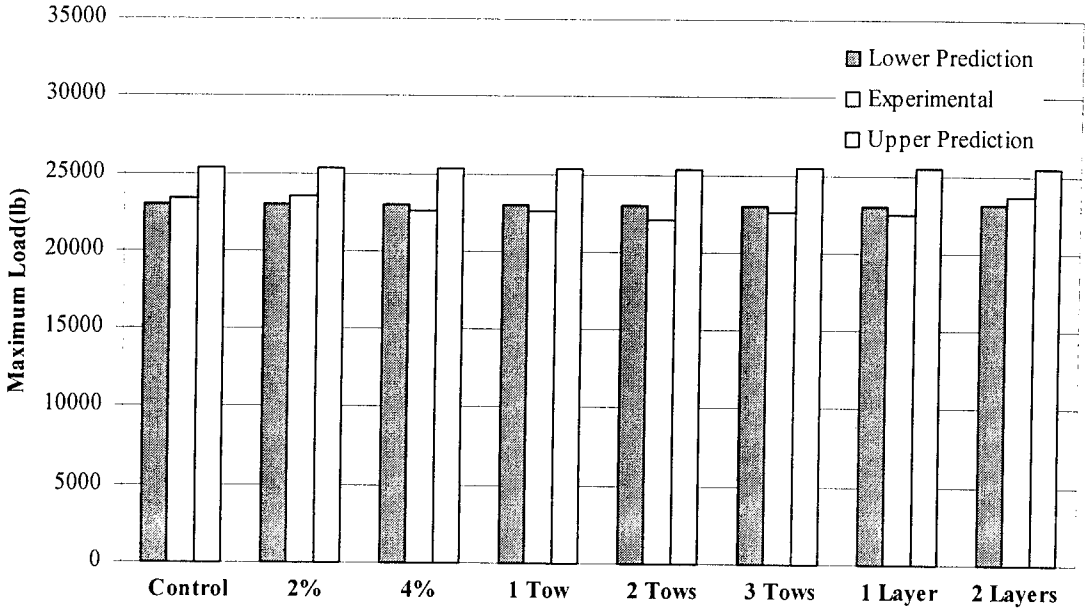

Fig. 6.12. Comparison of maximum loads

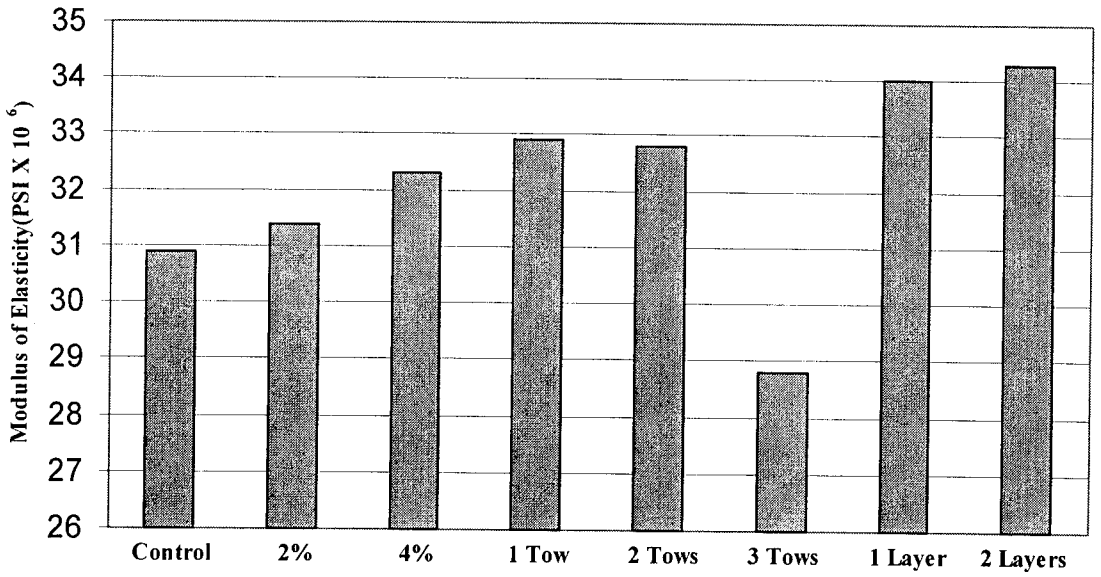

Fig. 6.13. Comparison of modulii of elasticity

Chapter 7

Reinforced Concrete Beams Strengthened with Carbon Fibers and Inorganic Matrix

7.1 Introduction

It is well known that the national infrastructure is in need of major repairs and rehabilitation. A number of repair and strengthening techniques are being promoted. Strengthening of reinforced concrete structures with externally bonded steel plates is one of the techniques developed in the 1960's. Recently, high strength carbon, glass, and aramid composite plates are being promoted as a better alternative to steel plates (ACI Committee 440). The major advantages in using the composite plates are: lightweight, corrosion resistance, and ease of application. The lightweight is a major advantage during construction because heavy equipment is not needed. The composites can also be applied layer by layer resulting in almost a homogeneous final structure.

The major disadvantage of composites is their lack of fire resistance and degradation under UV light leading to long term durability problems. The carbon and glass fabrics can withstand normal fire exposure and are durable under UV light. But the weak link is the organic polymers that are used to attach these fabrics to concrete. Hence, an investigation was undertaken to evaluate the use of the inorganic polymer.

7.2 Experimental Program

A number of investigators have evaluated beams strengthened with carbon fibers and organic polymers. The current experimental program was designed to simulate the research conducted at the Universite de Sherbrooke (M'Ba Zaa, Missihoun, and Labossiere, 1996). This strategy was used to reduce the number of beams to be tested for comparing organic and geopolymers. Four singly reinforced concrete beams that were similar to the Sherbrooke beams were cast and cured for 28 days. Then three of the beams were strengthened using carbon fabrics and geopolymer. Each of the four beams was tested as simply supported beams under four point loading. The details of the beams and experimental procedures are presented in the following sections.

7.3 Details of the Beams

Four reinforced concrete beams that were 10 ft. 6in. (3200 mm) long, 7.875 in. (200 mm) wide and 11.813 in. (300 mm) deep were constructed. These beams were tested over a simply supported span of 9 ft. 10 in. (3000 mm). The reinforcement details of the beams are shown in Figure 7.1. The tension reinforcement consisted of 2 #4 bars. The tension reinforcement was kept to a minimum in order to avoid the shear failure of strengthened beams. The compressive strength of the concrete was 6800 psi. The control cylinders made with all four beams provided consistent compressive strength results.

7.3.1 Strengthening of the Beams

Three beams were strengthened using 2, 3, and 5 layers of unidirectional carbon fabric. The fabric made of T300 carbon fibers had a density of 5 oz/yd^2. After curing,

the bottom surface of the beams were roughened, first by dry grinding followed by sand blasting. These operations removed the weak mortar layer, exposing some aggregates.

The rough surface was primed with a mixture of geopolymer to avoid the loss of geopolymer from fabrics to voids in concrete. The fabrics themselves were impregnated using hand pre-pregging and placed at the bottom surface of the beam. The beam with two layers was allowed to dry for 24 hours and heated to 80° C to cure the geopolymer. For the beams with three and five layers, after placing the fabrics, they were covered with bleeding cloth and a vacuum of about 28 in. of mercury was applied for better adhesion. These beams were also heated to 80° C to facilitate curing.

7.3.2 Instrumentation and Test Set-Up

The beams were instrumented to measure strains in concrete, tension steel, and the composite; and the deflections. The strain values in the composite can be considered only as average values because the gages were glued to both the fibers and the matrix. The beams were simply supported over a span of 9 ft. 10 in. (3000 mm) and two concentrated loads were applied at 3 ft. 3.3 in. (1000 mm) from the supports. The loads were measured using MTS data logging systems.

The loads were applied in 1000 or 500 lb. increments. For each increment of loading, strains, deflections, and crack pattern were recorded.

7.4 Results and Discussion

A summary of results is presented in Table 7.1 which shows loads corresponding to yield and final failure, and mid-span deflections at failure. The load-deflection

responses are presented in Figures 7.2-7.7. The performance of the inorganic-carbon composite and the comparison with the organic-carbon composite are discussed in the following sections.

Mode of Failure

All the strengthened beams failed by rupture of the composite. This shows that geopolymer provides effective adhesion even when five layers of fabric were used. In practice, the number of fabric layers would have been limited to three or four for economic reasons. Hence, if the repair system is properly carried out, failure by delamination of composite can essentially be eliminated. Since the beams were purposely under-reinforced with sufficient shear reinforcement, shear failure did not occur even when the moment capacity was increased by fifty percent over the control beam. As the number of layers increased, the length of composite that ruptures also increases.

Load-deflection behavior and crack patterns

As expected, the stiffness of the beam increased with the number of layers of fabric as indicated by the decrease in deflection shown in Figures 7.2-7.7. The depth of neutral axis seemed to increase with the number of layers. This should also be expected because increased tension force for a given curvature requires increased compressive force. Since the strength of the concrete is the same, the increased compressive force capacity has to come from increased compressive force provided by a larger depth of neutral axis.

The crack patterns of strengthened beams are different from the control beam. Strengthened beams had more cracks and were more closely spaced. As the number of layers increased, the length of the beam over which extensive cracking occurred also increased. Maximum crack widths were smaller for strengthened beams.

Comparison of organic and geopolymer

As mentioned earlier, the beams were designed so as to allow direct comparison of results obtained by Labossiere et al. at the Universite de Sherbrooke. Their control beam had a capacity of 14.3 kips, and their strengthened beam had a capacity of 22.4 kips. Hence, the strengthening provided an increase of about 50 percent. They used three layers of Tonen Unidirectional fabric. The amount of reinforcement in three layers of Tonen fabric is slightly higher than five layers of fabric used in the current study. The beam with five layers also sustained 50 percent more load than the control beam, Table 7.1.

The primary difference between the organic polymer and the geopolymer is the failure pattern. In the Sherbrooke study, the composite peeled off, wheras the composite ruptured in the current study. Delamination failure not only underutilizes the composite strength, but it is also extremely brittle. This type of failure must be avoided in order to provide warning of the impending failure.

The deflections and crack patterns of beams with organic and geopolymers are comparable. The composite in the current study recorded larger strains than the strains reported in the Sherbrooke study.

7.5 Summary

Based on the experimental results obtained in the current study and the results reported by other researchers (ACI Committee 440, 1996, Labossiere et al., 1996, and Nakamura et al., 1996), the following observations can be made.

- Geopolymer can be successfully used to bond carbon fabrics to reinforced concrete beams.
- With proper design and construction process, failure by delamination of composite can be eliminated.
- The performance of geopolymer is better than organic polymer in terms of adhesion. In addition, geopolymer is fire resistant, durable under UV light and does not involve any toxic substances. Geopolymer is water based and no special protective equipment other than gloves is needed. Excess material can be discarded as ordinary waste. This aspect is very important during the construction phase.

Table 7.1

Summary of test results

Beam Design	Load at yielding of steel, kips	Failure Load, kips	Deflection at Failure, in.	Flexural Stiffness kip-ft^2	Mode of failure
Organic Matrix					
Control	10.13	14.3	3.5	5589	Steel yield
Tonen	15.13	22.4	1.1	9409	Delamination
Inorganic Matrix					
Control	13	16.8	3.7	8575	Steel Yield
2 Layers	16.5	18.1	0.79	9610	Composite Rupture
3 Layers	17	20.7	0.92	10595	Composite Rupture
5 Layers	19	24.8	0.95	11768	Composite Rupture

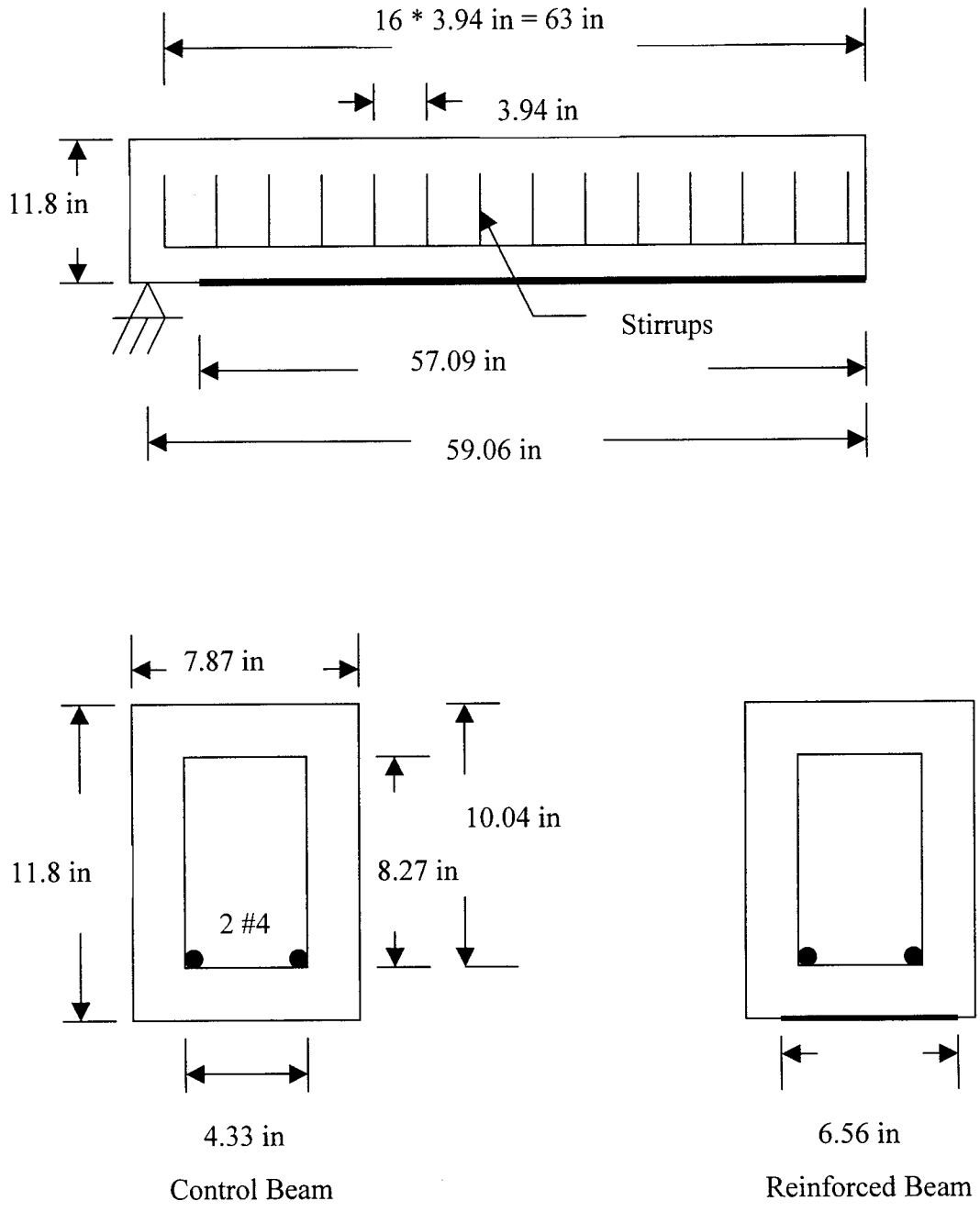

Fig. 7.1 Reinforced concrete beam cross sections

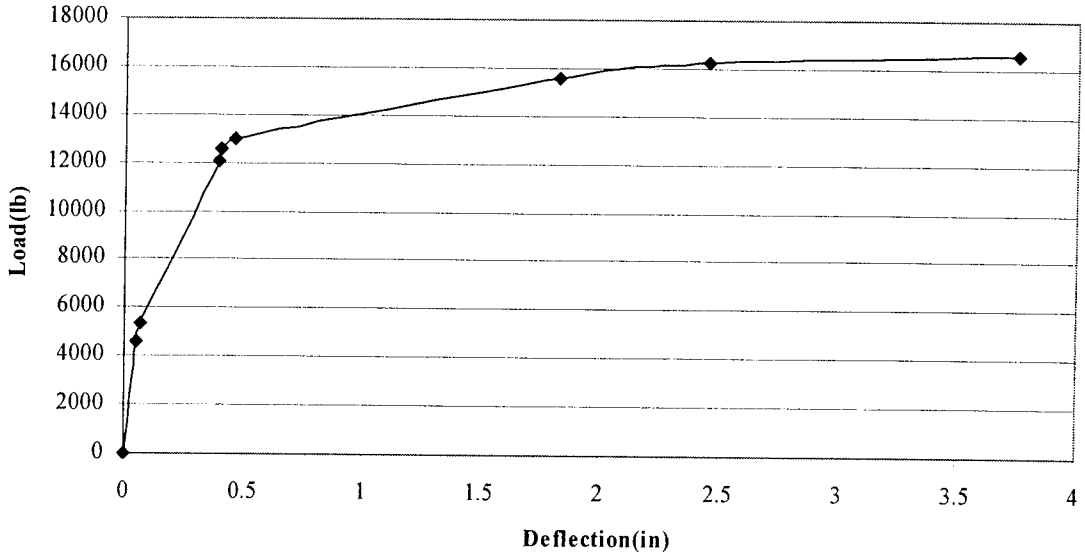

Fig. 7.2. Load-deflection response, control beam

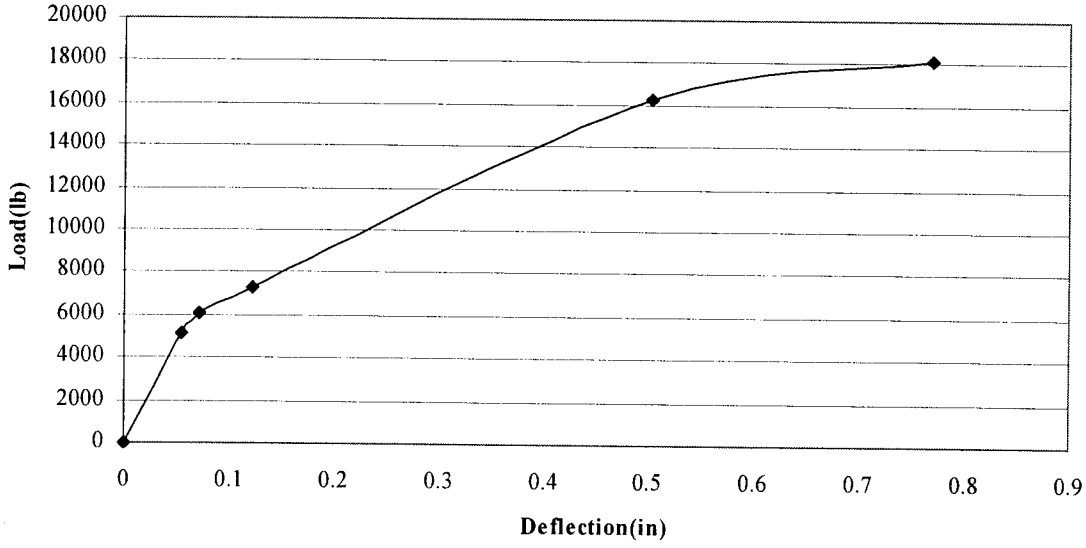

Fig. 7.3. Load-deflection response, beam strengthened with two layers CFRP

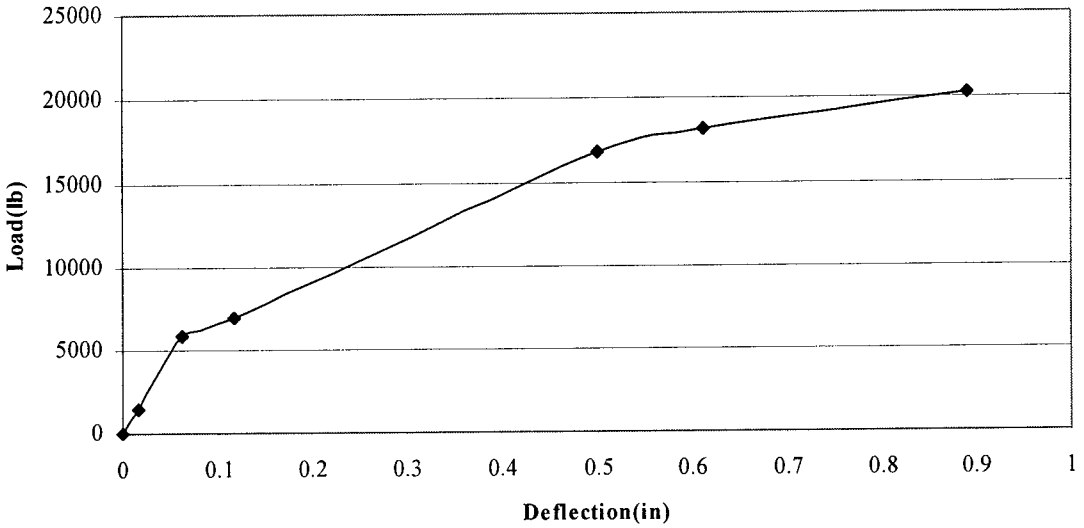

Fig. 7.4. Load-deflection response, beam strengthened with three layers CFRP

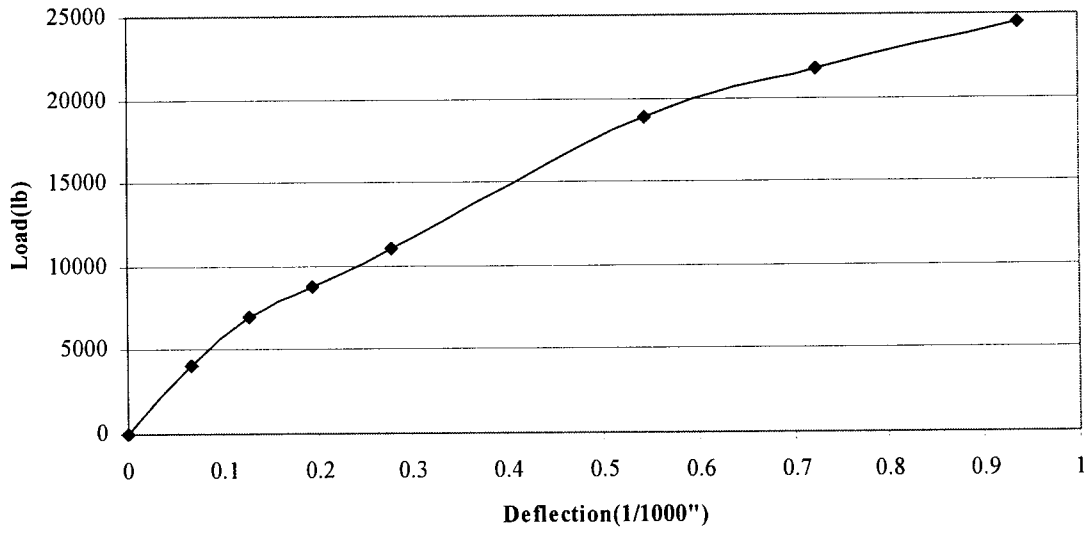

Fig. 7.5. Load vs. deflection response, beam strengthened with five layers CFRP

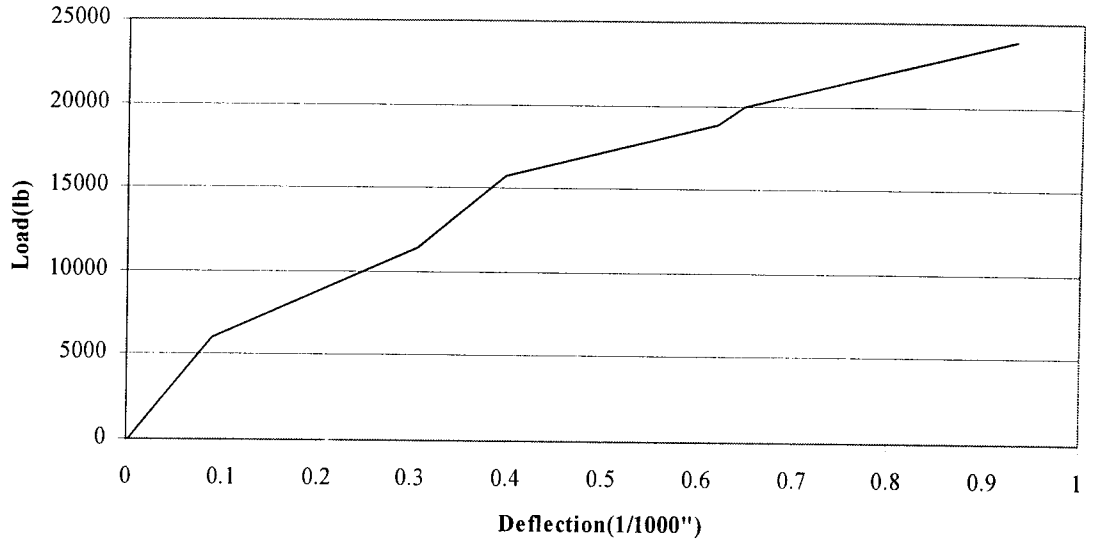

Fig. 7.6. Load vs. deflection response, beam strengthened with organic matrix

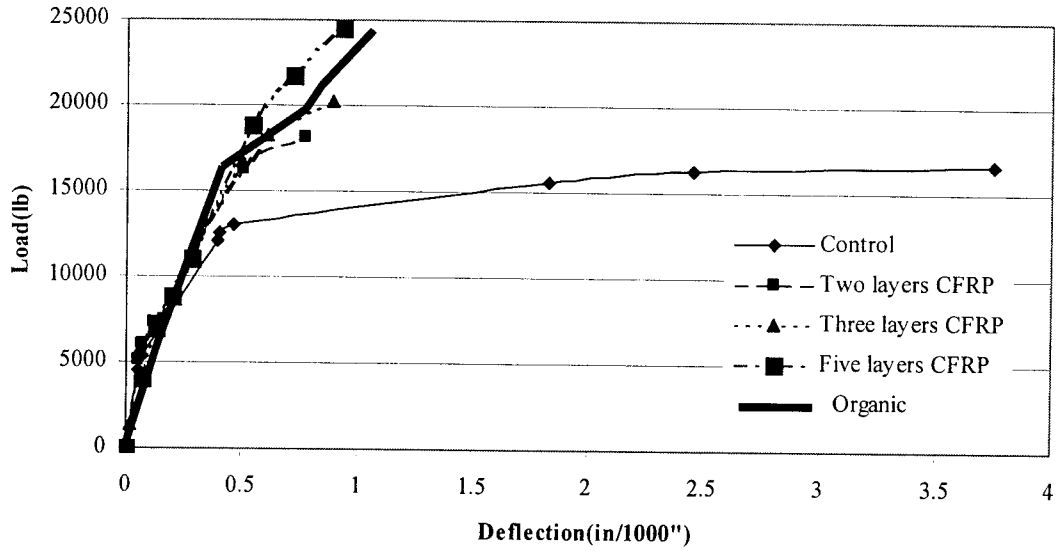

Fig. 7.7. Load vs. deflection response, all beams

Chapter 8

Analytical Investigation

8.1 Introduction

Analytical procedures have been developed by a number of authors for the analysis of reinforced concrete beams strengthened with carbon fibers and organic matrix (Saadatmanesh and Ehsani, 1991, Ritchie et al, 1991, and M'Bazaa et al, 1996). The procedures developed for organic matrices are not directly applicable to inorganic matrices because of their limited strain capacity. The results presented in this chapter focus on the following areas for which published information is lacking.

The first part deals with unreinforced concrete strengthened with high strength fibers. The results are applicable for unreinforced walls, abutments, and piers. Even though some reinforcement is provided in piers and abutments, the reinforcement ratio is very low and hence, their behavior is similar to unreinforced concrete. The analytical procedure for this class of structural elements was developed using the experimental results of plain concrete beams strengthened with both inorganic and organic matrices.

The second set of procedures was developed for reinforced concrete beams strengthened with carbon fibers and inorganic matrix. Existing procedures were modified to account for the lower modulus of the composite and cracking of the matrix. The cracking of the matrix reduces the fracture strain of the carbon fibers due to stress concentrations at the cracks.

The third part of this chapter deals with the design procedure for reinforced concrete beams strengthened using organic polymers. A parametric study was conducted

that focused on the following variables that have not been fully addressed in the published literature.

- Influence of failure carbon strain on the moment capacity of strengthened beams.
- Influence of the reinforcement ratio of the parent concrete on the magnitude of strength increase provided by high strength fibers.

These two factors have considerable impact on the design strength of rehabilitated beams.

A flow diagram was developed as an aid for the designer. This diagram is based on the established procedures and new guidelines for choosing the carbon strain. Both working stress and strength design approaches are presented.

8.2 Analytical Procedure – Plain Concrete with Inorganic and Organic Matrix

The classical mechanics of materials approach was used to analyze the behavior of the beams. In addition to the standard assumptions such as plane sections remain plane and perpendicular to the neutral axis, the following additional assumptions were made.

- Since the amount of reinforcement is small, the concrete was assumed to remain linearly elastic up to failure. This assumption was verified by computing the maximum stress in the concrete at failure.
- The behavior of the carbon fibers was assumed to be linearly elastic up to failure. Only fiber area was used for strength computations. Note that the inorganic matrix cracks at low strains and organic matrix has a very low modulus compared to the carbon and in both cases the force contribution of the matrix is negligible. The tows,

fabrics, and sheets were comprised of carbon fibers with a modulus of elasticity of 200 Gpa(29 X 10^6 psi). This value is based upon the results obtained for coupons cut from carbon composite plates (Foden, Balaguru, and Lyon, 1996) and the manufacturer's specifications for the unidirectional carbon sheet.

- The carbon fiber contribution depends upon the amount of reinforcement. Even though the fracture strain of carbon is 1.5%, this strain is never achieved in the beams. Carbon plate with inorganic matrix fractures at a lower strain because of the non-uniform distribution of stress and local micro-delamination at the cracks. In the case of organic matrix, a larger fiber volume promotes delamination before the failure, resulting in a lower average carbon strain at failure. The experimental results were used to estimate the fracture strain using the procedure described in the next section.

Estimation of carbon fiber strains at failure

Carbon fiber strains were computed using the deflection at peak load. A transformed section, similar to the one used for reinforced concrete was used to develop a relationship between moment and maximum stress. The cross section, strain, and stress distribution are shown in Figure 8.1. The tension force contribution of the concrete is neglected.

Since the concrete behavior is assumed to be linearly elastic, the depth of the neutral axis, kh, can be computed using the following equation:

$$b(kh)^2/2 = n_f A_f(h - kh) \qquad (8.1)$$

where A_f = area of the carbon fiber

b = width of the beam

h = thickness of the beam

kh = depth of the neutral axis

n_f = modular ratio(modulus of elasticity of carbon, E_f / modulus of elasticity of concrete, E_c)

The resisting moment, M, can be computed using the equation:

$$M = bkh(f_c / 2)(h - (kh)/3) \qquad (8.2)$$

where f_c = maximum concrete stress. Note that equations (8.1) and (8.2) are applicable for both working load and failure load as long as the maximum stress in the concrete does not exceed about 60 percent of the compressive strength.

Experimental results presented in Chapter 5 and the following procedure was used to estimate the strain in the carbon when failure occurred. Using the experimental failure load, the maximum concrete stress, f_c, was computed using equation (8.2). Once f_c is known, the maximum concrete strain, ε_c, was estimated as:

$$\varepsilon_c = f_c / E_c \qquad (8.3)$$

Using similar triangles, Figure 8.1c, carbon strain at failure, ε_{fu}, can be determined using:

$$\varepsilon_{fu} = \varepsilon_c[(h - kh) / h] \qquad (8.4)$$

The failure strains computed using equation (8.4) were found to be a function of the carbon area used for strengthening. The carbon area was expressed as a reinforcement ratio, ρ_f, using the equation:

$$\rho_f = A_f / bh \qquad (8.5)$$

Verification of ε_{fu} with respect to ρ_f is shown in Figure 8.2. A statistical regression showed that the relationship is exponential for both inorganic and organic matrices. The strain at failure for the inorganic matrix was lower than that for the organic matrix, Figure 8.2. The beams reinforced with one tow and the inorganic matrix were not used in the statistical regression because for these beams, the author believes that the tension force

contribution of the concrete should not be neglected. High failure loads indicate that both carbon fibers and tension zone concrete provide force contributions.

The maximum concrete stress at failure, f_c was much less than 50 percent of the compressive strength for all beams and therefore the assumption that the stress-strain behavior of concrete at failure was elastic is valid.

Computation of moment capacities

Based on the aforementioned discussion, the following procedure can be used for the computation of moment capacity of strengthened beams.

Given: section width, b; section thickness, h; area of carbon reinforcement, A_f; modulus of elasticity of carbon, E_f.

$$\text{Modular ratio, } n_f = E_f / E_c \qquad (8.6)$$

where E_f = modulus of elasticity of carbon

If E_c is not given, it can be estimated using the equation (ACI Committee 318, 1995):

$$E_c = 4730 \sqrt{f_c'} \text{ N/mm}^2 \qquad (8.7)$$

Compute depth of the neutral axis, kh, and moment capacity, M, using equations (8.1) and (8.2), respectively. In most instances, the concrete will be under a certain stress when the carbon is applied due to the existing loads. The author believes that this stress will be very low for plain concrete elements and hence can be neglected for the computation of ultimate moment capacity.

In equation (8.2), the value for maximum stress, f_c, can be estimated using the following procedure. Based on the carbon area, estimate the fracture strain of the carbon, ε_f, using the following equations:

$$\text{Organic matrix: } \varepsilon_{fu} = 0.0084e^{-120.04\rho_f} \qquad (8.8)$$

$$\text{Inorganic matrix: } \varepsilon_{fu} = 0.125e^{-315.95\rho_f} \qquad (8.9)$$

where ρ_f = carbon reinforcement ratio = A_f / (bh). Equations (8.8) and (8.9) were developed using the experimental results, Figure 8.2.

The maximum concrete strain, ε_c, can be computed using:

$$\varepsilon_c = \varepsilon_f [\, kh / (h-kh) \,] \qquad (8.10)$$

Then the maximum concrete stress:

$$f_c = E_c \varepsilon_c \qquad (8.11)$$

Evaluation of analytical model

The estimated failure loads are compared with experimental values in Tables 8.1 and 8.2. Since the failure strains of carbon were estimated using the experimental results, the predictions were accurate for the current set of data, Table 1.

The model was also evaluated using published results (Huang, 1995, Toutanji and Gomez, 1997). Moment capacities were predicted using 100 and 80 percent of the modulus of the carbon fiber. Typically, fiber tows and unidirectional fabrics tend to have a lower modulus because of undulations present in fiber bundles. The two sets of values can be used as lower and upper bounds for strength prediction. Huang tested concrete prisms reinforced with carbon tows and carbon fabrics using an inorganic polymer. He

also used more carbon reinforcement as compared to the current investigation. The results are compared in Table 2.

The model was also used to predict the results of an analysis conducted using a different organic matrix. The investigation conducted by Toutanji and Gomez deals with the effectiveness of externally bonded carbon in repair and rehabilitation of concrete structures. The predictions made by the failure strain model developed in this paper are shown in Table 2.

The failure strain model developed in this paper provides reasonably accurate results for samples tested by Huang. Experimental values for samples reinforced with six tows as well as two, three, and four layers of carbon fell within the range predicted by the model. The observed data for the specimen reinforced with nine carbon tows was slightly greater than the prediction. In the case of the organic matrix, for sample C1, the experimental maximum load is within the range. For sample C2, the model overpredicts the load by a small margin.

Summary

For both organic and inorganic matrices, the average fiber strain at failure decreases with an increase in fiber area. The analytical procedure presented in this section provides reasonably accurate results.

8.3 Analytical Procedure – Reinforced Concrete Strengthened with Carbon Fibers and Inorganic Matrix

Reinforced concrete beams strengthened with carbon fibers and organic matrix usually fail by delamination of the carbon composite plate. When an inorganic matrix is

used, however, failure is almost always by fracture of the carbon. An analytical procedure for predicting moment capacities when an organic matrix is used has been developed and it's accuracy has been verified with experimental data. The inorganic matrices are relatively new and the experimental data is limited to the results presented in Chapter 7. In this section, the ability to predict the moment capacity of reinforced concrete beams strengthened with inorganic matrix using the method developed for organic matrices is studied.

Details of Analytical Procedure: Ultimate Load

In the first step of the analysis procedure, the depth of the equivalent rectangular stress block was located by equating the compressive force of the concrete with the tension forces of the reinforcing steel and carbon plate. The strain in the extreme compression fibers of the concrete was assumed to be in the non-linear range at fracture of the carbon composite. The depth of the equivalent stress block, a, can be computed using:

$$a = (A_s f_y + A_f E_f \varepsilon_{fu}) / 0.85 b f'c \qquad (8.12)$$

where f'_c = compressive strength of the concrete

b = width of beam

f_y = yield stress of the steel reinforcement

A_s = area of the steel reinforcement

A_f = area of carbon reinforcement

E_f = modulus of elasticity of carbon

ε_{fu} = strain of carbon at failure

The nominal resisting moment of the beam was then found using equation (8.13).

$$M_n = A_s f_y (d - a/2) + A_f f_f (h - a/2) \qquad (8.13)$$

The concrete strain at failure of the carbon composite was determined, equation (8.14).

$$\varepsilon_c = \varepsilon_{fu}[\, c / (h-c)\,] \qquad (8.14)$$

where c = depth of the neutral axis = a / β_1 (ACI Committee 318, 1995)

$\beta_1 = 0.85$ for $0 < f'_c < 4000$ psi

$\beta_1 = 0.85 - 0.05[\,(f'_c - 4000) / 1000]$ for $4000 \text{ psi} < f'_c < 8000$ psi

$\beta_1 = 0.65$ for $f'_c > 8000$ psi

If ε_c calculated in equation (8.14) was greater than 0.002, the nominal moment capacity calculated in equation (8.13) is correct. However, if ε_c was less than 0.002, then the concrete was in the linear portion of the stress-strain relationship and an alternative method needs to be used to find the nominal moment capacity. The compression force, C, and the tension force, T, can be expressed as:

$$C = T$$

$$C = bc(f_c / 2) \qquad (8.15)$$

$$T = A_s f_y + A_f E_f \varepsilon_{fu} \qquad (8.16)$$

In equation (8.15), the depth of neutral axis, c, and the compressive stress of the concrete, f_c, are unknowns. Using similar triangles, a relationship between the depth of the neutral axis and the strain in the concrete at failure of the carbon composite can be expressed as:

$$c = h[\, \varepsilon_c / (\varepsilon_c + \varepsilon_{fu})] \qquad (8.17)$$

By substituting equation (8.17) into equation (8.15), the compressive force of the concrete is determined as,

$$C = (bh/2)[\varepsilon_c / (\varepsilon_c + \varepsilon_{fu})] E_c \varepsilon_c \qquad (8.18)$$

By equating the tension forces in equation (8.16) with the compressive force of the concrete in equation (8.18), the strain in the concrete at failure of the carbon, ε_c, is found. The depth of the neutral axis, c, is then determined using equation (8.17). The nominal moment capacity of the beam can be found using equation (8.19).

$$M_n = A_s f_y(d - c/3) + A_f E_f \varepsilon_{fu}(h - c/3) \qquad (8.19)$$

Details of Analytical Procedure: Working Loads

At working stress levels, deflection needs to be calculated for checking against maximum allowable deflection. Since the deflection is controlled by the flexural stiffness, EI, these values were computed and compared with experimental values. The depth of the neutral axis in the working stress analysis was determined in equation (8.20)

$$b(kd)^2/2 = n_s A_s(d - kd) + n_f A_f(h - kd) \qquad (8.20)$$

After solving equation (8.20) for k, the moment of inertia for the cracked section and the effective moment of inertia at working load are found using equations (8.21 and 8.22).

$$I_{cr} = b(kd)^3/3 + n_s A_s(d - kd)^2 + n_f A_f(h - kd)^2 \qquad (8.21)$$

$$I_{eff} = I_{cr} + (I_g - I_{cr})(M_{cr}/M_a)^3 \qquad (8.22)$$

Cracking moment;

$$M_{cr} = (I_g / 0.5h) f_r \qquad (8.23)$$

Modulus of rupture;

$$f_r = 7.5\sqrt{f'_c} \qquad (8.24)$$

I_g was assumed to be $bh^3/12$ and the working load (moment) was taken as 60 percent of the ultimate moment. Once I_{eff} is known, the flexural stiffness is:

$$\text{Flexural Stiffness} = E_c I_{eff} \qquad (8.25)$$

Comparison of predicted and experimental results

The experimental results presented in Chapter 7 were used for comparison. Moment capacities and flexural stiffness were calculated using equations (8.13, 8.19) and (8.25). Note that all beams failed by fracture of carbon followed by crushing of concrete. In the first set of calculations, the ultimate strain of the carbon given by the manufacturer, 0.015, was used as the failure strain. In the second analysis, the experimentally obtained failure strain was used. The resulting moment capacities and flexural stiffness are shown in Tables 8.3 and 8.4, respectively.

The predicted moment capacities (Table 8.3, Analysis 1) using a failure strain of 0.015 were all significantly greater than the experimental results. The prediction became less accurate as the carbon area increased. In sample IS3, where five layers of carbon were used, the error in the predicted moment capacity was greater than 40%. When the experimentally obtained failure strains were used in the analysis, the predicted moment capacities were within 20% of the observed values. Analysis of sample IS2 was the most accurate with an error of about 8%.

From Table 8.3, it can be seen that when lower carbon strains were used, the strains in the extreme concrete fibers were in the linear range. Therefore, equation (8.19) was used for the analysis.

The flexural stiffness values are compared in Table 8.4. The maximum moment was calculated using experimental carbon strains and the working load was taken as 60% of the maximum load. The error is less than 20%. However, the results are not extensive and further experimental results are needed for verification.

Summary

An analytical procedure exists for predicting the behavior of reinforced concrete beams strengthened with high strength fibers and organic matrix. An analytical model is presented in this section for use with organic matrices. The analytical models provide reasonably accurate results. More research is needed to estimate carbon strain at failure.

8.4 Reinforced Concrete Strengthened with Organic Matrix

. This section outlines the design procedure for reinforced concrete beams strengthened with carbon fibers and an organic matrix. A parametric study was conducted that focused on three variables that have been neglected in the published literature (Saadatmanesh and Ehsani, 1991, Ritchie et al, 1991, and M'Bazaa et al, 1996). The influence of the carbon failure strain and modulus of elasticity was studied. Additionally, the role of the reinforcement ratio of the parent concrete in the samples performance was determined. The influence of each of these variables on the moment capacity and working load deflection of the strengthened beams was determined. The traditional pound-inch system was chosen for this section because most of the analyses are done in these units.

8.4.1 Details of Analytical Procedure

The equations presented in this section are similar to the equations presented in section 8.3. However, they are repeated to provide comprehensive information and the

development of a flow chart. The sections were analyzed at three sections of loading, namely: pre-cracking, working load level, and ultimate load.

Pre-cracked section analysis

Section properties are needed at this level for the computation of deflections. The analysis completed using the principles of strength of materials require the moment of inertia and maximum flexural stress known as the modulus of rupture. Modulus of rupture, f_r, can be computed using the ACI guidelines (ACI Committee 318, 1995.)

$$f_r = 7.5\sqrt{f'_c} \qquad (8.26)$$

For moment of inertia the gross section can be used. Therefore, moment of inertia,

$$I_g = bh^3 / 12 \qquad (8.27)$$

where b =width of the beam section

h = depth of the beam section.

Cracking moment, M_{cr}, can be computed using the equation

$$M_{cr} = (I_g f_r) / 0.5h \qquad (8.27)$$

Working load analysis

Deflection in the beam is determined by completing a working load analysis. The depth of the neutral axis in the working stress analysis, kd, can be determined using equation (8.28).

$$b(kd)^2/2 = n_s A_s(d - kd) + n_f A_f(h - kd) \qquad (8.28)$$

where A_f = area of carbon reinforcement

A_s = area of steel reinforcement

d = effective depth

n_s = modular ratio of steel = E_s / E_c

n_f = modular ratio of carbon = E_f / E_c

Once kd is known, the cracked moment of inertia of the beam cross section is determined using equation (8.29).

$$I_{cr} = b(kd)^3/3 + n_s A_s(d - kd)^2 + n_f A_f(h - kd)^2 \qquad (8.29)$$

The effective moment of inertia for deflection calculations, I_{eff}, can be computed using

$$I_{eff} = I_{cr} + (I_g - I_{cr})(M_{cr} / M_a)^3 \qquad (8.30)$$

where M_a = maximum moment at working load. For the analysis presented in this section, M_a is assumed to be 60 percent of the nominal moment capacity, M_n.

$$\Delta = Pl^3 / 48E_c I_{eff} \qquad (8.31)$$

where P = load in pounds

l = length of the beam in inches

Δ = deflection of the beam in inches

Ultimate load analysis

For the ultimate load analysis, the following possibilities were considered.

Failure by fracture of the carbon and the maximum strain in the concrete more than or equal to 0.002. For this case, a rectangular stress block was assumed for the concrete force distribution.

Failure by fracture of the carbon and the maximum strain in the concrete less than 0.002. For this case, a triangular stress distribution was used for the concrete.

Failure by crushing of the concrete before fracture of the carbon. For this case, a rectangular stress block was assumed for the concrete.

In addition to the failure modes, the amount of reinforcement in the parent concrete and strain in the steel when the carbon was applied played an important role in the analysis.

The entire sequence of calculations is presented in the flow chart in section 8.6.

8.5 Parametric Study

As mentioned earlier, a parametric study was conducted to study the influence of carbon failure strain, carbon modulus, and the reinforcement ratio of the parent concrete. The dimensions and material properties are shown in Figure 8.3. The length of the beam was assumed to be 20 feet.

8.5.1 Influence of Carbon Failure Strain on Moment Capacity, M_n

The purpose of this section was to determine how variations in the failure strain of the carbon used in a strengthening effort would affect the resulting moment capacity. The modulus of elasticity of the carbon was assumed to be 30 X 10^6 psi and the reinforcement ratio of the parent concrete was $0.4\rho_b$. The failure strain of the carbon used in the reinforcement was varied between 0.008 and 0.015. Most of the experimental results report failure strains in the range of 0.008 to 0.01. The resulting moment capacities are shown in Table 8.5 and Figure 8.4.

As expected, the lowest carbon strain of 0.008 resulted in the minimum moment capacity. Insignificant increases in moment capacity were observed as the failure strain

of the carbon was increased to 0.01. At this point, the failure mode of the cross section changed from failure of the carbon to crushing of the concrete. Any additional increase in carbon failure strain is neglected because the concrete had already reached it's maximum allowable strain of 0.003. Unless the carbon area is very high as compared to the steel area, the reduction in strain capacity will not result in significant reduction in moment capacity.

8.5.2 Influence of Carbon Modulus of Elasticity on Moment Capacity, M_n

The modulus of the carbon was varied between 27 X 10^6 and 33 X 10^6 psi. The failure strain of the carbon was kept at a constant value of 0.015 for each of the analyses. Additionally, the reinforcement ratio of the parent concrete was $0.4\rho_b$. The moment capacities resulting from each of the analyses are shown in Table 8.6 and Figure 8.5.

The moment capacity of the strengthened samples was not dependent upon the modulus of elasticity of the carbon. Insignificant strength increases of less than two percent were observed as the modulus was increased from 27 X 10^6 to 33 X 10^6 psi, Figure 8.5. In each of the analyses, the failure mode was the fracture of the carbon in the composite plate.

8.5.3 Influence of Reinforcement Ratio of Parent Concrete on Moment Capacity

The effect of varying the reinforcement ratio of the parent concrete on the moment capacity of strengthened beams was determined in this section. In this series of analyses, the failure strain of the carbon was 0.015 and the modulus was 30 X 10^6 psi.

Reinforcement ratios between ten and seventy five percent of the balanced ratio were studied, Table 8.7.

The moment capacity increased with the reinforcement ratio of the parent concrete, Figure 8.6. A linear relationship was observed between the reinforcement ratio and the nominal resisting moment. When the reinforcement ratio was $0.1\rho_b$, the moment capacity was double the cracking moment of the plain concrete section. Strength increases of about 500 percent were observed as the reinforcement ratio was increased from $0.1\rho_b$ to $0.75\rho_b$. Therefore, increasing the reinforcement area, whether steel or carbon, is the most efficient way to increase the moment capacity.

8.5.4 Influence of the Carbon Modulus of Elasticity on Working Load Deflection

Deflection control is another important aspect of strengthening reinforced concrete beams with FRP. Although it may be advantageous to increase the moment capacity of the beams, the deflection must still be kept within allowable design limits. In this section, the influence of the carbon modulus of elasticity on the working load deflection of the beam was determined. As in section 8.5.2, the failure strain of the carbon and reinforcement ratio of the parent concrete remained constant while the carbon modulus was varied. The deflections were calculated for each beam at 60 percent of the nominal moment capacity, Table 8.8.

The deflection behavior of the reinforced concrete beams was not dependent upon the modulus of elasticity of the carbon in the strengthening effort, Figure 8.7. Insignificant increases in deflection were observed as the modulus of the carbon was increased.

8.5.5 Influence of Reinforcement Ratio of Parent Concrete on Working Load Deflection

The working load deflection was calculated at 60 percent of the nominal moment capacities calculated in section 8.5.3. The material properties of the external carbon reinforcement were held constant throughout the analyses. The variation in the computed deflections was the result of the reinforcement ratio of the parent concrete, Table 8.9.

The working load deflection increased with the reinforcement ratio of the parent concrete. A nonlinear relationship was observed. At low reinforcement ratios, large changes in displacement were observed in subsequent analysis. As the reinforcement ratio was increased, however, the variation in working load deflection was less dependent upon the reinforcement ratio. Between reinforcement ratios of $0.7\rho_b$ and $0.75\rho_b$, the variation in deflection was insignificant. The results show that limitations in deflections might control the design.

8.6 Design Procedure- Reinforced Concrete Beams with Organic Polymers

In this section, a flow chart has been developed for the analysis of reinforced concrete beams strengthened with carbon fibers and organic matrix.

A = Cross-sectional area
a = Depth of equivalent compression stress block
a_θ = Depth of equivalent compression stress block under fire conditions
A_{cr} = Area of crack face
A_e = Net effective slab bearing area
A_{ps} = Area of prestressed reinforcement
A_{vf} = Area of shear friction reinforcement
b = Width of compression face
b_w = Net web width of hollow core slab
C = Confinement factor
C = Compressive force
C = Seismic factor dependent on site and structure fundamental period
C = Factor for calculating steel relaxation losses as given in Table 2.2.3.2
c = Distance from extreme compression fiber to neutral axis
CR = Prestress loss due to concrete creep
C_s = Seismic coefficient
D = Dead load
d = Distance from extreme compression fiber to centroid of non-prestressed tension reinforcement
d_b = Nominal diameter of reinforcement
d_p = Distance from extreme compression fiber to centroid of prestressed reinforcement
DW = Distribution width
e = Distance from neutral axis to centroid of prestressed reinforcement
E_c = Modulus of elasticity of concrete
E_{ci} = Modulus of elasticity of concrete at the time of initial prestress
ES = Prestress loss due to elastic shortening of concrete
E_s = Modulus of elasticity of steel reinforcement
f'_c = Specified design compressive strength of concrete
f'_{ci} = Compressive strength of concrete at the time of initial prestress
f_{cir} = Net compressive stress in concrete at centroid of prestressed reinforcement at time of initial prestress
f_{cds} = Stress in concrete at centroid of prestressed reinforcement due to superimposed dead load
f_d = Stress at extreme tension fiber due to unfactored member self weight
F_i = Portion of base shear applied at level i
f_{pc} = Compressive stress in concrete at the centroid of the section due to effective prestress for non-composite sections or due to effective prestress and moments resisted by the precast section alone for composite sections
f_{pe} = Compressive stress in concrete at extreme fiber where external loads cause tension due to the effective prestress only
f_{ps} = Stress in prestressed reinforcement at nominal strength
$f_{ps\theta}$ = Stress in prestressed reinforcement at fire strength
f'_{ps} = Maximum steel stress in partially developed strand
f_{pu} = Specified tensile strength of prestressing steel
$f_{pu\theta}$ = Tensile strength of prestressing steel at elevated temperatures
F_{px} = Force applied to diaphragm at level under consideration
f_{se} = Effective stress in prestressing steel after all losses
f_{si} = Stress in prestressing steel at initial prestress
F_t = Additional portion of base shear applied at top level
f_u = Usable grout strength in a horizontal joint
f_y = Steel yield strength
h = Overall member depth
h_n = Net height of grout in keyway between slab units
I = Occupancy importance factor
I = Cross-sectional moment of inertia
J = Factor for calculating steel relaxation losses as given in Table 2.2.3.1
k = Fraction of total load in a horizontal joint in a grout column
K_{cir} = Factor for calculating elastic shortening prestress losses
K_{cr} = Factor for calculating prestress losses due to concrete creep
K_{es} = Factor for calculating prestress losses due to elastic shortening
K_{re} = Factor for calculating prestress losses due to steel relaxation as given in Table 2.2.3.1

K_{sh} = Factor for calculating prestress losses due to concrete shrinkage
K'_u = Factor from PCI Handbook Fig. 4.12.2 for calculating flexural design strength
L = Live load
ℓ = Span length
ℓ_d = Reinforcement development length
ℓ_e = Strand embedment length from member end to point of maximum stress
ℓ_f = Flexural bond length
ℓ_t = Strand transfer length
M = Service load moment
M_{cr} = Cracking moment
M_d = Unfactored dead load moment
M_g = Unfactored self-weight moment
M_n = Nominal flexural strength
$M_{n\theta}$ = Flexural strength under fire conditions
M_{max} = Maximum factored moment due to externally applied loads
= $M_u - M_d$
M_{sd} = Unfactored moment due to superimposed dead load
M_u = Factored design moment
M_θ = Applied fire moment
P = Effective force in prestressing steel after all losses
P_o = Effective prestress force at release prior to long term losses
P_i = Initial prestress force after seating losses
Q = First moment of area
R = Fire endurance rating
RE = Prestress loss due to steel relaxation
R_e = Reduction factor for load eccentricity in horizontal joints
RH = Ambient relative humidity
R_w = Seismic coefficient dependent on structural system type
S = Section modulus
SH = Prestress loss due to concrete shrinkage
T = Tensile force
t_g = Width of grout column in horizontal joint
V = Seismic base shear
V_c = Nominal shear strength of concrete
V_{ci} = Nominal shear strength of concrete in a shear-flexure failure mode
V_{cw} = Nominal shear strength of concrete in a web shear failure mode
V_d = Shear due to unfactored self weight
V_h = Horizontal beam shear
V_i = Factored shear force due to externa applied loads occurring simultaneou with M_{max}
= $V_u - V_d$
V_n = Nominal shear strength of a member
V_s = Nominal shear strength provided by she reinforcement
V_u = Design shear force
V/S = Volume to surface ratio
w = Uniformly distributed load
w = Bearing area length
W = Total dead load plus other applicab loads for seismic design
w_i = Portion of W at level i
w_{px} = Portion of W at level under consideration
y_b = Distance from neutral axis to extrem bottom fiber
y_t = Used as either distance to top fiber c tension fiber from neutral axis
Z = Seismic zone factor
β_1 = Factor defined in ACI 318-95, Sectio 10.2.7.3
γ_p = Factor for type of prestressing strand
δ_{all} = Limiting free end slip
δ_s = Actual free end slip
ε_{ps} = Strain in prestressed reinforcement a nominal flexural strength
ε_s = Strain in prestressed reinforcement
ε_{se} = Strain in prestressed reinforcement afte losses
μ = Shear friction coefficient
μ_e = Effective shear friction coefficient
ρ_p = Ratio of prestressed reinforcement
ρ' = Ratio of compression reinforcement
ϕ = ACI strength reduction factor
ω = $\rho f_y/f'_c$
ω' = $\rho' f_y/f'_c$
ω_p = $\rho_p f_{ps}/f'_c$
ω_w = Reinforcement index for flanged sections
ω'_w = Reinforcement index for flanged sections
ω_{pw} = Reinforcement index for flanged sections
ω_{pu} = $\rho_p f_{pu}/f'_c$
θ = Subscript denoting fire conditions

Step 1- Given information

Beam dimensions: width(b), depth(h), and distance to the tension steel reinforcement(d), length(l)
Concrete: compressive strength(f'_c)
modulus of elasticity = $E_c = 57000\sqrt{f'_c}$
Steel: area(A_s), modulus of elasticity(E_s), yield stress(f_y)
modular ratio = $n = E_s / E_c$
Carbon: ultimate strain(ε_{fu}), modulus of elasticity(E_f)
Existing loads: dead load(W_{dl}), live load(W_{ll})
Desired loads: dead load(W_{ndl}), live load(W_{nll})

Step 2- Desired information

Carbon: area(A_f)

Step 3- Determine if the section is cracked

Factored load(W_u) = $1.4W_{dl} + 1.7W_{ll}$
Existing moment(M_{exist}) = $W_u(l^2) / 8$
Cracking moment(M_{cr}) = $f_r(I / c)$
Where $f_r = 7.5\sqrt{f'_c}$
$I = bh^3 / 12$
$c = h / 2$
$M_{exist} > M_{cr}$, the section is cracked.

Step 4- Perform a cracked section analysis

$b(kd)^2/2 = nA_s(d - kd)$, solve for k

$\varepsilon_y = f_y / E_s$, ε_c @ yielding of steel $= \varepsilon_y[kd / (d - kd)]$

curvature at steel yield$(\phi_y) = \varepsilon_c / kd$

moment at yielding of steel$(M_y) = A_s f_y[d - (kd/3)]$

Check if the moment due to the revised loads > M_y.

If this is true, strengthening can not be accomplished

Step 5- Calculate nominal moment resistance of existing section

$C = T$

$0.85f'_c ba = A_s f_y$

$a = A_s f_y / 0.85f'_c b$

nominal moment resistance$(M_n) = A_s f_y(d - a/2)$

It is assumed that the section is under-reinforced.

Step 6- Determine strain at the bottom of the beam when carbon is attached

curvature at time of renovation(ϕ_{ren}) = $\phi_y(M_{exist} / M_y)$

strain at time of renovation(ε_{ren}) = $\phi_{ren}(h - kd)$

Step 7: Determine nominal moment at increased load

increased load(W_{nu}) = $1.4W_{ndl} + 1.7W_{nll}$

ultimate moment at increased load(M_u) = $W_{nu}(l^2) / 8$

nominal moment required(M_{nreq}) = $M_u / 0.9$

Step 8: Determine failure mode: crushing of concrete or carbon failure

calculate c for a balanced failure condition

$c_b = h\{ \varepsilon_{cu} / (\varepsilon_{cu} + \varepsilon_{fu} + \varepsilon_{ren}) \}$

calculate maximum tensile steel to allow for simultaneous failure

$A_{smax} = (0.85f'_c\beta c_b b) / f_y$

If $A_{smax} < A_{sprovided}$ then failure is by crushing of concrete (Go To Step 9a)

calculate area of carbon for balanced failure

$A_{fbal} = (A_{smax} - A_{sprovided})(f_y / f_{fu})$

calculate nominal moment resisted in balanced failure

$a = (A_s f_y + A_{fbal} f_{fu}) / 0.85f'_c b$

$M_{bal} = A_s f_y(d - a/2) + A_{fbal} f_{fu}(h - a/2)$

If $M_{nreq} > M_{bal}$, concrete crushing controls design (Go To Step 9b)

If $M_{nreq} < M_{bal}$, then carbon fracture controls design (Go To Step 9c)

To Step 9a

To Step 9b or 9c

To Step 9b or 9c

Step 9a: Concrete crushing controls design, no yielding of steel

Note: Code does not allow construction of a beam with a steel reinforcement ratio above $0.75\rho_b$, but the analysis will be completed here.

determine strain in carbon at crushing of concrete

$$(\varepsilon_f) = \{0.003((h - c) / c) - \varepsilon_{ren}\}$$

determine strain in steel at crushing of concrete

$$(\varepsilon_s) = \{0.003((d - c) / c) - \varepsilon_{ren}\}$$

solve force equilibrium equation

$$C = T$$

$$0.85f'_c b(0.85c) = A_s E_s \varepsilon_s + A_f E_f \varepsilon_f$$

The force equilibrium equation has two unknowns, c and A_f, so the moment equilibrium equation is also used.

moment capacity of the section = external moment

$$A_s E_s \varepsilon_s (d - (\beta_1 c)/2) + A_f E_f \varepsilon_f (h - (\beta_1 c)/2) = M_{nreq}$$

The two equations are solved simultaneously and the two unknowns, c and A_f, are determined. A_f is the area of carbon required to resist the additional load.

To Step 10

To Step 9b

To Step 9c

To Step 10

Step 9b: Concrete crushing controls design

determine strain in carbon at crushing of concrete

$$(\varepsilon_f) = \{0.003((h - c) / c) - \varepsilon_{ren}\}$$

solve force equilibrium equation

$$C = T$$

$$0.85f'_c b(0.85c) = A_s f_y + A_f E_f \varepsilon_f$$

The force equilibrium equation has two unknowns, c and A_f, so the moment equilibrium equation is also used.

moment capacity of the section = external moment

$$A_s f_y(d - (\beta_1 c)/2) + A_f E_f\{0.003((h - c) / c) - \varepsilon_{ren}\}(h - (\beta_1 c)/2) = M_{nreq}$$

The two equations are solved simultaneously and the two unknowns, c and A_f, are determined. A_f is the area of carbon required to resist the additional load.

To Step 9c

To Step 10

To Step 10

Step 9c: Carbon fracture controls design

Initially, a rectangular stress distribution for the concrete is assumed.

$$0.85b(\beta_1 c)f'_c = A_s f_y + A_f E_f \varepsilon_{fu}$$

$$A_s f_y(d - \beta_1 c/2) + A_f f_{fu}(h - \beta_1 c/2) = M_{nreq}$$

The two equations are solved for the two unknowns, c and A_f.

The concrete strain is determined from the calculated c.

$$\varepsilon_c = \{\varepsilon_{fu}(c / (h\text{-}c)) + \varepsilon_{ren}\}$$

If the $\varepsilon_c > 0.002$, the initial assumption was correct and the problem is solved. However, if $\varepsilon_c < 0.002$, the concrete stress distribution is triangular and the problem must be solved again.

Once again, $\varepsilon_c = \{\varepsilon_{fu}(c / (h\text{-}c)) + \varepsilon_{ren}\}$

$$C = T$$

$$C = (bc/2)E_c\varepsilon_c$$

$$T = A_s f_y + A_f E_f \varepsilon_{fu}$$

The relationship between c and ε_c is substituted into the equation for the compressive forces of the concrete. A second equation is developed with A_f and c as unknowns.

$$A_s f_y(d - c/3) + A_f E_f \varepsilon_{fu}(h - c/3) = M_{nreq}$$

The balance of force equation and required moment capacity equations are solved simultaneously and A_f and c are determined.

To Step 10

Step 10: Computation of deflection at service load

Analyze the beam as a composite section

$n_s = E_s / E_c$, $n_f = E_f / E_c$

composite section analysis

$b(kd)^2/2 = n_sA_s(d - kd) + n_fA_f(h - kd)$, solve for kd

determine the cracked moment of inertia of the beam

$(I_{cr}) = b(kd)^3/3 + n_sA_s(d - kd)^2 + n_fA_f(h - kd)^2$

determine the effective moment of inertia of the beam

$(I_{eff}) = I_{cr} + (I_g - I_{cr})(M_{cr}/M_a)^3$

M_a = maximum moment

determine the deflection for a simply supported beam under a concentrated mid-span load

$(\Delta) = Pl^3 / 48E_cI_{eff}$

For a uniformly distributed load, q:

$(\Delta) = ql^4 / 384E_cI_{eff}$

For flanged sections, flange width can be used for the width of the beam. In most cases, the depth of the neutral axis will be within the flange. If the depth of the neutral axis falls below the flange, the proper compression area should be used for computing the compressive force. For working stress analysis, I_{cr} should be computed using the web and flange areas. Equations can be found in text books on reinforced concrete.

8.6.1 Design Example #1

Step 1- Given information

b = 12 in, h = 36 in, d = 32 in, l = 48 ft
f'_c = 4000 psi
modulus of elasticity = $E_c = 4.03 \times 10^6$ psi
$A_s = 2.65in^2$, $E_s = 30 \times 10^6$ psi, f_y = 60000 psi
$N_s = E_s / E_c = 7.44$
$\varepsilon_{fu} = 0.015$, $E_f = 33 \times 10^6$ psi
W_{dl} = 400 lb/ft, W_{ll} = 150 lb/ft
Increased loads: dead load(W_{ndl}) = 700 lb/ft, live load(W_{nll}) = 420 lb/ft

Step 2- Desired information

Carbon: area(A_f)

Step 3- Determine if the section is cracked

W_u = 400 + 150 = 550 lb/ft
M_{exist} = 158.4 kip-ft
M_{cr} = 102.46 kip-ft
$M_{exist} > M_{cr}$, the section is cracked.

Step 4- Perform a cracked section analysis

$12(32k)^2/2 = (7.44)(2.65)(32 - 32k)$, $\therefore$ **k= 0.273**

ε_c @ yielding of steel = $0.002[kd / (d - kd)]$ = **0.0075**

$(\phi_y) = \varepsilon_c / kd = .0081/0.282$ = **0.000086**

$M_y = A_s f_y[d - (kd/3)]$ = **385.4 kip-ft**

Moment due to the new working loads = $1120(48)^2 /8$ = **322.56 kip-ft < M_y O.K.**

Step 5- Calculate nominal moment resistance of existing section

C = T

$0.85f'_c ba = A_s f_y$

$a = A_s f_y / 0.85 f'_c b = (2.65)(60)/(.85 \text{ X } 4 \text{ X } 12) = 3.9$ in

nominal moment resistance$(M_n) = A_s f_y(d - a/2) =$ **398 kip-ft**

Step 6- Determine strain at the bottom of the beam when carbon is attached

$\phi_{ren} = \phi_y(M_{exist} / M_y) = 0.000086(158.4/385.4) =$ **0.000035**

$\varepsilon_{ren} = \phi_{ren}(h - kd) = 0.000035(36 - 8.74) =$ **0.00095**

Step 7: Determine nominal moment at increased load

$W_{nu} = 1.4W_{ndl} + 1.7W_{nll} = 1.4(700) + 1.7(420) =$ **1694 lb/ft**

$M_u = W_{nu}(l^2) / 8 =$ **487.87 kip-ft**

$M_{nreq} = M_u / 0.9 =$ **542 kip- ft**

Step 8: Determine failure mode: crushing of concrete or carbon failure

$c_b = h\{ \varepsilon_{cu} / (\varepsilon_{cu} + \varepsilon_{fu} + \varepsilon_{ren}) \}$

$= 36\{ .003/ (.003 + .015 + .0009) =$ **5.71 in**

$A_{smax} = (0.85 f'_c \beta c_b b) / f_y$

$= (0.85 \text{ X } 4000 \text{ X } 0.85 \text{ X } 5.71 \text{ X } 12)/ 60000 =$ **3.3 in^2**

If $A_{smax} > A_{sprovided}$ $\therefore$ failure is by yielding of steel, **O.K.**

$A_{fbal} = (A_{smax} - A_{sprovided})(f_y / f_{fu})$

$= (3.29 - 2.65)(60/505) =$ **0.077 in^2**

calculate nominal moment resisted in balanced failure

$a = (A_s f_y + A_{fbal} f_{fu}) / 0.85 f'_c b = [2.65(60000) + 0.77(505000)/.85(4000)(12)] =$ **4.84 in.**

$M_{bal} = A_s f_y(d - a/2) + A_{fbal} f_{fu}(h - a/2) =$ **500.66 kip -ft**

$M_{nreq} > M_{bal}$, **(542 > 500.66) concrete crushing controls design (Go To Step 9b)**

Step 9b: Concrete crushing controls design

$(\varepsilon_f) = \{0.003((h - c) / c) - \varepsilon_{ren}\}$

$\varepsilon_f = \{0.003((36 - c) / c) - 0.0009\}$

solve force equilibrium equation

$C = T$

$0.85f'_c b(0.85c) = A_s f_y + A_f E_f \varepsilon_f$

$0.85(4)(12)(0.85c) = (2.65 \text{ X } 60) + A_f(33.66 \text{ X } 10^3) \{0.003((36 - c) / c) - 0.0009\}$

moment capacity of the section = external moment

$A_s f_y(d - (.85c)/2) + A_f E_f\{0.003((h - c) / c) - \varepsilon_{ren}\}(h - (.85c)/2) = M_{nreq}$

$2.65(60)(32 - (.85c)/2) + A_f(33 \text{ X } 10^3)\{0.003((36 - c) / c) - 0.001\}(36 - (.85c)/2) = (542$

X 12)

The two equations are solved simultaneously and the two unknowns,

c and A_f, are determined.

$A_f = 0.117 \text{ in}^2$

c = 6.2 in.

Step 10: Computation of deflection at service load

Analyze the beam as a composite section

$n_s = 7.44$, $n_f = 8.36$

composite section analysis

$12(32k)^2/2 = 7.44(2.65)(32 - 32k) + 8.36(0.117)(36 - 32k)$

k = 0.279, kd = 8.95 in

$(I_{cr}) = 12(8.95)^3/3 + (2.65)(7.44)(32 - 8.95)^2 + 0.117(8.36)(36 - 8.95)^2$

I_{cr} = 11513.31 in^4

$M_a = \phi M_n = 0.6(542) =$ **325.2 kip-ft**

$(I_{eff}) = 11513.31 + (46656 - 11513.31)(102.46/325.2)^3$

I_{eff} = 12612.43 in^4

M = Pl/4, l= 48 ft, P = M/12

P = 325.2/12 = 27.1 kips = 27100 lb

$(\Delta) = Pl^3 / 48E_cI_{eff}$

$\Delta = 27100(48 \text{ X } 12)^3/[48(4.03 \text{ X } 10^6)(12612.43)] = 2.12$ in

This deflection should be checked against allowable deflections.

8.6.2 Design Example #2

Design problem 1 was analyzed while taking into account creep effects on the concrete.

Step 1- Given information

b = 12 in, h = 36 in, d = 32 in, l = 48 ft
f'_c = 4000 psi
modulus of elasticity = $E_c = 2.42 \text{ X } 10^6$ psi
$A_s = 2.65in^2$, $E_s = 30 \text{ X } 10^6$ psi, f_y = 60000 psi
$n_s = E_s / E_c = 12.4$
$\varepsilon_{fu} = 0.015$, $E_f = 33 \text{ X } 10^6$ psi
W_{dl} = 400 lb/ft, W_{ll} = 150 lb/ft
Increased loads: dead load(W_{ndl}) = 700 lb/ft, live load(W_{nll}) = 420 lb/ft

Step 2- Desired information

Carbon: area(A_f)

Step 3- Determine if the section is cracked

W_u = 400 + 150 = 550 lb/ft
M_{exist} = 158.4 kip-ft
M_{cr} = 102.46 kip-ft
$M_{exist} > M_{cr}$, the section is cracked.

Step 4- Perform a cracked section analysis

$12(32k)^2/2 = (12.4)(2.65)(32 - 32k)$, $\therefore$ **k= 0.337**

ε_c @ yielding of steel = $0.002[kd / (d - kd)]$ = **0.001**

$(\phi_y) = \varepsilon_c / kd = .001/10.784$ = **0.000093**

$M_y = A_s f_y[d - (kd/3)]$ = **376.4 kip-ft**

Moment due to the new working loads = $1120(48)^2 /8$ = **322.56 kip-ft < M_y O.K.**

Step 5- Calculate nominal moment resistance of existing section

C = T

$0.85f'_c ba = A_s f_y$

$a = A_s f_y / 0.85f'_c b = (2.65)(60)/(.85 \text{ X } 4 \text{ X } 12) = 3.9$ in

nominal moment resistance(M_n) = $A_s f_y(d - a/2)$ = **398 kip-ft**

Step 6- Determine strain at the bottom of the beam when carbon is attached

$\phi_{ren} = \phi_y(M_{exist} / M_y) = 0.000093(158.4/376.4)$ = **0.0000391**

$\varepsilon_{ren} = \phi_{ren}(h - kd) = 0.0000391(36 - 10.784)$ = **0.00099**

Step 7: Determine nominal moment at increased load

$W_{nu} = 1.4W_{ndl} + 1.7W_{nll} = 1.4(700) + 1.7(420)$ = **1694 lb/ft**

$M_u = W_{nu}(l^2) / 8 =$ **487.87 kip-ft**

$M_{nreq} = M_u / 0.9 =$ **542 kip- ft**

Step 8: Determine failure mode: crushing of concrete or carbon failure

$c_b = h\{ \varepsilon_{cu} / (\varepsilon_{cu} + \varepsilon_{fu} + \varepsilon_{ren}) \}$

$= 36\{ .003/ (.003 + .015 + .00099) =$ **5.69 in**

$A_{smax} = (0.85f'_c \beta c_b b) / f_y$

$= (0.85 \text{ X } 4000 \text{ X } 0.85 \text{ X } 5.71 \text{ X } 12)/ 60000 =$ **3.29 in^2**

If $A_{smax} > A_{sprovided}$ $\therefore$ failure is by yielding of steel, **O.K.**

$A_{fbal} = (A_{smax} - A_{sprovided})(f_y / f_{fu})$

$= (3.29 - 2.65)(60/505) =$ **0.08 in^2**

calculate nominal moment resisted in balanced failure

$a = (A_s f_y + A_{fbal} f_{fu}) / 0.85f'_c b = [2.65(60000) + 0.08(505000)/.85(4000)(12)] =$ **4.88 in.**

$M_{bal} = A_s f_y(d - a/2) + A_{fbal} f_{fu}(h - a/2) =$ **504.66 kip -ft**

$M_{nreq} > M_{bal}$, **(542 > 504.66) concrete crushing controls design (Go To Step 9b)**

Step 9b: Concrete crushing controls design

$(\varepsilon_f) = \{0.003((h - c) / c) - \varepsilon_{ren}\}$

$\varepsilon_f = \{0.003((36 - c) / c) - 0.00099\}$

solve force equilibrium equation

$C = T$

$0.85f'_c b(0.85c) = A_s f_y + A_f E_f \varepsilon_f$

$0.85(4)(12)(0.85c) = (2.65 \text{ X } 60) + A_f(33.66 \text{ X } 10^3)\ \{0.003((36 - c) / c) - 0.00099\}$

moment capacity of the section = external moment

$A_s f_y(d - (.85c)/2) + A_f E_f\{0.003((h - c) / c) - \varepsilon_{ren}\}(h - (.85c)/2) = M_{nreq}$

$2.65(60)(32 - (.85c)/2) + A_f(33 \text{ X } 10^3)\{0.003((36 - c) / c) - 0.00099\}(36 - (.85c)/2) =$

(542 X 12)

The two equations are solved simultaneously and the two unknowns,

c and A_f, are determined.

$A_f = 0.123 \text{ in}^2$

c = 6.2 in.

Step 10: Computation of deflection at service load

Analyze the beam as a composite section

$n_s = 12.4$, $n_f = 13.9$

composite section analysis

$12(32k)^2/2 = 12.4(2.65)(32 - 32k) + 13.9(0.123)(36 - 32k)$

k = 0.345, kd = 11.04 in

$(I_{cr}) = 12(11.04)^3/3 + (2.65)(12.4)(32 - 11.04)^2 + 0.123(13.9)(36 - 11.04)^2$

$I_{cr} = 20883.55 \text{ in}^4$

$M_a = \phi M_n = 0.6(542) =$ **325.2 kip-ft**

$(I_{eff}) = 20883.55 + (46656 - 20883.55)(102.46/325.2)^3$

$I_{eff} = 21689.61 \text{ in}^4$

M = Pl/4, l= 48 ft, P = M/12

P = 325.2/12 = 27.1 kips = 27100 lb

$(\Delta) = Pl^3 / 48E_cI_{eff}$

$\Delta = 27100(48 \text{ X } 12)^3/[48(2.42 \text{ X } 10^6)(21689.61)] = 2.06$ in

This deflection should be checked against allowable deflections.

8.7 Summary

Analytical procedures were presented in this chapter that focused on areas for which the published information is currently lacking. Both inorganic and organic matrices can be effectively used for strengthening unreinforced concrete. At excessive loads the inorganic matrix composite develops micro cracks and failure occurs by fracture of the carbon whereas in the organic matrix, failure occurs due to delamination of the plates. The average fiber strain at failure reduces with an increase in fiber area for both matrix types. Load redistribution through a crack plays a major role in the failure mechanism and should be considered in repair design.

The parametric study showed that the fracture strain and modulus of the carbon do not play a significant role in increasing the nominal moment capacity and working deflections. Increase in reinforcement ratio plays a significant role both in moment capacity and change in deflections.

A flow chart is presented for the design of reinforced concrete beams strengthened with carbon composite. Both working and ultimate stress methods are outlined to determine the additional reinforcement required when loads on a reinforced concrete beam increase above the design loads. Design examples are also presented to further clarify the design procedure.

Table 8.1

Comparison of experimental and predicted maximum loads, experimental results from current investigation

Peak load, kN		
Beam	Experimental	Fiber modulus, 100%
O-T1	9	7
O-T2	11	11
O-T3	15	15
O-L1	14	14
O-L2	25	25
O-TONEN	23	23
I-T1	13	11
I-T2	12	14
I-T3	14	15
I-L1	15	15
I-L2	17	16

Table 8.2

Comparison of experimental and predicted maximum loads, (experimental results from Huang, 1995 and Toutanji and Gomez, 1997.)

Peak load, kN			
Beam	Experimental	Predicted Fiber modulus, 100%	Fiber Modulus, 80%
I-T6	5.09	5.66	4.54
I-T9	6.43	6.26	5.03
I-L2	6.35	7.09	5.71
I-L3	7.72	9.09	7.32
I-L4	9.1	11.3	9.08
C1	3.74	4.27	3.45
C2	4.86	6.86	5.54

Table 8.3
Comparison of predicted and experimental moment capacities: Reinforced concrete beams

Beam	Experimental M_n(kN-m)	ε_c	Analysis 1 M_n(kN-m)	error	ε_c	Analysis 2 M_n(kN-m)	error
IS1	44.73	0	53.2	18.9%	.001	35.93	-19.7%
IS2	51.06	.0025	65.18	27.7%	.0011	42.05	-8.5%
IS3	61.16	.0036	88.35	44.4%	.0013	54.1	-11.5%

Table 8.4
Comparison of predicted and experimental flexural stiffness: Reinforced concrete beams

Beam	Experimental FS(kN-m^2)	Analysis 2 FS(kN-m^2)	error
IS1	3972	5461	37.49%
IS2	4379	4656	6.3%
IS3	4864	4156	-14.6%

Table 8.5
Results of parametric study: Influence of carbon failure strain on moment capacity, M_n

$E_f = 30 \times 10^6$psi $\rho = 0.4\rho_b$	
ε_{fu}	M_n(kip-ft)
0.008	670.875
0.009	678.053
0.01	684.89
0.011	660.343
0.012	660.343
0.013	660.343
0.014	660.343
0.015	660.343

Table 8.6
Results of parametric study:
Influence of carbon modulus
on moment capacity, M_n

$\varepsilon_{fu} = 0.015$ $\rho = 0.4\rho_b$ E_f(psi)	M_n(kip-ft)
27×10^6	656.47
28×10^6	657.77
29×10^6	659.06
30×10^6	660.34
31×10^6	661.62
32×10^6	662.89
33×10^6	664.15

Table 8.7
Results of parametric study:
Influence of reinforcement ratio
on moment capacity, M_n

$\varepsilon_{fu} = 0.015$ $E_f = 30 \times 10^6$ psi ρ	M_n(kip-ft)
$0.1\rho_b$	238.11
$0.2\rho_b$	398.87
$0.3\rho_b$	535.66
$0.4\rho_b$	660.34
$0.5\rho_b$	783.95
$0.6\rho_b$	902.98
$0.7\rho_b$	1015.24
$0.75\rho_b$	1069.78

Table 8.8
Results of parametric study:
Influence of carbon modulus
on working load deflection

$\varepsilon_{fu} = 0.015$ $\rho = 0.4\rho_b$ E_f(psi)	Deflection(in)
27×10^6	0.301
28×10^6	0.3013
29×10^6	0.302
30×10^6	0.3026
31×10^6	0.3033
32×10^6	0.304
33×10^6	0.3046

Table 8.9
Results of parametric study:
Influence of reinforcement ratio of parent concrete
on working load deflection

$\varepsilon_{fu} = 0.015$ $E_f = 30 \times 10^6$ psi ρ	Deflection(in)
$0.1\rho_b$	0.1547
$0.2\rho_b$	0.2687
$0.3\rho_b$	0.2932
$0.4\rho_b$	0.3026
$0.5\rho_b$	0.3166
$0.6\rho_b$	0.3331
$0.7\rho_b$	0.3499
$0.75\rho_b$	0.3569

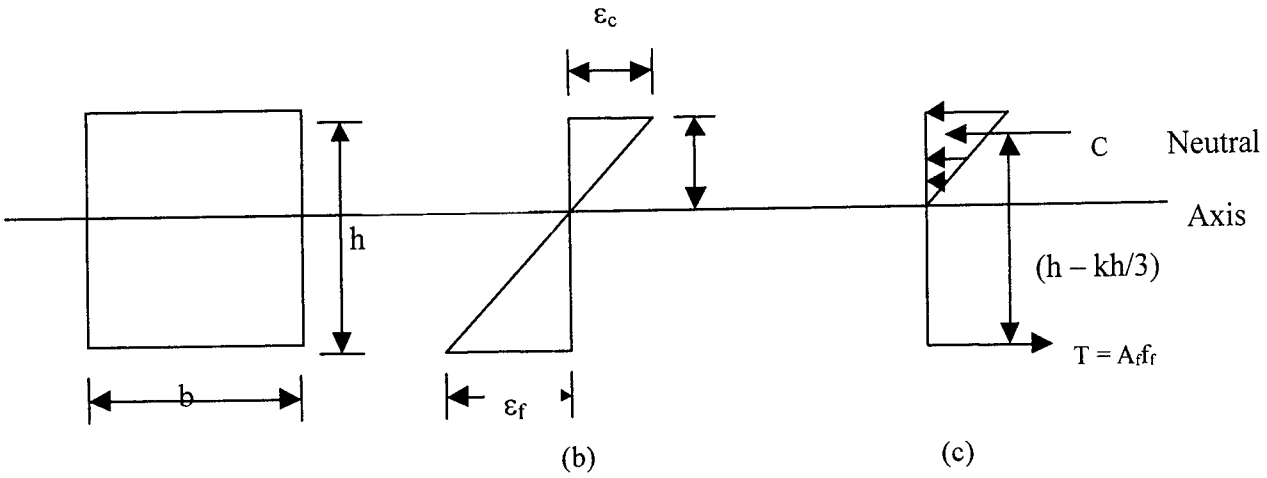

Fig. 8.1. Stress and strain distribution across beam depth: (a) beam cross section; (b) strains; (c) stress distribution

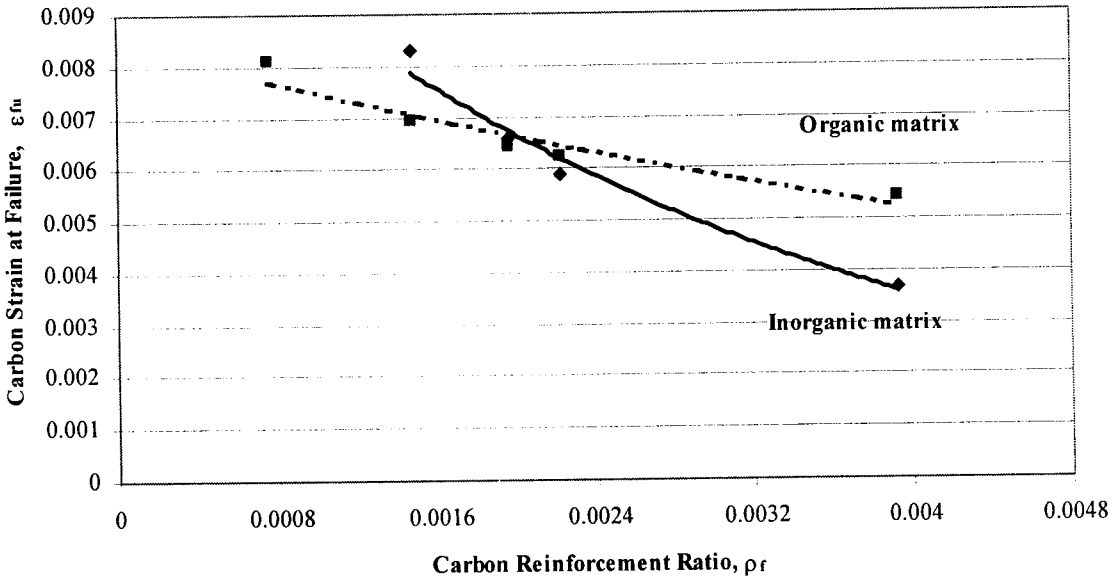

Fig. 8.2. Carbon reinforcement ratio vs. carbon strain at failure

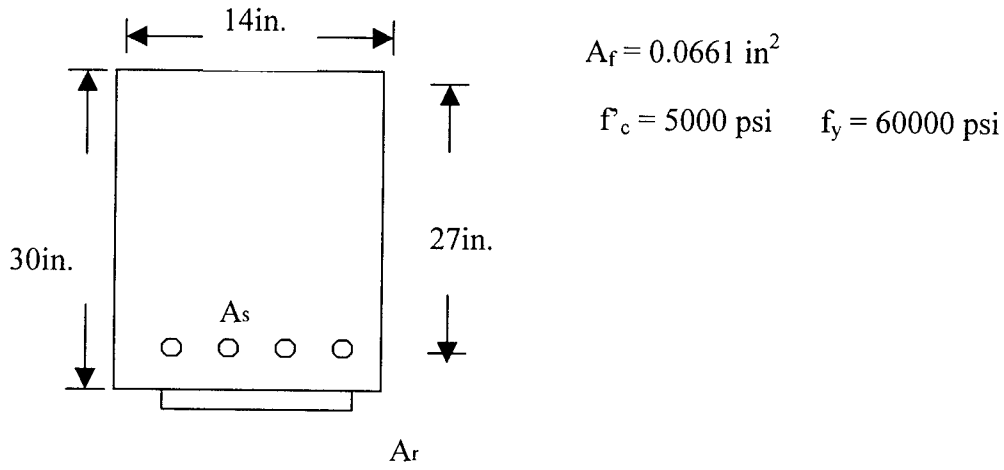

Fig. 8.3. Rectangular beam cross section for parametric study

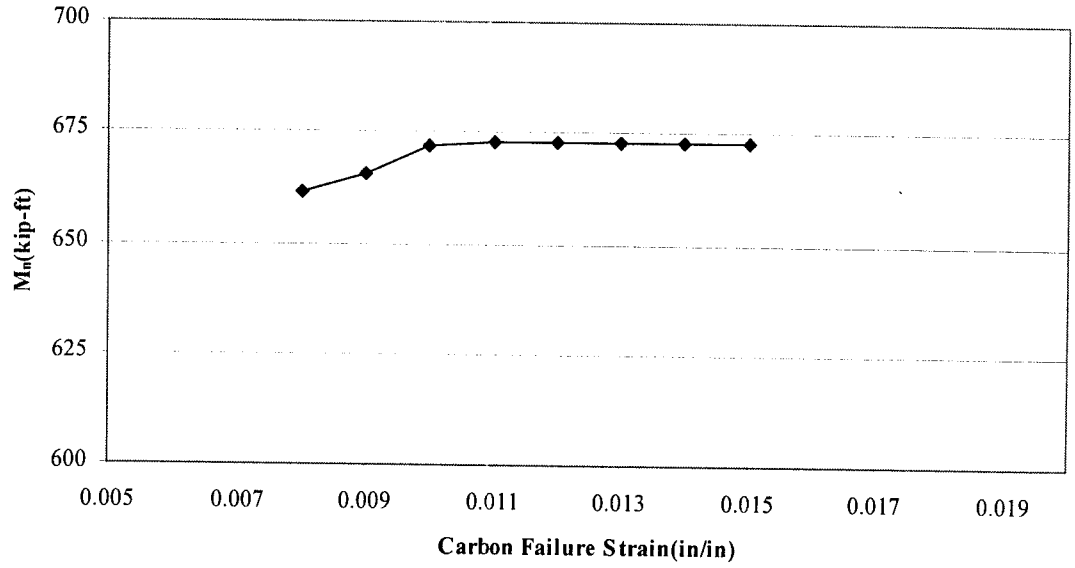

Fig. 8.4. Influence of carbon failure strain on moment capacity, M_n

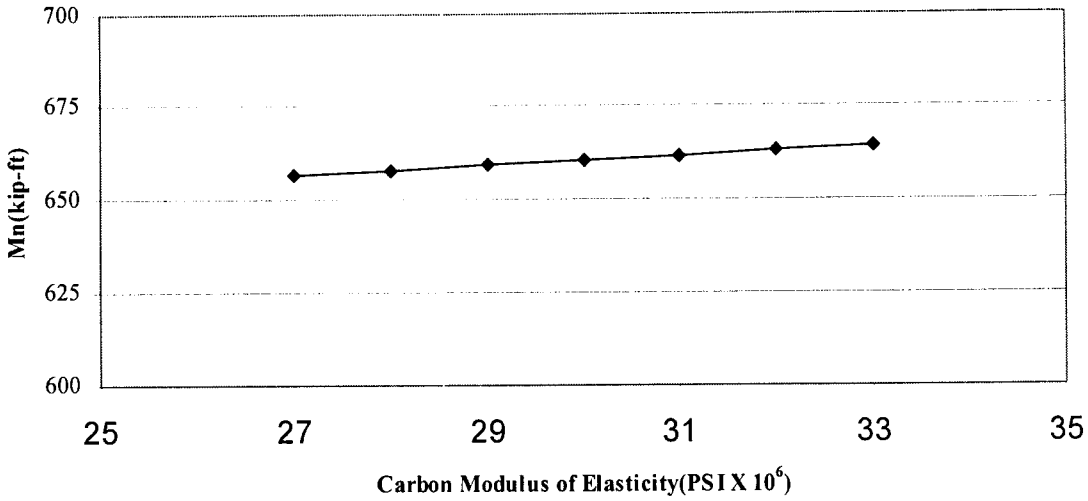

Fig. 8.5. Influence of carbon modulus of elasticity on moment capacity, M_n

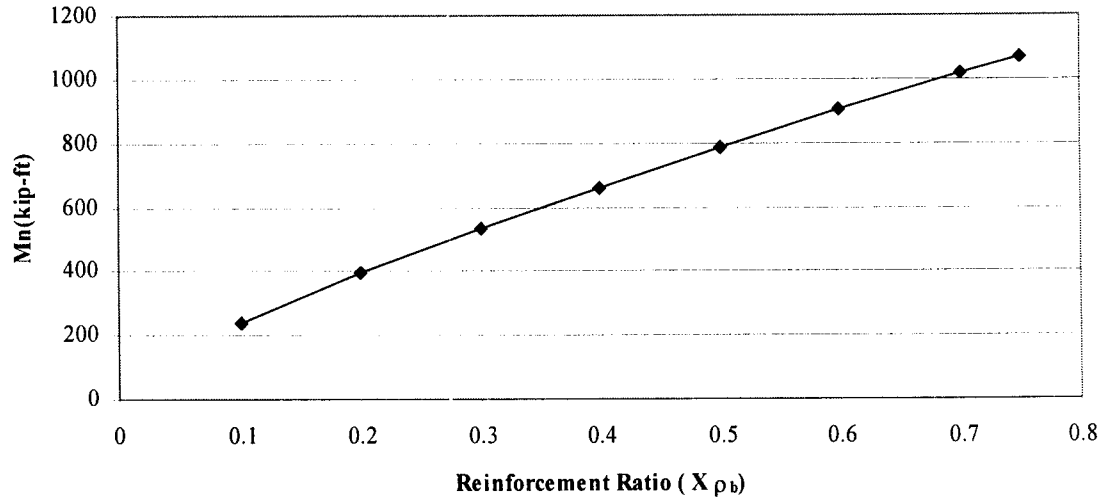

Fig. 8.6. Influence of reinforcement ratio of parent concrete on moment capacity, Mn

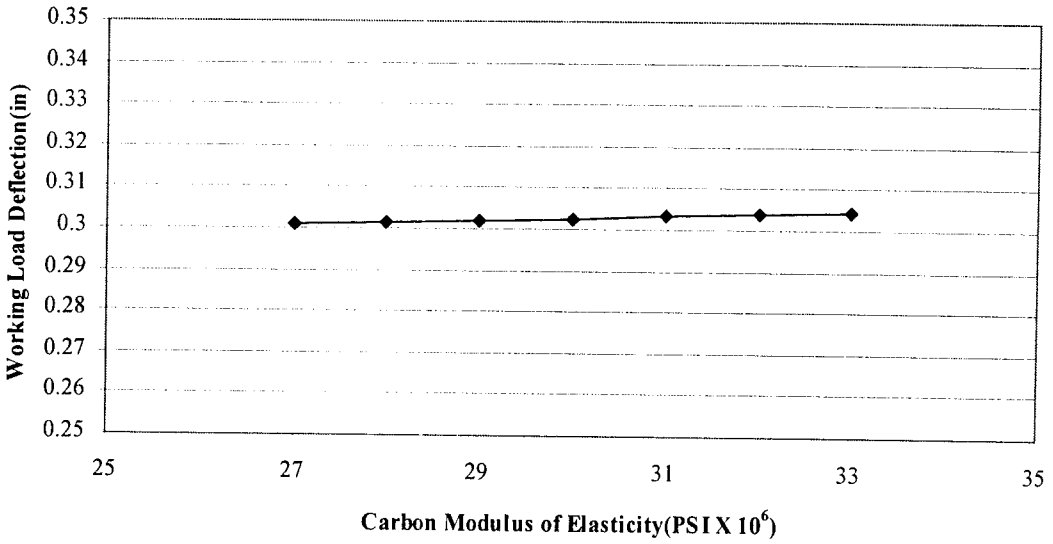

Fig. 8.7. Influence of carbon modulus of elasticity on working load deflection

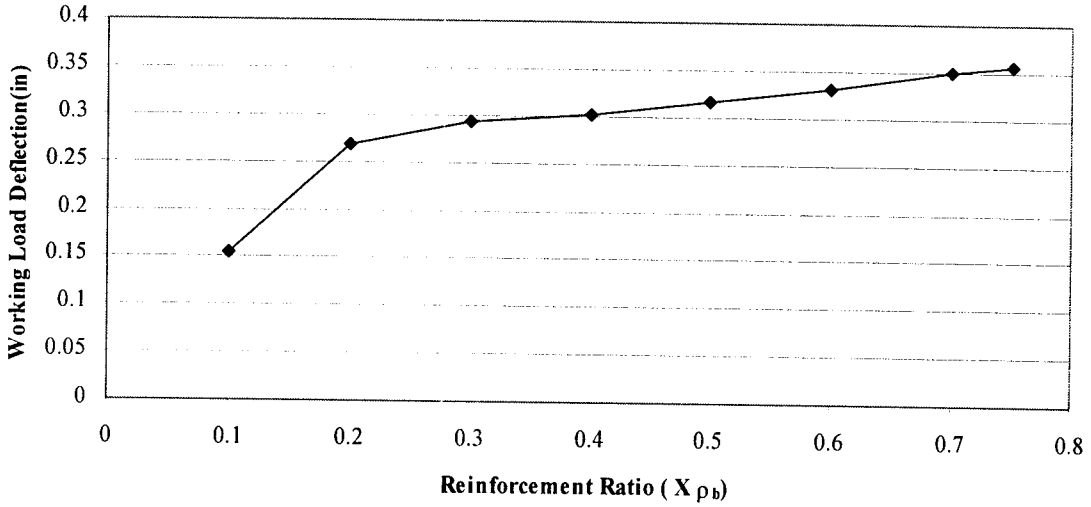

Fig. 8.8. Influence of reinforcement ratio of parent concrete on working load deflection

Chapter 9

Field Applications

Field trials were carried at three locations in Rhode Island. In all cases the surfaces were pre-wetted. The coating consisted of liquid and powder components. They were mixed in the field using high shear mixers. The compositions were based on formulations tested for durability. Field evaluation should be continued to confirm durability.

The first application was on New Jersey barrier, located near seawater. Two formulations with two levels of fillers were applied using a spatula and brush. It was felt that the working time was too short. Therefore the formulations were modified using a retarder.

The second set of applications was at the bridge on Route 1 in South County. Parapet walls near road and an abutment surface were coated with brush, Fig 9.1. Eventhough, a light rain started after 6 hours and continued for 3 days, the coatings performed well. Water running from the road through the expansion joints washed out some of the cementing agent in the pier surface. Inspite of this the coating is in excellent shape after 2 years.

The third application was done under the bridge carrying Route 295 near Providence. This application was done using a sprayer. There was some difficulty because the compressor capacity was not sufficient. The spraying equipment are shown in fig 9.2 and 9.3. the most recent application, which was on New Jersey barrier Route 1 (NJ) is shown in fig 9.4.

A commercial level compressor and spraying equipment are needed to carry out an application involving a large area. It is recommended that 3 more field trials are carried out either using a paint (coating) contractor, or DOT maintenance crew. These applications can be a part of a follow-up project on field implementation of protective coatings. These applications will confirm the productivity rate and coating thickness.

Based on the current experience, the following limits can be set for specifications. These limits are applicable to all the inorganic and polymer modified coatings.

Surface Preparation

The surface shall be free of thick dirt or other foreign material. Any organic material such an algae should be removed. The surface should be pre-wetted with no standing water.

Mixing and Application

The manufacturer's recommendations shall be followed for mixing. Typically, the mixing should be done with high shear mixers. High torque, high-speed drills can be used with mixing vanes. The mixing should be done till the mixture becomes homogenous. Mixing time could vary from 1 to 4 minutes.

The application can be done with brush or sprayer. For economic reasons, sprayer is the preferred method for application.

Typical coating thickness is about 1 mm (0.04 in).

Climate Conditions

The temperature should be higher than 40 °F for t 24 hours. The coatings should be protected from running water for 24 hours.

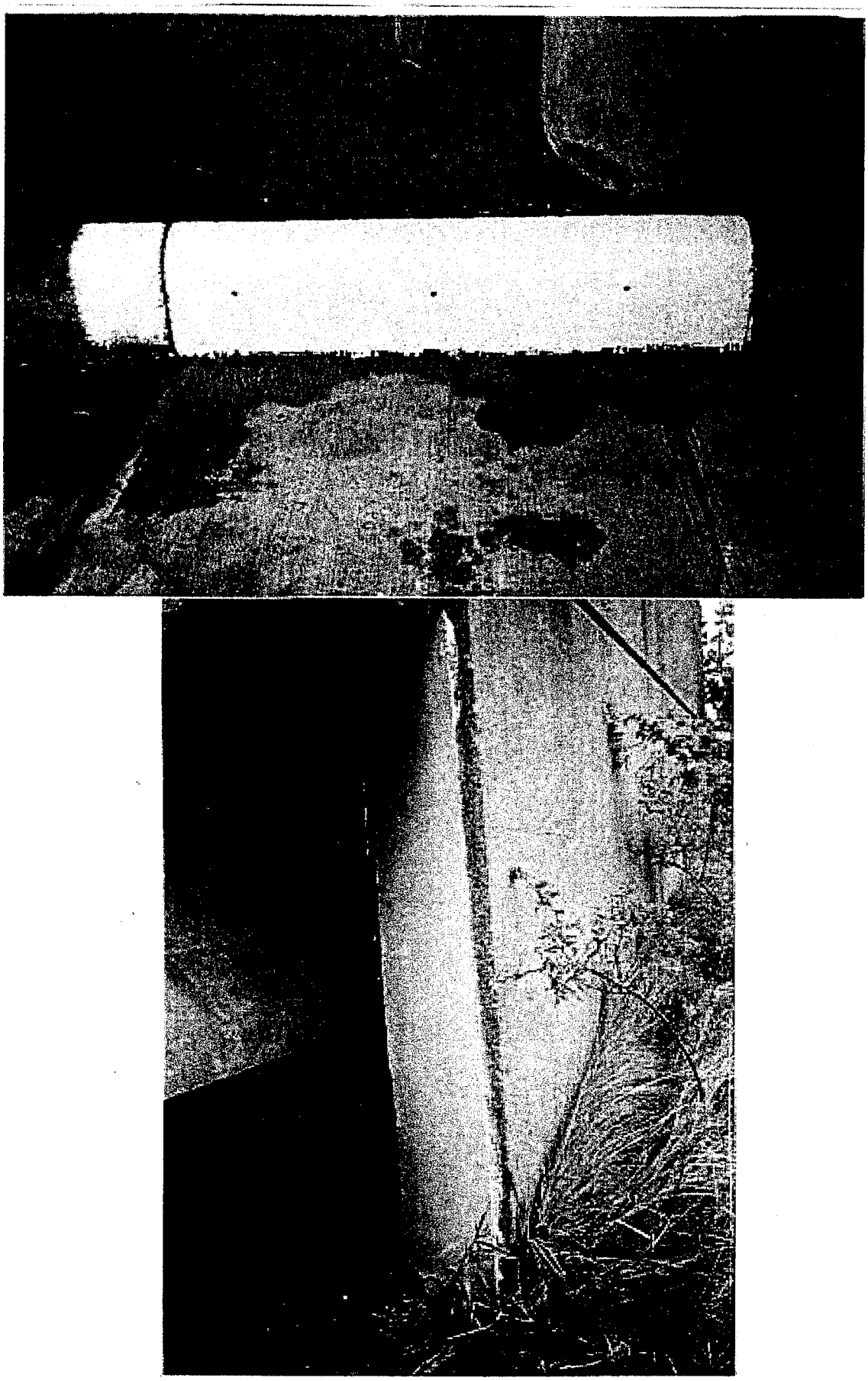

Fig. 9.1 Application of thin white coating, curb and abutment, Rt. 1, Rhode Island

Fig. 9.2. Spray system used for demonstration.

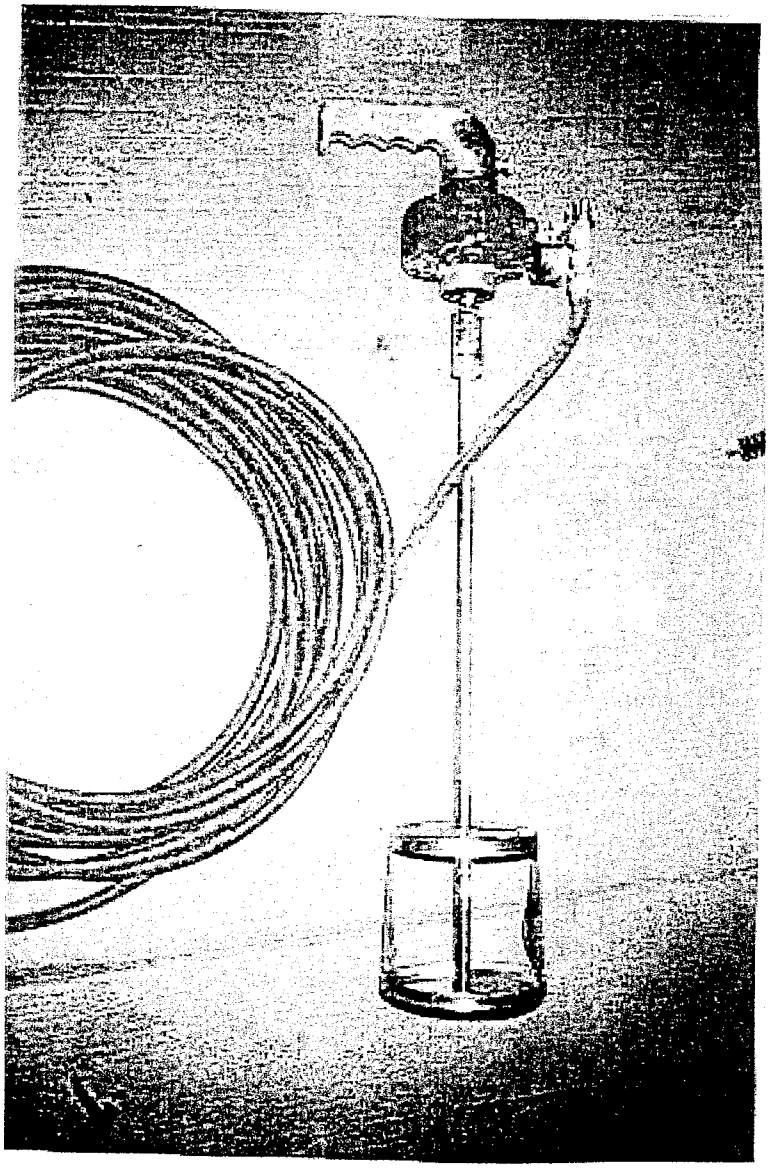

Fig. 9.3 Set up for field mixing

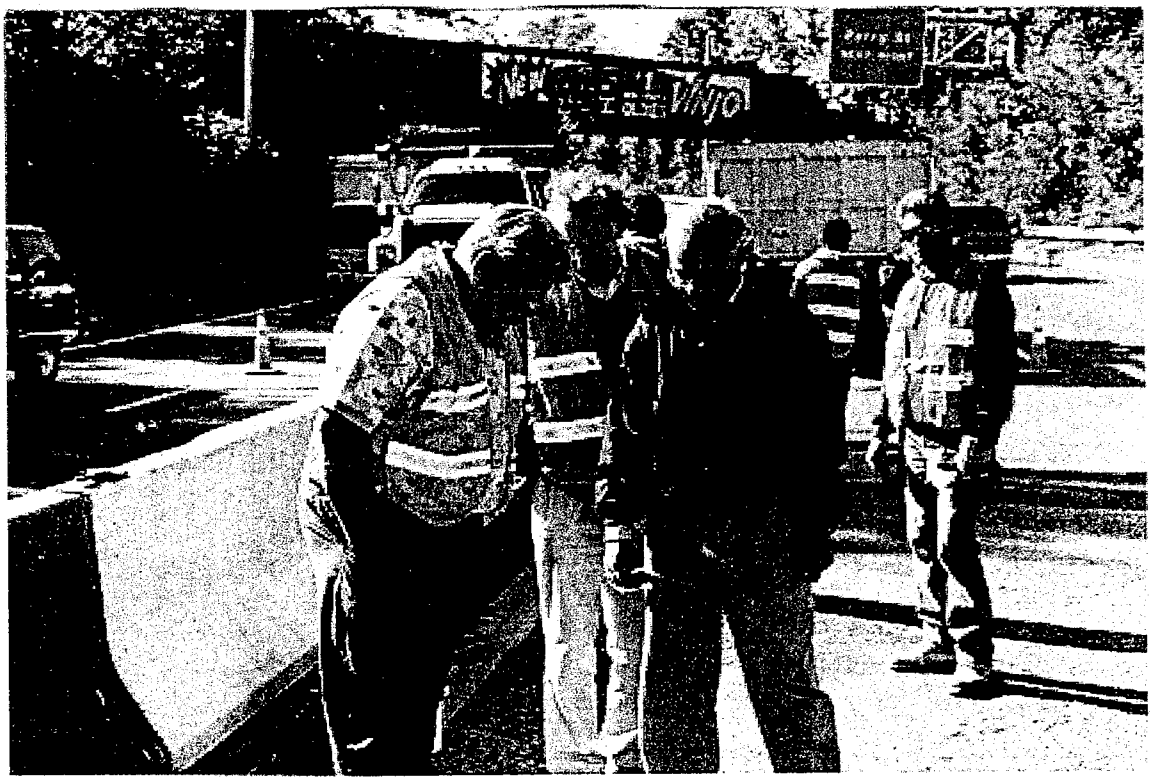

Fig. 9.4 Application on Rt. 1 Barrier, New Jersey

Chapter 10

Conclusions and Recommendations

The results presented in this report focus on the development of an inorganic matrix that can be used both as a coating and also as a matrix with micro, discrete, and continuous fibers. It is expected that the results will help to widen the application of high strength composites in infrastructure applications.

Study of the existing literature led to the following conclusions.

- Coating material should be less permeable than concrete and should not form an impermeable membrane. If the water inside the member is not allowed to escape, the impermeable membrane will delaminate.
- Polymer modified cementitious materials can be formulated to develop matrices with low permeability.
- The inorganic alumino silicate being developed as a fire proof matrix for high strength composites can also be used as a coating material.

Durability studies conducted using one organic matrix, two polymer modified cementitious materials, and three formulations of alumino silicate matrices lead to the following conclusions. The exposure conditions were: wetting and drying, freezing and thawing, and scaling. The samples were evaluated using a non-destructive test method.

- All of the systems performed well in wetting and drying conditions. The coatings and interfaces were durable.

- Under scaling conditions, damage to the surface of the samples could be slowed or prevented. Each of the matrices performed well.
- The coatings were durable under freezing and thawing but they could not protect concrete without entrained air. Therefore, if the structure is susceptible to freezing and thawing, coating alone will not protect the structure.

Evaluation of plain concrete strengthened with inorganic matrix and subjected to wetting and drying and scaling conditions lead to the following conclusions.

- The inorganic matrix in combination with tows and sheets can be used to strengthen plain concrete members.
- Evaluation of prismatic members in flexure indicate that the carbon does not reach it's fracture strain of 0.015 at failure. Since the inorganic matrix cracks, stress concentrations at these cracks result in early failure. The fracture strain of the carbon was also found to be dependent upon the amount of carbon reinforcement. As the amount of reinforcement increases, the fracture strain decreases.
- The fracture strain of carbon is higher when organic matrix was used for strengthening. However, the increase was not very significant.
- Wetting and drying and scaling conditions do not degrade the strength. In some cases, a slight decrease in toughness was found to occur.

It is also possible to use the inorganic matrix for strengthening reinforced concrete members.

- The inorganic matrix can be successfully used to bond carbon fabrics to reinforced concrete beams.
- With proper design and construction process, failure by delamination of composite can be eliminated.
- The performance of the inorganic matrix is better than organic polymer in terms of adhesion. In addition, it is fire resistant, durable under UV light and does not involve any toxic substances. The alumino silicate matrix is water based and no special protective equipment other than gloves is needed. Excess material can be discarded as ordinary waste. This aspect is very important during the construction phase.

The strengthening systems were also evaluated for use with steel samples. The results indicate that the matrix is compatible with steel and can be used as a protective system. To improve strength and stiffness, large carbon areas are needed.

Analytical methods were developed to analyze plain and reinforced concrete members strengthened with inorganic matrix.

- The analytical procedure provides reasonably accurate results. The factor that is most difficult to estimate is the carbon strain at failure for both the inorganic and organic matrices.
- The parametric study indicates that carbon strain and carbon modulus do not significantly affect the moment capacity. Therefore, small errors in the assumption of carbon fracture strain may not significantly affect the nominal moment calculations.

A flow chart and design example is provided for the analysis at working load levels and strength design.

The field trials proved the viability of the system. However a larger site applications should be carried out before developing detailed specifications.

Recommendations

The results of this investigation show that it is possible to use inorganic matrix as a protective coating material. The matrix can also be used for strengthening in combination with carbon fibers. The authors strongly recommend that field demonstration projects be carried out for both applications. Since coating involves less risk, we recommend that this project be carried out in the following summer.

The project should be co-operative effort of the University team and a DOT team. A contractor or the DOT maintenance crew should do the application. The authors envision the major tasks.

Task 1. Identify three sites in the New England region. It is preferable to distribute these sites geographically.

The application should cover a large area. An entire column, abutment or a few hundred yards of a barrier or curbs should be minimum.

Task 2. Application of Coating.

Apply the coating using industrial level crews. The conditions for surface preparation, mixing and application should simulate the real-world conditions.

The entire operation should be videotaped for future reference.

Task 3. Monitoring.

The applications should be monitored for atleast 3 years. Since no degradation is expected, the DOT inspection team can perform this task during their regular visit to the site.

Task 4. Report Preparation.

The report should contain all the information on surface preparation, mixing and application procedures. Using the experience, model specifications should be written.

The project can be funded part as research and as part maintenance. The research part to be conducted by the university will consist of co-ordinating the site selection, monitoring (including videotaping) of applications, and report preparation. The project cost of this part is $ 30,000 over one year period.

References

ACI Committee 318. (1999.) *Building Code Requirements for Reinforced Concrete*, ACI Standard 318-99, Section 8.5.1, American Concrete Institute, Detroit, MI.

ACI Committee 440. (1996). "State-of-the-Art Report on Fiber Reinforced Plastic(FRP) Reinforcement in Concrete Structures," ACI Standard 440R-96, American Concrete Institute, Detroit, MI, 68pp.

ACI Committee 503. (1989). "Use of Epoxy Compounds with Concrete," ACI Standard 503-89, American Concrete Institute, Detroit, MI, 28 pp.

ACI Committee 515. (1986). "A Guide to the Use of Waterproofing, Dampproofing, Protective, and Decorative Barrier Systems for Concrete," ACI Standard 515-86, American Concrete Institute, Detroit, MI, 44 pp.

ACI Committee 548. (1995). "State-of-the-Art Report on Polymer Modified Concrete," ACI Standard 548-95, American Concrete Institute, Detroit, MI, 47 pp.

American Society for Testing and Materials(1993). "Standard Test Method for Scaling Resistance of Concrete Surfaces Exposed to De-icing Chemicals." Standard C-672, Section 4, Volume 2, pp. 345-347.

American Society for Testing and Materials(1993). "Resistance of Concrete to Rapid Freezing and Thawing." Standard C-666A, Section 4, Volume 2, pp. 326-331.

Balaguru, P., Kurtz, S., and Rudolph, J. (1996). "Geopolymer for Repair and Rehabilitation of Reinforced Concrete Beams," *Civil Engineering Report 96-14*, Rutgers University, 19pp.

Balaguru, P., Shah, S.P. (1992.) Fiber Reinforced Cement Composites, McGraw-Hill, New York, NY, 535pp.

Balaguru, P., Slattum, K. (1995.) "Test Methods for Durability of Polymeric Fibers in Concrete and UV Light Exposure," *American Concrete Institute - Special Publication Number 155*, Detroit, MI, pp. 115-136.

Bean, D.L. (1988.) "Surface Treatments to Minimize Concrete Deterioration: Survey of Field and Laboratory Applications and Available Products," *Technical Report REMR_CS-17*, Report 1, U.S. Army Engineer Waterways Experiment Station, Vicksburg, MS.

Berset, J.D. (1992.) "Strengthening of Reinforced Concrete Structures for Shear Using Composite Materials," *M.S. Thesis, Massachusetts Institute of Technology.*

Carter, P.D. (1989.) "The Use of Penetrating Sealers on Concrete Bridge Decks," *Proceedings of the Sessions Related to Structural Materials at Structures Conference 1989,* San Francisco, CA, pp. 292-302.

Chajes, M.J., Mertz, D.R., and Thomson, J.R. (1994.) "Durability of Composite Material Reinforcement," *Proceedings of the Third Materials Engineering Conference*, ASCE, pp. 598-605.

Davidovits, J. (1991.) "Geopolymers: Inorganic Polymeric New Materials," *Journal of Thermal Analysis*, volume 37, pp. 1633-1756.

Davidovits, J., and Davidovics, M. (1991.) "Geopolymer: Ultra High Temperature Tooling Material for the Manufacture of Advanced Composites," *36th International SAMPE Symposium*, June 30 – May 5.

Dolan, C., Rizkalla, S., and Nanni, A., (editors, 1999.), Fiber Reinforced Polymer Reinforcement for Reinforced Concrete Structures, *American Concrete Institute – Special Publication Number* 188, Detroit, MI, 1152 pages.

Ehsani, M.R., Saadatmanash, H., Abdelghany, I.H., and Elkafrawy, W. (1993.) "Flexural Behavior of Masonry Walls Strengthened With Composite Fabrics," *American Concrete Institute – Special Publication Number 128*, Detroit, MI, pp. 492-507.

Foden, A., Balaguru, P., and Lyon, R. (1996A.) "Mechanical Properties and Fire Response of Geopolymer Structural Composite," *41st International SAMPE Symposium, May 30 – June 3.*

Foden, A., Balaguru, P., and Lyon, R. (1996B.) "Mechanical Properties of Carbon Composites Made Using an Inorganic Polymer," *ANTEC*, pp. 3013-3018.

Foden, A., Balaguru, P., Lyon, R., and Davidovits, J. (1997.) "Flexural Fatigue Properties of an Inorganic Matrix-Carbon Composite," *41st International SAMPE Symposium, May 29 – June 2.*

Foden, A., Lyon, R., and Balaguru, P. (1996.) "A High Temperature Inorganic Resin for Use in Fiber Reinforced Composites," *Proceedings of the First International Conference on Composites in Infrastructure*, NSF, Tucson, Arizona, pp. 166-177.

Gomez, J., and Casto, B. (1996.) "Freeze-Thaw Durability of Composite Materials," *Proceedings of the First International Conference on Composites in Infrastructure*, NSF, Tucson, Arizona, pp. 947-955.

Hamid, J., Larralde, J., and Salama, A. (1993.) "Properties of Hollow Concrete Masonry Reinforced with Fiberglass Composite," *American Concrete Institute – Special Publication Number 128*, Detroit, MI.

Harmon, T.G. and Slattery, K.T. (1992.) "Advanced Composite Conferment of Concrete," *Proceedings of the First International Conference on Advanced Composite Materials in Bridges and Structures*, Sherbrooke, Quebec, Canada, pp. 299-306.

Huang, G.G. (1995.) "An Inorganic Polymer for Use in Fiber Composites," Special Project Report Submitted to Rutgers, The State University, May 1995, 73 pp.

Husbande, T.B., and Causey, F.E. (1989.) "Surface Treatments for Concrete," *Proceedings of the Sessions Related to Structural Materials at Structures Congress 1989*, pp. 282-291.

Javed, S., Kumar, S.V., and GangaRao, V.S. (1996.) "Experimental Behavior of Concrete Beams with Externally Bonded Carbon Fiber Tow Sheets," *Presented at the 51st Annual Meeting of SPI/CI Conference & Exposition.*

Lavelle, J.A. (1988.) "Acrylic Latex-Modified Portland Cement," *ACI Materials Journal*, volume 85, number 1, Jan-Feb 1988, pp. 41-48.

Li, M.W., Saadatmanash, H., and Ehsani, M.R. (1992.) "Behavior of Externally Confined Concrete Columns," *Proceedings of the Materials Engineering Congress*, Atlanta, Ga, pp. 677-690.

Lyon, E., Sorathia, U., Balaguru, P., Foden, A., and Davidovits, J. (1996.) "New Fire Safe Material for Cabin Interiors," *AGARD Conference Proceedings*, 587, pp. 27.1-27.8.

Lyon, R., Sorathia, U., Balaguru, P., and Foden, A. (1996.) "Fire Response of Geopolymer Structural Composites," *Proceedings of the First International Conference in Composites in Infrastructure*, NSF, Tucson, Arizona, pp. 972-981.

Lyon, R E. Balaguru, P N. Foden, A. Sorathia, U. Davidovits, J. Davidovics, M. (1997.) "Fire-resistant aluminosilicate composites," *Fire & Materials*, volume 21, number 2, Mar-Apr 1997, pp. 67-73.

Marusin, S.L. (1989.) "Enhancing Concrete Durability by Treatment with Sealers," *Proceedings of the Sessions Related to Structural Materials at Structures Congress 1989,* pp. 270-281.

Marusin, S.L. (1987.) "Improvement of Concrete Durability Against Intrusion of Chloride Laden Water by Using Sealers, Coatings, and Various Admixtures," *American Concrete Institute – Special Publication Number 100.*

M'Ba Zaa, I., Missihoun, M., and Labossiere (1996.) "Strengthening of Reinforced Concrete Beams with CFRP Sheets," *Fiber Composites in Infrastructure,* 1996, pp. 746-759.

Meier, U. (1987.) "Bridge Repair with High Performance Composite Materials," *Material UND Technik*, Vol. 4, pp. 125-128.

MPA. (1987.) "Bonding of Steel and GFRP Plates in the Area of Coupling Joints, Talbruk Kattenbusch," *Federal Institute for Material Testing(MPS),* Braunschweig, Research Report, No. 312611429.

Nanni, A., Editor, Fiber Reinforced Plastic(FRP) Reinforcement for Concrete Structures: Properties and Applications, Elsevier Science Publishers, B.V., 450pp.

Nakamura, M., Sakai, H., Yagi, K., and Tanaka, T. (1996.) "Experimental Studies on the Flexural Reinforcing Effect of Carbon Fiber Sheet Bonded to Reinforced Concrete Beam," *Fiber Composites in Infrastructure*, pp. 746-759.

Plevris, N., and Triantafillou, T.C. (1994.) "Time-dependent behavior of RC members strengthened with FRP laminates," *Journal of Structural Engineering-ASCE*, volume 120, number 3, March 1994, pp. 1016-1042.

Plevris, N., Triantafillou, T.C., and Veneziano, D. (1995.) "Reliability of RC members strengthened with CFRP laminates," *Journal of Structural Engineering-ASCE*, volume 121, number 7, July 1995, pp. 1037-1044.

Priestley, M.J.N., Seible, F., and Fyfe, E. (1992.) "Column Seismic Retrofit Using Fiberglass/Epoxy Jackets," *Proceedings of the First International Conference on Advanced Composite Materials in Bridges and Structures*, Sherbrooke, Canada, pp. 287-298.

Rahman, A.H., Kingsley, and Crimi, J. (1996.) "Durability of a FRP Grid Reinforcement," *Proceedings of the Second Annual International Conference on Advanced Composite Materials in Bridges and Structures*, Montreal, Canada, pp. 681-690.

Ritchic, P.A., Thomas, D.A., Lu, L.W., and Connelly, G.M. (1991.) "External Reinforcement of Concrete Beams Using Fiber Reinforced Plastics," *American Concrete Institute Structural Journal*, volume 88, number 4, pp. 490-500.

Saadatmanash, H., and Ehsani, M. (1991.) "RC Beams Strengthened with GFRP Plates: Part I Experimental Study," *Journal of Structural Engineering-ASCE*, volume 117, number 10, pp. 3417-3433.

Saadatmanash, H., and Tannous, F. (1998.) "Durability of Fiber Reinforced Plastic(FRP) Rebars and Tendons in Aggressive Environments," *Repair and Rehabilitation of Reinforced Concrete Structures*, ASCE, pp. 120-133.

Sadatmanesh, H., and Ehasani, M., Editors. (1996.) Fiber Composites in Infrastructure, *Second International Conference on Composites in Infrastructure*, Tucson, Arizona, January 5-7, 1999.

Sen, R., Mariscal, D., and Shahawy, M. (1993.) "Durability of fiberglass pretensioned beams," *ACI Structural Journal*, volume 90, number 5, Sep-Oct 1993, pp. 525-533.

Soudki, K.A., and Green, M.F. (1996.) "Freeze-Thaw Durability of Concrete Beams Strengthened with Carbon Fiber Sheets," *ACI Fall Convention*, New Orleans, November 1996.

Toutanji, H.A., and Balaguru, P. (1998.) "Durability FRP Encased Columns," Under Review, *Journal of Materials - ASCE.*

Toutanji, H.A., and Gomez, W. (1997.) "Durability Characteristics of Concrete Beams Externally Bonded with FRP Composite Sheets," *Cement and Concrete Composites*, volume 19, pp. 351-358.

Walters, P.G. (1992.) "VAE Redisposable Powder Hydraulics Cement Admixtures," *Concrete International*, volume 14, number 4, pp. 30-34.